ABSTRACT

The effect of short, strong radiofrequency pulses on the nuclear spin system is examined. Providing the durations of the pulses are short with respect to coupling constants within the spin system, they may be described by simple rotation operators which are exponential functions of the angular momentum operators. Operator algebra can be used to define the interaction of such pulses with the spin system, and the mutual interaction of a sequence of pulses. The case of a simple coupled spin system is examined in detail and it is found that a vector model can be used to describe the motion of the expectation values of the observables. This model also allows treatment of such 'non-classical' effects as coherence transfer and multiple-quantum coherence. The proposal is also made that certain types of pulse imperfection may be compensated by using specially constructed sequences of small numbers of pulses, which are termed 'composite pulses'. Their compensatory action is illustrated by computer simulation, and by experimental results. In the case of certain symmetrical composite pulses, operator algebra can be used to understand their overall effect in the presence of pulse imperfections, suggesting their use in such critical applications as multiple spin echo trains. Another class of symmetrical composite pulses provides rotations by arbitrary angles around the z-axis of the rotating reference frame, and is expected to be of use in multiple-quantum spectroscopy.

NEW TECHNIQUES IN

NUCLEAR MAGNETIC RESONANCE

A thesis submitted for the degree of Doctor of Philosophy

by

Malcolm Harris Levitt

March 1981

Keble College,
Oxford.

Physical Chemistry Laboratory,
Oxford.

ACKNOWLEDGEMENTS.

This research was made possible by the contributions of many people, and it is a pleasure to record here my debt to them. I thank Geoffrey Bodenhausen, Gareth Morris and David Turner for their assistance with machine-code programming, the use of their existing programs, and their essential hardware modifications. Most of the experimental results derived from collaborative work with Stewart Kempsell, and I thank him. I thank all of the above and also Ad Bax, Tony Avent, Pei Feng-Kui, James Keeler, Tom Frenkiel, Tom Mareci and Reinhard Niedermeyer for much illuminating discussion and encouragement. Special thanks are reserved for my supervisor, Dr. R. Freeman, who has been an enormously helpful, experienced and imaginative guide.

CONTENTS.

CHAPTER ONE

INTRODUCTION

CHAPTER 1

INTRODUCTION

1.1 The high-resolution NMR spectrum

Of all the various forms of spectroscopy, nuclear magnetic resonance has some unique properties which have ensured its great interest both for the theoretician and the practical chemist. It is a low energy spectroscopy, and it is a high resolution spectroscopy. NMR transitions occur between the energy levels of magnetic nuclei immersed in a strong magnetic field; the very low energies involved (0.1 $Jmol^{-1}$) ensure that the probability of spontaneous transitions taking place is essentially zero (1). Thus the exchange of nuclear spin energy with the surroundings relies on the presence of transitions stimulated by incident photons; the photons may originate either from the coherent irradiation fields of the spectrometer, or from incoherent local fields generated by neighbouring magnetic species. In certain cases, particularly that of isotropic diamagnetic liquids, the latter effect is very weak; the natural lifetimes of the nuclear spin states can be very long (up to tens of seconds) so that the lifetime broadening of the NMR resonances is very small. Indeed the effective resolution (the ratio of natural linewidth to transition frequency) of NMR is one of the smallest of all forms of spectroscopy (about 0.01 Hz in 100 MHz, or 1 in 10^{10}). Thus NMR spectra have an exceedingly high potential information content, although in practice the frequency range of the resonances of a given nuclear species is quite small, and the practical effective resolution much reduced.

Because NMR operates at such a low frequency, sensitivity is a considerable problem. The difference in thermal equilibrium populations of two typical nuclear energy levels is only about 1 in 10^5. Hence a resonant detection technique is used in which a coherent oscillation of the nuclear spin magnetization is detected, rather than the incoherent absorption normally used in high-energy spectroscopies. The method now almost universally employed is that of pulse-Fourier-transformation, introduced in 1966 (2). A coherent pulse of radio-frequency photons is applied to the sample. Now the interaction between the irradiation field and the nuclear spins may be expressed as a rotation of the nuclear spin magnetization vector in a rotating frame of reference (3). If the photons are of a frequency corresponding to the hyperfine splitting of the chosen nuclear isotope in the strong magnetic field, and the pulse has the appropriate duration, energy is absorbed and the nuclear magnetization is rotated by $\pi/2$ radians to a position perpendicular to the field. The precessional motion which is so induced stimulates an electrical signal in a suitably positioned coil. The observed effect is that the pulse creates a ringing transient which slowly decays due to incoherent internal fields ('spin-spin relaxation'), or to variations in the magnetic field, and hence the ringing frequencies, through the sample volume. After filtration and mixing down to an audio frequency, the transient can be digitized and stored in the memory of the dedicated computer which is now invariably part of modern NMR spectrometers. Digital Fourier transformation of the signal (often called the 'free induction decay') results in the NMR spectrum, with peaks corresponding to the various NMR frequencies of the given isotope.

The signal-to-noise ratio of a spectrum produced in this way is usually enhanced by repeating the experiment after a delay of some seconds to allow thermal equilibration of the magnetic spin system. The results can be coadded. If this is repeated N times, the signal-to-noise ratio increases according to $\sqrt{N}$, assuming uncorrelated, stationary noise. Other manipulations are regularly performed by the computer on the digitized free induction decays before Fourier transformation. These include enhancement of the signal-to-noise ratio at the expense of resolution, and vice-versa (2). Other more sophisticated schemes, now in routine use, include comparison of the decaying radio-frequency transient with <u>two</u> reference signals of the same frequency but in quadrature phase (4). A quadrature Fourier transform can be applied to these two independent sets of data to give a spectrum in which frequencies greater and smaller than the reference frequency can be distinguished. This has the advantage that less pulse power is required to excite a given range of NMR resonance frequencies.

When obtained the NMR spectrum can provide a great deal of information on molecular structure and dynamics. The resonance frequencies of the lines are strongly affected by magnetic interactions with electrons, particularly if these are unpaired. The large magnetic moment associated with electronic ground states of finite electronic angular momentum has a strong influence on the local magnetic fields at the nuclei and may result in large frequency shifts of the resonances. For this reason small amounts of paramagnetic lanthanide ions are sometimes added to solutions to spread out the resonances and enhance resolution (5). But even in diamagnetic substances, the

application of a magnetic field can introduce participation of paramagnetic excited states (6). Local electronic currents are induced which give rise to small local variations in the magnetic flux density. These produce relative perturbations of resonance frequencies which are proportional to the applied magnetic field. The effect is known as the 'chemical shift' (7). Despite a general lack of success in 'ab initio' calculations of shift values (8), they remain probably the single most informative NMR parameter to the chemist. An enormous number of empirical correlations of chemical shifts with molecular structure have been made. Many NMR spectra can be fully assigned on the basis of chemical shifts alone, and conclusions about conformation and other fine structural details can often be drawn (9).

Besides electrons, interactions between magnetic nuclei usually have an influence on the NMR spectrum. The interaction of the greatest magnitude is the direct through-space coupling of magnetic dipoles, but this does not usually affect resonance frequencies in isotropic liquids because it is averaged to zero by rapid random molecular tumbling (10). A weaker mechanism is responsible for the observed splitting of the resonances - this is the indirect scalar coupling (11,12) attributed to mediation of the bonding electrons (13). Scalar couplings cause a splitting of the resonance from a given nucleus into a multiplet of several lines, often with a binomial distribution of intensities. This situation is not quite so simple if the scalar interaction is comparable to the difference in chemical shifts of the coupled nuclei ('strong coupling'). Here the interaction is strong enough to cause mixing of the wavefunctions, resulting in

perturbation of both the frequencies and intensities of the resonances (14). But in the absence of strong coupling effects, the multiplet structure provides a particularly direct means of access to molecular structural information. Multiplicities indicate the number of neighbouring magnetic nuclei, and the magnitude of the couplings may also be used to advantage. In particular the long-range couplings (especially 'vicinal' couplings over three bonds), are related in a simple way to bond dihedral angles, in favourable cases (15).

But chemical shifts and scalar couplings still do not constitute all the information contained in the NMR spectrum. Each resonance also possesses at least two relaxation time constants, the spin-lattice relaxation time T_1 and the spin-spin relaxation time T_2. The former quantifies the rate of exchange of energy between the nuclear spin ensemble and the 'lattice' - the continuum of energy levels associated with the thermal motion of the molecules which compose the medium. The second relaxation time expresses the natural rate of transitions across the two energy levels which define the chosen resonance. This transition rate is responsible for the finite natural linewidth of a NMR response, and is due to incoherent interactions with surrounding magnetic species. Note that not every transition between nuclear energy levels leads to energy exchange between the spin system and the surroundings. For example a nuclear transition may be accompanied by a similar one in the opposite direction somewhere else in the ensemble, (a 'flip-flop process'), so that energy is conserved. Hence T_2 is always shorter than or equal to T_1.

Probably the strongest relaxation mechanism for nuclear spins is quadrupole coupling. Nuclei of magnetic quantum number $I \geqslant 1$ may have an electric quadrupole moment - asymmetric distribution of electric charge. This can interact strongly with electric field gradients at the nucleus according to the strength of the electric quadrupole moment eQ(1). This provides a strong relaxation mechanism and greatly broadens the resonances of quadrupolar nuclei. Accordingly spin-$\frac{1}{2}$ nuclei such as ^{1}H and ^{13}C are normally favoured for NMR work. For these nuclei the quadrupolar relaxation mechanism is absent.

The second major relaxation mechanism involves interaction with neighbouring magnetic dipoles, such as those produced by unpaired electrons, or other magnetic nuclei. As usual unpaired electrons have much the strongest effect and traces of paramagnetic substances can cause a dramatic increase in relaxation rates. Hence it is important to remove dissolved oxygen from samples in which the relaxation properties are of interest. In the absence of unpaired electron spins and of quadrupolar relaxation, it is the direct, through-space, dipole-dipole interaction between magnetic nuclei which is the dominant mechanism. As mentioned above, dipolar interactions do not affect NMR resonance frequencies in isotropic liquids, but their magnitude may be assessed from relaxation properties in favourable cases. If there is fast isotropic molecular tumbling (the 'extreme narrowing limit') and assuming a rigid molecular framework, the contribution to the relaxation rate of one nucleus from dipolar coupling with another is simply proportional to the inverse sixth power of the internuclear separation (10).

Accordingly the dipolar contribution falls off very rapidly at high internuclear distances, so that all but intramolecular nearest-neighbour interactions can usually be ignored. With these assumptions and in favourable cases, relaxation rates can provide accurate estimates of relative liquid-state internuclear distances (16). But for large molecules, when molecular motion is typically slow, anisotropic and non-rigid, theoretical analysis is much more difficult and no single model has been found to provide an universal quantitative description of relaxation behaviour (17-22). However semi-quantitative information can often be obtained such as the relative degrees of mobility of the side chains in a large, non-rigid biomolecule (23). A full analysis may require both field-dependent and temperature-dependent studies of relaxation rates, and measurement of both T_1 and T_2.

In a system of coupled spins many resonances share energy levels, so that spin-lattice relaxation must be described by a set of coupled differential equations (24). As there may be many different pathways for the relaxation of one given resonance, the approach to thermal equilibrium generally proceeds according to a sum of exponential terms, rather than the single exponential time-course usually assumed (25). It is also possible for the individual lines of a given multiplet to have different spin-lattice relaxation times. This is particularly the case if there is a degree of anisotropy in the molecular tumbling (26).

Dipolar spin-spin relaxation rates and spin-lattice relaxation rates have a rather different form of temperature-dependence (10). Both depend on the 'rotational correlation time' of the random molecular

motions, which expresses the average rate of molecular reorientation, and is a function not only of temperature but also of molecular size and solution viscosity. Spin-lattice relaxation requires that the molecular motion generates a component of incoherent dipolar fields at a frequency close to that of the NMR transition. Only then can energy be exchanged between the molecular motions and the nuclear magnetic polarisation. Thus T_1's are the longest both at <u>low</u> temperatures (where molecular motion is slow and there is insufficient energy available at the NMR frequency), and at <u>high</u> temperatures (where the motion is fast and the available energy is spread over such a wide range of frequencies that there is only a little available at the required condition). Therefore there is a minimum in the plot of spin-lattice relaxation time against temperature. Around this condition T_1 varies very little as the temperature is changed, and T_2 may then be more informative (27). The temperature dependence of T_2 does not display a minimum (10).

T_2 is also sensitive to many factors which have no influence on T_1. For example spin-spin relaxation can be used to study chemical exchange over rather more rapid time-scales than T_1 (28). T_2's are also affected indirectly by spin-lattice relaxation of coupled spins (29): If the nucleus of interest has a scalar coupling interaction with a second nucleus which happens to have a short spin-lattice relaxation time, this furnishes a mechanism for spin-spin relaxation of the first nucleus. This is important in cases such as proton-coupled carbon-13 spectroscopy, and is often known as 'scalar relaxation'. It can also be responsible for differential spin-spin relaxation rates of the individual components of a scalar-coupled multiplet (24).

Apart from the dipolar interaction, other mechanisms are known for both spin-spin and spin-lattice relaxation. These are almost invariably much weaker than the dipole-dipole mechanism and are not observed except in special cases. They include chemical shift anisotropy (30) and spin-rotation (31). Both of these involve interactions between paired electron spins, the magnetic field, and molecular rotation, but will not be treated further here.

1.2 NMR of isotopes of low natural abundance

With such a large amount of information contained in a high-resolution NMR spectrum, it is not too surprising that one of the major problems encountered is that of resolution and assignment of the many resonances. Even using the high fields now available in contemporary superconducting magnets, the size of molecule for which a conventional proton spectrum can be resolved is very limited. Hence once the old problem of sensitivity had been alleviated by using the new high fields and a Fourier transform technique, attention turned to spin-$\frac{1}{2}$ isotopes of low natural abundance, such as carbon-13 and nitrogen-15. These isotopes have many advantages, summarised below for the case of carbon-13:

(i) The low natural abundance ensures the absence of homonuclear coupling structure from the spectrum, because it is unlikely that two carbon-13 nuclei are to be found in the same molecule. (there is in fact a very small fraction of molecules which do contain two carbon-13 nuclei, and which are responsible for weak 'satellite' lines in the spectrum. The importance of these molecules will be investigated later). The absence of homonuclear coupling constitutes a very important spectral simplification;

(ii) Coupling with the abundant protons may be eradicated by noise-modulated irradiation in the region of the proton transition frequencies (32). This simplifies the spectra still further, which now consist of a series of decoupled single lines, one for each chemically distinct carbon site in the molecule. There are also other advantages associated with noise-modulated irradiation of the protons. Firstly, the intensity of the resonance from a given carbon is increased because the signal strength is no longer spread out over several multiplet components; Secondly, the carbon-13 magnetization may be enhanced by a relaxation phenomenon known as the Nuclear Overhauser Effect (33). Finally, the natural linewidth of the carbon-13 resonances is reduced because the scalar coupling mechanism for spin-spin relaxation is removed. (See above).

(iii) The spread in chemical shifts is greater by a factor of about 20 for carbon-13 as against protons, and greater still for ^{15}N. This is mainly because protons lack low-lying p-orbitals, whose participation is necessary for the production of the induced electronic currents responsible for the chemical shift. The nearest available proton p-orbitals are of considerable energy, so that induced currents must be small; and

(iv) The information provided by ^{13}C NMR is at worst complementary, and at best more directly useful than that provided by protons. The central situation of the carbon nuclei in the backbone of the molecule makes them more easily influenced by important conformational changes and less sensitive to solvent effects and other intermolecular interactions.

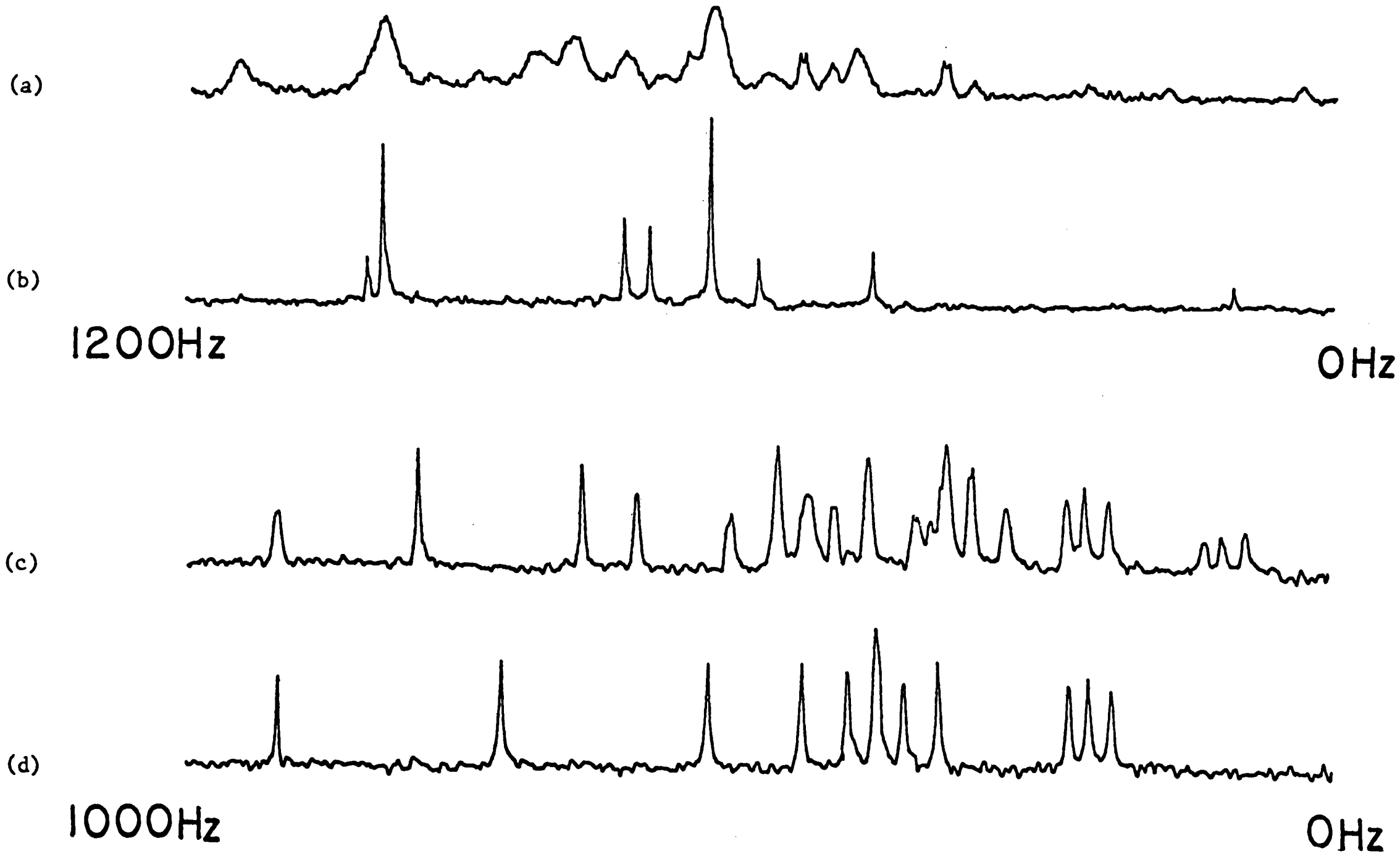

Fig.1.1. The proton-coupled (a) and proton-decoupled (b) carbon-13 spectra of the aliphatic region of 2(1-methylcyclohexyl)-4,6-dimethylphenol. (c) and (d); the coupled and decoupled spectra of sucrose.

These advantages should of course be weighed against the great sensitivity disadvantages of these isotopes. Apart from the very low natural abundance (1% for carbon-13 and only 0.2% for nitrogen-15), these nuclei have low gyromagnetic ratios, further degrading the achievable sensitivity. In addition relaxation times tend to be longer than those of protons, particularly for ^{15}N.

1.3 Two-dimensional spectroscopy

Once a simplified NMR spectrum has been obtained by observing a rare isotope under proton-decoupled conditions, the problem remains of assigning the individual resonances to specific sites in the molecule. This can be difficult, because with all coupling structure eliminated from the spectrum, it is necessary to rely purely on chemical shifts to make the assignment. In many cases shifts do not provide sufficient information. It may then be necessary to revert to the proton-coupled mode. The coupling structure can be of considerable use, providing it can be resolved. The multiplicities indicate the number of directly-bonded protons, and the magnitudes of the couplings, and the nature of any long-range coupling fine structure which can be seen, are also helpful. But again the very richness of information present in the proton-coupled carbon-13 spectrum is itself a source of difficulty. The coupled spectrum consists of many superimposed, overlapping multiplets. It is frequently impossible to disentangle these from each other and isolate the multiplet components of a single carbon site (see Figure 1.1). There seems to be this inherent difficulty in carbon-13 spectroscopy. The decoupled spectrum enjoys good

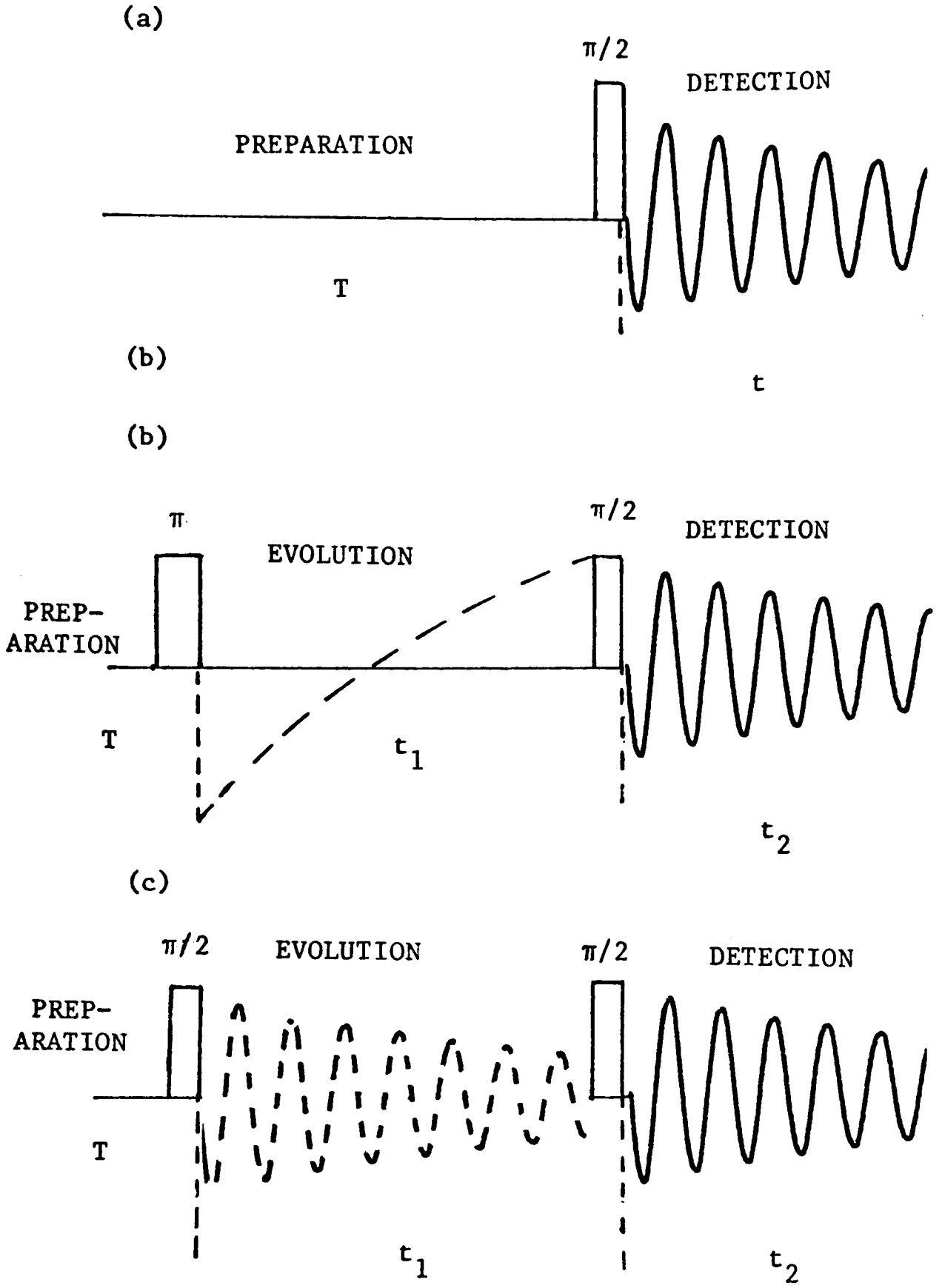

Fig.1.2 Fourier transform experiments.

(a) Conventional experiment, consisting of a preparation period in which reproducible populations are established, followed by a $\pi/2$ pulse for excitation of transverse magnetization.

(b) Relaxation time measurement by the 'inversion-recovery' method. A variable evolution period t_1 has been introduced in which the populations, initially perturbed by the π pulse, are re-established with characteristic time constants.

(c) Two-dimensional spectroscopy. Here the evolution during t_1 consists of the oscillation of coherences, producing a modulation of the signals acquired during t_2 which may be analysed by a second Fourier transformation.

resolution but has a poor information content, whilst the coupled spectrum is rich in information, little of which can be distinguished. This apparent impasse is only resolved by a drastic modification of the mode of operation of the NMR experiment, and a revision of the concept of the NMR spectrum to include additional frequency dimensions.

The principle of two-dimensional spectroscopy may be illustrated by using an example from the different field of proton spectroscopy, in which it is the homonuclear couplings which are the major factor responsible for resolution difficulties. In this field an important method of resonance assignment is to map out the connectivity of the lines in the spectrum - that is, to find out which resonances share energy levels and hence originate from a common group of coupled spins. Such information is vital for assignment of proton spectra of large molecules, but in the past has relied on rather messy double-resonance techniques (34,35,36).

The pulse sequence used for the mapping of connectivity by two-dimensional spectroscopy is shown in Figure 1.2 (c), and is a very simple sequence of just two $\pi/2$ pulses, separated by an 'evolution period' t_1 and followed by the usual detection period t_2, in which oscillating magnetization is detected, digitized, and stored in the computer memory. To understand how this experiment works it is useful to make an analogy with the familiar inversion-recovery method for the measurement of spin-lattice relaxation times, Figure 1.2(b) (37,38). This experiment begins with a long preparation period T, during which thermal equilibrium is established. The net magnetization at this time is longitudinal, i.e. aligned along the static magnetic field. On application of a π

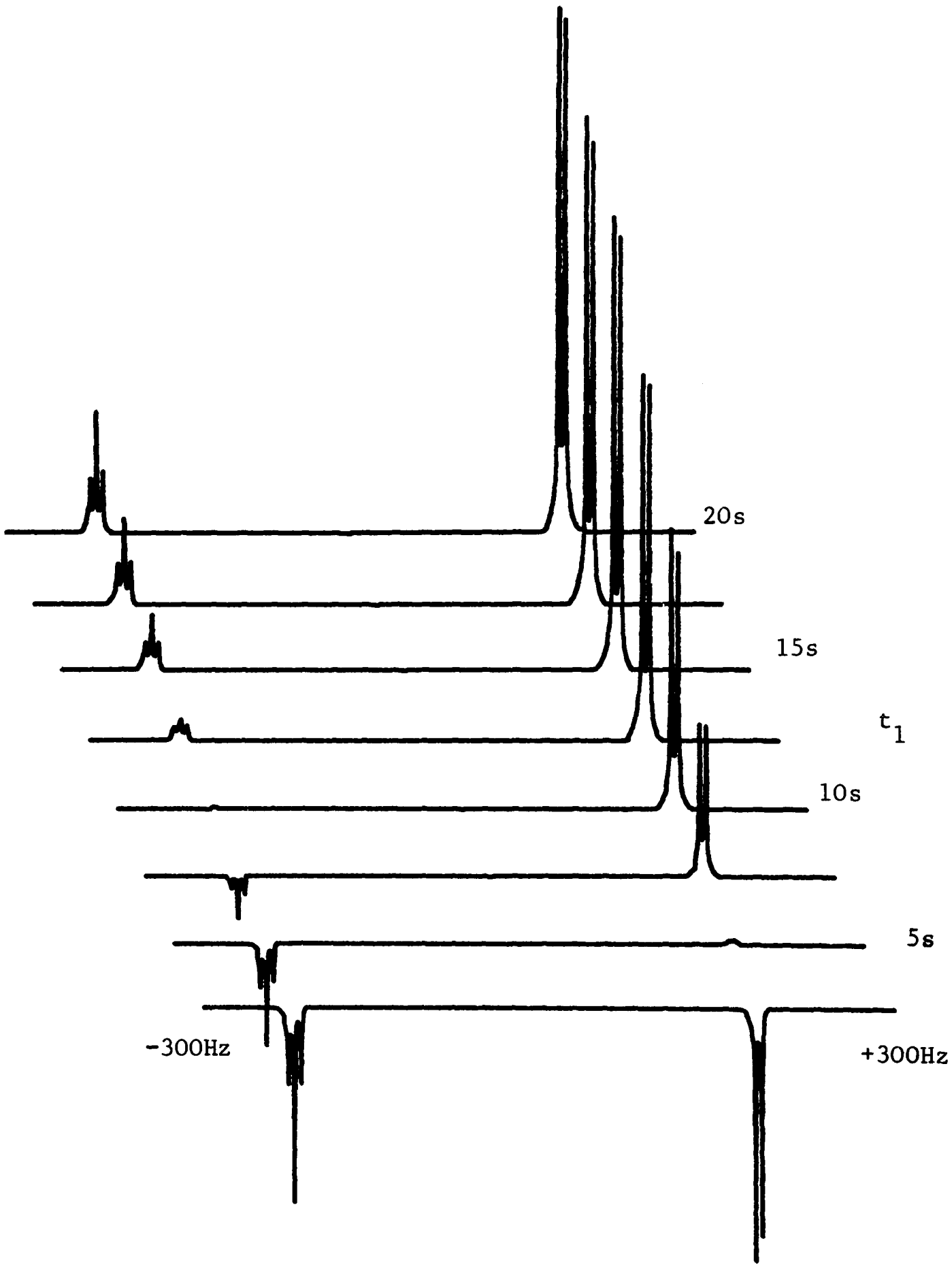

Fig.1.3. A typical inversion-recovery relaxation time measurement - the proton spectrum of 1,1,2-trichloroethane measured on the XL-200.

pulse, the spin system absorbs energy, and equilibrium is destroyed, to be slowly restored as the excess energy is redistributed into the 'lattice' by relaxation processes. The π pulse has the effect of inverting the initial magnetization, so that if a series of spectra are acquired for increasing values of t_1, the intensity of each line is also seen to relax with an individual time constant T_1; it is at first inverted, then passes through a null, and finally reassumes its thermal equilibrium value (Figure 1.3). The time course of each resonance can be analysed to extract the individual spin-lattice relaxation time.

The two-dimensional correlation experiment of Figure 1.2(c) operates in a not dissimilar fashion. It differs only in the substitution of a $\pi/2$ pulse for the initial π pulse, but this small change has far-reaching consequences. The magnetization excited by the first pulse is now transverse rather than longitudinal. Being perpendicular to the static field, it immediately embarks on a precessional motion, as illustrated. Detection and transformation of this oscillation would simply give a conventional spectrum, but instead it is allowed to evolve for a period t_1, which ends with a second $\pi/2$ pulse. Now it is not wished to delve too deeply into the subtle effects associated with this second pulse. A full description requires a deep quantum mechanical analysis (39), and similar problems will be faced in Chapter 3. Here it is sufficient to indicate that the most important property for the purposes of this section is that the pulse 'mixes together' the magnetizations of all the transitions of a set of coupled spins. Thus if spin A is coupled to spin B, some of the magnetization elements which during t_1 were precessing at a frequency characteristic of spin A

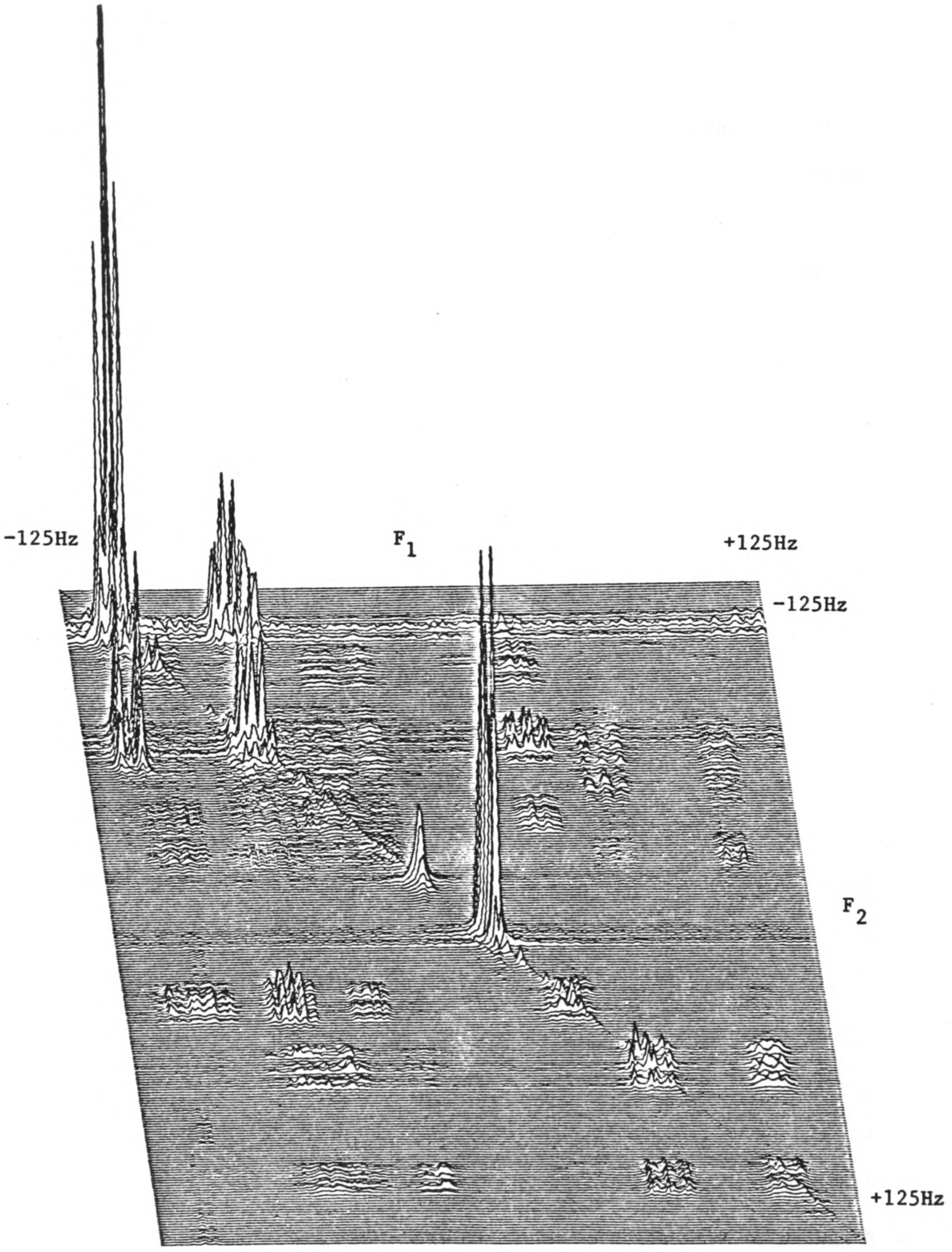

Fig.1.4. A typical two-dimensional spectrum - the proton Jeener spectrum of 2-ethylpiperidine, obtained on the XL-200 spectrometer. A slight modification of the simple pulse sequence of Fig.1.2(c) was employed in order to discriminate negative and positive F_1 frequencies (see reference 160). Peaks which lie on the obvious diagonal are due to components which precessed at the same frequency during t_1 and t_2, and hence did not experience coherence transfer. The off-diagonal peaks represent components which did experience coherence transfer and give a particularly direct display of the connectivity of the proton transitions.

suddenly find themselves precessing at a spin B frequency during the detection period t_2 - and vice versa. This phenomenon is known in general as 'coherence transfer'.

The key point is that those magnetization components which are now spin B, but used to be spin A, 'remember' their past history. The historical information is stored in the amplitude of the transferred components of magnetization, for as t_1 is increased, a part of the spin B signals is modulated at the frequency of the A spins, so revealing its immigrant status, as it were. In fact the modulation pattern of each resonance is a weighted sum of all the frequencies of the connected resonances. This complicated modulation pattern can be analysed by a second Fourier transformation. The result is a two-dimensional spectrum such as that of Figure 1.4. Peaks on the diagonal have the same frequencies in both t_1 and t_2 periods, and so arise from magnetization components not transferred by the second $\pi/2$ pulse. But the off-diagonal peaks are produced by coherence transfer and provide a direct map of the connectivity of the proton resonances. This was in fact the first double-Fourier transform experiment ever suggested and is due to Jeener (40).

To summarise again the experimental procedure: First there is a preparation period in which reproducible equilibrium or steady-state populations are established. Then precessing transverse magnetization is excited and detected by some pulse sequence just as in one-dimensional Fourier transform spectroscopy. But in the two-dimensional experiment the exciting pulse sequence is not fixed but is varied by steadily increasing one or more of the component

intervals t_1 in regular increments. The computer is programmed to store the time-averaged free-induction decays for each value of t_1 in separate storage locations, so that eventually it accumulates a large data matrix $S(t_1,t_2)$. Double Fourier transformation of the matrix yields the two dimensional spectrum, $S(F_1,F_2)$. This is plotted out, as a sequence of traces stacked so as to give an illusion of three-dimensionality as in Figure 1.4, or, in certain applications, as a contour plot.

The two-dimensional spectrum is characterised by its 'projections' onto the two Cartesian axes (41). These are the results of coadding all cross-sections which run parallel to the axis of projection. The projections define the nature of the evolutions during the t_1 and t_2 periods. Since during the t_2 period, ordinary precessing transverse magnetization is observed, the projection onto the F_2 axis always corresponds to a conventional spectrum. (The F_2 axis is consistently depicted in this thesis as 'going into the paper'). But the properties during t_1 are much more amenable to manipulation and much of the interest of two-dimensional spectroscopy lies in the unusual evolutions which can be devised for this period. In the Jeener spectrum described above, t_1 consists of uninterrupted free precession of transverse magnetization, just as does the t_2 period, so that the projections onto the two axes are identical, the utility of the two-dimensional spectrum residing solely in connectivity information. However a class of two-dimensional experiments may be devised in which the two periods are not equivalent, so as to allow correlation of evolution frequencies under two <u>different</u> effective Hamiltonians. An example

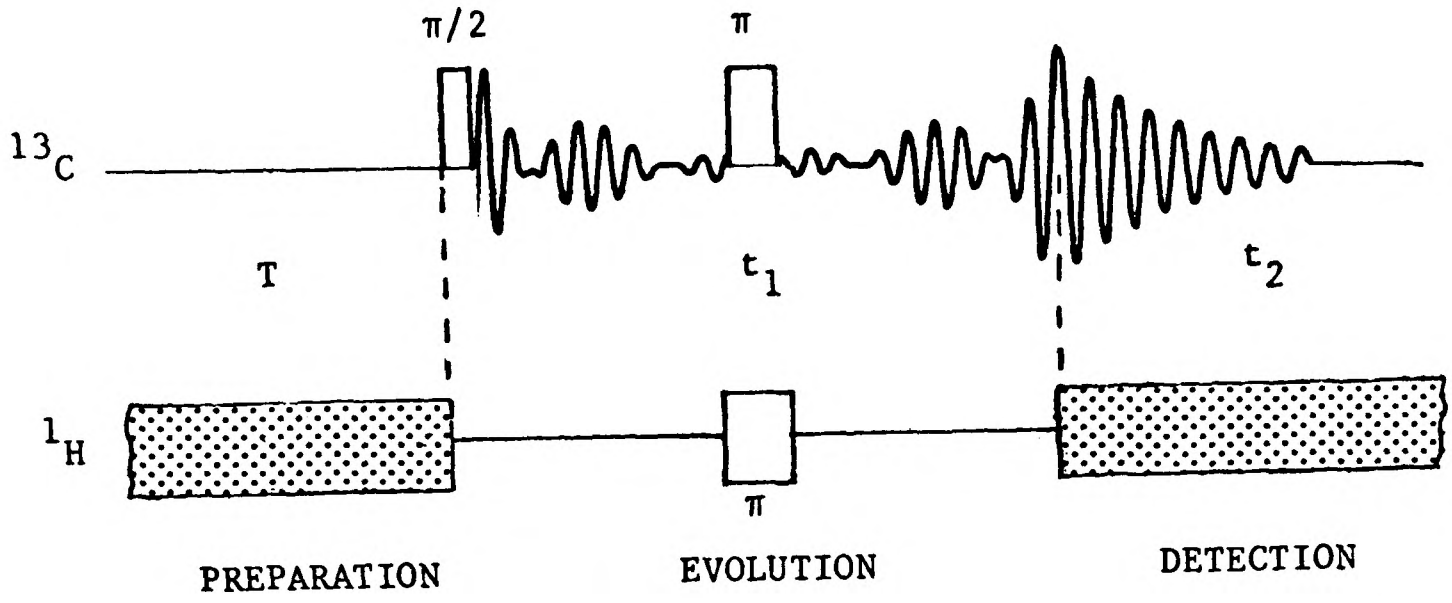

Fig.1.5. Pulse sequence used to generate a heteronuclear two-dimensional J-spectrum.

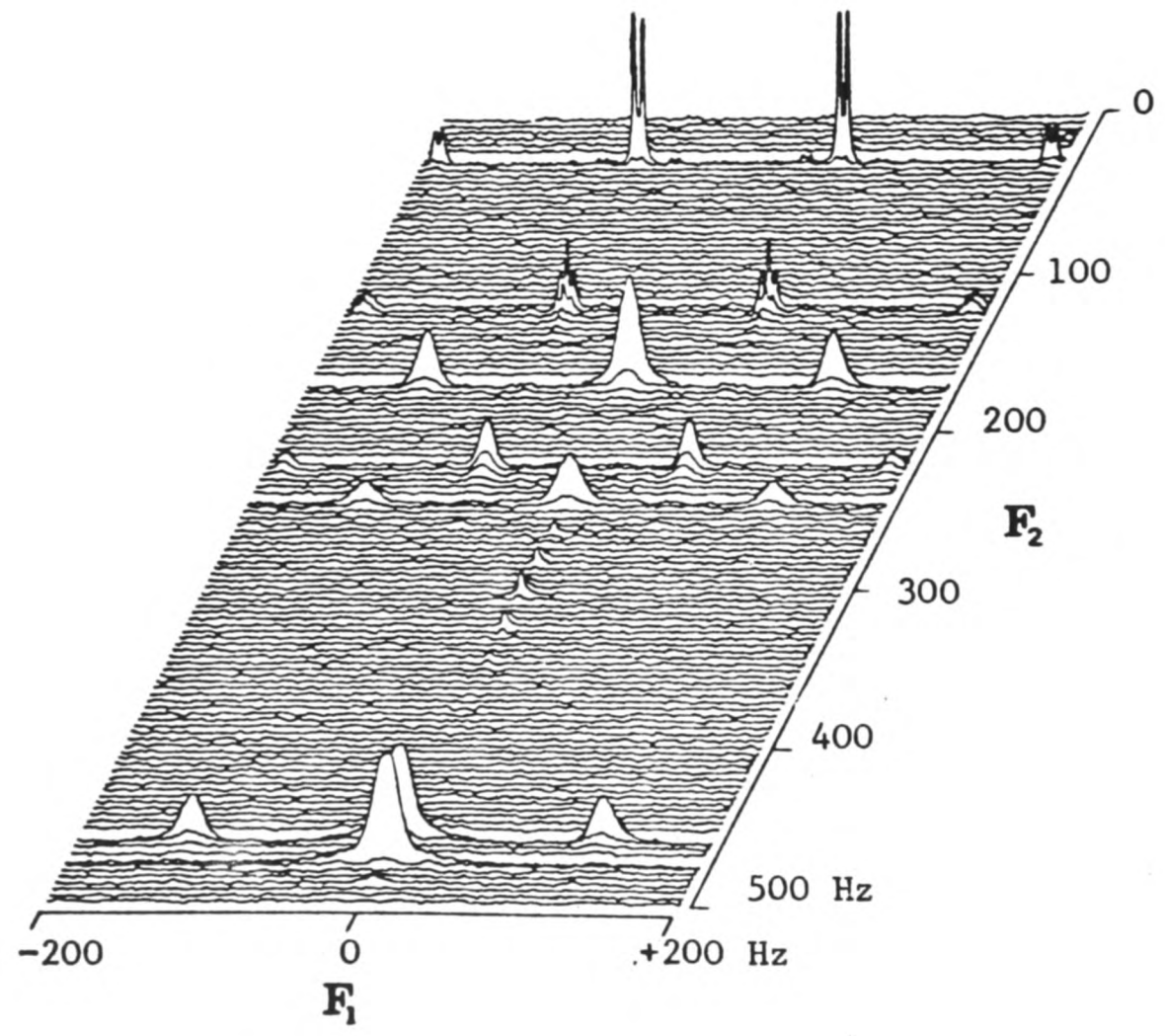

Fig.1.6. The proton coupled carbon-13 two-dimensional J-spectrum of 2(1-methylcyclohexyl)-4,6-dimethylphenol, obtained on the CFT-20 spectrometer. Five lines from the lock material (acetone-d^6) may also be seen. Note the clear separation of proton-decoupled chemical shifts (in the F_2 dimension) from direct proton-carbon couplings (in the F_1 dimension). Some long-range carbon-proton coupling structure may also be discerned on two of the multiplets.

is provided by 'two-dimensional heteronuclear J-spectroscopy', which assists the assignment of carbon-13 spectra by allowing study of proton-carbon couplings while avoiding the resolution difficulties normally associated with the proton-coupled spectra (42-48). By using a two-dimensional separation of proton coupling structure and chemical shifts, the impasse described at the beginning of this section can be avoided.

One of the pulse sequences which can be used is shown in Figure 1.5. As can be seen this sequence requires synchronised manipulation of both the carbon-13 and the proton spin systems. This facility is routinely available on modern spectrometers. The pulse sequence begins with long period of noise irradiation of the proton spin system in order to establish Overhauser-enhanced steady-state carbon-13 populations (33), and ends with the acquisition of a proton-decoupled carbon-13 free induction decay during the period t_2. But between these a period t_1 is inserted during which the proton irradiation is interrupted, so that evolution occurs under proton-coupled conditions. No signal is observed during t_1, but the effect of the proton-coupled evolution is carried through as a modulation of the decoupled carbon-13 free induction decays detected during t_2. It is not wished to enter into too much detail over the precise operation of the pulse sequence as this will be done in Chapter 2. In summary the evolution during t_1 is designed to include only heteronuclear couplings, the effect of chemical shifts being eliminated. This is done by forming a carbon-13 spin echo by applying a π pulse in the centre of the evolution period. This reverses the sign of the effective precession frequency during the first half of t_1 so that it

cancels out exactly at the end of t_1. This refocussing effect is inhibited for the heteronuclear couplings by applying a π pulse to the proton system at the same time as the carbon-13 refocussing pulse - the so-called 'proton flip' method (47). The result is that evolution during t_1 occurs under an 'average Hamiltonian' which contains only terms associated with carbon-proton coupling. Accordingly the projection of the two-dimensional spectrum onto the F_1 axis is a 'J-spectrum' (49,50), containing only heteronuclear coupling frequencies and no chemical shifts. The latter information is contained in the projection onto the F_2 axis, which is a proton-decoupled carbon-13 spectrum, so that the full two-dimensional spectrum contains all the information of the conventional proton-coupled spectrum but with a neat separation of shifts and couplings. The advantages of this can be verified by comparing the two-dimensional J-spectrum of Figure 1.6 with the one-dimensional coupled spectrum of Figure 1.1(a). In principle both contain the same information, but in the two-dimensional version, this has been separated out, rather like the opening of a Venetian blind.

Now both of these examples produce spectra of a form reasonably familiar from older and more conventional experiments; in one case a connectivity map of a homonuclear coupled spectrum (such as can be obtained less directly from double-resonance techniques such as INDOR (35)), and in the second case, a proton-coupled carbon-13 spectrum, albeit presented in a rather unfamiliar fashion, with the coupling structure rotated into a second dimension. However two-dimensional spectroscopy is not subject to the same restrictions as conventional methods as to the range of

transitions which can be observed. In conventional Fourier transform spectroscopy, it is precessing transverse magnetization which is detected, and usually that of one specific isotope only, because the bandwidth of the receiver electronics must be severely restricted on sensitivity grounds. Thus precessing proton magnetizations do not induce detectable signals in a probe tuned for carbon-13, and their frequencies are inaccessible to the standard Fourier transform experiment, although they can be deduced in an indirect and unsatisfactory fashion from double-resonance studies (51,52). Another quite different restriction is evident from the quantum-mechanical description of the properties of coupled spin systems, or of systems containing spins with $I > \frac{1}{2}$. Quantum mechanics predicts the existence of another class of coherent oscillations, also incapable of inducing direct signals, but this time because they do not contribute at all to system magnetization. These arise from 'forbidden' transitions with $\Delta M \neq \pm 1$, ΔM being the change in total magnetic quantum number across the transition. These 'multiple-quantum coherences' may be thought of as 'magnetic vibrations' of whole groups of coupled nuclei, rather than the isolated resonance of a single nucleus in the local field produced by its neighbours. They were observed at an early stage in continuous-wave studies using high irradiation fields (53,54), but are completely inaccessible to conventional Fourier transform NMR. This is unfortunate because multiple-quantum coherences may have many advantages over conventional dipolar magnetizations.

This can be emphasized by considering a system of N coupled, non-equivalent spin-$\frac{1}{2}$ nuclei. The 'order' of a given multiple-quantum coherence is the value of ΔM across the transition; thus conventional transverse magnetization is associated with coherences of order $\Omega = 1$. It can be shown that in a system of N coupled non-equivalent spins, there may exist the whole range of coherences of order 0 to N. Each order Ω is represented by $n(\Omega)$ transitions, where

$$n(\Omega) = (N-|\Omega-1|)2^{(N-1-|\Omega-1|)} \qquad 1.1$$

This means that in a complicated system of many coupled spins, there are far fewer high-order multiple-quantum transitions than single-quantum. If it were possible to observe multiple-quantum coherences and separate out specific high orders, much spectral simplification would ensue. Secondly, multiple-quantum precession frequencies can provide information on the connectivity of the single-quantum spectrum, an alternative to Jeener spectroscopy (53-56). Thirdly, some forms of multiple-quantum coherence have very special properties indeed. Homonuclear zero-quantum coherence is insensitive to small variations in magnetic field and thus persists in inhomogeneous or variable fields whilst other coherences are rapidly destroyed (55). Fourthly, the relaxation rates of multiple-quantum coherences can provide information on molecular motions which is complementary to that obtained from conventional relaxation measurements (57-59).

Fortunately the instrumental or theoretical restrictions on

the observation of hidden coherences are lifted in two-dimensional spectroscopy because the observation process is indirect. All that is required is that the coherence, having evolved in the t_1 period, is transferred into observable single-quantum magnetization by some sequence of pulses. The decays during the t_2 period then contain a component modulated at the frequency of the hidden coherences so that they appear in the F_1 dimension of the two-dimensional spectrum (55,56). This leads to another class of two-dimensional spectroscopies in which the peaks are spread out in the F_1 dimension according to frequencies which are normally inaccessible. Apart from multiple-quantum NMR, this class includes indirect detection of proton precession frequencies (60-65), proton relaxation times (66), and proton-proton couplings (67), all observed indirectly through their effect on the carbon-13 spectra. The advantage of such a complicated mode of operation is apparent for large molecules in which individual decoupled carbon-13 resonances are resolvable whilst the proton spectrum is not. The correlation of proton and carbon chemical shifts is a particularly useful experiment (63,64). Here a two-dimensional spectrum can be produced whose peaks characterize individual CH, CH_2 or CH_3 groups. Each of these moeities gives rise to a single peak in the two-dimensional spectrum located in F_2 at the carbon-13 chemical shift, and in F_1 at the resonance frequency of the directly-bonded protons. This informative experiment has also been applied to other pairs of nuclei, such as ^{1}H-^{11}B (68). But it is fair to say that the possibilities opened up by indirect detection have so far remained largely unexploited.

It is not possible to give a more comprehensive review of two-dimensional spectroscopy here. For a fairly complete account of two-dimensional methods in high-resolution liquid-state NMR the reader is referred to the article by Morris and Freeman (69). This of course does not touch upon the increasing number of difficult and highly sophisticated experiments which have been performed in the solid-state (70-77).

The two-dimensional experiment is not free from technical difficulties and the author has been involved to some extent in seeking a solution to these problems. As this work is now seen to be of rather peripheral importance it is presented here only in outline.

The first problem concerns the presentation of the two-dimensional data. A complex and versatile program was written in machine code to allow operator-interactive display of any small section of the data matrix. This program also facilitates the troublesome phase-correction of the two-dimensional data (78). As this program consists of about 5000 lines of machine code its development represented a considerable investment of time and effort.

The second problem is concerned with two-dimensional lineshapes. The 'natural' lineshape of a two-dimensional resonance turns out to be a complicated mixture of absorption and dispersion-mode Lorentzians, widely known as the 'phase twist' (45). If a series of sections through the line are taken parallel to one of the frequency axes, they appear as dispersion-mode Lorentzians far from the line centre but rapidly switch to absorption mode,

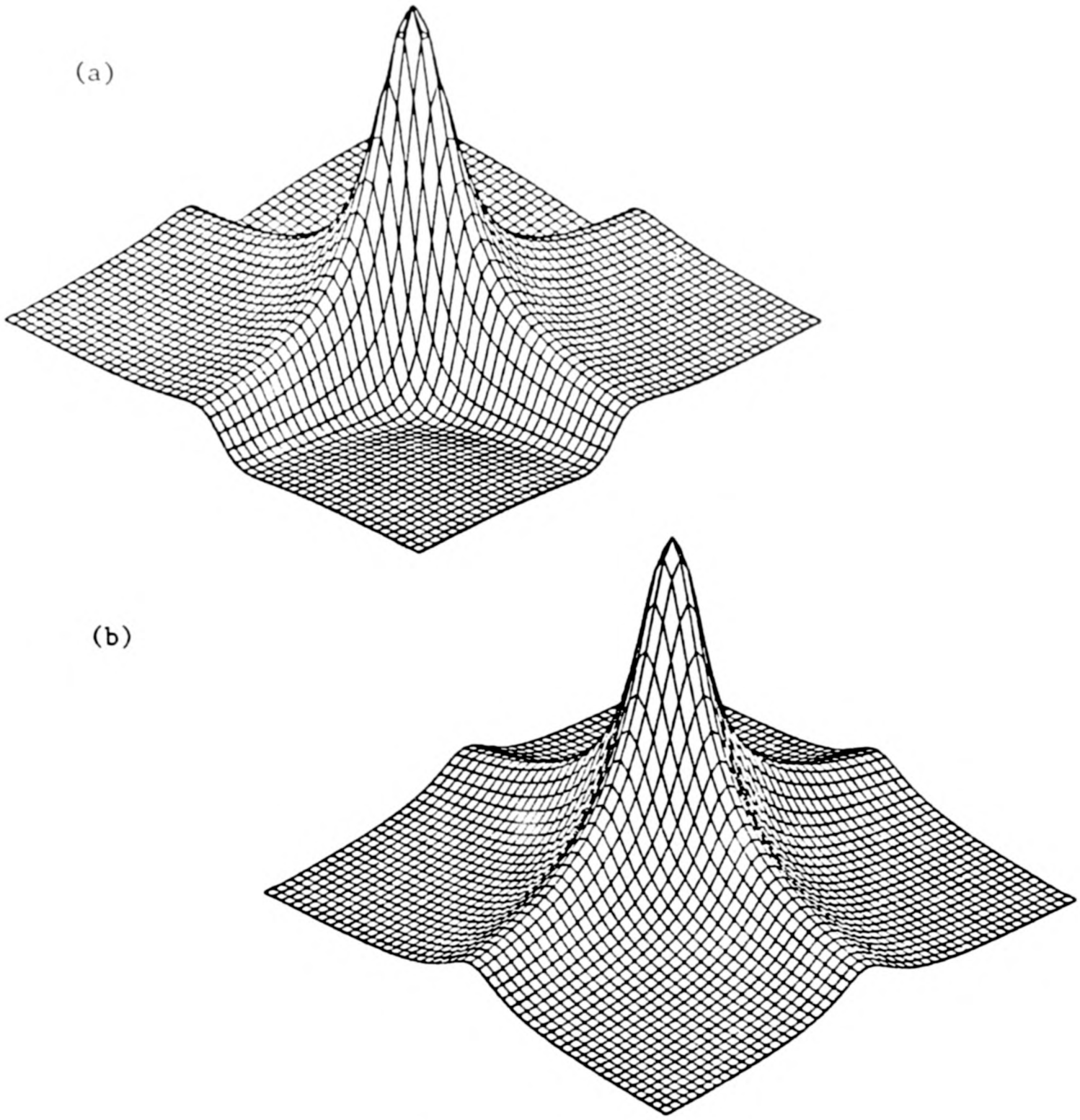

Fig.1.7. Computer simulated two-dimensional lineshapes. (a) The phase twist' lineshape which is the normal result of double Fourier transformation. (b) The 'absolute value lineshape, usually employed to counteract the problems associated with (a). (c) The double-absorption mode Lorentzian lineshape, which is generated by some forms of two-dimensional spectroscopy.

on-resonance . (See Figure 1.7a). This characteristic is most inconvenient in applications where interference between neighbouring lines can lead to misleading results, or where skew projections of the data matrix are desired (41). The usual solution is then to display the absolute value of the data, which is shown in Figure 1.7b. Unfortunately the absolute-value mode introduces its own problems of loss of resolution, of interference between neighbouring lines, and suppression of the relative sign of peaks. Particularly when a skew projection is required, the loss of resolution can be disastrous. However, in certain cases, it was found that the dispersion-mode contributions to the phase-twist line can be eliminated by combining two sets of two-dimensional data, which differ only in the sign of the effective precession frequency in the t_1 period (79). The result is the double-absorption mode lineshape of Figure 1.7c, which proves to be the optimum shape for almost all applications. But it must be said that the solution found was not particularly general and may now be seen to have been superseded by more recent developments (80,81).

A third problem is associated with the optimisation of the data storage requirements of the two-dimensional experiment. In many applications the bulk of the data matrix is redundant. For instance, the majority of traces in many two-dimensional spectra consist only of noise. Furthermore, in some experiments only the broadest features of the F_1 cross-sections are of interest. An example is in two-dimensional heteronuclear J-spectroscopy, in which the proton-coupled carbon-13 multiplets are displayed in the F_1 dimension, but it is usually only the multiplicities which are of importance, the magnitudes of the splittings ofen being

similar and uninformative. In such a case the acquisition of the full data matrix, followed by double Fourier transformation, may be seen to represent an excessive waste of computer time and space. All that is required from such an experiment is a separation of the lines in the decoupled carbon-13 spectrum into those originating from quaternary carbon, CH, CH_2 and CH_3 groups by a simple appraisal of the proton-coupled multiplicities. A means was found to fulfil this simple requirement without requiring appreciably more data storage space than a conventional one-dimensional experiment (82). The proton couplings are made to modulate the decoupled spectra in a series of experiments just as in heteronuclear J - spectroscopy described above. But the modulations are not analysed by a second Fourier transformation but simply by comparison with a small number of time-domain 'masks' prepared beforehand by the experimenter. In some cases the sensitivity of this method exceeds that of the full two-dimensional experiment and approaches that of the conventional decoupled spectrum.

But more pressing problems in two-dimensional spectroscopy are really associated with the nature of the preparation and evolution periods, and how these should be designed to have a specific effect. Both periods are usually composed of a sequence of strong pulses separated by intervals of free precession, and it is necessary to understand the influence of such pulses in coupled spin systems. Now there are many effects such as coherence transfer, and multiple-quantum coherence, which are very important in these experiments and yet are not comprehensible on the basis of the familiar model of precessing magnetizations due to Bloch (3).

Accordingly quantum-mechanical treatments such as that of the density matrix (83) are favoured. But although accurate, the density matrix furnishes little insight into the processes under way, and the transparency of a vector model such as Bloch's is greatly missed.

A related problem is provided by pulse imperfections in two-dimensional experiments. In conventional experiments the effect of imperfections in the pulses is usually simply to influence the intensities and phases of the spectral lines. Apart from in some relaxation experiments, such effects are easily allowed for. But imperfections have a more complicated influence if they concern the pulses which compose the evolution period in a two-dimensional experiment. New lines may appear in the two-dimensional spectrum, which can lead to erroneous interpretations if not understood, or (better) eliminated. Although these artefacts can sometimes be removed by exploiting their different phase properties to the desirable signals (84), there is a class of imperfections which do not respond in this way (85,86). Then the suppression of artefacts requires either ensuring completely perfect, correctly set pulses, or some way of internally compensating each pulse in the sequence. A means to do this is described in Chapter 4.

1.4 Spin-lattice relaxation time measurements

The close relationship between two-dimensional spectroscopy and methods of measuring spin-lattice relaxation times, such as the inversion-recovery method, has already been pointed out. Both experiments start with a preparation period in which some non-equilibrium initial condition is set up, usually by perturbing a

system either in thermal equilibrium or in some reproducible steady state. By definition the non-equilibrium state evolves in some way during the following variable period t_1. In both experiments this evolution is followed by generating precessing transverse magnetization at the end of t_1 and detecting it during a further interval t_2. This set of transients, on Fourier transformation, gives a series of spectra modulated in some way by the processes going on during the evolution period t_1. The two experiments really differ only in the form of the modulation and the analysis technique which this dictates. In two-dimensional spectroscopy the typical evolution during t_1 is the oscillation of some coherence, so that the signals are modulated in a sinusoidal fashion. These oscillations are best analysed by a second Fourier transformation, to produce the two-dimensional spectrum, with peaks in the F_1 dimension corresponding to the modulation frequencies during t_1.

The inversion-recovery method for measurement of spin-lattice relaxation times differs in that the perturbed state does not contain oscillating coherences but simply inverted energy level populations (see Figure 1.2(b)). Thus the evolution during t_1 is not oscillatory but is a simple relaxation of the individual components of longitudinal magnetization back to their respective equilibrium values. Mathematically:

$$[M_z(t_1) - M_o] = [M_z(0) - M_o]\, e^{-t/T_1} \qquad 1.2$$

M_o is the equilibrium magnetization, and $M_z(t_1)$ the partially relaxed magnetization after an interval t_1. A single exponential form of relaxation has been assumed. $M_z(0)$ is the inverted

magnetization immediately after the preparatory π pulse; ideally this would be $(-M_o)$ but imperfections may cause deviations from that value. The appropriate analysis technique for the time-course of equation 1.3 is not to perform a second Fourier transformation but to plot $\ln[M_o-M_z(t_1)]$ against t_1. The slopes of the semi-log plots give the individual T_1 values. Although providing an accurate value of T_1 insensitive to most instrumental imperfections, this method is not completely satisfactory. Reliable results require a sufficiently long waiting period T between experiments - but this condition is not only incompatible with optimisation of the sensitivity of the experiment but also implies prior knowledge of the range of T_1 values to be encountered, so that an acceptably short period T can be arranged. Furthermore, it is essential to make numerous measurements of M_o, preferably at intervals during the course of the experiment, to counteract the errors due to possible instrumental drift (87). This inefficient use of experimental time can be completely prohibitive when examining unstable species or biological systems. Accordingly alternatives have been devised which reduce the overall experimental time. The 'null-point' method uses the property that, assuming exponential relaxation from a fully inverted equilibrium magnetization, the value of t_1 at which the relaxing longitudinal magnetization passes through zero is alone sufficient to define the relaxation time constant. Thus in principle, just one measurement is necessary, in practice the null being located by interpolation between two or more measurements as close as possible on either side of it. Allowance can be made for non-linear relaxation over this short time period.

If t_{1N} is the measured null-point delay,

$$T_1 = t_{1N}/\ln 2 \qquad 1.3$$

The null-point method has the operational disadvantage that a good estimate of T_1 is necessary in order to know 'where to look' for the null in the range of t_1-values. This is often not a serious problem when for example, it is wished to follow the small changes in T_1 of a single resonance with temperature. A more serious defect is that a perfect inversion of equilibrium population is necessary - only then is $M_z(0)$ equal to $-M_o$. Unfortunately the π pulses used for the initial population inversion are particularly susceptible to instrumental defects such as irradiation fields of imperfect homogeneity, errors due to the finite offset frequency from resonance, or inaccurate or irreproducible pulse lengths. Accordingly the simple inversion-recovery null-point method is a very poor technique in most spectrometers. However its use may be resurrected by the use of pulse sequences which to a large extent are capable of compensating these effects (89). This possibility will be discussed in detail in Chapter 4.

Other means of improving the operational efficiency of the inversion-recovery method rely on relaxing the stringent initial condition of full thermal equilibrium. Two common alternative methods use saturation as the initial condition, rather than thermal equilibrium. Transverse magnetization can easily be destroyed by applying a magnetic field gradient, allowing all longitudinal magnetization to be also set to zero by the application of a $\pi/2$ pulse. Thus this initial condition is much more easily satisfied than

that of full thermal equilibrium, so that experiments can be repeated much more quickly with a useful enhancement of the overall sensitivity. This is known as 'saturation-recovery' (90).

Further suggestions dispense altogether with the waiting period between experiments. In the 'progressive-saturation' method (91) a steady-state is set up by applying an unbroken train of $\pi/2$ pulses, separated by intervals comparable to T_1. The signals generated by each of these pulses are detected and coadded to produce a spectrum with a particularly high signal-to-noise ratio per unit time. The signal strengths decrease if the pulses are brought closer together and under certain conditions the rate of this decrease is simply related to T_1.

In a second method, called 'fast inversion-recovery' (92), a train of inversion-recovery sequences, $(\pi - t_1 - \pi/2 - t_2)$, are applied in quick succession, again with no attempt to allow thermal equilibration between them. Surprisingly enough it can be shown that the series of spectra obtained behave in the same general way as when the full interval is left between experiments. Spin-lattice relaxation times can be extracted from semilog plots in the usual fashion.

However all of these more sophisticated methods suffer to a greater or lesser degree from sensitivity to pulse imperfections. This is particularly so in the 'fast' methods, which essentially consist of one long pulse sequence, so that pulse errors can accumulate and cause gross distortions. Although it is sometimes possible to compensate for the distortions by complex data manipulations (93), the 'fast' techniques are generally thought

to be unreliable and are not much used. Once more the error compensation schemes to be described in Chapter 4 may redress this situation.

1.5 Spin-spin relaxation time measurements

Spin-spin relaxation is the process by which transverse magnetization irreversibly decays due to the incoherence introduced by interactions with neighbouring magnetic species. As was noted above, spin-spin relaxation is sometimes more informative than spin-lattice relaxation. For example, T_2 is sensitive to the presence of chemical exchange over much shorter time-scales than T_1. At worst spin-spin relaxation is a complementary source of information. However, the experimental determination of T_2's is notoriously difficult. This is because it is not easy to exclude any instrumental effects which may also introduce incoherence.

The most important of such factors is the spatial inhomogeneity of the static magnetic field. This causes relative dephasing and destructive interference between precessing magnetization vectors in different regions of the sample. To combat this it is necessary to construct an evolution period for the transverse magnetization in which the dephasing effect of the inhomogenous magnetic field is effectively suppressed. This is done by placing a π pulse in the centre of t_1 (Carr-Purcell method 'A' (94)), so that the sequence becomes:

$$T - \frac{\pi}{2} - \tfrac{1}{2}t_1 - \pi - \tfrac{1}{2}t_1 - \text{acquisition} \qquad 1.4$$

The π pulse 'refocusses' the precession of the vectors during the first half of t_1 so that they form an 'echo' at the end of the evolution period as phase coherence is restored. Fourier transformation of a series of decaying half-echoes created with increasing evolution periods t_1 gives a set of spectra in which the intensity of each resonance decays with its individual spin-spin relaxation time constant. The formation of the echo is not perfect if there are any factors which cause a variation in the precession frequencies of the individual magnetization 'isochromats' over the evolution period. Thus the sample should be kept stationary rather than spinning it as is usually done to improve resolution. But even in a stationary sample it is impossible to avoid microscopic physical diffusion of the spins into regions of different magnetic field. This has been shown to cause a premature decay in echo amplitudes for long evolution times (94). The effect of this can be much reduced if the single π pulse is replaced by a whole train of n refocussing pulses operating over the same total time (Carr-Purcell method 'B' (94)). This strongly restricts the phase dispersion of the isochromats so that spin diffusion exerts a much reduced influence. A further important modification to this experiment was introduced by Meilboom and Gill (95). They introduced a radio-frequency phase shift of $\pi/2$ radians between the pulses of the preparation and evolution periods, to give

$$T - (\pi/2)_x - (\tau-\pi_y-\tau)^n - \text{acquisition} \qquad 1.5$$

where $t_1 = 2n\tau$. The phase shift is indicated by the subscripts x and y.

This modification is necessary to combat the effects of cumulative pulse imperfections, which otherwise can be yet another source of premature decay. It can be shown (see Chapter 4) that when the phase-shift is present, pulse imperfections do not have a cumulative effect but cancel to first order on the even-numbered echoes in the sequence. In this respect the Meiboom-Gill modification may be considered to anticipate the development of composite pulses described in a later chapter.

Despite these ingenious experiments, T_2 measurements were still considered difficult. This may be attributed to the fact that the considerations above really only apply to spins with no scalar coupling interactions with their neighbours. This is a rare occurrence in NMR. Signals from rare isotopes in natural abundance, such as carbon-13, approach this situation quite closely providing they are fully decoupled from proton neighbours. However it is difficult to ensure complete decoupling of all protons. Noise-modulated proton irradiation, which would normally be used for this purpose, is inadvisable in this context since it itself may introduce incoherent effects associated with magnetization transfer processes (96,97). However even more serious problems arise if T_2 measurements are conducted under coupled conditions. Firstly if there is <u>strong</u> coupling present anywhere in the spin system, the π pulses do not have a simple effect and complicated modulations ensue (46,47,98). Fortunately the incidence of strong coupling has been much reduced by the introduction of high-field superconducting magnets. But even if there is only weak coupling, and it is between nuclei of the same isotopic species ('homonuclear coupling') the π

pulses cannot be prevented from affecting both the nucleus of interest and those coupled to it. The result is that the lines in the transformed half-echoes display a sinusoidal phase modulation superimposed on the exponential decay in amplitude. This may be removed by taking the absolute value of the Fourier transform spectra, which is insensitive to phase variations. A more serious problem is that under these coupled conditions, the pulse errors no longer cancel on even-numbered echoes. A messy modulation of the transformed half-echoes is observed as the pulse errors accumulate, from which it is impossible to deduce reliable relaxation time constants. Hence accurate T_2 measurements have made extreme demands on the spectrometer of good stability and perfect irradiation field homogeneity. However, it if were possible to compensate internally each refocussing pulse for its imperfections, these severe constraints would be alleviated. Once again this possibility is discussed in Chapter 4.

Finally, a different method for measuring transverse relaxation rates should be mentioned. In the 'spin-locking' technique, the relaxation of transverse magnetization is studied in the presence of a continuous radio-frequency field (99). Transverse magnetization is first created along the y-axis of the rotating frame by the usual pulse of $\pi/2$ radians about the x-axis. The phase of the radio-frequency irradiation field is then shifted by $\pi/2$ radians, just as in the Meiboom-Gill method. However instead of creating a train of spin echoes by applying a sequence of π pulses, the irradiation is left on continuously, representing an effective field vector also along the y-axis of the rotating frame. The relaxing components of transverse magnetization can be shown to be constrained to a position

of relative phase coherence parallel to this vector ('spin locking'). The rate of decay has been shown to be insensitive to both magnetic field inhomogeneities and pulse imperfections, although off-resonance effects can be a problem. Nevertheless the method does have some disadvantages. Firstly, the transverse relaxation time constant in the presence of the rotating-frame field is not the same as the unimpeded value, and is usually given the symbol $T_{1\rho}$. Some relaxation mechanisms which influence T_2 to not effect $T_{1\rho}$, for example the scalar relaxation mechanism (100), and also chemical exchange, which is on the other hand one of the major motivations for the study of T_2. Thirdly, the power input required to spin-lock wide spectra may be unacceptably high. If thermal damage to the sample or probe is to be avoided, one is restricted to the study of only small sections of the spectrum at a time.

CHAPTER TWO

BASIC THEORY

CHAPTER 2

BASIC THEORY

2.1 The Bloch equations

In the complete absence of interactions between the magnetic species in a given ensemble, the interaction between the nuclear magnetization and static or oscillating magnetic fields may be described by the equations of classical electrodynamics. The magnetization of the nuclear spin system is represented as a vector $\underline{M}$ which experiences a torque when immersed in an applied magnetic field $\underline{B}$. The classical equation of motion is:

$$\dot{\underline{M}} = \gamma \underline{M} \Lambda \underline{B} \qquad 2.1$$

γ is the gyromagnetic ratio, a constant for each magnetic nuclear isotope, and determinesthe precession frequency of the nucleus in a given field. In practice $\underline{M}$ may need to be treated as a sum of several components $\underline{M}_i$ ('isochromats'), each of which experience slightly different local fields $\underline{B}_i$.

In the case where $\underline{B}$ is the sum of a large static field $\underline{B}_o$, applied along the z-axis of a reference frame, and an oscillating transverse radio-frequency field of amplitude $2B_1$, frequency ω and phase ϕ,

$$\underline{B} = 2B_1 \cos(\omega t+\phi)\underline{i} + B_o\underline{k} \qquad 2.2$$

This covers most situations commonly encountered. In this and in

following equations, $\underline{i}$, $\underline{j}$ and $\underline{k}$ represent unit vectors along the x, y and z-axes.

The classical method of solving the equation of motion, eqn 2.1, under the time-dependent field of eqn 2.2 is to make a transformation into a reference frame in which the oscillating field appears stationary. At high field strengths a good approximation is first to decompose the amplitude-modulated part of B_1 into two counter-rotating components. Viewed from a reference frame which rotates synchronously with one of the components, the other rotates too fast to have an appreciable overall effect and may safely be neglected (101). With these approximations $\underline{B}$ is represented as an effective field in the rotating frame:

$$\underline{B}^{eff} = B_1(\underline{i}\cos\phi + \underline{j}\sin\phi) + (B_o - \frac{\omega}{\gamma})\underline{k} \qquad 2.3$$

Since the quantum mechanical equivalent of the transformation from 2.2 to 2.3 will be dealt with shortly only the important features of the result will be pointed out. Firstly note that the effective field is now time-independent, so that equation 2.1 can now be readily solved. Secondly, the large static field B_o has been greatly reduced to a residual rotating frame value $B_o - \omega/\gamma$, and vanishes completely if the radiofrequency field is applied on resonance ($\omega = \gamma B_o$). Then the effective field lies exactly in the equatorial plane of the rotating frame so that it has the maximum effect on equilibrium magnetization components which lie parallel to the static magnetic field along the z-axis. However, if the irradiation is applied off-resonance, so that $\omega \neq \gamma B_o$, the effective field is

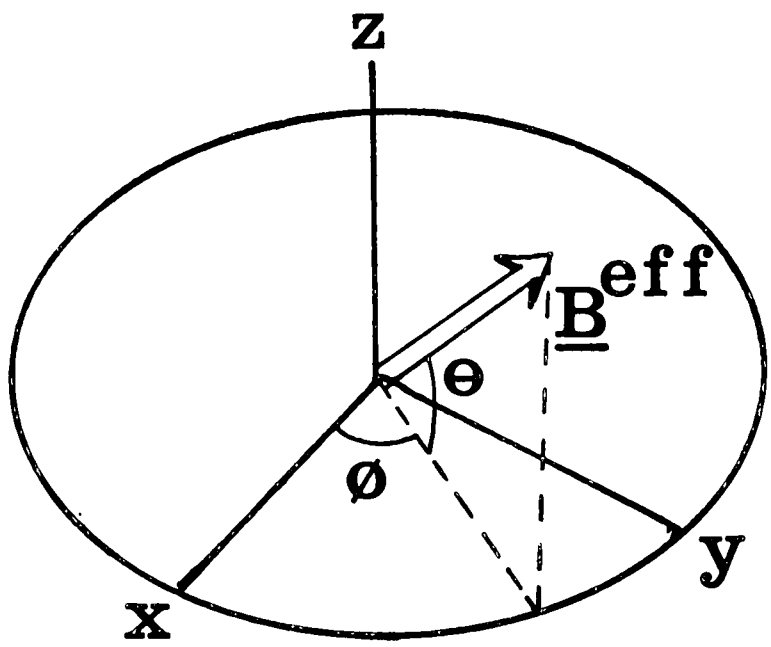

Fig.2.1. The effective field vector in the rotating reference frame.

tilted somewhat away from the transverse plane. Far off-resonance it lies almost along the z-axis, and has no appreciable influence on equilibrium magnetizations. This explains why it is necessary to apply radiofrequency irradiation close to the Larmor frequency γB_o in order to influence the spin magnetizations.

The magnitude and direction of the effective field of eqn.2.3 are conveniently expressed in terms of polar coordinates (see Figure 2.1). The field vector has a magnitude $|B^{eff}|$ given by:

$$|B^{eff}|^2 = B_1^2 + (\frac{\Delta\omega}{\gamma})^2 \qquad 2.4$$

where $\Delta\omega$ represents the offset of the irradiation frequency from the resonance condition:

$$\Delta\omega = \gamma B_o - \omega \qquad 2.5$$

The direction of the effective field is specified by the two angles θ and ϕ: ϕ indicates the relative phase of the radio-frequency irradiation field with respect to some invariant reference signal. In many applications it is desired to switch the phase of the effective field, so that it may operate along different axes in the equatorial plane of the rotating frame. This is usually done in steps of $\pi/2$ radians, so as to allow pulses along the x, y, -x or -y axes, although smaller phase jumps are feasible. The jumps are accomplished under computer control by switching of analogue or digital circuitry and have become a regular facility of most modern instruments.

The second angle θ represents the tilt of the effective field away from the equatorial plane of the rotating frame. It is related to the ratio of resonance offset to irradiation field strength:

$$\tan\theta = \frac{\Delta\omega}{\gamma B_1} \qquad 2.6$$

Effective field tilt is generally undesirable and can be minimised by using more powerful radio-frequency amplifiers and optimising the design of the probe. However technological developments in these areas have been matched by an increase in the static magnetic fields available, so that field tilt is likely to remain a problem for the forseeable future. For a typical carbon-13 spectrum of width 200 ppm, observed at 50 MHz with a radio-frequency field strength of $\gamma B_1/2\pi$ = 30 kHz, the tilt varies across the spectrum between $\pm$ 9^o.

If interactions between spins can be ignored, the solution of equation 2.1 becomes a simple problem in spherical geometry. The magnetization vectors nutate about the tilted effective field of Figure 2.1, at a rate of $\gamma|B^{eff}|$ radians per second. However this treatment is inadequate if there is spin-spin interaction as in coupled systems. Equation 2.1 also fails if there is finite relaxation, since this too involves internuclear interactions. However in this case the interactions are small and incoherent so that account can be taken of them in a reasonably adequate way by adding two extra terms to equation 2.1. This produces the Bloch equations, which can be summarised as:

$$\dot{\underline{M}} = \gamma \underline{M} \Lambda \underline{B} - \frac{1}{T_2}(M_x \underline{i} + M_y \underline{j}) - \frac{1}{T_2}(M_z - M_o)\underline{k} \qquad 2.7$$

The two extra terms account for the separate processes of spin-spin and spin-lattice relaxation. The first leads to a decay of transverse magnetization due to the small fluctuations in local magnetic fields produced by the presence of neighbouring spins. The second term allows energy exchange between nuclear magnetization and the rest of the universe, so that there is a tendency for the longitudinal component of magnetization M_z to relax towards its thermal equilibrium value M_o. Both these processes are assumed to be exponential.

Now in Fourier transform NMR the spin system is usually subjected to either of two extreme conditions. Either a very strong burst of radio-frequency irradiation is applied, or free evolution is allowed in the absence of perturbing fields. The motions of the magnetization in these two cases are both described by eqn. 2.7. For a pulse of duration much shorter than the two relaxation times, the extra terms in equation 2.7 can be ignored, so that the magnetization nutates about a tilted effective field as described before. If the field is applied on-resonance, or if the magnitude of B_1 is large enough to make off-resonance effects negligible ($\gamma B_1 >> \Delta\omega$) the tilt angle is zero and the effective field lies in the equatorial plane of the rotating frame. Equilibrium magnetization vectors, initially along the z-axis, nutate towards the xy plane, intersecting it at a time t given by

$$\gamma B_1 t = \pi/2 \qquad 2.8$$

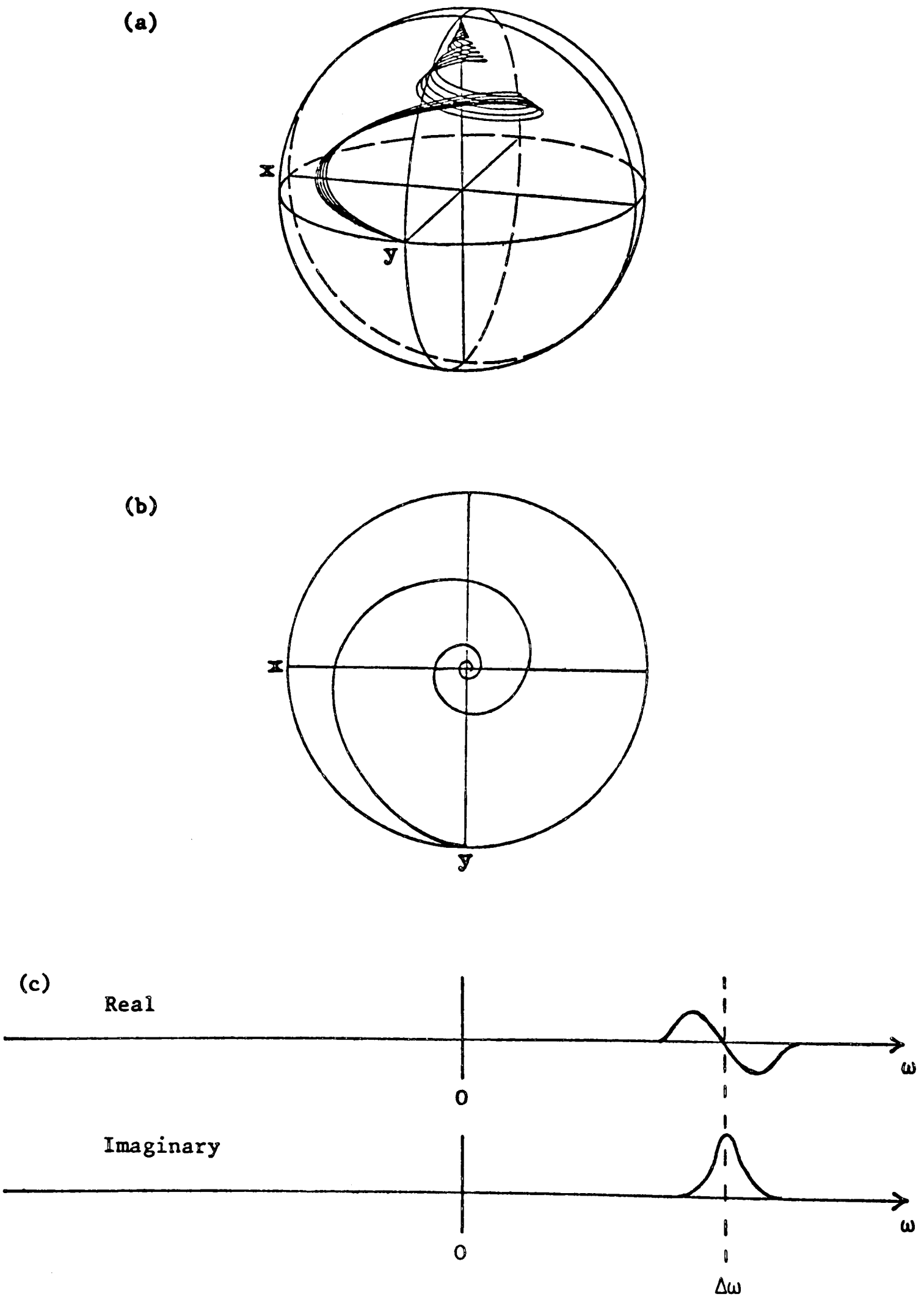

Fig.2.2. (a) The precessional motion of a family of magnetization vectors, viewed from a reference frame rotating slightly off-resonance.
(b) The evolution of the transverse components of one such magnetization vector.
(c) The result of Fourier transforming the signal corresponding to (b).

This is the familiar condition for a pulse of length $\pi/2$ radians, and results in the maximum possible conversion of longitudinal magnetization into transverse magnetization. If the pulse duration is doubled, the vectors are rotated by π radians, so that the longitudinal magnetization is inverted and no transverse magnetization is produced. Such an inversion pulse is used in the inversion-recovery method for the determination of spin-lattice relaxation times described in the previous chapter.

In the intervals between the pulses, evolution must be described by the full version of equation 2.7. The typical motion of magnetization vectors is then a spiral trajectory as precession occurs around the z-axis with simultaneous relaxation towards the north pole of the rotating frame. This is depicted in the computer simulation of Figure 2.2(a) which concerns the trajectories traced out by a family of vectors of slightly different precession frequencies, as viewed from a frame rotating at slightly off the resonance condition. They start out in the xy plane of the rotating frame and precess about the residual field, which is along the z-axis. At the same time relaxation occurs, and because the two relaxation times were made to be equal in this particular simulation, their spiral courses all lie on the surface of the sphere. It is not possible to observe directly the full evolution of Figure 2.2(a), but the development of just the transverse part of the magnetization can be detected as the free induction decay. This decaying transient is proportional to the sum of all transverse magnetization components in the sample, and displays the same spiral time-course as the projection of Figure 2.2(a) onto the

equatorial plane (Figure 2.2(b)). For only one resonance,

$$S(t) = iS(0)e^{-(i\Delta\omega+\lambda)t} \qquad 2.9$$

which is a complex number representation of the clockwise precession of Figure 2.2(b). (Note that it is possible to detect both the x and y components of the free induction decay by using two reference signals in quadrature phase (4).) Here λ indicates the rate of decay of macroscopic transverse magnetization, due to a combination of magnetic field inhomogeneity and true spin-spin relaxation effects.

The complex signal is subjected to Fourier transformation:

$$S(\omega) = \int_0^\infty S(t)e^{i\omega t}dt \qquad 2.10$$

$$= S(0)\int_0^\infty ie^{[i(\omega-\Delta\omega)-\lambda]t}dt \qquad 2.11$$

$$= -\frac{S(0)(\omega-\Delta\omega)}{[(\omega-\Delta\omega)^2+\lambda^2]} + \frac{i\lambda S(0)}{[(\omega-\Delta\omega)^2+\lambda^2]} \qquad 2.12$$

The real part of the result is a dispersion-mode Lorentzian line; the imaginary part is an absorption-mode Lorentzian of width at half height 2λ Hz. Both are centred about the angular frequency $\omega = \Delta\omega$, as illustrated in Figure 2.2(c). Thus Fourier transformation of the free induction decay from a single resonance gives a direct display of the offset of the precession frequency of the resonance from that of the reference signal. Since Fourier transformation is a linear operation, when there are many resonances, the spectrum is just the sum of the Lorentzian lines from each one, each positioned at its appropriate offset. Normally the imaginary part of the

Fourier transform is taken, since this should contain absorption-mode Lorentzian lines, but if there is a phase error it may be necessary to take a carefully adjusted linear combination of real and imaginary parts in order to generate the desired absorption-mode spectrum. Phase errors arise when the precessing components of transverse magnetization do not start off exactly along the y-axis at time t = 0, and this can occur if the effective field of the preparatory pulse is appreciably tilted, or if an interval must be left between the pulse and the start of data acquisition. In both cases the phase errors generated are approximately a linear function of frequency, and the spectra can easily be adjusted for absorption-mode by the use of an operator-interactive display.

2.2 Spin echoes

The desire to measure spin-spin relaxation times led to the very early development of a range of techniques which have since proved exceptionally useful. The natural decay of the transverse magnetization, which is responsible for the finite minimum linewidth of the lines in the NMR spectrum, is augmented by the inevitable spread in static magnetic fields throughout the sample volume. Each free induction decay is a superposition of signals from many isochromats which precess at slightly different frequencies, so that they lose phase coherence and destructively interfere. This effect makes it impossible to use the NMR linewidths as a direct measure of spin-spin relaxation times. The possibility that this effect might be reversible was realised by Hahn who added a second pulse after transverse magnetization had been created and allowed to precess for an arbitrary interval. An echo was

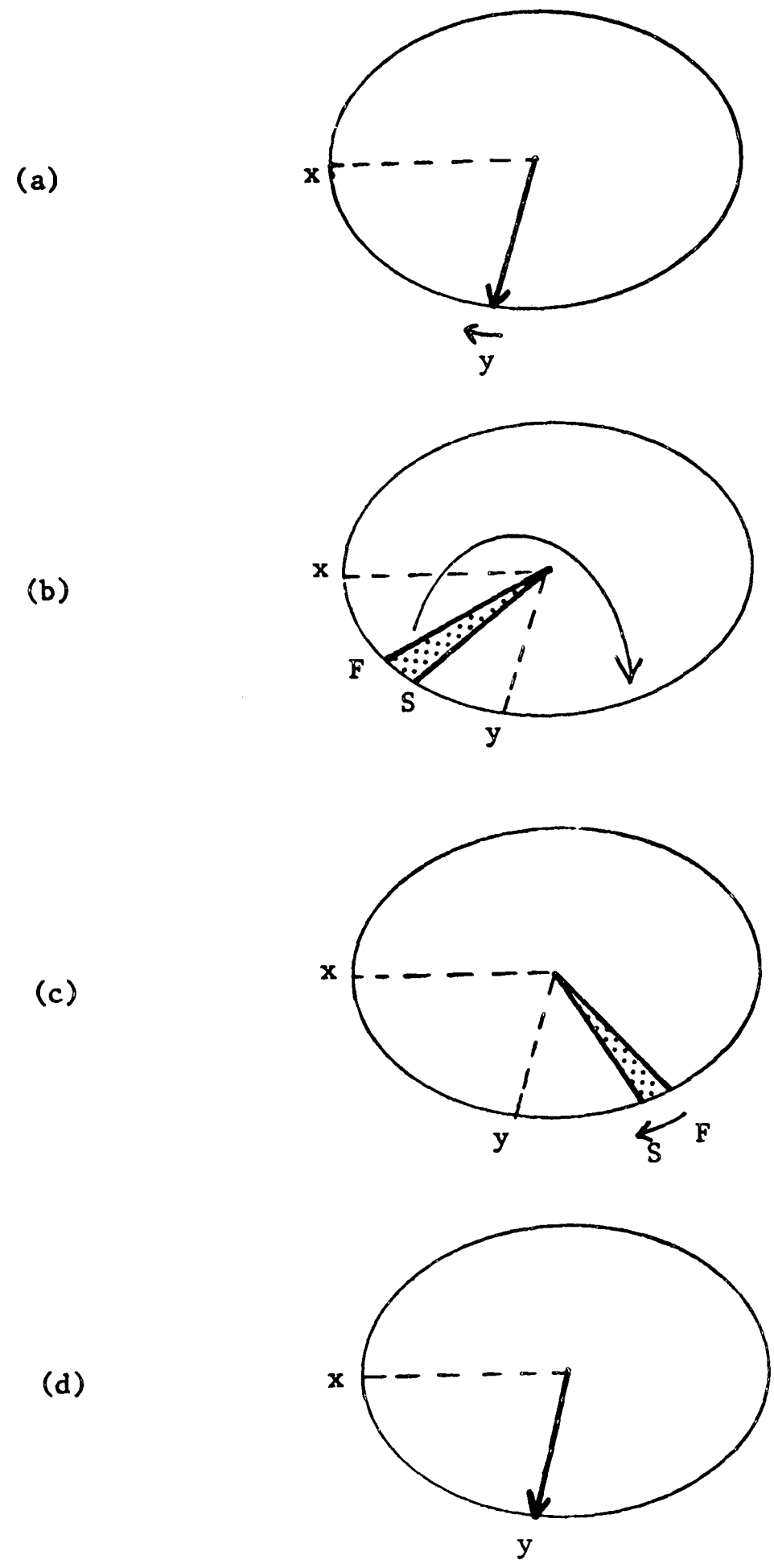

Fig.2.3. Formation of a spin echo.
(a) An initial $\pi/2$ pulse creates transverse magnetization along the y-axis.
(b) The components of transverse magnetization disperse due to different local B_o fields. Components which experience high local fields ('F') precess faster than those experiencing small fields ('S').
(c) A π pulse, applied about the y-axis, places the vectors in mirror-image positions with respect to the yz plane.
(d) The difference in relative precession frequencies now causes a 'refocussing' of all vectors onto the y-axis at time 2τ.

observed at an equal time after the second pulse, indicating that the reversal of the effects of magnet inhomogeneity had been successful (102). Much later, Carr and Purcell (94) and Meiboom and Gill (95) developed and improved Hahn's idea as described above in Chapter 1. In the most sophisticated versions of the experiment, a train of many hundreds of consecutive echoes is induced, in which the effects of both static and slow dynamic variations in magnetic field are much reduced.

The operation of the spin echo experiment is illustrated in Figure 2.3. Magnetization isochromats, starting out in relative phase coherence along the y-axis, progressively dephase as they precess at different rates. This is represented by the shaded area in Figure 2.3(b), in which the positions of those isochromats which precess at the highest and lowest rates are indicated by 'F' and 'S', (for fast and slow). After a time $\frac{1}{2}t_1$, a pulse of length π radians is applied about the y-axis of the rotating frame. This rotates the vectors into a mirror-image position with respect to the yz plane, such that on further precession at the same frequencies, they come back into phase coherence along the y-axis after a further time $\frac{1}{2}t_1$. The observed effect is that the signal, initially attenuated by destructive interference between the isochromats, is resurrected at time t_1 to an extent only dependent on true spin-spin relaxation during the formation of the echo. The experiment can be repeated for different values of the evolution time t_1. Fourier transformation of the decaying half-echoes (corresponding to the period after Figure 2.3(d)), produces a series of spectra in which the intensity of each resonance decays with respect to t_1 according to

its individual spin-spin relaxation time. If desired, the experiment can be made more insensitive to slow time-dependent changes in magnetic field (such as those produced by diffusion), by stimulating not one but a whole series of such echoes in the same total evolution time. The principle remains unchanged.

An interesting result is obtained if a Fourier transform is made of the whole echo, not just the decaying half (80). If the magnet homogeneity is bad enough that the decay of the signal due to the dephasing of the isochromats greatly exceeds that arising from spin-spin relaxation, the echo envelope is symmetrical about the centre of the echo. (If this condition is not satisfied naturally, it can be imposed by artificial weighting of the echo signal). Defining zero time as the centre of the echo, the signal observed from a single resonance may be expressed:

$$S(t) = iS(0)e^{(-i\Delta\omega-\lambda)t} \qquad \text{for } t > 0 \qquad 2.13$$

but

$$S(t) = iS(0)e^{(-i\Delta\omega+\lambda)t} \qquad \text{for } t < 0 \qquad 2.14$$

This symmetrical signal can be subjected to Fourier transformation. Now the transform which must be used is not quite the same as that applied to free induction decays, because in this case the signal exists for negative times. The full form of the Fourier transform must be used, with integration limits from $-\infty$ to $+\infty$:

$$S(\omega) = \int_{-\infty}^{\infty} S(t)e^{i\omega t}dt \qquad 2.15$$

$$= iS(0)\{\int_{o}^{\infty} e^{[i(\omega-\Delta\omega)-\lambda]t}dt + \int_{-\infty}^{o} e^{[-i(\omega-\Delta\omega)+\lambda]t}dt\} \qquad 2.16$$

The variable of the second integral can be changed to give

$$S(\omega) = iS(0)\{\int_{o}^{\infty} e^{[-(\omega-\Delta\omega)-\lambda]t}\,dt + \int_{o}^{\infty} e^{[i(\omega-\Delta\omega)-\lambda]t'}dt'\} \qquad 2.17$$

This is almost the same as equation 2.11 but contains an additional term in which the sign of $(\omega-\Delta\omega)$ has been reversed. Thus the part of the NMR spectrum (equation 2.12), which is antisymmetrical in this quantity is cancelled out and the result is:

$$S(\omega) = \frac{2i\lambda S(0)}{[(\omega-\Delta\omega)^2+\lambda^2]} \qquad 2.18$$

which contains no dispersion-mode contributions. This property is extremely useful, especially if there are phase errors present. In the conventional spectrum produced by the transformation of a free induction decay, an absorption mode signal is generated by taking suitable linear combinations of the real and imaginary parts of the Fourier transform. This only works in a spectrum of many lines if any phase errors present vary regularly and not too heavily across the spectrum. However in some forms of spectroscopy, the lines are produced with irregular phases, and then this form of phase correction does not work.

Whole-echo transformation is an attractive alternative. A phase error ϕ in the echo signal S'(t) is carried through into the frequency domain as follows:

$$S'(t) = S(t)\ e^{i\phi} \qquad 2.19$$

$$\text{so that} \quad S'(\omega) = \frac{2ie^{i\phi}\lambda S(0)}{[(\omega-\Delta\omega)^2+\lambda^2]} \qquad 2.20$$

This simply represents an absorption-mode Lorentzian line distributed between the real and imaginary parts of the transform. If the absolute-value of this spectrum is taken:

$$[S'(\omega)S'(\omega)^*]^{\frac{1}{2}} = \frac{2\lambda S(0)}{[(\omega-\Delta\omega)^2+\lambda^2]} \qquad 2.21$$

This is a pure absorption-mode signal of the full intensity, free from phase errors and dispersion-mode Lorentzian contributions (80).

An important application of whole-echo transformation arises when the spin echoes are modulated for some reason. This is the case if it desired to derive relaxation times in proton spectroscopy, where there are coupling interactions with other protons. In the presence of homonuclear spin-spin couplings, echoes are not stimulated along the y-axis of the rotating frame, but along a phase-shifted axis which depends on the coupling J_{HH} and the echo evolution time. As t_1 is increased, each resonance not only decreases in intensity due to T_2 processes, but also undergoes a phase-modulation at a frequency corresponding to the scalar coupling it experiences (12,49,50). The reason for this can be seen

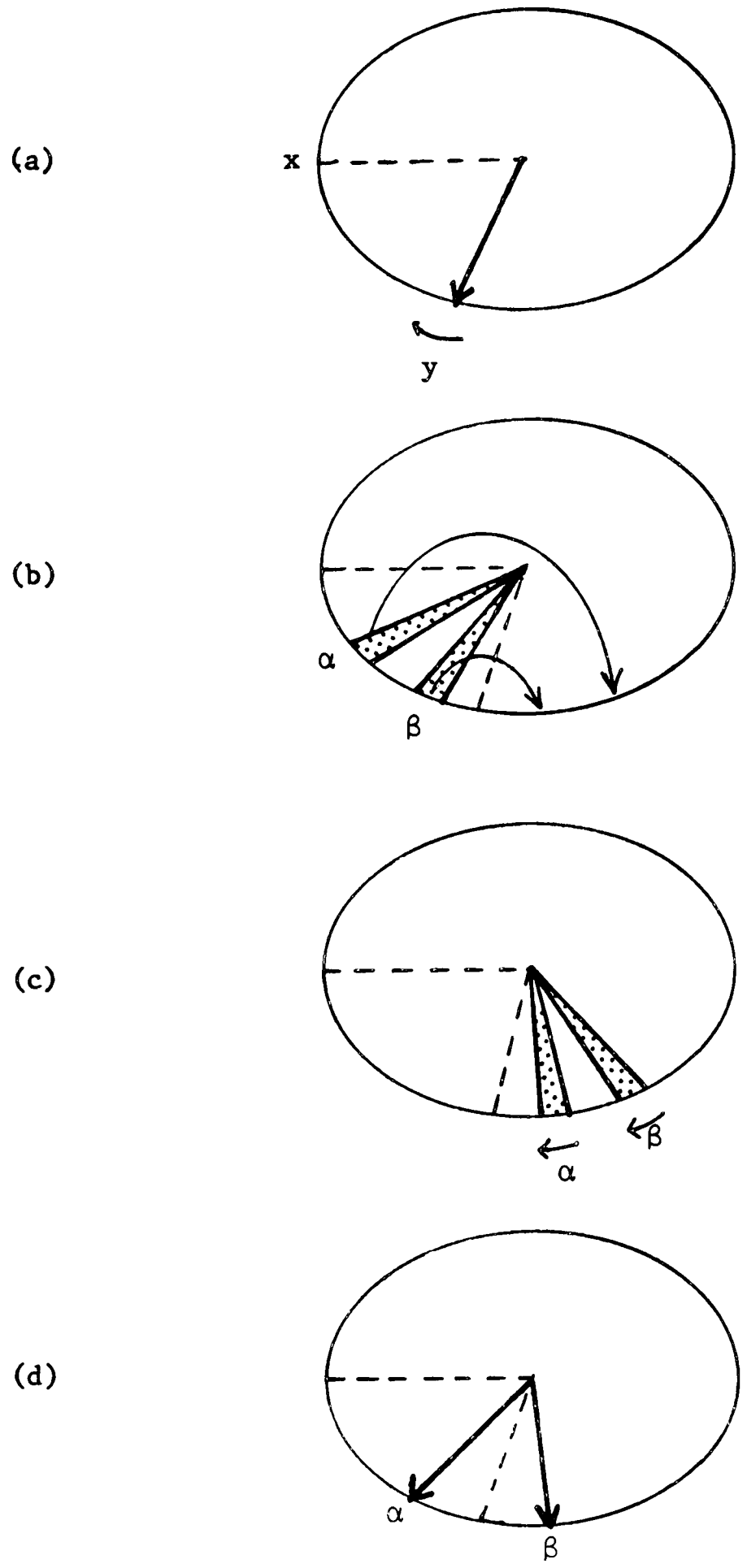

Fig.2.4. Modulation of a spin echo by weak homonuclear coupling.
(a) An initial $\pi/2$ pulse creates transverse magnetization along the y-axis.
(b) The vectors split into two sets according to the state of the coupled spin, α or β.
(c) The π pulse places the vectors in mirror-image positions, but also interchanges the states of the coupled spin, $\alpha \leftrightarrow \beta$.
(d) At time 2τ, the effect of B_o inhomogeneity has been refocussed, but there remains a divergence in phase between the α and β vectors. The result is a modulation of the echo amplitude with respect to τ at frequency J Hz.

from Figure 2.4. This concerns the transverse magnetization components of a spin which has a homonuclear coupling with another. The state of the second spin is indicated by α and β; this spin may be either parallel or anti-parallel to the magnetic field, so that it either augments or decreases the local field experienced by the nucleus of interest. Thus the transverse magnetization splits into two components which precess at frequencies either higher or lower than the chemically-shifted frequency by $\pm \frac{1}{2}J_{HH}$ Hz (Figure 2.4(b)). Fourier transformation of the decaying signal produced by such transverse magnetization would give a doublet of two lines at frequencies $\delta \pm \frac{1}{2}J_{HH}$ Hz, where δ is the chemically shifted frequency.

To generate the echo a π pulse is applied about the y-axis as usual. This places the vectors in mirror-image positions. However if the coupled spin is of the same isotopic species, it too is affected by the π pulse, so that its states α and β are interchanged. (Figure 2.4(c)). This breaks the symmetry of the echo formation process so that the two components no longer refocus along the y-axis but along axes shifted in phase by amounts $\pm \pi Jt_1$ radians (Figure 2.4(d)). Fourier transformation of the decaying half-echoes would produce spectra in which each line oscillates between absorption and dispersion-mode at a rate $\frac{1}{2}J$ Hz. This impedes the measurement of the spin-spin relaxation times. It is possible to take the absolute value of the Fourier transformed decaying half-echoes, which is insensitive to phase. However the conventional absolute-value mode is associated with problems of loss of resolution, and interference between adjacent lines (41,103). Much better is to calculate the absolute-value of the whole-echo

transform, as described above. This function is free from both phase modulation and interference effects. Smooth non-oscillatory decays of the intensities of each signal should be observed, very suitable for measurement of the spin-spin relaxation times.

It is possible to turn the modulation of the echoes to good use. If an absolute-value is not used, and a series of spectra are taken for increasing evolution times t_1, each resonance is seen to decay due to natural spin-spin relaxation, with a superimposed modulation at the coupling frequency. Thus the Fourier transform of the modulation envelope, (rather than the echoes themselves), is a 'J-spectrum' with lines at the coupling frequencies and a linewidth smaller than that determined by magnet inhomogeneity (49,50). In 'two-dimensional homonuclear J-spectroscopy' (104), a $(\pi/2\text{-}\tau\text{-}\pi\text{-}\tau)$ sequence is used as the evolution period of a two-dimensional experiment. The resultant two-dimensional spectrum is characterised as usual by the nature of its projections onto the two frequency axes. The projection onto F_2 is a conventional spectrum containing both chemical shifts and homonuclear couplings, and is frequently not resolvable, for the same reasons as proton-coupled carbon-13 spectra - a surfeit of information. But the projection onto F_1 is a 'J-spectrum', containing only homonuclear couplings. Thus it is possible to tilt the two-dimensional data matrix by $\pi/4$ radians to produce a complete separation of chemical shifts from homonuclear couplings, a goal long sought in proton spectroscopy (104). This technique has greatly increased the maximum size of molecule accessible to study by proton NMR (105-108).

Echo modulation is not observed when coupling is only present

(a)

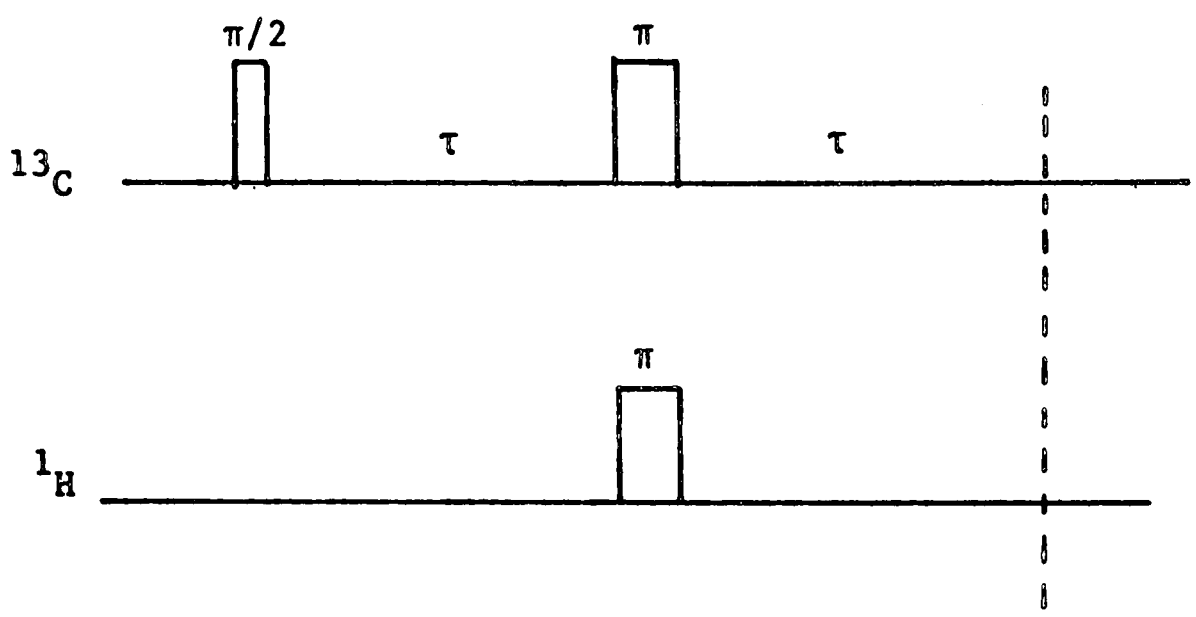

(b)

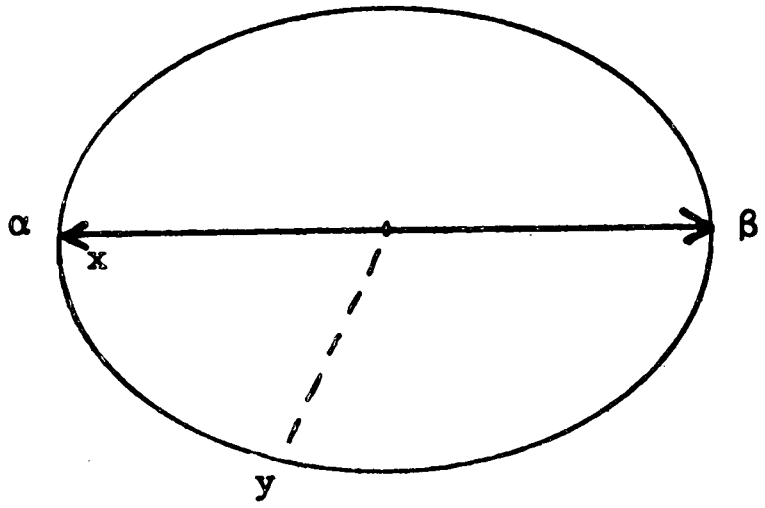

Fig.2.5. In heteronuclear coupled systems, the echo amplitude is not normally modulated by scalar coupling. Modulation can be introduced by employing a π pulse to the coupled spins at the same time as the refocussing pulse (a). Then, for an AX ^{13}C-^{1}H system, sequence (a) prepares the two components of carbon-13 magnetization in an antiparallel relative orientation along the x-axis, (b), providing $\tau = 1/(4J_{CH})$. This state is a starting point for various 'non-classical' manipulations of the spin system. (See Ch.3).

to spins of a different isotopic species. (Although weak effects can be observed in certain strongly-coupled cases (98,109)). Only one spin is affected by the refocussing pulse, so that the effect of the coupling is cancelled out at the time of the echo, just like the magnet inhomogeneity. However the modulation can be introduced by perturbing the coupled spin system with a π pulse at the same time as the refocussing pulse. An example of this is in carbon-13 proton-coupled J-spectroscopy. (See Figure 1.5). The effect of the extra π pulse is to interchange the labels of the coupled spins just as in Figure 2.4, and so induces echo modulation, this time due to the heteronuclear spin-spin coupling. When used as the evolution period of a two-dimensional experiment, a separation of carbon-13 chemical shifts from carbon-13 - proton couplings can be achieved, as described in Chapter 1, section 3. Because it is possible to decouple the carbon spins from the protons in the detection period by using high-power proton irradiation, a tilt of the data matrix is unnecessary in this case.

Finally, an application of modulated spin echoes will be mentioned which is of particular relevance to the following chapter. Many interesting 'non-classical' effects can be observed in coupled spin systems by manipulating a system which has been prepared such that the components of transverse magnetization of a given spin have an antiparallel relative orientation (Figure 2.5(b)). These include coherence transfer, and the creation of multiple-quantum coherence. The state of Figure 2.5(b) is usually achieved by use of a modulated spin echo. In the AX system of a carbon-13 nucleus coupled to a single proton, the sequence of Figure 2.5(a) produces

the required state if $\tau = 1/(4J_{CH})$. (When there are more couplings present, the values of the intervals may need to be modified). The effects which can be induced in a system corresponding to Figure 2.5(b) will be examined in detail in the following chapter. This will require knowledge of the quantum-mechanical description of coupled spin systems.

2.3 Density matrix theory

2.3.1 Definitions

Although the semi-classical model of precessing magnetization vectors is invaluable for understanding many NMR phenomena, it has been found to be inadequate in cases such as coupled spin systems. Much is left unexplained unless the quantum-mechanical nature of the spin system is explicitly taken into account. There are several equivalent quantum-mechanical formalisms which can be used. The one which is the most well-suited for NMR is that of the density matrix (83). Its use will be introduced by a study of an ensemble of non-interacting spin-$\frac{1}{2}$ nuclei.

Of fundamental importance in all quantum-mechanical theories is the Hamiltonian operator $\hat{H}$, which contains all factors which determine the energy of the system, and hence defines the equation of motion of all observable quantities. There are a set of rules for constructing the Hamiltonian (6): In this simple case, the Hamiltonian expresses an interaction between an applied magnetic field $\underline{B}$, and a nuclear magnetic moment $\underline{m}$:

$$\hat{H} = -\hat{\underline{m}}.\underline{B} \qquad 2.22$$

For systems more complicated than spin-$\frac{1}{2}$, there will be additional terms expressing couplings, and/or quadrupole interactions. The nuclear magnetic moment is proportional to the nuclear angular momentum:

$$\hat{\underline{m}} = \gamma\hat{\underline{I}} \qquad 2.23$$

The proportionality constant γ is a property of each nuclear isotope and may be positive, as for ^{1}H and ^{13}C, or negative, as for ^{15}N. (The electron also has a negative magnetogyric ratio). The angular momentum operator is usually expressed in terms of its three Cartesian components I_x, I_y and I_z:

$$\hat{\underline{I}} = \underline{i}\hat{I}_x + \underline{j}\hat{I}_y + \underline{k}\hat{I}_z \qquad 2.24$$

where $\underline{i}$, $\underline{j}$ and $\underline{k}$ are unit vectors along the three axes of the Cartesian reference frame.

The Hamiltonian becomes

$$\hat{H} = -\gamma(B_x\hat{I}_x + B_y\hat{I}_y + B_z\hat{I}_z) \qquad 2.25$$

where B_i are the Cartesian components of applied magnetic field. Now the components of the angular momentum operator do not commute with each other. Their important commutation properties can be expressed:

$$\begin{aligned} [\hat{I}_x,\hat{I}_y] &= iI_z \\ [\hat{I}_y,\hat{I}_z] &= iI_x \\ [\hat{I}_z,\hat{I}_x] &= iI_y \end{aligned} \qquad 2.26$$

For simplicity the numerical constant $\hbar$ has been omitted.

How that the Hamiltonian $\hat{H}$ has been constructed it is possible to proceed to the evolution of the wavefunction Ψ which expresses the state of the spin ensemble. The equation of motion of Ψ under the influence of the Hamiltonian is the Schrödinger equation:

$$\hat{H}\Psi = i\dot{\Psi} \qquad 2.27$$

The wavefunction Ψ is deemed to contain all possible knowledge of the spin ensemble. In quantum mechanics the value of some observable quantity Ω can never be defined with absolute certainty, but its 'expectation value', the statistically most likely value, can be stated as:

$$\langle\Omega\rangle = \int \Psi^* \hat{\Omega} \Psi \, d\tau \qquad 2.28$$

where $d\tau$ signifies an integration over all spatial coordinates, and $\hat{\Omega}$ is the operator for Ω.

All of these equations can be restated in a form more suitable for NMR by using the density matrix formalism. Firstly, Ψ is expanded as a linear combination of time-independent basis functions ϕ_i:

$$\Psi = \sum_i c_i \phi_i \qquad 2.29$$

Note that any time-dependence in Ψ is carried entirely in the time-dependence of the expansion coefficients c_i: in the density matrix theory it is never necessary to refer explicitly to the basis functions ϕ_i. (This is particularly useful in NMR problems where the rather

mysterious spin wavefunctions are used). The density matrix $\underline{\underline{\sigma}}$ is composed of binary products of these coefficients. Specifically,

$$\sigma_{mn} = \overline{c_m c_n^*} \qquad 2.30$$

where the bar signifies an ensemble average.

Note therefore that the density matrix is necessarily Hermitian:

$$\sigma_{mn} = \sigma_{nm}^* \qquad 2.31$$

or equivalently,

$$\underline{\underline{\sigma}}^{\sim *} = \underline{\underline{\sigma}} \qquad 2.32$$

The operators $\hat{\Omega}$ are also expressed in matrix form by using a definition of the matrix elements:

$$\Omega_{mn} = \int \phi_m^* \hat{\Omega} \phi_n d\tau \qquad 2.33$$

This allows a reformulation of the expectation value of an observable in terms of the trace of a matrix product

$$\langle \Omega \rangle = \mathrm{Tr}(\underline{\underline{\Omega\sigma}}) \qquad 2.34$$

For example, the expectation value of the z-component of nuclear spin magnetization can be calculated as

$$\langle M_z \rangle = \gamma \mathrm{Tr}(\underline{\underline{I_z \sigma}}). \qquad 2.35$$

The Schrödinger equation can also be restated as an equation of motion of the density matrix (83):

$$\dot{\underline{\underline{\sigma}}} = -i[\underline{\underline{H}},\underline{\underline{\sigma}}] \qquad 2.36$$

in which relaxation has been neglected.

Armed with these two equations it is possible to calculate the motion of the expectation values of the observables of the system. For example it is possible to show, by using the commutation rules of eqn. 2.26 and the Hamiltonian of equation 2.25, that the expectation value of the magnetization vector behaves in a classical fashion, neglecting relaxation (110):

$$\dot{\langle \underline{M} \rangle} = \gamma \langle \underline{M} \rangle \wedge B \qquad 2.37$$

This should not be too surprising because so far nothing has been said to differentiate an ensemble of spin-$\frac{1}{2}$ nuclei from a macroscopic rotating magnet. The angular momentum components in both cases are described by operators $\hat{I}_x$, $\hat{I}_y$ and $\hat{I}_z$ which have the same commutation properties and thus give rise to the same equation of motion. The difference between the two systems lies only in the number of basis functions ϕ_i which must be used in the expansion of the wavefunction, equation 2.29. By convention, these functions are usually eigenfunctions of the z-component of the angular momentum operator $\hat{I}_z$, so that

$$\hat{I}_z \phi_i = m_i \phi_i \qquad 2.38$$

For a macroscopic rotating body, the total angular momentum $I\hbar$ is very large compared to $\hbar$. There are a very large number of

eigenfunctions ϕ_i available, corresponding to 2I+1 eigenvalues of I_z, from $m_i = -I$ to $m_i = +I$. Thus the density matrix is very large, of dimensions 2I+1 by 2I+1. In contrast for a spin-$\frac{1}{2}$ nucleus, the total angular momentum is only of the order of $\hbar$. (Precisely, $\frac{1}{2}\hbar\sqrt{3}$). There are only two eigenfunctions of $\hat{I}_z$, denoted α and β and distinguished by their eigenvalues:

$$\hat{I}_z|\alpha\rangle = +\tfrac{1}{2}|\alpha\rangle \qquad 2.39$$
$$\hat{I}_z|\beta\rangle = -\tfrac{1}{2}|\beta\rangle$$

The density matrix is of dimension 2 x 2. Nevertheless there is no detectable difference in the motion of the magnetization vector between the spin-$\frac{1}{2}$ case, and the classical limit of infinite total angular momentum. The restricted number of states available to the ensemble of nuclear spins only becomes important in the presence of more complicated Hamiltonians.

2.3.2 The motion of the density matrix

In the absence of a radiofrequency field, the Hamiltonian is simply composed of an interaction between the nuclear magnetic moment and the static field of magnitude B_o applied along the z-axis:

$$\hat{H} = -\gamma B_o \hat{I}_z \qquad 2.40$$

It can be shown that for a spin-$\frac{1}{2}$ system, the density matrix comes to equilibrium through relaxation processes and assumes the value (83):

$$\underline{\underline{\sigma}}_o = \underline{\underline{1}} + \frac{\gamma B_o}{kT} \hat{I}_z \qquad 2.41$$

This equation assumes a temperature high enough that $kT >> \hbar\gamma B_o$ which is almost always easily satisfied. Normally the constants in this equation are omitted for the sake of brevity, so that a reduced density matrix σ' is used, given by:

$$\underline{\underline{\sigma}}' = \frac{kT}{\gamma B_o} (\underline{\underline{\sigma}} - \underline{\underline{1}}) \qquad 2.42$$

The use of the reduced density matrix will be implied in all subsequent equations. Note therefore that a factor $\hbar\gamma B_o/kT$ should be taken to multiply the values of any expectation values deduced. As a further simplification the use of circumflex to denote operators and double-underlining to indicate matrices will now be dropped. The meaning of symbols should be clear from the context. With these simplifications the equilibrium reduced density matrix is denoted:

$$\sigma_o = I_z \qquad 2.43$$

Now the choice of the basis set in which the density matrix and the operators are expressed is quite arbitrary. However the simplest expressions are obtained if the eigenfunctions of the equilibrium Hamiltonian are chosen. These are also the eigenfunctions of I_z, α and β. With this basis set, the matrix representations of the three Cartesian components of the angular momentum operator are the three Pauli matrices:

$$I_x = \frac{1}{2}\begin{pmatrix} 0 & 1 \\ 1 & 0 \end{pmatrix} \quad I_y = \frac{1}{2i}\begin{pmatrix} 0 & 1 \\ -1 & 0 \end{pmatrix} \quad I_z = \frac{1}{2}\begin{pmatrix} 1 & 0 \\ 0 & -1 \end{pmatrix} \qquad 2.44$$

It is easy to show that these matrix representations satisfy the commutation relationships of equation 2.26.

It is now possible to find the expectation values of the components of magnetization in terms of the elements of the density matrix:

$$\begin{aligned} \langle M_x \rangle &= \gamma Tr(\sigma I_x) = \frac{1}{2}(\sigma_{12}+\sigma_{12}^*) = Re\sigma_{12} \\ \langle M_y \rangle &= \gamma Tr(\sigma I_y) = \frac{1}{2i}(\sigma_{12}-\sigma_{12}^*) = Im\sigma_{12} \\ \langle M_z \rangle &= \gamma Tr(\sigma I_z) = \frac{1}{2}(\sigma_{11}-\sigma_{22}) \end{aligned} \qquad 2.45$$

Thus M_x and M_y are associated with the off-diagonal elements of the density matrix, whilst M_z is proportional to a difference between the diagonal elements. The significance of these diagonal elements is revealed by a re-examination of the definition of the density matrix. From equation 2.30,

$$\sigma_{ii} = |\overline{c_i}|^2 \qquad 2.46$$

so that the diagonal element σ_{ii} is a measure of the weight with which an eigenfunction ϕ_i is represented in the full wavefunction Ψ. In other words, the relative population of state i. Thus the diagonal elements of the density matrix represent energy level populations.

This conclusion is supported by calculating the evolution of a general density matrix under the influence of the Hamiltonian

of equation 2.40. The equation of motion 2.36 can be much simplified, because the Hamiltonian is diagonal when expressed in the basis set of its own eigenfunctions:

$$\begin{aligned} \dot{\sigma}_{mn} &= -i[H,\sigma]_{mn} \\ &= -i \sum_i (H_{mi}\sigma_{in} - \sigma_{mi}H_{in}) \\ &= -i\sigma_{mn}(H_{mm} - H_{nn}) \end{aligned} \qquad 2.47$$

The differential equation can be solved to give

$$\sigma_{mn}(t) = \sigma_{mn}(0)\exp[-it(H_{mm} - H_{nn})] \qquad 2.50$$

This shows that the diagonal elements, for which m = n, do not vary in time, just as would be expected if they signified unperturbed energy level populations. In contrast, the off-diagonal elements ($m \neq n$) do oscillate at a rate proportional to the difference in energy between the connected levels, $H_{mm} - H_{nn}$. It is hard to get a physical picture of the significance of these off-diagonal elements. A nomenclature is frequently used in which the presence of a non-zero element σ_{mn} denotes a 'coherence' between states m and n. This tries to convey a sense of oscillation without implying an exchange of populations between the two energy levels, which would be incorrect. In this particular case the coherence is closely associated with oscillating magnetization, for the combination of equations 2.45 with equation 2.50 gives the familiar Bloch picture of a precessing transverse magnetization vector. However, in the next chapter some forms of coherence will

be encountered which do not appear to be associated with magnetization.

It is perhaps not surprising that it is hard to get a physical grasp of the concept of coherence because it is really a quantum-mechanical phenomenon. In the macroscopic world of very large quantum numbers, all that is experienced is a combination of vast numbers of coherences, which may interfere so as to give an impression of concerted motion. The individual coherences can only really be experienced in the quantum-mechanical world of nuclear spin systems, with their small numbers of energy levels and long time-scales.

2.3.3 Rotation operators

The motion of the density matrix under the influence of a pulse of radiofrequency irradiation will now be examined. This is despite the fact that the answer is already known. The magnetization vectors follow the classical equation of motion, and since the elements of the density matrix have already been given in terms of the components of magnetization, the final density matrix could already be deduced without the need for quantum-mechanical calculation. The motivation for performing the treatment is different. Firstly it provides a useful introduction to unitary transformations; secondly, the treatment will be generalised in the following chapter for the case of coupled spins. Finally, it provides an expression for the rotation operators which act on the density matrix during the pulse. The properties of these operators will be seen to be of importance in Chapter 4, in which

many rotations are chained together to produce a useful combined effect ('composite pulses'). This represents a shift in emphasis from the effect of rotation operators on the density matrix to the effect of rotation operators on each other.

As usual the Hamiltonian operator is the starting point: In the presence of radio-frequency irradiation it is given by

$$H = -2\gamma B_1 \cos(\omega t + \phi) I_x - \gamma B_o I_z \qquad 2.51$$

As in the classical theory the amplitude-modulation of the radio-frequency field may be represented as the sum of two counter-rotating components, one of which can be ignored:

$$H = -\gamma B_1 \cos(\omega t+\phi) I_x - \gamma B_1 \sin(\omega t+\phi) I_y - \gamma B_o I_z \qquad 2.52$$

The rotating field is usefully expressed by using exponential operators (83):

$$H = \gamma B_1 e^{-i(\omega t+\phi) I_z} I_x e^{+i(\omega t+\phi) I_z} - \gamma B_o I_z \qquad 2.53$$

The properties of exponential operators are summarised in Appendix 1. Of particular importance is the set of identities:

$$e^{i\alpha I_z} I_y e^{-i\alpha I_z} = I_y \cos\alpha + I_x \sin\alpha \qquad 2.54$$

$$e^{i\alpha I_z} I_x e^{-i\alpha I_z} = I_x \cos\alpha - I_y \sin\alpha \qquad 2.55$$

Each of these is subject to cyclic permutation of the subscripts x, y and z. They derive from the commutation properties of the components of angular momentum and can be proved by using differential equations (83). They will be encountered repeatedly throughout this thesis.

Returning to equation 2.53, this Hamiltonian is time-dependent so that the equation of motion cannot be solved immediately. First a unitary transformation into a rotating reference frame must be performed in which the Hamiltonian appears stationary. The transformation operator U is given by

$$U = e^{-i\omega t I_z} \qquad 2.56$$

with the transformed density matrix σ^r:

$$\sigma^r = U\sigma U^{-1} \qquad 2.57$$

This can be shown to follow the equation of motion

$$\dot{\sigma}^r = -i[H^r,\sigma^r] \qquad 2.58$$

where the transformed Hamiltonian H^r is given by:

$$H^r = UHU^{-1} + \omega I_z \qquad 2.59$$

This can be evaluated as the following expression which is time-independent:

$$H^r = -\gamma B_1 \, e^{-i\phi I_z} \, I_x e^{i\phi I_z} - \Delta\omega I_z \qquad 2.60$$

where

$$\Delta\omega = \gamma B_o - \omega \qquad 2.61$$

This rotating-frame Hamiltonian clearly represents an interaction between the nuclear angular momentum operator $\underline{I}$ and a tilted rotating-frame effective field as given in Figure 2.1. This conclusion is supported by a little calculation to put equation 2.40 into the form:

$$H^r = -\gamma |B^{eff}| e^{-i\phi I_z} \, e^{i\theta I_y} \, I_x \, e^{-i\theta I_y} \, e^{i\phi I_z} \qquad 2.62$$

where $|B^{eff}|$ and θ take their usual values given in equations 2.4 and 2.6.

It still remains to solve the equation of motion of the rotating-frame density matrix eqn. 2.58. This is now easily done because H^r, although quite complicated, is time-independent. The general solution of eqn. 2.58 for a time-independent H^r is

$$\sigma^r(t) = e^{-iH^r t} \, \sigma^r(0) e^{+iH^r t} \qquad 2.63$$

with H^r given by the expression 2.62. Fortunately the operator $\exp(-iH^r t)$, which is apparently an exponential of a product of exponentials, can be much simplified by reasoning such as:

$$\exp(UAU^{-1}) = 1 + UAU^{-1} + \frac{1}{2!} UAU^{-1}.UAU^{-1} + ...$$

$$= U(1 + A + \frac{1}{2!} A^2 + ...) U^{-1}$$

$$= Ue^{A}U^{-1} \qquad 2.64$$

So that the equation of motion of the rotating-frame density matrix becomes

$$\sigma^r(t) = R(\alpha,\theta,\phi)\sigma^r(0)\ R^{-1}(\alpha,\theta,\phi) \qquad 2.65$$

where

$$R(\alpha,\theta,\phi) = R_{-z}(\phi)R_y(\theta)R_x(\alpha)R_{-y}(\theta)R_z(\alpha) \qquad 2.66$$

The flip angle α under the effective field has the usual value:

$$\alpha = \gamma|B^{eff}|t \qquad 2.67$$

and the rotation operators are given by expressions such as

$$R_{-z}(\phi) = \exp(-i\phi I_z) \qquad 2.68$$

(Note that $R_{-z}(\phi) = R_z(-\phi)$).

Equation 2.65 is the general equation of motion of the density matrix in a radiofrequency irradiation field, relaxation having been ignored. (This restricts the equation to application to pulses of duration much shorter than the relaxation times.)

One important feature of the motion should be pointed out. The trace of the density matrix is invariant under the perturbation. This can be proved formally as follows:

$$\begin{aligned} \mathrm{Tr}(R\sigma R^{-1}) &= \mathrm{Tr} (R^{-1}R\,\sigma) \\ &= \mathrm{Tr}\,\sigma \end{aligned} \qquad 2.69$$

$$\text{since} \quad \mathrm{Tr}(ABC) = \mathrm{Tr}(BCA). \qquad 2.70$$

As the trace of the density matrix represents the sum of the populations of the energy levels, this is to be expected. The pulse simply redistributes the populations throughout the energy levels.

If the irradiation field strength γB_1 greatly exceeds the resonance offset $\Delta\omega$, so that $\theta \simeq 0$, and there are no phase shifts, then $R(\alpha,\theta,\phi)$ takes the simple form $R_x(\alpha)$. If desired the matrix representation of this operator can be evaluated by the recipe of equation 2.33, and for the spin-$\frac{1}{2}$ case can be shown to be (see Appendix 2):

$$R_x(\alpha) = \begin{pmatrix} c & is \\ is & c \end{pmatrix} \qquad 2.71$$

where $c = \cos \frac{1}{2}\alpha$ and $s = \sin \frac{1}{2}\alpha$. As usual the basis set (α,β) has been used. Without these simplifications the pulse operator must be expressed as a product of up to five such matrices, equation 2.66. Note that this equation is an example of a general theorem

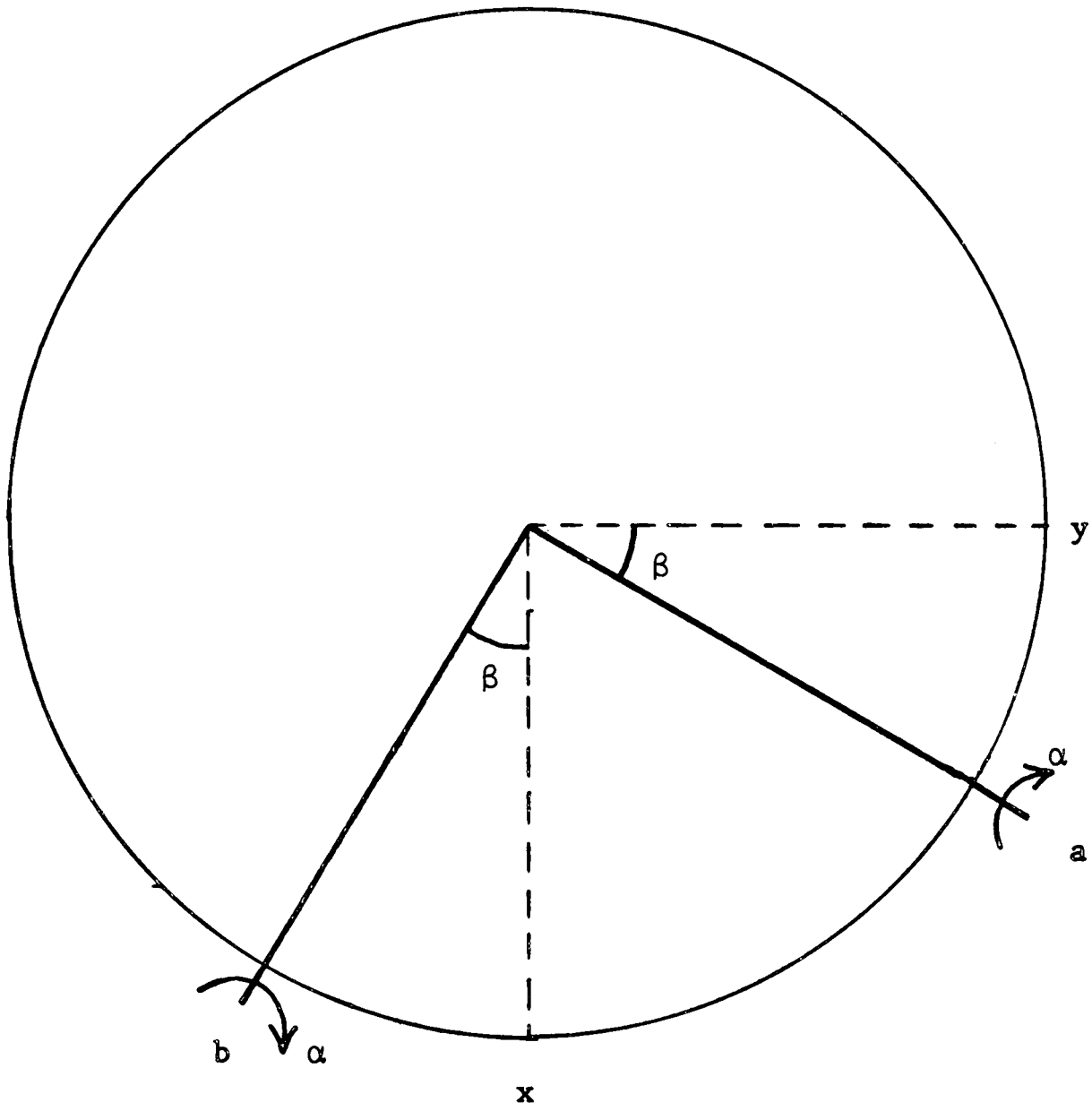

Fig.2.6.

which states that any combination of two or more successive rotations is another rotation. (As distinct from other possible operations, such as reflections or inversions). In the parlance of group theory, the set of rotations which leave a sphere unchanged form a group, and this property will be put to good use in Chapter 4.

In most cases the product of two or more rotations gives a complicated result. Although the overall operator is certain to be another rotation, it is often difficult to derive an expression for this in the general case. But certain symmetrical groups of three successive rotations do have a simple overall effect, as expressed by the following identities:

$$R_z(\beta)R_y(\alpha)R_{-z}(\beta) = \exp[i\alpha(I_y\cos\beta + I_x\sin\beta)] \qquad 2.72$$

$$R_z(\beta)R_x(\alpha)R_{-z}(\beta) = \exp[i\alpha(I_x\cos\beta - I_y\sin\beta)] \qquad 2.73$$

These two operators represent rotations by α radians about the axes a and b in Figure 2.6. As usual they are subject to cyclic permutation of the subscripts x, y and z. Note the resemblance between these identities and equations 2.54 and 2.55. They can be derived from each other by use of equation 2.64.

Particularly important special cases of eqns 2.72 and 2.73 occur when β takes the value $\pi/2$ or π radians. Thus

$$R_z(\pi/2)R_y(\alpha)R_{-z}(\pi/2) = R_x(\alpha) \qquad 2.74$$

$$R_z(\pi)R_y(\alpha)R_{-z}(\pi) = R_{-y}(\alpha) \qquad 2.75$$

Other examples of rotations combining to produce a simple overall effect will be found in Chapter 4.

CHAPTER THREE

A VECTOR MODEL OF THE AX SYSTEM

CHAPTER 3

A VECTOR MODEL OF THE AX SYSTEM

3.1 Non-classical effects in the AX system

One of the simplest cases for which the Bloch picture breaks down is the AX spin system, consisting of an ensemble of pairs of weakly interacting nuclei each of spin-$\frac{1}{2}$. Even in this simplest of cases many effects can be observed which are truly inexplicable using classical magnetization vectors. These not only include rather esoteric phenomena such as multiple-quantum coherence and coherence transfer, but may be observed in very simple pulse sequences, as is shown below.

For example, consider a heteronuclear AX system, consisting of coupled spins of different isotopic species. The wide difference in Larmor frequencies for the two isotopes makes it easy to excite selectively just one of them. Thus if thermal equilibrium is established and a pulse of length $\pi/2$ radians is applied at the B-spin frequency, transverse B-magnetization is produced and starts to precess in the static magnetic field. (The symbol B is used for the name of the spins rather than X, to avoid confusion with the x-axis of Cartesian reference frames. Nevertheless, a weakly-coupled AX system, not a strongly-coupled AB system, is always implied.) The precessing magnetization splits into two components according to the state of the A-spin, α or β. Detection and Fourier transformation of the decaying transient would produce

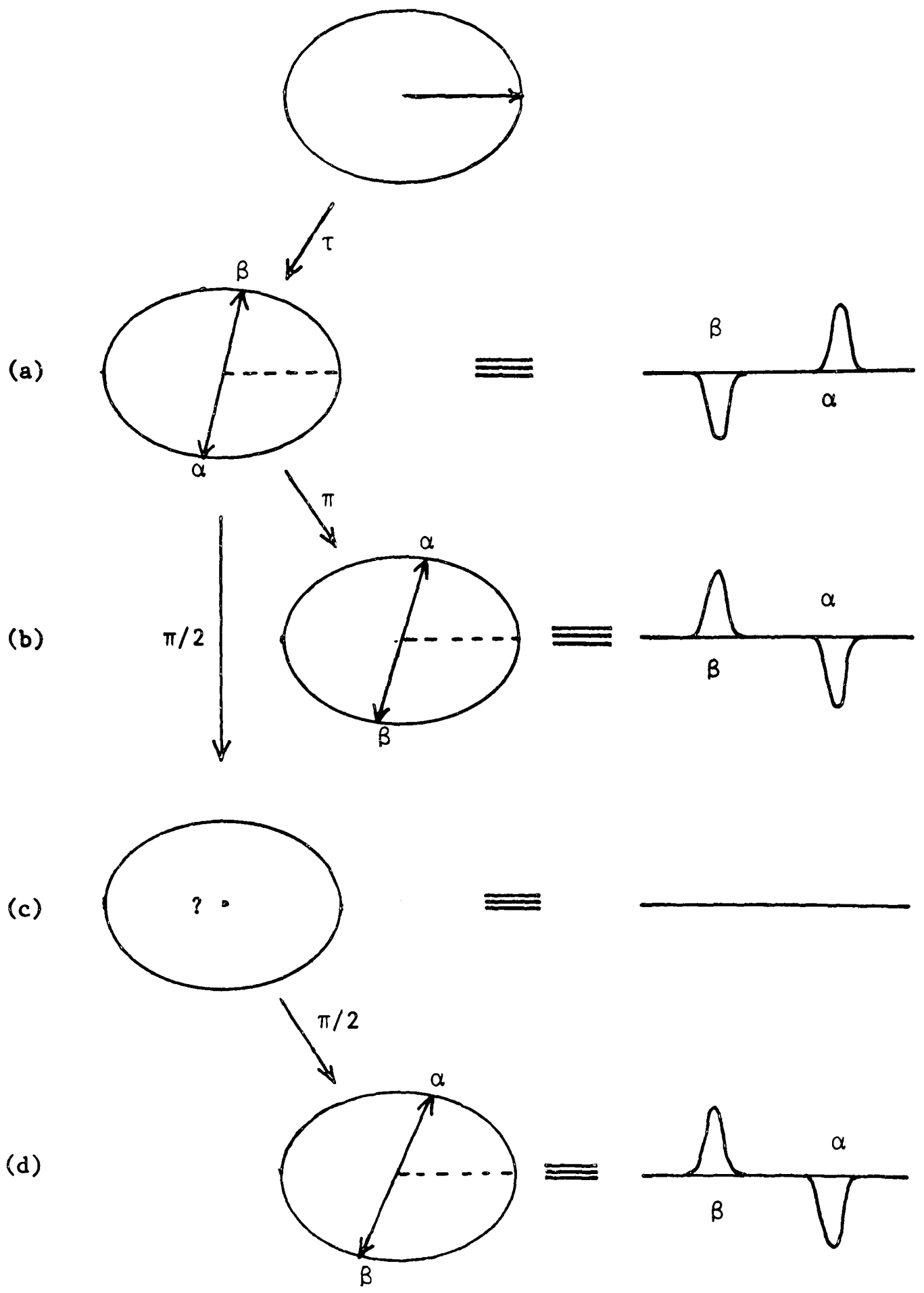

Fig.3.1(a) Components of transverse ^{13}C magnetization are prepared in an antiparallel orientation along the x-axis.

(b) A π pulse to the protons interchanges these two vectors.

(c) A π/2 pulse to the protons destroys the ^{13}C magnetization.

(d) A further π/2 proton pulse restores the ^{13}C magnetization to give the same overall result as (b).

a spectrum with two lines symmetrically disposed about the chemically-shifted B-spin precession frequency, with splitting J Hz.

Interesting effects are produced if the B-spin magnetization is allowed to precess for a time, and a pulse is applied to the A-spins, before detection and Fourier transformation. Suppose that a time $\tau = 1/(2J)$ seconds is left. Then a phase difference of π radians accumulates between the two components of precessing B-magnetization, so that they are described by antiparallel vectors in the rotating reference frame. If the reference frequency for the B-spins is the exact mean of the precession frequencies of the components, the two vectors assume antiparallel orientations along the $\pm$ x axis at this time. Detection and transformation of the subsequent transient (without manipulation of the A-spins) produces a spectrum with two lines of opposite sign (Figure 3.1(a)).

Now consider a pulse of length π radians applied to the A-spins just before the start of data acquisition. The effect of this is well-known. The pulse interchanges the A-spin states $\alpha \leftrightarrow \beta$, so that the amplitudes of the two components of B-magnetization are also interchanged (Figure 3.1(b)). This phenomenon has been mentioned prevously in the context of modulated spin echoes (Chapter 2, section 2). It can be accommodated in the Bloch picture without too much discomfort.

It is a different matter if the pulse to the A-spins is made of length $\pi/2$ radians (Figure 3.1(c)). The observed effect is that

the B-magnetization vanishes (Figure 3.1(c)). Now this too can be explained to some extent by postulating that the $\pi/2$ pulse accomplishes an incomplete inter-conversion of the B-spin states, and ends up 'mixing' the two-components of magnetization, which then mutually cancel. To the theorist this should produce a rather uncomfortable feeling, because only coherent perturbations have been applied to the spin system, so that it is unlikely that these could combine so as to produce a complete destruction of magnetization. Nevertheless, this is the observed effect: The B-magnetization does indeed disappear, and if the state of Figure 3.1(c) is allowed to evolve, never reappears until relaxation processes produce longitudinal magnetization again.

The unsatisfactory nature of this description become glaringly obvious if a further $\pi/2$ pulse is applied to the A-spins. The combined effect of the two consecutive $\pi/2$ pulses has to be the same as that of a single π pulse, so that the result (Figure 3.1(d)) is the same as Figure 3.1(b) - two antiparallel components of B-magnetization. But this magnetization cannot have appeared out of nothing, as Figure 3.1(c) seems to suggest. It is clear that there must exist some form of 'coherence' in the spin system which does not appear in conventional magnetization vector diagrams, but which is present in state (c), and which exerts an obvious influence when a second pulse is applied.

Thus even in this very simple sequence of pulses, there are some rather subtle effects which demand a satisfactory explanation. It is the aim of this chapter to clarify such phenomena and in so doing present an expanded version of the Bloch diagram which allows

the advantages of a pictorial representation to be retained.

It will be found that a full description of the behaviour of the AX system requires the use of not less than six Cartesian reference frames. Four of these concern the rotations of the four components of magnetization (two components each for both the A and B spin systems). The extra two frames have some rather special properties and are concerned with the interconversion of transverse magnetization components with zero- and double-quantum coherence. One frame rotates at the reference frequency of the A spins and will be referred to as the 'AZDQ frame'. The other rotates at the B reference frequency and is the 'BZDQ frame'. (The two reference signals being one and the same for the homonuclear AX system.) All six frames are 'coupled': That is to say, the rotation of a vector in a given frame affects the positions of vectors in at least one other of the six frames. An example of this is already familiar. The longitudinal components in the four magnetization frames are connected because they represent population differences across shared energy levels. This type of connectivity can give rise to some familiar effects such as the nuclear Overhauser effect (33), and non-exponential spin-lattice relaxation (25). But far more suble connectivity effects can be demonstrated which involve the transverse components of the magnetization frames and will be discussed below.

Before proceeding further the limitations of the model should be pointed out. The restriction to the AX system is an obvious disadvantage because such spin systems are quite rare in nature. But simple extensions to systems involving equivalent spins are

probably quite feasible. However it is unlikely that a workable vector model can be developed for systems more complicated than AX, A_2X, A_3X, etc. Even the strongly coupled AB system is beyond the scope of the present model. Furthermore, only a restricted variety of perturbations to the AX system can be treated. This includes free precession, and strong pulses over time periods short compared to the inverse coupling 1/J, but not weak, very selective pulses. As the two former perturbations comprise the great majority of useful manipulations in liquid-state NMR this restriction is not serious in practice. However some interesting 'non-classical' effects involving weak, highly-selective pulses have been demonstrated (111-113). To repeat, the present treatment only handles pulses strong and short enough to be nonselective between the two transitions of a single spin isotopic species. As such it is most suitable for liquid-state work, where the coupling interactions are almost always small. But in anisotropic media, where dipole-dipole couplings are involved and can be considerable, it is probably better to use the single-transition operator formalism of Vega and others (114-116).

Despite these clear deficiences, it should be emphasized that alternative schemes are invariably inadequate or more complicated. For example, it is always possible to perform the full density matrix calculation, but the numerous matrix multiplications are tedious and to most people provide little insight.

3.2 The density matrix of the AX system

It is the first requirement of any successful model that it should be consistent with the conclusions of quantum mechanics. Accordingly the density matrix and its motion under pulses is used as the scaffolding on which this treatment is based. In fact the model which will be described could be viewed as a way of predicting the motion of the density matrix without recourse to direct calculation. The advantages of such diagrammatic representations of quantum-mechanical evolutions are well-known and have long been used in nuclear physics, for example.

The basis set which should be used to construct the density matrix is as usual the set of eigenfunctions of the unperturbed Hamiltonian H_o:

$$H_o = -\gamma_A B_o I_{zA} - \gamma_B B_o I_{zB} + J_{AB} \underline{I}_A \cdot \underline{I}_B \qquad 3.1$$

The last term expresses the coupling between the spins as a quantity proportional to the scalar product between the two angular momentum vectors. In the AX case, the interaction is weak so that off-diagonal elements can be ignored (117) so that the Hamiltonian becomes:

$$H_o = -\gamma_A B_o I_{zA} - \gamma_B B_o I_{zB} + J_{AB} I_{zA} I_{zB} \qquad 3.2$$

The eigenfunctions of this are simply the four possible products of the single spin wavefunctions

(a)

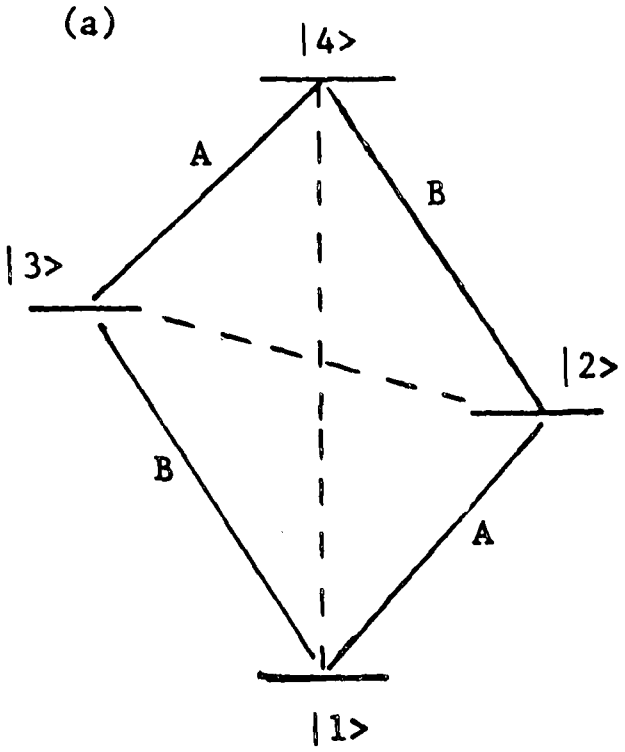

(b)

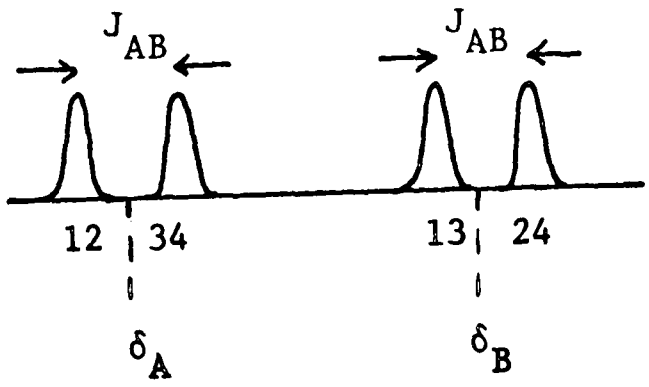

(c)

$$\begin{pmatrix} P_1 & \sigma_{12} & \sigma_{13} & \sigma_{14} \\ \sigma_{12}^* & P_2 & \sigma_{23} & \sigma_{24} \\ \sigma_{13}^* & \sigma_{23}^* & P_3 & \sigma_{34} \\ \sigma_{14}^* & \sigma_{24}^* & \sigma_{34}^* & P_4 \end{pmatrix}$$

(d)

$$\begin{pmatrix} 0 & \frac{1}{2} & \frac{1}{2} & 0 \\ \frac{1}{2} & 0 & 0 & \frac{1}{2} \\ \frac{1}{2} & 0 & 0 & \frac{1}{2} \\ 0 & \frac{1}{2} & \frac{1}{2} & 0 \end{pmatrix}$$

Fig.3.2 (a) Energy levels and transitions for the AX system. Full lines represent allowed single-quantum transitions. Dotted lines represent the 'forbidden' zero- and double-quantum transitions.

(b) The frequencies of the single-quantum transitions.

(c) The density matrix of the AX system.

(d) The matrix representation of the operator I_x.

$$|1\rangle = |\alpha\alpha\rangle, \quad |2\rangle = |\beta\alpha\rangle, \quad |3\rangle = |\alpha\beta\rangle, \quad |4\rangle = |\beta\beta\rangle \qquad 3.3$$

which have the four eigenvalues

$$\begin{aligned} E_1 &= -\tfrac{1}{2}\gamma_A B_o - \tfrac{1}{2}\gamma_B B_o + \tfrac{1}{4}J_{AB} \\ E_2 &= +\tfrac{1}{2}\gamma_A B_o - \tfrac{1}{2}\gamma_B B_o - \tfrac{1}{4}J_{AB} \\ E_3 &= -\tfrac{1}{2}\gamma_A B_o + \tfrac{1}{2}\gamma_B B_o - \tfrac{1}{4}J_{AB} \\ E_4 &= +\tfrac{1}{2}\gamma_A B_o + \tfrac{1}{2}\gamma_B B_o + \tfrac{1}{4}J_{AB} \end{aligned} \qquad 3.4$$

These represent the four energy levels of Figure 3.2(a).

Thus the density matrix is a 4 x 4 matrix, as shown in Figure 3.2(c). The Hermidity of the matrix has been stated explicitly. As usual the four diagonal elements indicate the relative populations of the four energy levels, $P_1 \ldots P_4$. The sum of these elements, being the trace of the matrix, is invariant under any perturbation. Four more elements, with their complex conjugates, represent the four allowed transitions indicated by solid lines in Figure 3.2(a), and correspond to the Fourier transform spectrum of Figure 3.2(b); two A transitions (σ_{12} and σ_{34}) and two B transitions (σ_{13} and σ_{24}).

There remain two elements, with their complex conjugates, σ_{14} and σ_{23}, which are coherences between energy levels not joined by an allowed transition. Indicated by dotted lines in Figure 3.2(a) they link levels separated by changes in angular momentum of $\Delta M = 0$ and ± 2, and accordingly are known as zero- and double-quantum coherences.

These multiple-quantum coherences do not contribute to system magnetization. This can be verified by evaluating the transverse magnetization of a general density matrix. The transverse angular momentum operator I_x for an AX system is given in Figure 3.2(d). Its expectation value can be calculated as:

$$\langle I_x \rangle = Tr(\sigma I_x) \qquad 3.5$$

and becomes

$$\langle I_x \rangle = \frac{1}{2}(\sigma_{12}+\sigma_{12}^*) + \frac{1}{2}(\sigma_{34}+\sigma_{34}^*) + \frac{1}{2}(\sigma_{13}+\sigma_{13}^*) + \frac{1}{2}(\sigma_{24}+\sigma_{24}^*)$$

$$= Re\ (\sigma_{12}+\sigma_{34}+\sigma_{13}+\sigma_{24}) \qquad 3.6$$

Similarly

$$\langle I_y \rangle = Im(\sigma_{12}+\sigma_{34}+\sigma_{13}+\sigma_{24}). \qquad 3.7$$

As anticipated these expressions only involve coherences of allowed transitions.

3.3 Submatrix rotations

If the zero- and double-quantum coherences do not represent magnetization, how then are they involved in the observable behaviour of the system?

The answer is that their influence is always indirect: The zero- and double-quantum coherences (ZDQ) may be inter-converted with transverse magnetization by the action of radio-frequency pulses. Hence a rigorous vector model of the AX system must provide a description of this inter-conversion process, and it is on precisely this point that the classical magnetization vector model tends to fail, since it can provide no explanation, or representation, of multiple-quantum coherence.

Let us now examine the motion of the density matrix under a radio-frequency pulse and see if it suggests the form that a more rigorous vector model would take. To simplify matters as much as possible at first consider a <u>selective</u> pulse, applied near the precession frequencies of the A spins and too weak to affect the B spins appreciably. Nevertheless the pulse should be strong enough that off-resonance effects may be ignored. For a heteronuclear AX system, with the A and B spins of different isotopic species, this would be the normal state of affairs. (It is important to distinguish such a partially selective pulse from a 'very selective pulse' which is weak enough to have a differential effect between the two transitions of a single spin).

The operator for this pulse may be represented $\exp(i\alpha I_{xA})$ and has the block-diagonal form of equation (3.8):

$$\exp(i\alpha I_{xA}) = \begin{pmatrix} c & is & & \\ is & c & & 0 \\ & & c & is \\ & 0 & is & c \end{pmatrix} \qquad 3.8$$

Note that each of these diagonal blocks is of the same form as $\exp(i\alpha I_x)$ for the isolated spin-$\frac{1}{2}$ case of equation 2.71. A notation will be used in which 4 x 4 matrices are split into their four component 2 x 2 submatrices. Accordingly $\exp(i\alpha I_{xA})$ becomes:

$$\exp(i\alpha I_{xA}) = \begin{pmatrix} [R] & 0 \\ 0 & [R] \end{pmatrix} \text{where} \quad [R] = \begin{pmatrix} c & is \\ is & c \end{pmatrix} \qquad 3.9$$

The density matrix can be decomposed in a similar fashion:

$$\sigma = \begin{pmatrix} [\sigma_{11}][\sigma_{13}] \\ [\sigma_{31}][\sigma_{33}] \end{pmatrix} \quad \text{where } [\sigma_{1m}] = \begin{pmatrix} \sigma_{1m}, & \sigma_{1,m+1} \\ \sigma_{1+1,m}\sigma_{1+1,m+1} \end{pmatrix} \qquad 3.10$$

Then the effect of $\exp(i\alpha I_{xA})$ on the density matrix σ can be expressed

$$\begin{pmatrix} [R] & 0 \\ 0 & [R] \end{pmatrix} \begin{pmatrix} [\sigma_{11}][\sigma_{13}] \\ [\sigma_{31}][\sigma_{33}] \end{pmatrix} \begin{pmatrix} [R]^{-1} & 0 \\ 0 & [R]^{-1} \end{pmatrix} = \begin{pmatrix} [\sigma_{11}^{+}][\sigma_{13}^{+}] \\ [\sigma_{31}^{+}][\sigma_{33}^{+}] \end{pmatrix} \qquad 3.11$$

where $$[\sigma_{ij}^{+}] = [R][\sigma_{ij}^{-}][R]^{-1} \qquad 3.12$$

The symbol (-) denotes the density matrix before and (+) after the pulse. Thus each of the four submatrices of σ are independently rotated by the operation [R].

Now let us examine the implications of this result for each of the four submatrices.

(i) <u>For submatrices 11 and 33</u>, the rotations are expressed diagrammatically by the precession of a vector through an angle α

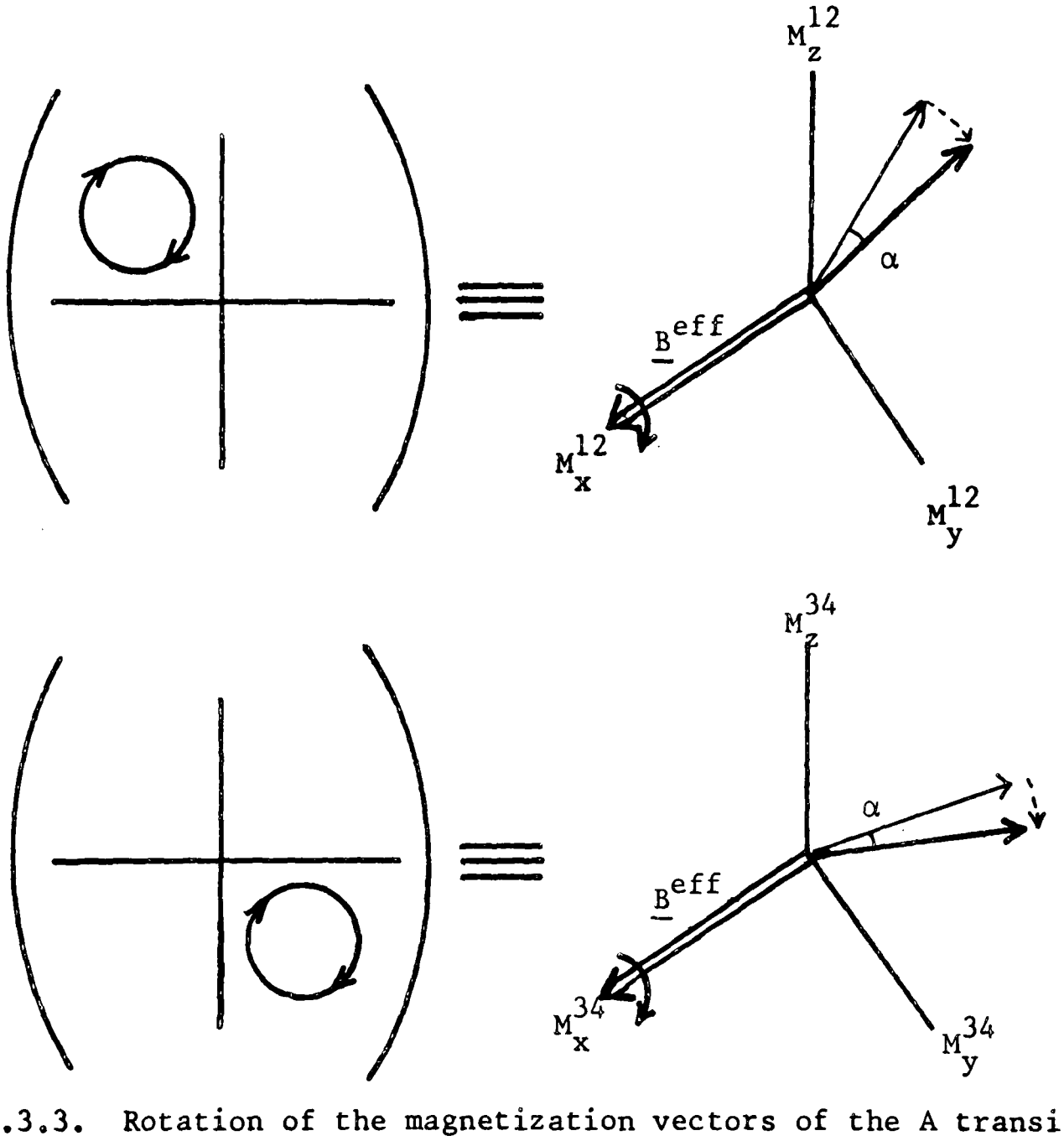

Fig.3.3. Rotation of the magnetization vectors of the A transitions about effective fields along the x-axes of the rotating frames, and the associated motion of the diagonal submatrices.

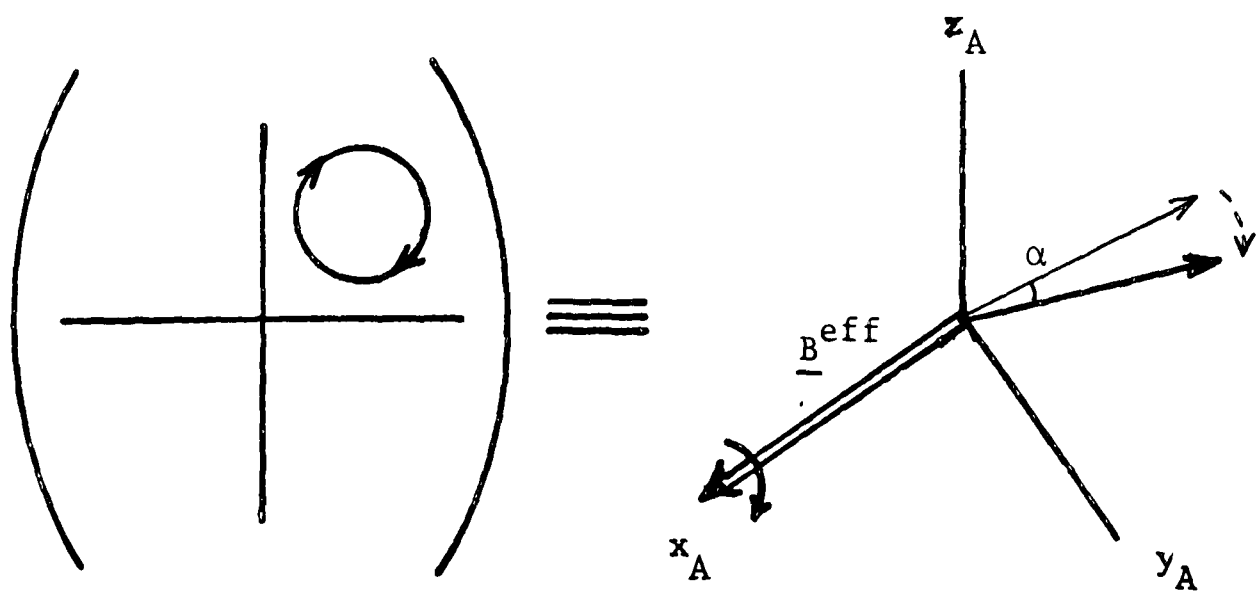

Fig.3.4 The analogous motion of an off-diagonal submatrix, with its vector representation.

about a pulse field along the x-axis of a reference frame. The Cartesian components of the vector are given by the expectation values:

$$\begin{aligned} \langle x \rangle &= Tr([\sigma][I_x]) \\ \langle y \rangle &= Tr([\sigma][I_y]) \\ \langle z \rangle &= Tr([\sigma][I_z]) \end{aligned} \qquad 3.13$$

where $[I_i]$ are here the three Pauli matrices of Equation 2.44. Thus for each of these two diagonal submatrices, equation 3.12 expresses the classical rotations of the individual magnetizations of the two A transitions by the pulse field, as depicted in Figure 3.3.

However the master equation 3.12 also suggests rotations of the off-diagonal submatrices of σ by the field applied to the A-spins. For our purposes this is the feature of greatest interest, since the off-diagonal submatrices involve the multiple quantum elements, which cannot be described by classical ideas.

(ii) Rotation of submatrices $[\sigma_{13}]$ and $[\sigma_{31}]$.

The off-diagonal submatrix $[\sigma_{13}]$ of σ contains four elements. Two, σ_{13} and σ_{24} represent the two-components of B single-quantum magnetization. The other two, σ_{23} and σ_{14}, are the non-classical zero- and double-quantum coherences.

The rotation of this submatrix describes the following behaviour -

a) the effect of a pulse, applied to the A spins, on B magnetization, and

(b) the participation of zero- and double-quantum coherence.

A vector representation of this submatrix will now be developed by analogy with the diagonal submatrices $[\sigma_{11}]$ and $[\sigma_{33}]$. The three Cartesian projections of the vector which should be used are idenified as:

$$\begin{aligned} \langle x_A \rangle &= \mathrm{Tr}([\sigma_{13}][I_x]) = \tfrac{1}{2}(\sigma_{14}+\sigma_{23}) \\ \langle y_A \rangle &= \mathrm{Tr}([\sigma_{13}][I_y]) = \tfrac{1}{2i}(\sigma_{14}-\sigma_{23}) \\ \langle z_A \rangle &= \mathrm{Tr}([\sigma_{13}][I_z]) = \tfrac{1}{2}(\sigma_{24}-\sigma_{13}) \end{aligned} \qquad 3.14$$

where again the three Pauli matrices have been used:

$$[I_x] = \tfrac{1}{2}\begin{pmatrix} 0 & 1 \\ 1 & 0 \end{pmatrix}, [I_y] = \tfrac{1}{2i}\begin{pmatrix} 0 & 1 \\ -1 & 0 \end{pmatrix}, [I_z] = \tfrac{1}{2}\begin{pmatrix} 1 & 0 \\ 0 & -1 \end{pmatrix} \qquad 3.15$$

Thus to represent the rotation of submatrix $[\sigma_{13}]$ under the influence of a pulse applied to the A spins, a vector $\underline{v}_A$ is used, defined as

$$\underline{v}_A = \langle x_A \rangle \underline{i} + \langle y_A \rangle \underline{j} + \langle z_A \rangle \underline{k} \qquad 3.16$$

where $\underline{i}$, $\underline{j}$ and $\underline{k}$ are the unit vectors along the x, y and z axis of the Cartesian reference frame. The vector may then be rotated around the applied pulse field, as in Figure 3.4.

As indicated by Equations 3.14, the transverse components of $\underline{v}_A$, x_A and y_A, represent combinations of double- and zero-quantum coherence. The rather unusual properties of these components will be treated shortly in much more detail. Examining now the z-component it may be seen that this does not involve ZDQ coherence but single-quantum coherences of the B-spins - that is, transverse magnetization of the spin species which is not directly affected by the pulse. To make this clear the z-component may be written:

$$z_A = \frac{1}{2\gamma_B}\left[(M_x^{24} - M_x^{13}) + i(M_y^{24} - M_y^{13})\right] \qquad 3.17$$

This is a complex number representation of the difference vector between the two components of transverse magnetization of the B spins.

At this stage two important and unusual properties of the vector $\underline{v}_A$ must be pointed out:

(a) Each one of the Cartesian components of this vector is not observable directly. The two transverse components x_A and y_A involve coherences of forbidden transitions, and these have already been seen to contribute nothing to observable magnetization. The longitudinal component z_A does involve magnetizations, as discussed above, but not in an observable form. This is because only the total magnetization of the A or B spins is observable at a given time; for example the total transverse magnetization of the B-spins:

$$\underline{M}_{xy}^{tot}(B) = \underline{M}_{xy}^{13} + \underline{M}_{xy}^{24} \qquad 3.18$$

This vector, when represented as a complex number, is proportional

to the trace of the off-diagonal submatrix $[\sigma_{13}]$:

$$M_{xy}^{tot}(B) = \gamma_B(\sigma_{13}+\sigma_{24}) = \gamma_B Tr[\sigma_{13}] \qquad 3.19$$

and as usual this trace is unaffected during the rotation (compare eqn. 2.69). Physically this means that the total B-magnetization is constrained to be unchanged (in both magnitude and direction) on pulsing the A-system, which is reasonable. Nevertheless, the individual components of B-magnetization may change, and this is expressed in the variation of the difference magnetization z_A of equation 3.17.

(ii) Secondly, the vector $\underline{v}_A$ has the unusual property that each of its three Cartesian components is a complex number. This in sharp contrast to classical magnetization vectors, whose Cartesian components are of course real. This property emphasizes the strictly non-physical representation of Figure 3.4, and originates from the Hermicity of the complete density matrix. In general Hermitian matrices have real expectation values, whilst non-Hermitian matrices will give complex or imaginary expectation values. On examination, only the diagonal submatrices $[\sigma_{11}]$ and $[\sigma_{33}]$ are Hermitian. The off-diagonal submatrices $[\sigma_{13}]$ and $[\sigma_{31}]$ are non-Hermitian and therefore the Cartesian components of the vector $\underline{v}_A$ are complex quantities.

Now since complex numbers may be thought of as a representation of a point in a two-dimensional space, it is clear that the vector of Figure 3.4, which has three components, that may all be independent complex numbers, is actually a representation of a

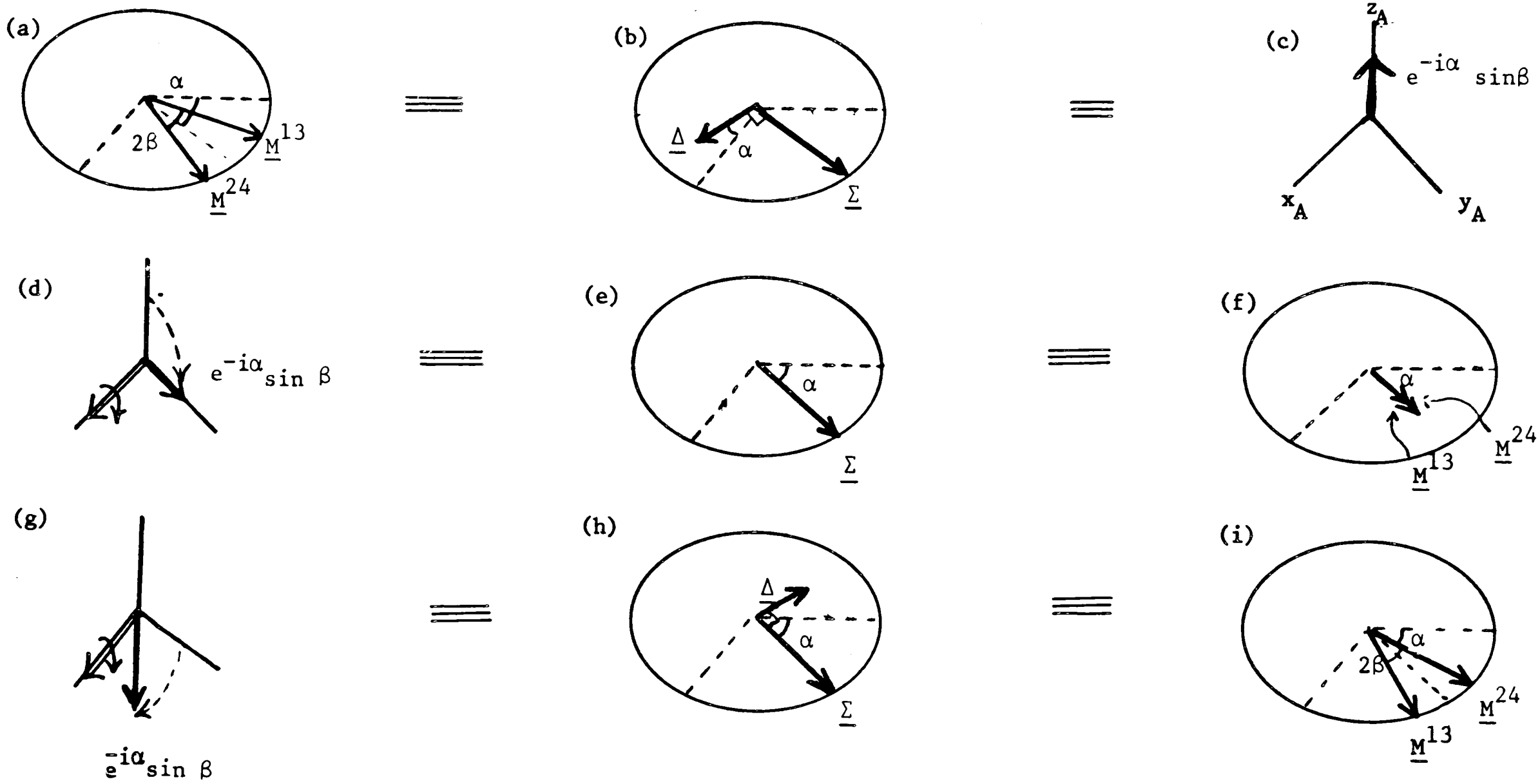

Fig.3.5. (a) Initial B magnetizations. (b) The equivalent sum vector $\underline{\Sigma}$ and difference vector $\underline{\Delta}$. (c) The representation of $\underline{\Delta}$ in the ZDQ frame. (d) Rotation of the vector in the ZDQ frame by the action of a $\pi/2$ pulse to the A spins. (e) This rotation has destroyed $\underline{\Delta}$ so that the modified components of transverse B magnetization are as in (f). (g) Further rotation in the ZDQ frame results in an overall inversion of the z-component. This is equivalent to reversing the difference vector $\underline{\Delta}$ (h). The overall result is an interchange of $\underline{M}^{13}$ and $\underline{M}^{24}$ (i).

of a vector in a six-dimensional space. This leads to some unusual properties as will be seen later.

Despite these rather daunting hidden complexities, ZDQ vectors are actually quite simple to use, as is readily illustrated by a simple application.

Consider the effect of applying a pulse to the A-spins on the rather general B-magnetization of Figure 3.5(a). The two components of transverse B magnetization $\underline{M}_{xy}^{13}$ and $\underline{M}_{xy}^{24}$ have been prepared each with intensity $\frac{1}{2}\gamma$ but differing in phase by an arbitrary angle 2β in the xy plane. For convenience their mean phase in the xy plane is denoted as $(\frac{\pi}{2} - \alpha)$.

To calculate the effect on the B-magnetization components when an A-pulse is applied, the sum vector $\underline{\Sigma}$ and the difference vector $\underline{\Delta}$ of the two transverse magnetization components is required. These may be calculated by simple trigonometry and are represented in Figure 3.5(b).

$$\underline{\Sigma} = \underline{M}_{xy}^{24} + \underline{M}_{xy}^{13}$$

$$\text{and} \qquad \underline{\Delta} = \underline{M}_{xy}^{24} - \underline{M}_{xy}^{13} \qquad 3.20$$

As discussed above, the sum vector $\underline{\Sigma}$ is unaffected by pulses applied to the A spins, whilst the difference vector may be represented as a z-component in the ZDQ frame, and may thus be rotated about the pulse field. $\underline{\Delta}$ should first be written as a complex number, thus

$$\Delta = \frac{1}{2}\gamma i\, e^{i(\beta-\alpha)} - \frac{1}{2}\gamma e^{-i(\beta+\alpha)}$$

$$= \frac{1}{2}\gamma e^{-i\alpha}\sin\beta \qquad 3.21$$

then $$z_A = e^{i\alpha}\sin\beta \qquad 3.22$$

This representation is given in Figure 3.5(c). Note that diagrams 3.5(a-c) are each completely equivalent representations of the same initial state of B transverse magnetization. However representation (c) is the one appropriate for discussion of the influence of pulses, applied to the A spins, on B magnetization components.

If a $\pi/2$ pulse is now applied to the A spins (the axis is not important), the vector of Figure 3.5(c) is rotated away from the z-axis into the transverse plane, where as we have seen it indicates non-zero zero- and double-quantum coherence. The z-component, now being zero (Figure 3.5(d)) indicates that the B-magnetization difference vector $\underline{\Delta}$ has been set to zero, whilst the sum vector $\underline{\Sigma}$ remains unchanged (Figure 3.5(e)). The new values of $\underline{M}_{xy}^{24}$ and $\underline{M}_{xy}^{13}$ may be recalculated from equations 3.20 , revealing that the two vectors have now assumed the same, mean, phase angle, but with intensities reduced by a factor $\cos\beta$. Incidentally, if the components of B magnetization had initially been prepared in an antiparallel state, so that β were $\pi/2$ radians, all B magnetization would be destroyed at this point, having been completely converted into zero- and double-quantum coherence.

The argument can be extended by applying a second $\pi/2$ pulse to the A system, as in Figure 3.5(g). In all this is equivalent to a π pulse, and the overall effect becomes evident. The inversion of the z-component in the ZDQ frame is equivalent to reversing the sign of the difference vector $\underline{\Delta}$, which is in turn the same as interchanging the positions of $\underline{M}_{xy}^{13}$ and $\underline{M}_{xy}^{24}$ in Figure 3.5(a). This is indeed the observed effect (often called 'interchange of spin labels') and is well-known. Note again, that if β were $\pi/2$ radians, all B-magnetization would be destroyed by the first $\pi/2$ pulse to the A-spins, but would then appear to be resurrected from nowhere by the second pulse. This is the problem mentioned in the introduction to this chapter and is inexplicable on the basis of conventional magnetization vector pictures. In contrast the ZDQ vector picture offers a simple explanation: The total transverse magnetization vector of the B-spins, $\underline{\Sigma}$, is immune to manipulations of the A-spin system, but the difference vector, $\underline{\Delta}$, between the components of B-spin magnetization is inter-converted with zero- and double-quantum coherence by the action of the pulse. Hence the two components of B-magnetization, given by

$$\underline{M}_{xy}^{24} = \frac{1}{2}(\underline{\Delta} + \underline{\Sigma})$$
$$\underline{M}_{xy}^{13} = \frac{1}{2}(\underline{\Sigma} - \underline{\Delta}) \qquad 3.23$$

assume a range of magnitudes and directions between the extremes of Figures 3.5(a) and (i).

PULSES TO THE A SPINS

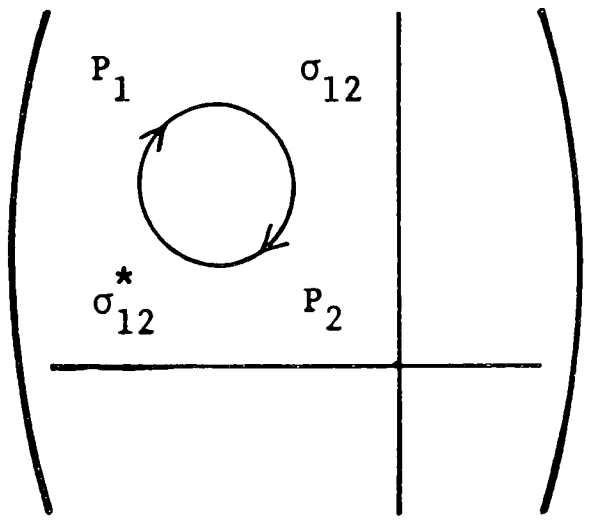

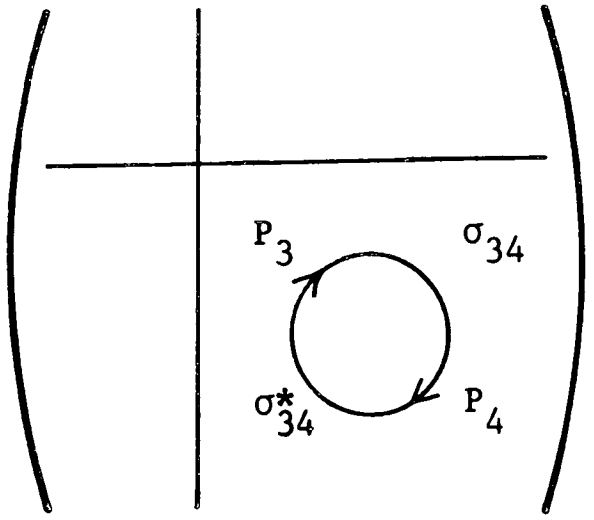

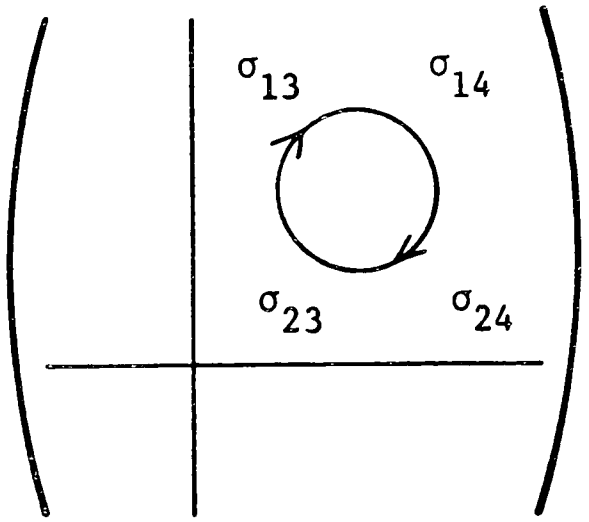

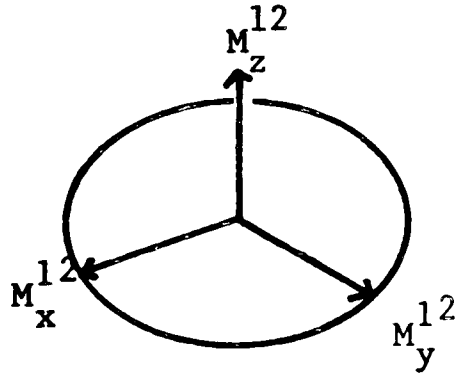

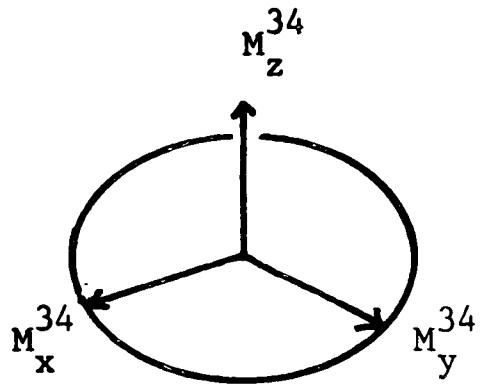

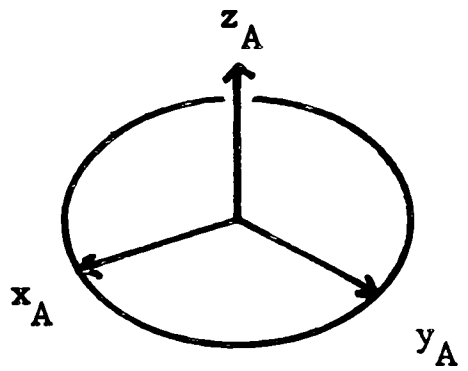

$(1/\gamma_A)M_z^{12} = \frac{1}{2}(P_1 - P_2)$

$(1/\gamma_A)M_x^{12} = \text{Re}\ \sigma_{12} = \frac{1}{2}(\sigma_{12}+\sigma_{12}^*)$

$(1/\gamma_A)M_y^{12} = \text{Im}\ \sigma_{12} = \frac{1}{2i}(\sigma_{12}-\sigma_{12}^*)$

$(1/\gamma_A)M_z^{34} = \frac{1}{2}(P_4 - P_3)$

$(1/\gamma_A)M_x^{34} = \text{Re}\ \sigma_{34} = \frac{1}{2}(\sigma_{34}+ \sigma_{34}^*)$

$(1/\gamma_A)M_y^{34} = \text{Im}\ \sigma_{34} = \frac{1}{2i}(\sigma_{34}- \sigma_{34}^*)$

AZDQ FRAME

$z_A = \frac{1}{2}(\sigma_{24} - \sigma_{13})$

$x_A = \frac{1}{2}(\sigma_{14} + \sigma_{23})$

$y_A = \frac{1}{2i}(\sigma_{14} - \sigma_{23})$

Fig.3.6(a) Reference frames used when pulsing the A spins.

PULSES TO THE B SPINS

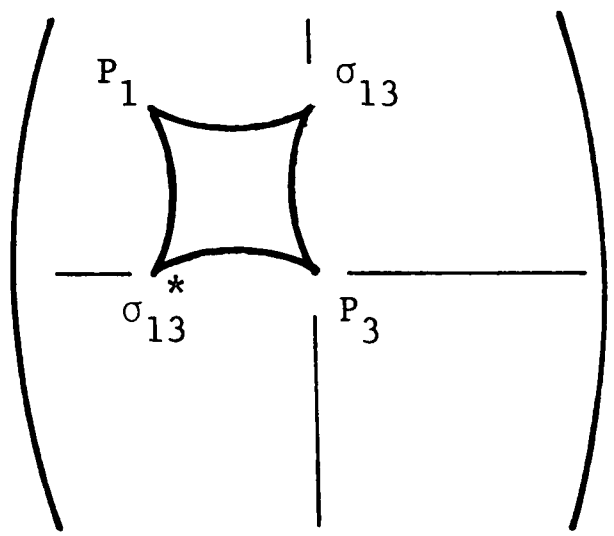

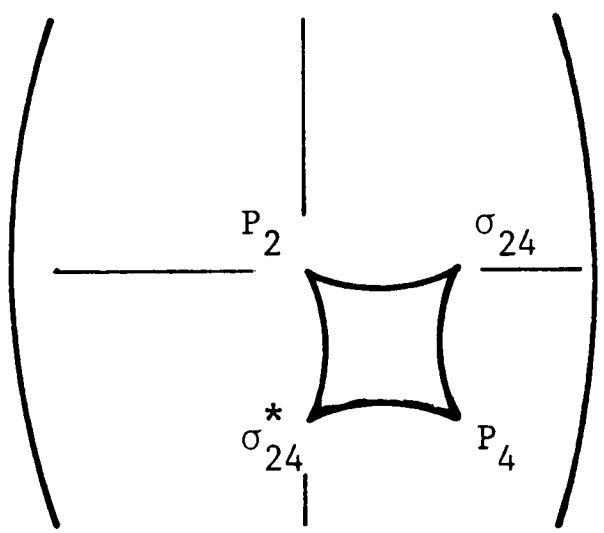

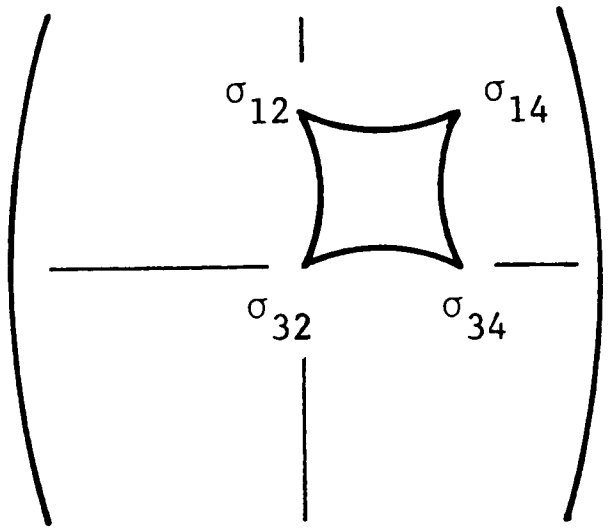

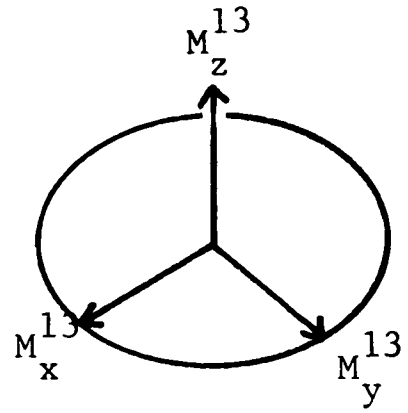

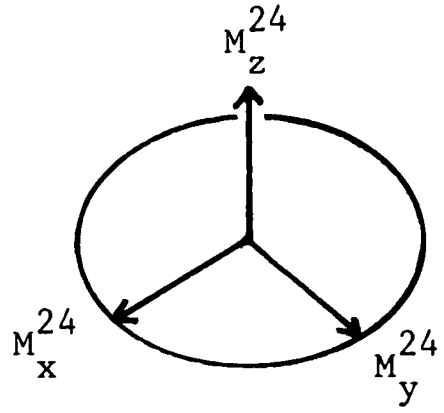

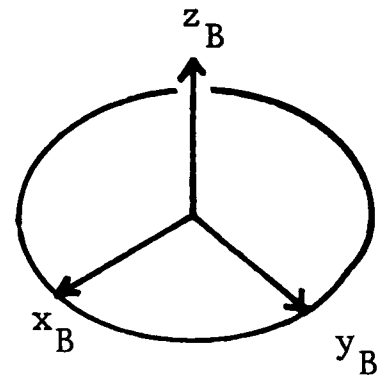

$(1/\gamma_B)M_z^{13} = \frac{1}{2}(P_3 - P_1)$

$(1/\gamma_B)M_x^{13} = \text{Re } \sigma_{13} = \frac{1}{2}(\sigma_{13} + \sigma_{13}^*)$

$(1/\gamma_B)M_y^{13} = \text{Im } \sigma_{13} = \frac{1}{2i}(\sigma_{13} - \sigma_{13}^*)$

$(1/\gamma_B)M_z^{24} = \frac{1}{2}(P_4 - P_2)$

$(1/\gamma_B)M_x^{24} = \text{Re } \sigma_{24} = \frac{1}{2}(\sigma_{24} + \sigma_{24}^*)$

$(1/\gamma_B)M_y^{24} = \text{Im } \sigma_{24} = \frac{1}{2i}(\sigma_{24} - \sigma_{24}^*)$

BZDQ FRAME

$z_B = \frac{1}{2}(\sigma_{34} - \sigma_{12})$

$x_B = \frac{1}{2}(\sigma_{14} + \sigma_{32})$

$y_B = \frac{1}{2i}(\sigma_{14} - \sigma_{32})$

Fig.3.6(b) Reference frames used when pulsing the B spins.

3.4 'Conjugate Frames'

It is not difficult to extend the submatrix treatment given above to include pulses applied to the B-spins. The density matrix is again divided into four 2 x 2 submatrices, and each of these submatrices is associated with a vector which rotates about the B pulse field. However the elements contained in each of the four submatrices differ in the two applications, as illustrated in Figure 3.6. This is because the density matrix is now partitioned in such a way that elements linked by a B transition, rather than an A transition, are joined.

The three extra frames created by this process are displayed in Figure 3.6(b). As in the above section, there are now two Bloch-type frames corresponding to the two diagonal submatrices and which are concerned with the ordinary magnetizations $\underline{M}^{13}$ and $\underline{M}^{24}$ of the allowed B transitions. As is familiar, a pulse applied to the B spins interconverts the longitudinal and transverse magnetizations of these two transitions. The third frame, labelled the B zero- and double-quantum frame (BZDQ) is appropriate for treatment of the effect of B pulses on A transverse magnetizations - the exact reverse of the discussion above. Identical manipulations may be performed using this frame as were previously demonstrated for the AZDQ frame.

Now it is important to realise that the six Cartesian frames of Figure 3.6 are not as independent as this diagram appears to indicate. They are implicitly connected, because the same density matrix elements always appear in the Cartesian coordinates of vectors in

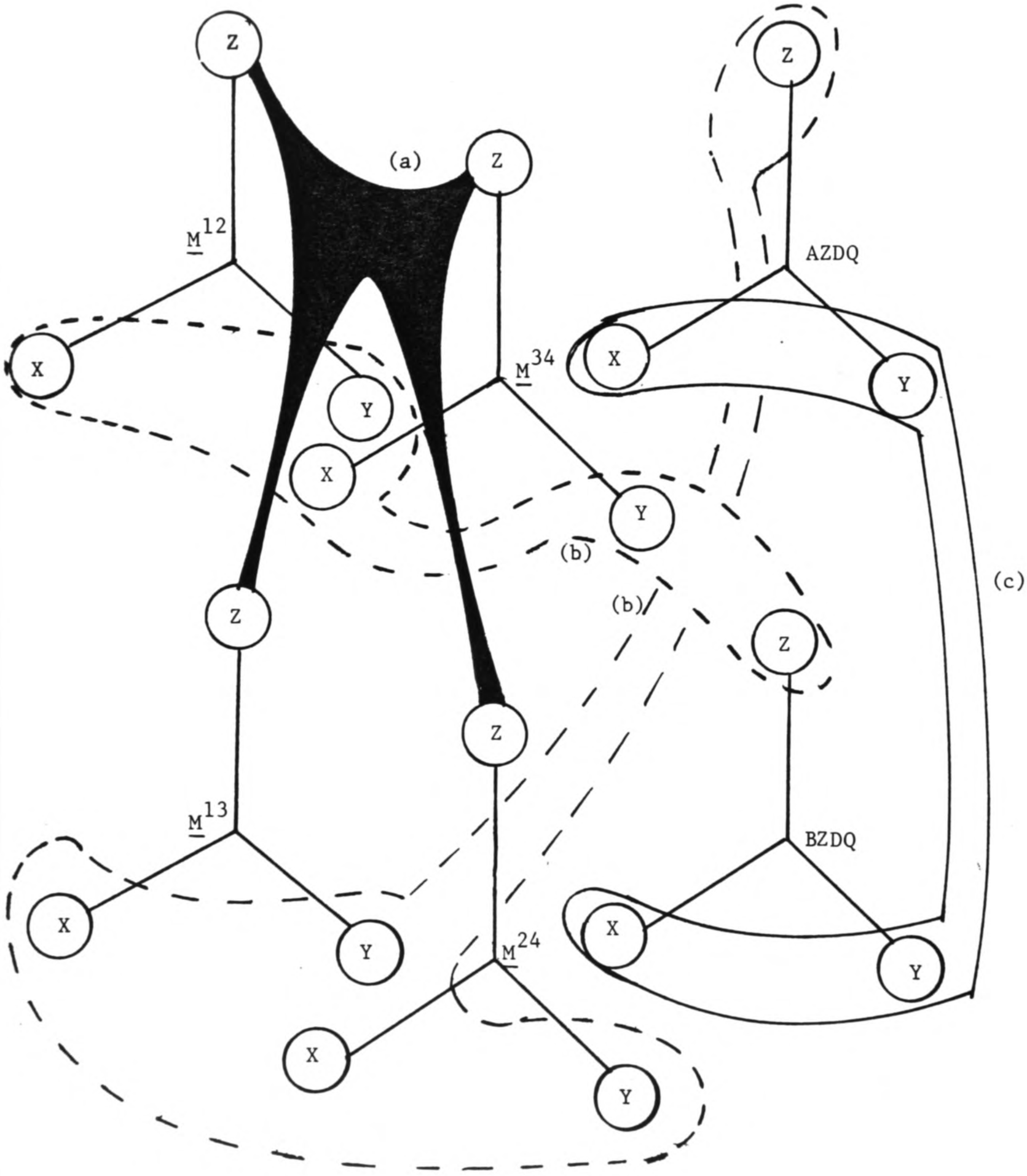

Fig.3.7. The connectivity of the six reference frames.

at least two separate frames. For example, the diagonal density matrix element P_1 participates in the z-components of the $\underline{M}^{12}$ as well as the $\underline{M}^{13}$ frame. This connectivity gives rise to familiar effects. Perturbation of the longitudinal magnetizations of one set of transitions may also affect the longitudinal magnetizations of a different but connected set of transitions. These effects are easily analysed and suffice it to say that such possibilities should not be overlooked when predicting the result of a given pulse sequence. This type of connectivity is indicated symbolically by the shape (a) in Figure 3.7.

A further connection between the frames has also been analysed in some detail and corresponds to the loops (b) of Figure 3.7. This is the relationship between the transverse magnetization components of the B spins with the z-component of the AZDQ frame, and vice versa. The difference vector between the two components of transverse magnetization of the B spins, when expressed as a complex number, becomes the z-component of the AZDQ vector, and thus may be rotated by pulses applied to the A spins.

The third connection between the frames, indicated (c), is between the transverse planes of the two ZDQ frames. Examination of the elements indicated in Figure 3.6 shows that the x and y coordinates of a vector in these frames share the matrix elements σ_{14} and σ_{23}, or their complex conjugates. Hence a vector in the transverse plane of the AZDQ frame must have some different vector representation in the BZDQ frame, although this representation is not immediately obvious.

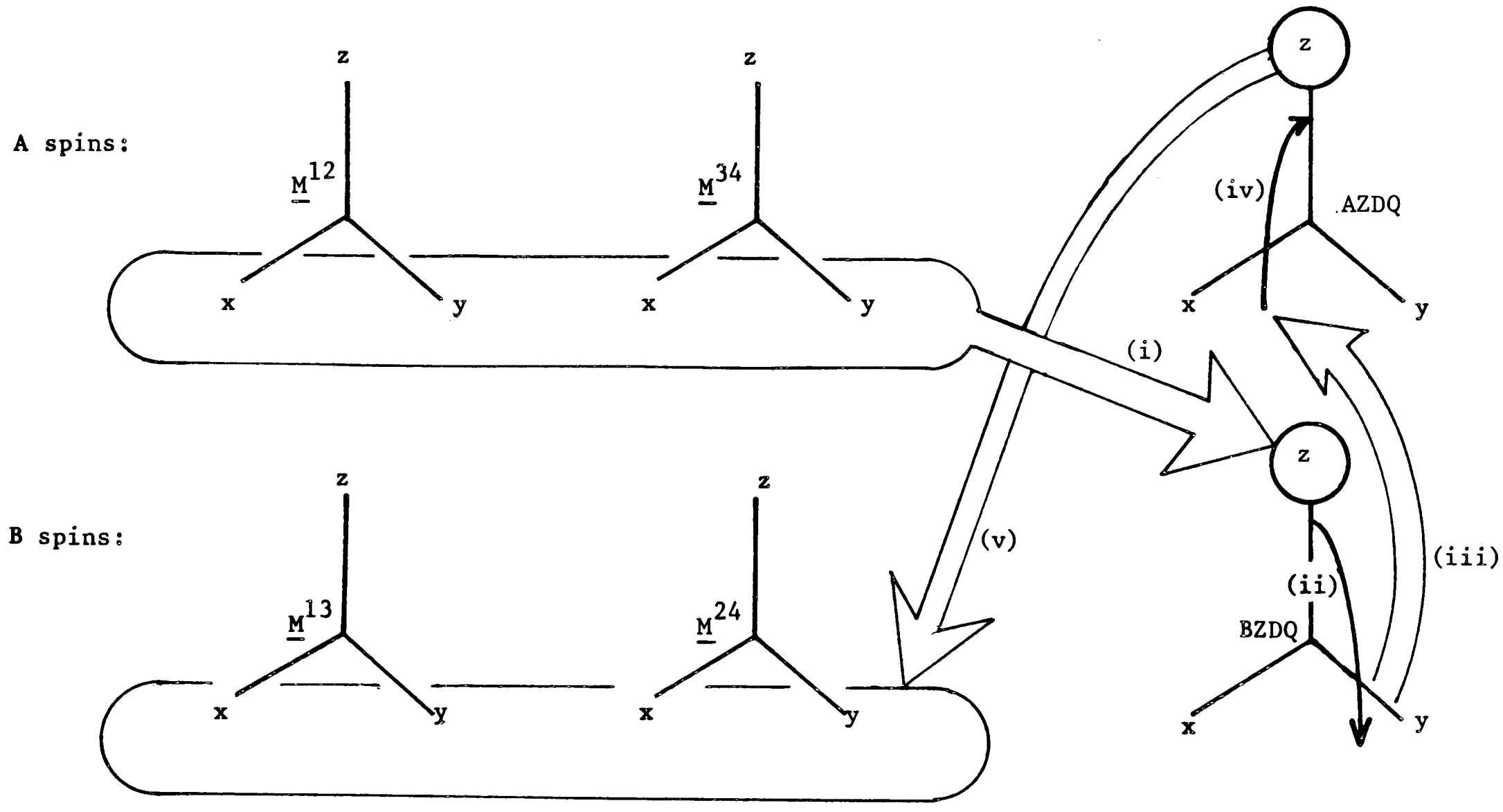

Fig.3.8 A mechanism for transfer of magnetization from the A spins to the B spins.

This type of connectivity gives rise to certain interesting possibilities, such as coherence transfer. For example, it may be desired for some reason to transfer transverse magnetization from the A spin system into the B spin system by means of some pulse sequence. The connection between the transverse planes of the ZDQ frames can then be used as a way of doing this. A possible mechanism might be:

(i) Transverse A-magnetization is prepared such that it represents a vector z_B in the BZDQ frame. (Connection (b)).

(ii) This vector is rotated into the transverse plane of the BZDQ frame by applying a $\pi/2$ pulse to the B spins.

(iii) The transverse vector in the BZDQ frame must have some equivalent representation as vector in the transverse plane of the AZDQ frame (connection (c)).

(iv) The transverse vector in the AZDQ frame is rotated to the z-axis of that frame by the action of a $\pi/2$ pulse, this time applied to the A spins, and

(v) This z-vector represents transverse magnetization components of the B spins (connection (b)).

Thus steps (i)-(iv) represent a means of transferring transverse magnetization from A to B spins, as indicated in Figure 3.8.

This full process is analysed in more detail shortly with reference to the INEPT pulse sequence (118) which does indeed follow this procedure. Firstly though, the transformation (iii), the

connection between the vectors in the two transverse ZDQ frames, must be discussed. If a geometrical relationship between the two vectors could be found, this would allow a pictorial representation of the processes (i)-(iv) without recourse to algebraic analysis. Fortunately the transformation required turns out to be quite easy to apply. It simply requires an interchange of the 'transverse' and 'imaginary' dimensions of the vector. This statement will now be clarified.

Firstly recall the unusual properties of a vector $\underline{v}$ in the transverse plane of a ZDQ frame. The position in the transverse plane is given by the equation

$$\underline{v}_A = \underline{i}\, x_A + \underline{j}\, y_A \qquad 3.24$$

remembering that the components x_A and y_A are complex numbers. (Here $\underline{i}$ and $\underline{j}$ represent unit vectors along the x and y axes). Take the simplified case in which the components x and y have the same phase α in the imaginary dimension, so

$$\begin{aligned} x_A &= |x_A| e^{i\alpha} \\ y_A &= |y_A| e^{i\alpha} \end{aligned} \qquad 3.25$$

The position of $\underline{v}_A$ in the transverse plane of this frame could also be expressed by using a transverse phase angle β such that

$$\begin{aligned} |x_A| &= |v| \cos\beta \\ \text{and} \qquad |y_A| &= |v| \sin\beta \end{aligned} \qquad 3.26$$

where

$$|x_A|^2 + |y_A|^2 = |v|^2 \qquad 3.27$$

Thus $\underline{v}_A$ can be expressed

$$\begin{aligned} x_A &= |v|e^{i\alpha}\cos\beta \\ y_A &= |v|e^{i\alpha}\sin\beta \end{aligned} \qquad 3.30$$

as shown in Figure 3.9(a).

It will now be shown that the transformation of this ZDQ vector into the BZDQ frame can easily be accomplished by interchanging the transverse and imaginary phase angles of the vector. i.e. interchanging the two angles α and β. The Cartesian components are identified as combinations of zero and double-quantum matrix elements according to equation 3.14:

$$\begin{aligned} x_A &= |v|e^{i\alpha}\cos\beta = \tfrac{1}{2}(\sigma_{14}+\sigma_{23}) \\ y_Z &= |v|e^{i\alpha}\sin\beta = \tfrac{1}{2i}(\sigma_{14}-\sigma_{23}) \end{aligned} \qquad 3.31$$

Accordingly σ_{23} and σ_{14} may be calculated:

$$\begin{aligned} \sigma_{14} &= x_A + iy_A = |v|e^{i(\alpha+\beta)} \\ \sigma_{23} &= x_A - iy_A = |v|e^{i(\alpha-\beta)} \end{aligned} \qquad 3.32$$

From this information the position of the vector in the BZDQ frame may be constructed:

(a)

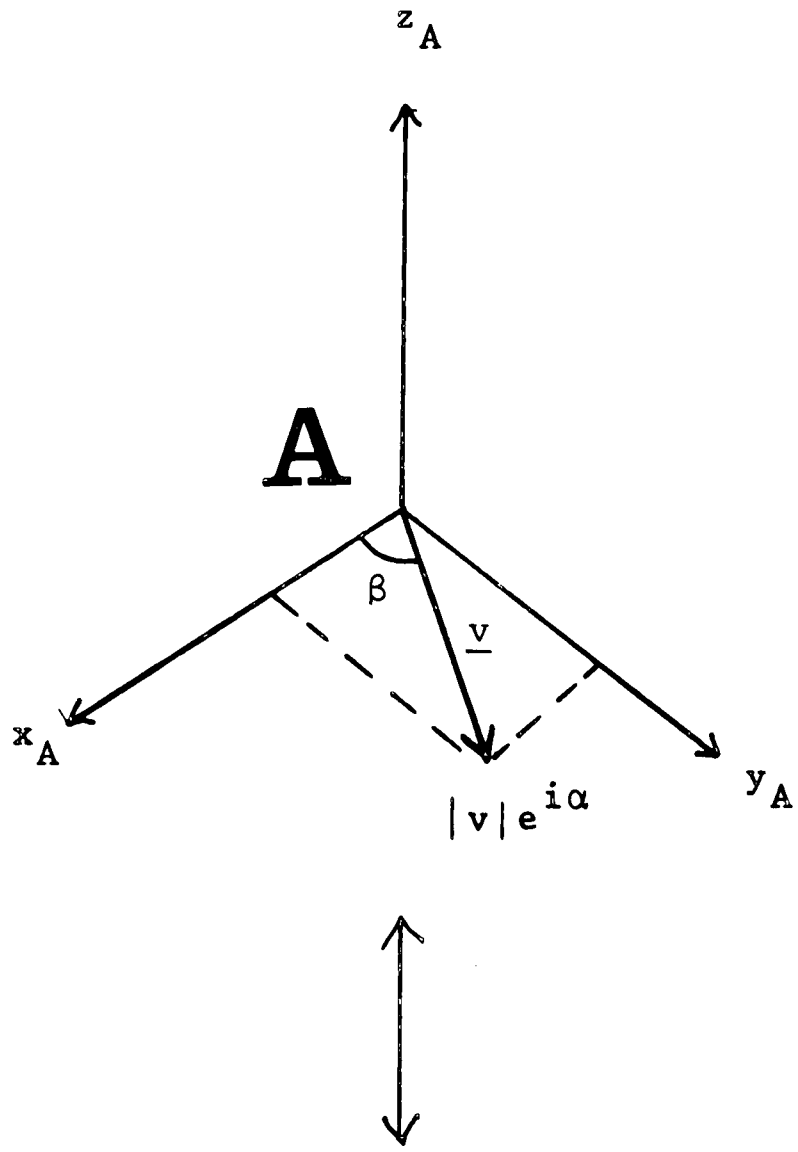

(b)

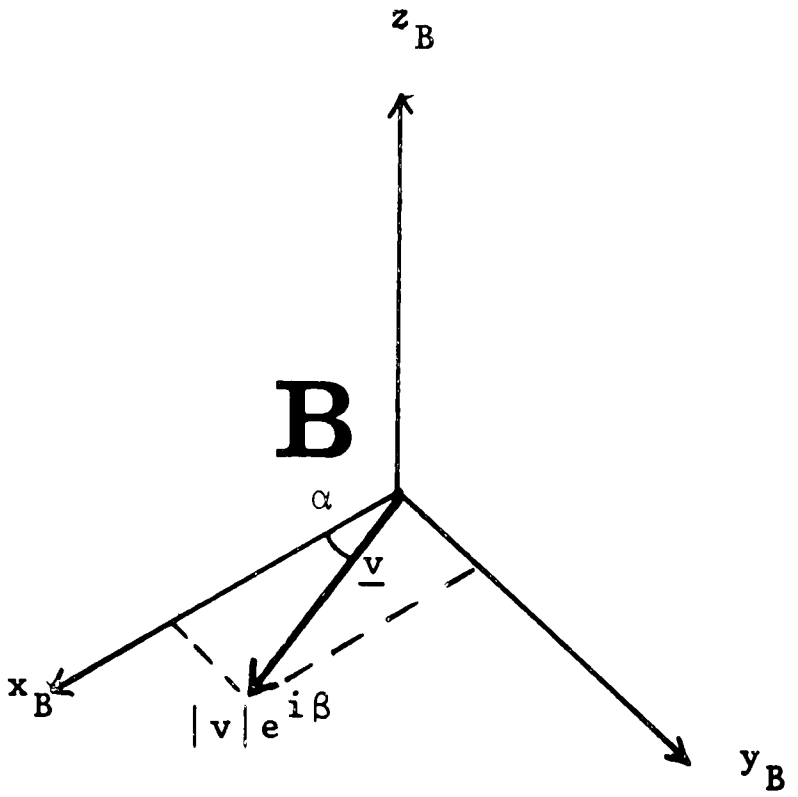

Fig.3.9. 'Conjugate transformation'.

$$x_B = \frac{1}{2}(\sigma_{14} + \sigma_{32}) = |v|e^{i\beta}\cos\alpha$$

and $$y_B = \frac{1}{2}(\sigma_{14} - \sigma_{32}) = |v|e^{i\beta}\sin\alpha \qquad 3.33$$

which corresponds to the diagram of Figure 3.9(b).

The diagrams Figures 3.9(a) and (b) have been linked by a double-headed arrow to indicate that they represent the same information. As has already been observed, the ZDQ frames are implicitly six-dimensional in nature, and the two three-dimensional Cartesian frames which are drawn are in fact projections of the six-dimensional information onto three-dimensional spaces. To our eyes there is no obvious symmetry transformation linking the two representations of Figs. 3.9(a) and (b). Similarly a three-dimensional object may look quite different when viewed from perpendicular directions in space. Nevertheless the transformation of the vector (a) $\leftrightarrow$ (b), consisting of the transposition of transverse and imaginary phases, is not so difficult to apply in practice. For the purposes of illustration some examples are given in Figure 3.10. A rather tentative nomenclature will be now used in which the interchange of transverse and imaginary phases is known as a 'conjugate transformation' of a vector between 'conjugate planes'.

This discussion completes all the links suggested in Figure 3.7. Connectivity in the AX system may be summarised:

(a) Connectivity of longitudinal magnetizations, because these are proportional to population differences across transitions which may share an energy level.

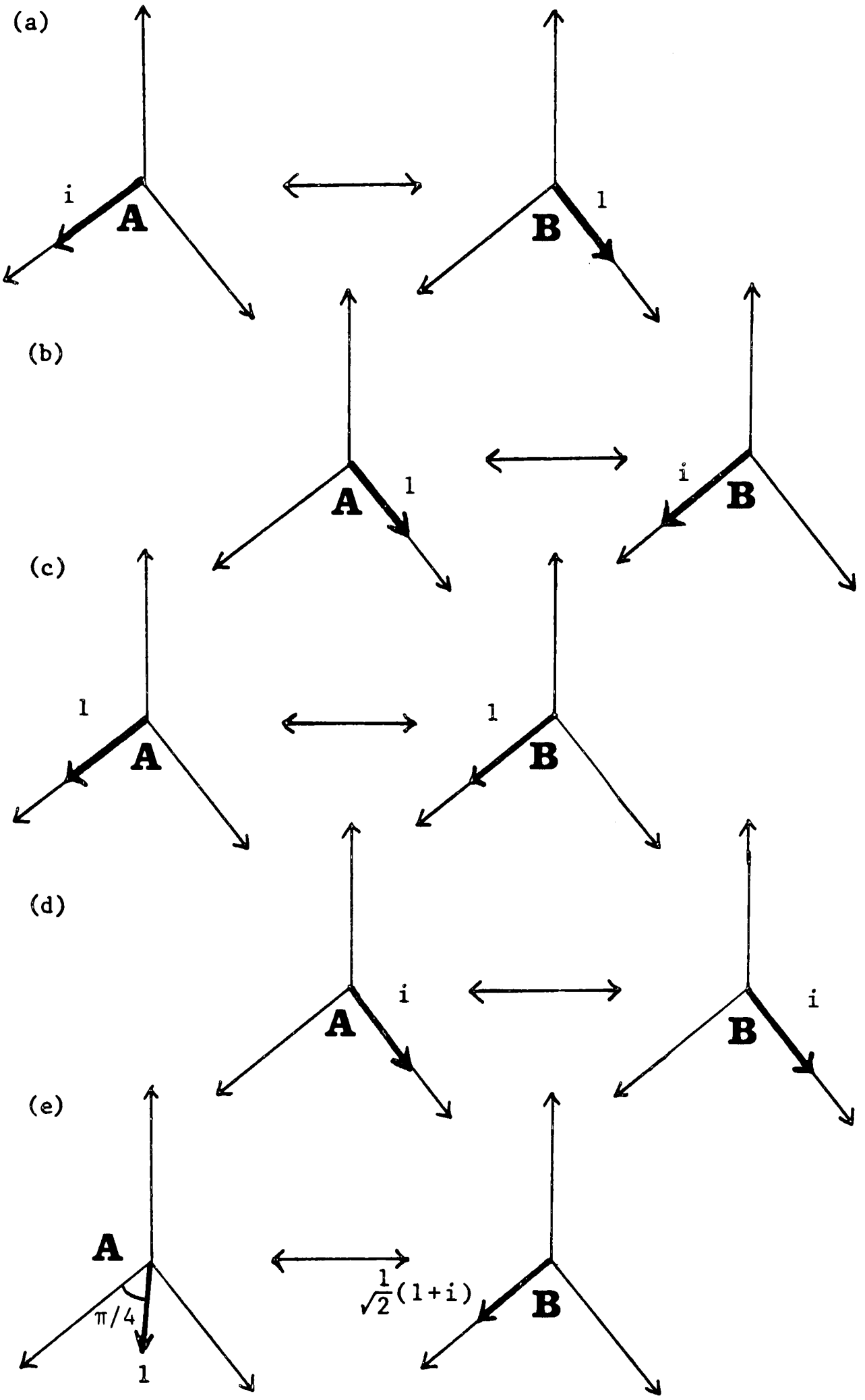

Fig.3.10. Some examples of 'conjugate transformation'.

(b) Connection of transverse magnetizations with the ZDQ frames. The difference vector between the two components of transverse magnetization of one set of spins, expressed as a complex number, becomes the z-component in the ZDQ frame of the other set of spins. Thus rotation in the ZDQ frame allows modification of the transverse magnetization components of one set of spins upon pulsing the other spin system.

(c) the connection between the 'transverse' and 'imaginary' dimensions of the two ZDQ frames, which are related by a 'conjugate transformation'.

3.5 Coherence Transfer

The general scheme suggested in Figure 3.8 for transfer of transverse magnetization from one spin system to another can now be analysed more fully.

For clarity reference will be made to a ^{13}C-^{1}H AX system, and the transfer process is conducted in the direction $^{1}H \rightarrow {}^{13}C$. The principles are however quite general for all AX systems.

Examine Figure 3.8, and consider the A spins to be the protons and the B spins carbon-13. The five-step process shown includes the application of two $\pi/2$ pulses, one to the carbon-13 spins (rotation (ii)), and one to the protons (rotation (iv)). It is clear that to enjoy maximum transfer of proton magnetizations into the carbon-13 system, the following conditions should be fulfilled:

(a) the proton transverse magnetization should be prepared such that the difference vector between the two components of transverse proton magnetization is of the greatest possible magnitude (since this becomes the z-component in the ^{13}C - ZDQ frame (step (i)). Accordingly, the two components should be prepared in an antiparallel state;
and (b) the pulse fields must be of the correct phase in order to accomplish the rotations to and from the z-axes of the ZDQ frames.

Note that if conditions (a) and (b) are fulfilled exactly, there is a full transfer of proton magnetization into carbon-13 magnetization. Because the magnetization produced may be represented as a z-vector in a ZDQ frame, the resultant carbon-13 magnetization appears as antiparallel components, just like the source proton magnetization.

A transfer scheme which fulfils all these conditions is the INEPT pulse sequence (118), which has proved to be a very useful method of enhancing the magnetizations of nuclei of small or negative gyromagnetic ratio such as carbon-13 or nitrogen-15 (119).
The source of magnetization is invariably the directly bonded protons which have a large gyromagnetic ratio and also relax quickly, furnishing a source of longitudinal magnetization of favourable magnitude and which is quickly replenished. The overall increase in sensitivity can be orders of magnitude for favourable cases such as ^{15}N.

The pulse sequence used is illustrated in Figure 3.11. The

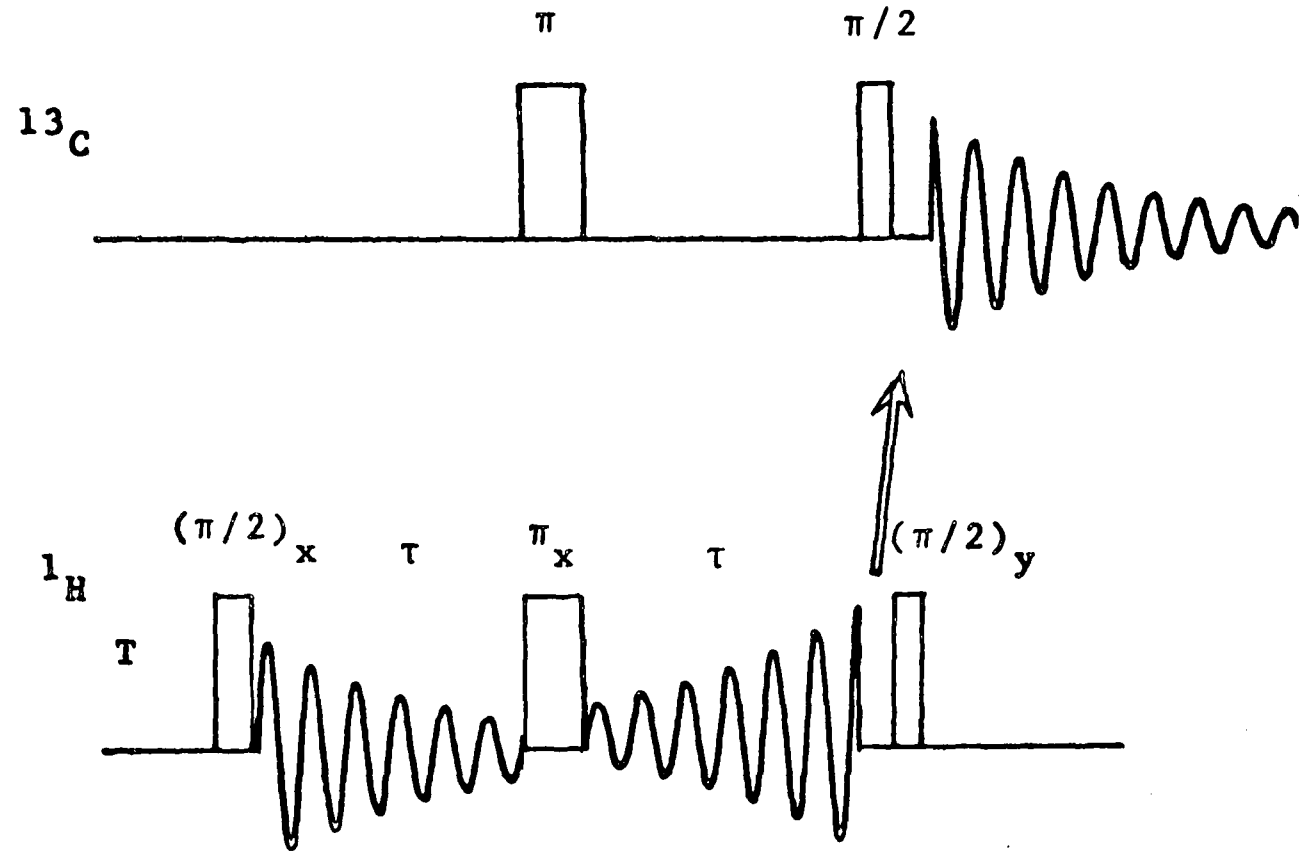

$$\tau = 1/(4J_{CH})$$

Fig.3.11. The INEPT pulse sequence for transfer of magnetization from protons to carbon-13.

experiment starts with the usual preparatory period T to allow full relaxation of the proton longitudinal magnetization ($T > 5T_{1H}$). Proton transverse magnetization is then created by a $\pi/2$ pulse and brought to a spin echo at a time 2τ by the $(\tau - \pi - \tau)$ sequence. The small number of protons which are coupled to carbon-13 spins possess two magnetization components which precess at different rates according to the state of the coupled carbon-13 spin (these give rise to the carbon-13 satellites in the normal proton spectrum). The introduction of a π carbon-13 pulse at the same time as the π proton refocussing pulse causes the phase divergence between these components to continue to evolve during the duration of the spin echo, and if τ is chosen such that $\tau = 1/4J$, at the time of the echo the components of transverse magnetization are antiparallel and along the x-axis of the proton rotating frame, as illustrated in Figure 3.12(a) (see Section 2.2). This fulfils condition (a) above and the proton transverse magnetization is now ready for the coherence transfer process.

There now follow two $\pi/2$ pulses applied to each of the carbon-13 and proton spin systems. If the pulses are short enough it is immaterial in which order they are applied. The case is taken here in which the carbon-13 pulse is deemed to precede slightly the proton pulse, although the opposite case can also be analysed (118). For simplicity it is also assumed that no carbon-13 magnetization exists at this time, so that all carbon-13 magnetization produced originates from the proton spins via the coherence transfer. A more general case would be easily treated. The condition of proton magnetization vectors at time 2τ is such that they are antiparallel

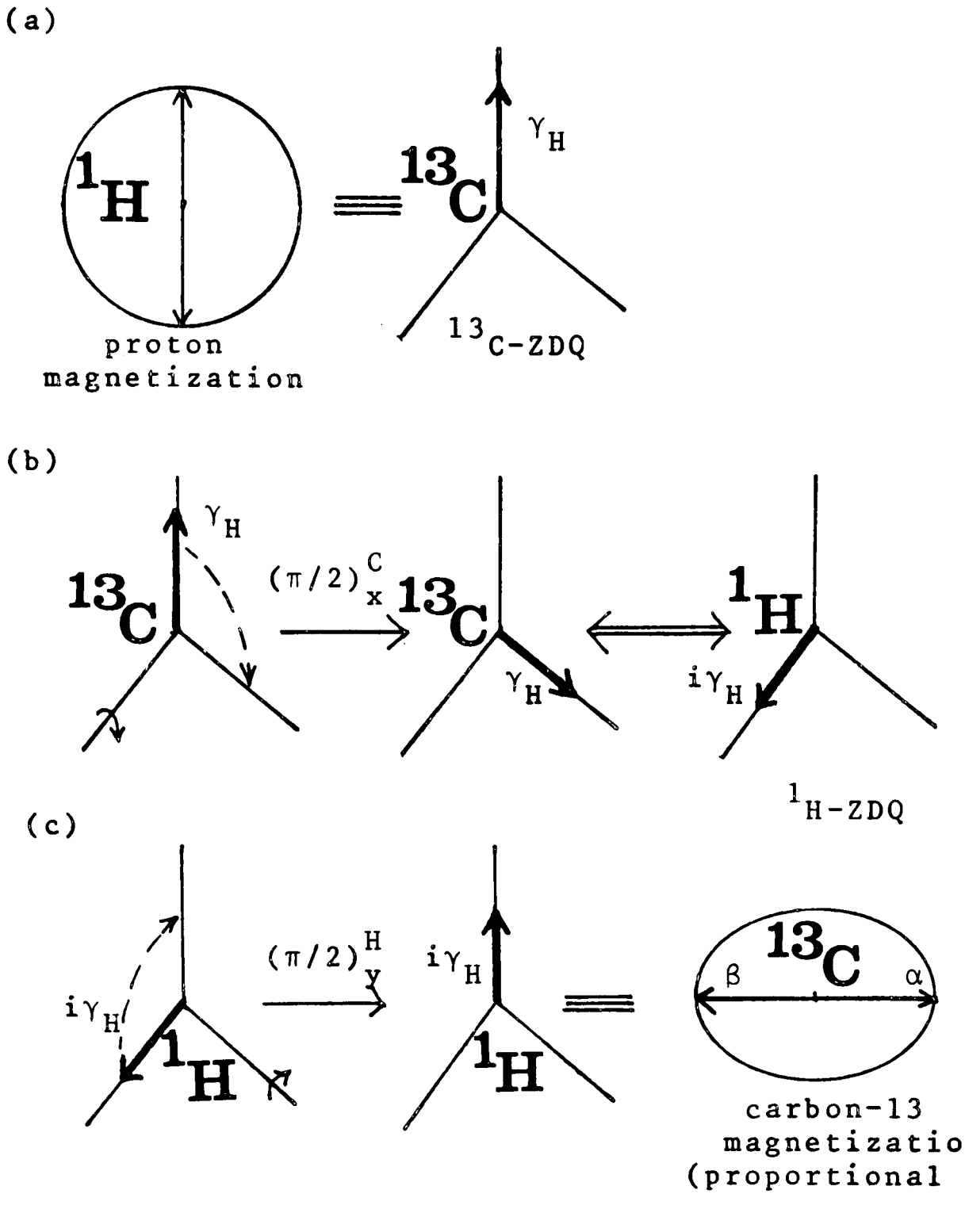

Fig.3.12 Coherence transfer in the INEPT pulse sequence.

(a) Antiparallel components of transverse proton magnetization are prepared by means of a modulated spin echo (compare Fig.2.5). This state may be represented by a real number of magnitude γ_H along the z-axis of the ^{13}C-ZDQ frame.

(b) This z-component is rotated into the transverse plane of the ^{13}C-ZDQ frame by the $\pi/2$ carbon-13 pulse. Therefore all proton transverse magnetization is converted into zero- and double-quantum coherence. The real number γ_H along the y-axis of the ^{13}C-ZDQ frame is equivalent, under 'conjugate transformation', to an imaginary number $i\gamma_H$ along the x-axis of the ^{1}H-ZDQ frame.

(c) The vector is now rotated to the z-axis of the ^{1}H-ZDQ frame by the $(\pi/2)_y^H$ pulse. Note that a phase shift of the proton reference signal is neccessary to accomplish the rotation. The complex number along the z-axis indicates antiparallel components of transverse ^{13}C magnetization along the y-axis, as illustrated.

along the $\pm x$ axis of the rotating reference frame. As this transverse magnetization originated from longitudinal proton magnetization, each vector is of a magnitude proportional to the proton gyromagnetic ratio γ_H, ignoring relaxation during 2τ. Thus the representation of the proton transverse magnetization is a vector along the z-axis of the carbon-13 ZDQ frame, of real value γ_H as shown in Figure 3.12(a). A $\pi/2$ ^{13}C pulse is now applied. This rotates this vector down into the transverse plane of the ^{13}C-ZDQ frame, as shown in Figure 3.12(b). At this time the proton transverse magnetization has been converted into zero- and double-quantum coherence. This coherence will now be converted into carbon-13 transverse magnetization by applying a $\pi/2$ proton pulse. To treat this the ZDQ vector must first be transformed from the transverse plane of the ^{13}C-ZDQ frame to the transverse plane of the ^{1}H-ZDQ frame, which is a 'conjugate transformation'. Applying this transformation to the vector of real value γ_H along the y-axis of the ^{13}C-ZDQ frame, it becomes a vector of imaginary value $i\gamma_H$ along the x-axis of the ^{1}H-ZDQ frame, as shown. The $\pi/2$ proton pulse may now be applied. To accomplish the rotation of the vector from the x-axis to the z-axis of the ^{1}H-ZDQ frame, it must be applied along the y-axis. This constitutes a phase shift of $\pi/2$ radians in the phase of the proton transmitter signal. The result of this phase-shifted $\pi/2$ proton pulse is a vector of imaginary value γ_H along the z-axis of the proton ZDQ frame, where it may be interpreted as components of transverse ^{13}C magnetization, lying in phase opposition along the y-axis of their rotating frame, as illustrated. Thus the overall effect of this sequence is to transfer magnetization from the protons to the carbon-13 spins, via

the scalar coupling interaction. This process greatly enhances the sensitivity of carbon-13 spectroscopy. The equilibrium proton longitudinal magnetization is of a much greater magnitude than the equilibrium carbon-13 magnetization, because of the ratio of gyromagnetic ratios, $\gamma_H/\gamma_C \simeq 4$. Furthermore the short relaxation times of the protons allow experiments to be repeated more quickly, with further increase in signal-to-noise per unit time. For ^{13}C the advantage to be gained over the conventional nuclear Overhauser enhancement is somewhat marginal, but for nuclei of negative gyromagnetic ratio such as ^{15}N, for which the nuclear Overhauser effect can be unfavourable, there are orders of magnitude in sensitivity to be gained (119).

It is beyond the scope of this work to describe other important applications of coherence transfer, some of which were mentioned in Chapter 1, section 3. It is used in a range of experiments in two-dimensional spectroscopy (39,60-65,120-121). All of these processes are fully described for the AX system by using the vector model presented here.

3.6 The Interaction Frame

The vector picture developed so far is actually only suitable for describing evolution of the spin system over infinitesimal time periods, such as during short, powerful radio-frequency pulses. It will now be generalised so that finite time periods may be treated. This will be seen to result in only a minor increase in complexity, and will allow discussion of the evolution of the density matrix during periods of free precession, or under the influence of long, off-resonance pulses. However an important assumption must

be made. Time periods cannot be treated which are long enough that the coupling term in the Hamiltonian has an appreciable effect. This excludes the case of pulses which are long and weak enough to be appreciably selective between the two transitions of one of the spin species. Such very selective pulses are known to give rise to some very strange effects in the AX system (111-113) and no explanation is offered here. In these cases resort must be made to single-transition operators (114-116).

Consider a rotating field of strength B_{1A}, angular frequency ω_A and phase ϕ applied to the A spins. Neglecting far off-resonance fields, the laboratory frame Hamiltonian is:

$$H^L = -I_{zA}\omega_A^{\,o} - I_{zB}\omega_B^{\,o} + J_{AB}I_{zA}I_{zB} - \gamma_A B_{1A} e^{iI_{zA}(\omega_A t+\phi)} I_{XA} e^{-iI_{zA}(\omega_A t+\phi)} \qquad 3.34$$

Off-diagonal elements of the coupling term $J\hat{\underline{I}}_A.\hat{\underline{I}}_B$ have also been neglected. The angular frequencies $\omega_i^{\,o}$ represent Larmor angular frequencies of the nuclear species i in the absence of coupling. $\hbar$ has been set to unity for simplicity.

The motion of the density matrix is most conveniently expressed in an interaction frame defined by the equation

$$H_o = -I_{zA}\omega_A - I_{zB}\omega_B \qquad 3.35$$

where ω_A and ω_B are reference frequencies for A and B spins respectively.

The density matrix is transformed into the interaction frame as follows:

$$\sigma = e^{iH_o t}\ \sigma^L\ e^{-iH_o t} \qquad 3.36$$

where σ^L is the laboratory frame density matrix. The appropriate interaction frame Hamiltonian H is given by:

$$H = e^{iH_o t}\ (H^L - H_o)\ e^{-iH_o t} \qquad 3.37$$

and may be evaluated as the time-independent expression:

$$H = -\Delta\omega_A I_{zA} - \Delta\omega_B I_{zB} + J_{AB} I_{zA} I_{zB} - \gamma_A B_{1A} e^{iI_{zA}\phi}\ I_{xA}\ e^{-iI_{zA}\phi} \qquad 3.38$$

where $\Delta\omega_i$ are the resonance offsets $\Delta\omega_i = \omega_i^o - \omega_i$.
The interaction frame density matrix now responds to this time-independent Hamiltonian with the equation of motion:

$$\sigma(t) = e^{-iHt}\ \sigma(0) e^{iHt} \qquad 3.39$$

Note that the interaction frame appears to rotate at different frequencies (the two transmitter reference frequencies) for the two nuclear species. In this way symmetry is preserved between the A and B spins.

Now the important assumption is made that the pulse field is strong enough not to be selective between the two transitions of the A spins, which allows neglect of the coupling terms in eqn. 3.38.

$$H \simeq -\Delta\omega_A I_{zA} - \Delta\omega_B I_{zB} - \gamma_A B_{1A} e^{iI_{zA}\phi} I_{XA} e^{-iI_{zA}\phi} \qquad 3.40$$

Hence H is now the sum of two commuting terms applied to the A and B spins independently. The motion of the density matrix can be expressed as a succession of a rotation of the A spins about the A pulse field, with an independent precession of the B spins:

$$\sigma(t) = e^{-iH_A t} e^{-iH_B t} \sigma(o) e^{iH_B t} e^{iH_A t} \qquad 3.41$$

$$H_B = -\Delta\omega_B I_{zB} \qquad 3.42$$

$$H_A = -\Delta\omega_A I_{zA} - \gamma_A B_{1A} e^{iI_{zA}\phi} I_{xA} e^{-iI_{zA}\phi} \qquad 3.43$$

Now each of the submatrices of σ has its own vector representation. The effect of this double evolution on each submatrix vector will now be examined. To do this the operators must be constructed which generate the Cartesian components of each of these vectors. For example, the operator I_{xA} can be used to present the total x-magnetization of the A spins, in that:

$$< M_{xA} > \propto Tr(\sigma I_{xA}) \qquad 3.44$$

If however only the x-magnetization of the 12 transition is required, a new operator I_{xA}^{12} must be found such that

$$<M_{xA}^{12}> \propto Tr(\sigma I_{xA}^{12}) \qquad 3.45$$

This operator may be deduced to be:

$$I_{xA}^{12} = \frac{1}{2}I_{xA} + I_{xA}I_{zB} \qquad 3.46$$

and in general the three operators which generate the three Cartesian components of magnetization of the 1-2 transition are:

$$I_{\nu A}^{12} = \frac{1}{2}I_{\nu A} + I_{\nu A}I_{zB} \qquad 3.47$$

where the subscript ν takes the values x, y and z.

The expectation values for these three components are:

$$\langle M_{\nu A}^{12} \rangle = \gamma \mathrm{Tr}(\sigma I_{\nu A}^{12}) \qquad 3.48$$

Similarly, for the other transition of the A spins, the 3-4 transition,

$$I_{\nu A}^{34} = \frac{1}{2}I_{\nu A} - I_{\nu A}I_{zB} \qquad 3.49$$

and for the two B-spin transitions:

$$I_{\nu B}^{13} = \frac{1}{2}I_{\nu B} + I_{\nu B}I_{zA} \qquad 3.50$$

$$I_{\nu B}^{34} = \frac{1}{2}I_{\nu B} - I_{\nu B}I_{zA} \qquad 3.51$$

It is now of interest to calculate the effect on expectation values of these operators on allowing the density matrix to evolve according to equation 3.41. Accordingly the calculation is made:

$$\langle M_{\nu A}^{12}\rangle^{+} = \gamma Tr\{e^{-iH_A t}\, e^{-iH_B t}\, \sigma(o)\, e^{iH_B t}\, e^{iH_A t}\, (\tfrac{1}{2}I_{\nu A} + I_{\nu A} I_{zB})\} \quad 3.52$$

$$= \gamma Tr\{\, \sigma(o)\, e^{iH_A t}\, e^{iH_B t}\, (\tfrac{1}{2}I_{\nu A} + I_{\nu A} I_{zB})\, e^{-iH_B t}\, e^{-iH_A t}\,\} \quad 3.53$$

since H_B commutes with I_{zB}, (equation 3.42) this may be written:

$$\langle M_{\nu A}^{12}\rangle^{+} = \gamma Tr\{\sigma(o) I_{\mu A}^{12}\} = \langle M_{\mu A}^{12}\rangle^{-} \quad 3.54$$

where I_μ is a rotated form of I_ν :

$$I_\mu = e^{iH_A t}\, I_\nu\, e^{-iH_A t} \quad 3.55$$

In other words, the three Cartesian components of magnetization of the 12 transition are rotated about the A pulse field, without interconversion with the magnetizations of other transitions. The rotation may be about a tilted effective field if the pulse were applied significantly off-resonance. Similar considerations apply to the magnetization of the 34 transition.

A rather more sophisticated treatment is necessary when the Cartesian components of the vectors associated with an off-diagonal submatrix are considered. The Cartesian components are again expectation values of operators, but in this case the operators are not Hermitian. Thus for the Cartesian components x_A,y_A and z_A of the vector in the AZDQ frame, the operators may be found to be:

$$I_{\nu}^{(AZDQ)} = I_{B+}I_{\nu A} \qquad 3.56$$

where the 'shift operator' I_{B+} is given by

$$I_{B+} = I_{xB} + iI_{yB} \qquad 3.57$$

It may be verified that the expectation values of this set of operators are indeed the expressions previously deduced and used:

$$\langle x_A \rangle = Tr[I_x^{(AZDQ)}\sigma] = Tr[I_{B+}I_{xA}\sigma] = \frac{1}{2}(\sigma_{23}+\sigma_{14}) \qquad 3.58$$

$$\langle y_A \rangle = Tr[I_y^{(AZDQ)}\sigma] = Tr[I_{B+}I_{yA}\sigma] = \frac{1}{2i}(\sigma_{23}-\sigma_{14}) \qquad 3.59$$

$$\langle z_A \rangle = Tr[I_y^{(AZDQ)}\sigma] = Tr[I_{B+}I_{zA}\sigma] = \frac{1}{2}(\sigma_{13}-\sigma_{24}) \qquad 3.60$$

Similarly the operators for the components of the vector in the BZDQ frame are

$$I_{\nu}^{(BZDQ)} = I_{A+}I_{\nu B} \qquad 3.61$$

where

$$I_{A+} = I_{xA} + iI_{yA} \qquad 3.62$$

These operators are also non-Hermitian.

Note that this operator representation expresses the 'conjugate frame' relationship rather concisely - the operators concerned with the transverse planes of the AZDQ and BZDQ frames being connected by the relationship:

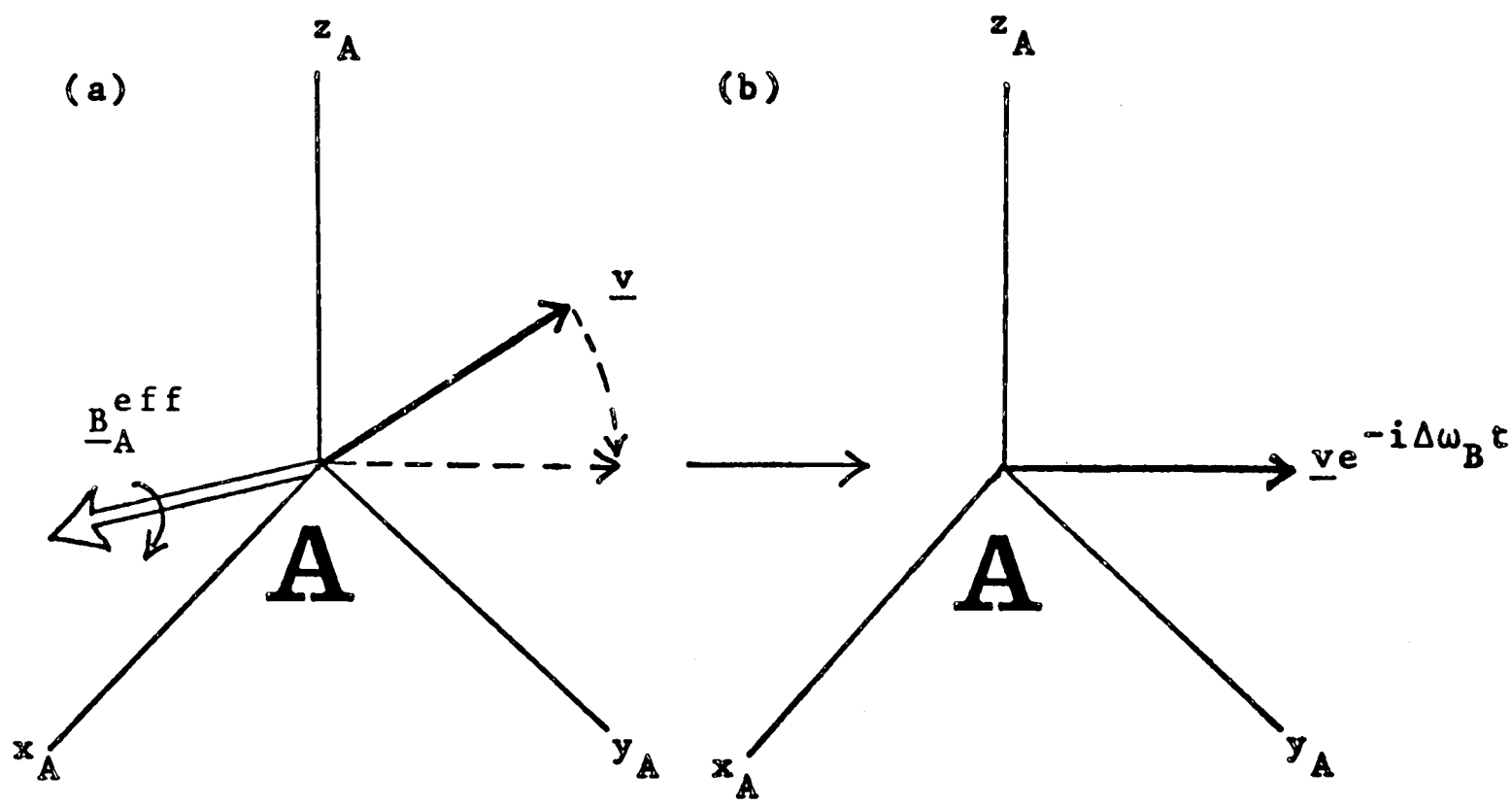

Fig.3.13. Rotation of a vector $\underline{v}$ in the AZDQ frame about a tilted effective field $\underline{B}_A^{eff}$. Evolution has also occurred in the 'conjugate frame' leading to an additional factor $\exp(-i\Delta\omega_B t)$.

$$I_x^{(AZDQ)} + iI_y^{(AZDQ)} = I_x^{(BZDQ)} + iI_y^{(BZDQ)}. \qquad 3.63$$

$I_\nu^{(AZDQ)}$ and $I_\nu^{(BZDQ)}$ can now be used to study the effect of a pulse on the ZDQ vectors, just as was done above for transition magnetizations.

For the AZDQ vector:

$$\langle I_\nu^{(AZDQ)} \rangle^+ = \gamma Tr\{e^{-iH(A)t}\, e^{-iH(B)t}\, \sigma(0) e^{iH(B)t} e^{iH(A)t} I_{B+} I_{\nu A}\} \qquad 3.64$$

$$= \gamma Tr\{\sigma(0)(e^{iH(A)t} I_{\nu A} e^{-iH(A)t})(e^{iH(B)t} I_{B+} e^{-iH(B)t})\} \qquad 3.65$$

The end result has two parts; the effect of exp(iH(A)t) on the component $I_{\nu A}$, and that of the rotation exp(iH(B)t) on the shift operator I_{B+}. Now exp(iH(A)t) acts as usual on $I_{\nu A}$ so as to rotate it into a new position $I_{\mu A}$. But this time H(B) does not commute with I_{B+} so this part must also be evaluated. The result is:

$$e^{iH(B)t} I_{B+} e^{-iH(B)t} = e^{-i\Delta\omega_B I_{zB} t} (I_{xB} + iI_{yB}) e^{i\Delta\omega_B I_{zB} t} \qquad 3.66$$

$$= e^{-i\Delta\omega_B t} I_{B+} \qquad 3.67$$

Therefore the total rotation becomes:

$$(I_\nu^{(AZDQ)})^+ = e^{-i\Delta\omega_B t} I_\mu^{(AZDQ)} \qquad 3.68$$

Thus the vector is rotated as usual to a new position in the AZDQ frame but it must also be multiplied by a complex factor $\exp(-i\Delta\omega_B t)$.

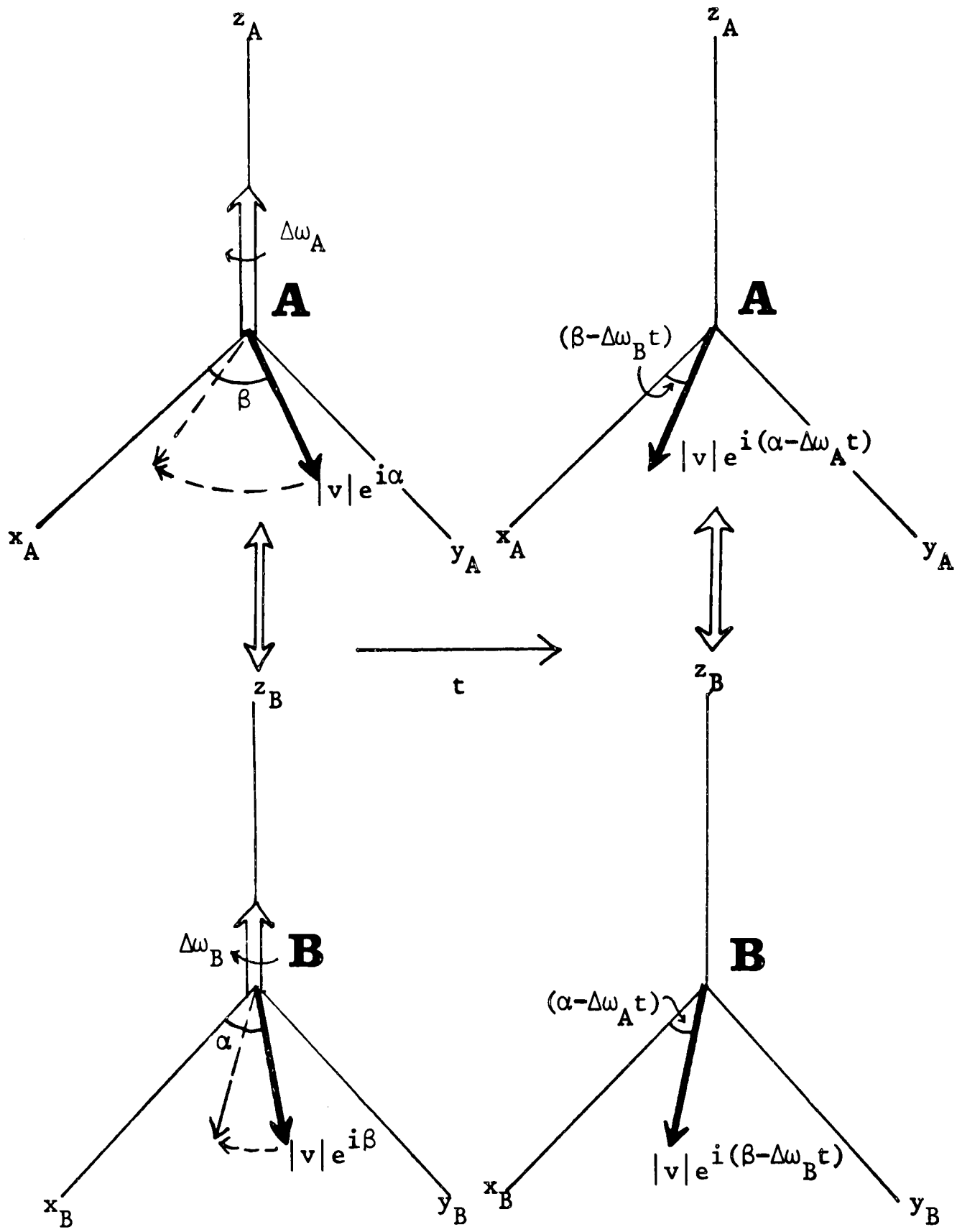

Fig.3.14. Precession in the 'conjugate' frames.

This has the following interpretation: At the same time as the A spins nutate about the effective pulse field, the B spin system is also evolving. The B-spin vectors are also rotating about their effective field which in the absence of B irradiation is a residual field along the z-axis proportional to the resonance offset from the B spin reference frequency. Now this rotation of vectors in the transverse plane of the BZDQ frame must also be interpreted as an evolution in the imaginary dimension of the AZDQ frame, because they are linked by a 'conjugate transformation'. This is the origin of the complex factor $\exp(-i\Delta\omega_B t)$ in equation 3.68.

This general result can also be applied to the precessional motion of ZDQ vectors, in which the effective field on the A spins simply assumes the value $\gamma\Delta\omega_A$ and lies along the z-axis. The A-vectors precess in the transverse plane about this effective field as do the B-vectors about their corresponding effective field. Then according to the 'conjugate' relationship between the two frames the two transverse precessions must also be represented as evolution in the imaginary dimension of the opposite ZDQ frame (Figure 3.14). This simple picture allows application of the vector model to periods of free precession and to pulses applied off-resonance. However it should be remembered that an assumption was made that the coupling term in the Hamiltonian has only a small effect. This restricts the treatment to evolution over time intervals τ for which $J\tau$ is only a small rotation. This excludes the case of pulses long enough to have a differential effect between the two transitions of the A or B spins.

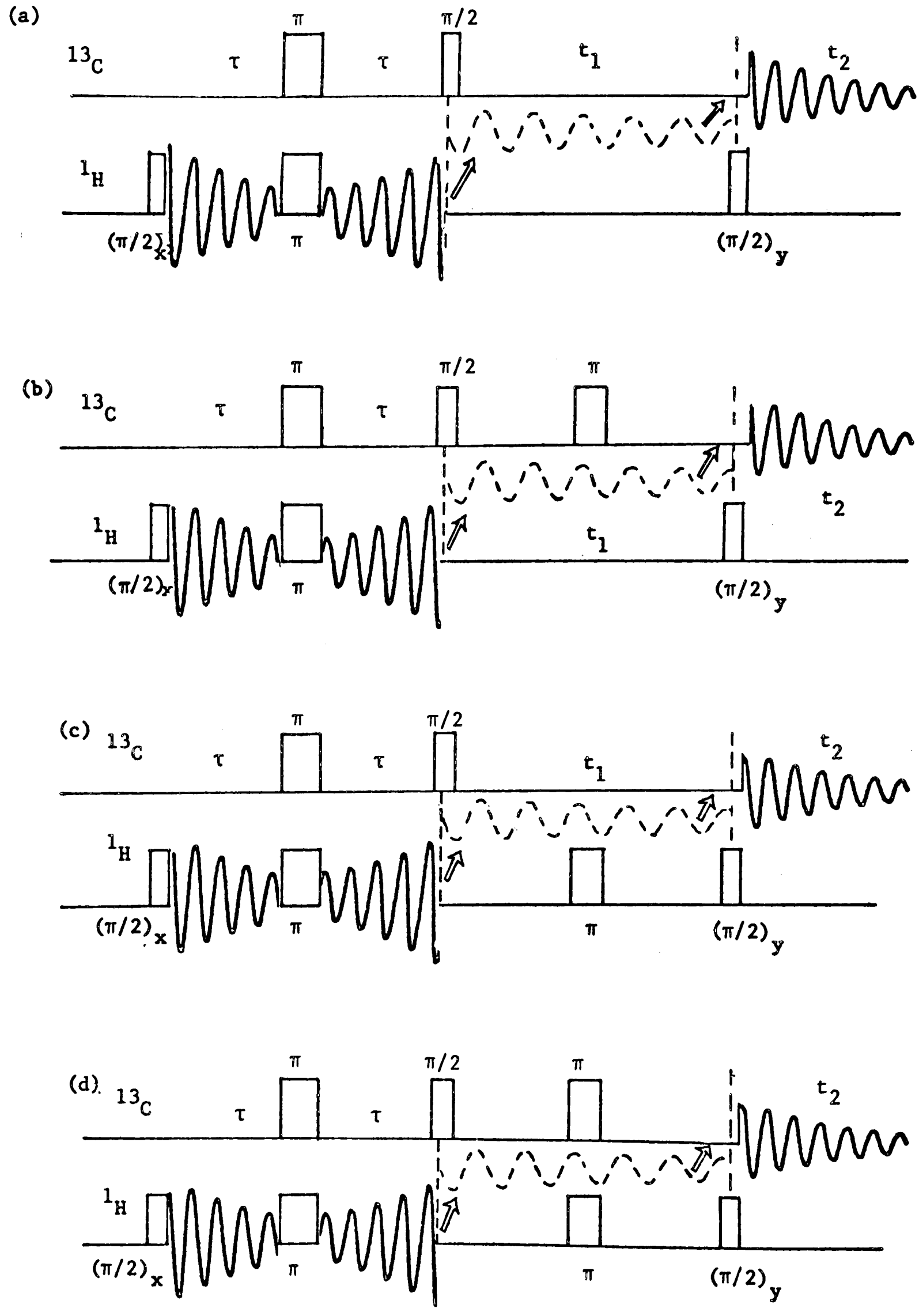

Fig.3.15. Pulse sequences used for the study of ZDQ precession in the heteronuclear AX system.
Transverse proton magnetization is created and converted into ZDQ coherence by the $\pi/2$ ^{13}C pulse, allowed to evolve for a time t_1, and converted into observable ^{13}C magnetization by the $\pi/2$ proton pulse.

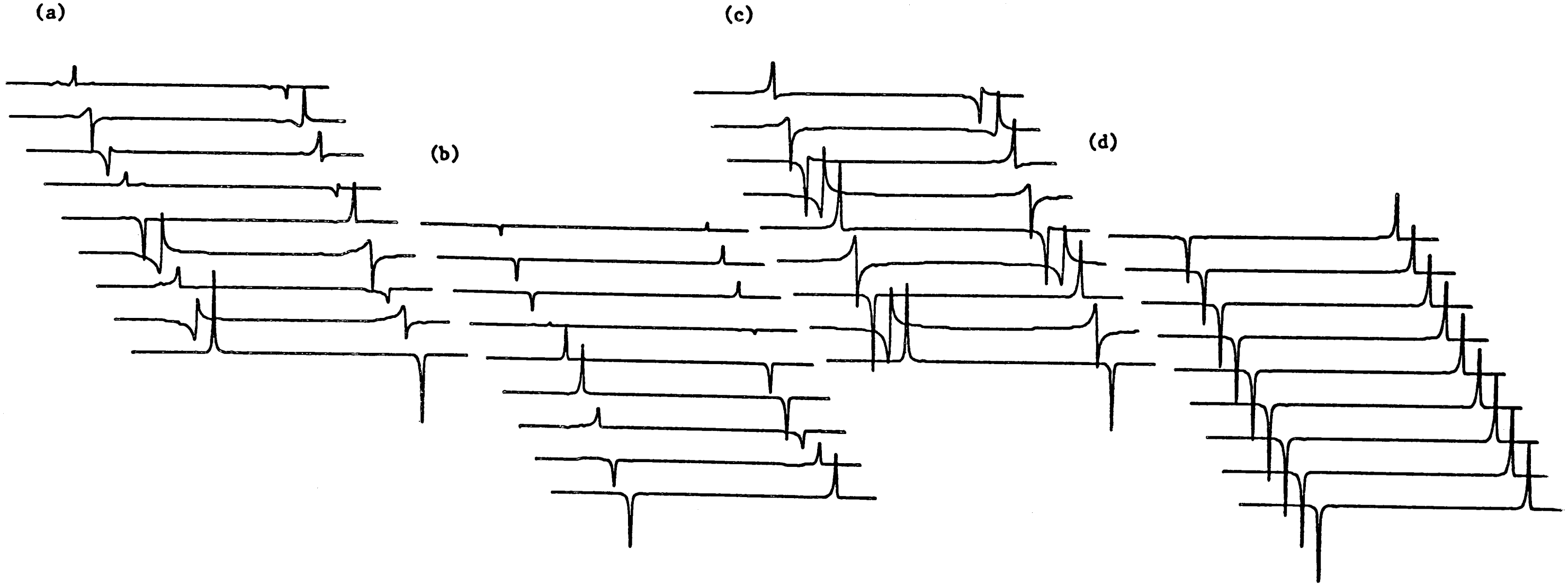

Fig.3.16. Experimental results for the pulse sequences of Fig.3.15, using the heteronuclear AX system of formic acid, on the XL-200 spectrometer. The spectra are 350Hz wide, and t_1 has been incremented from 0 to 17.5ms in 2.5ms steps.

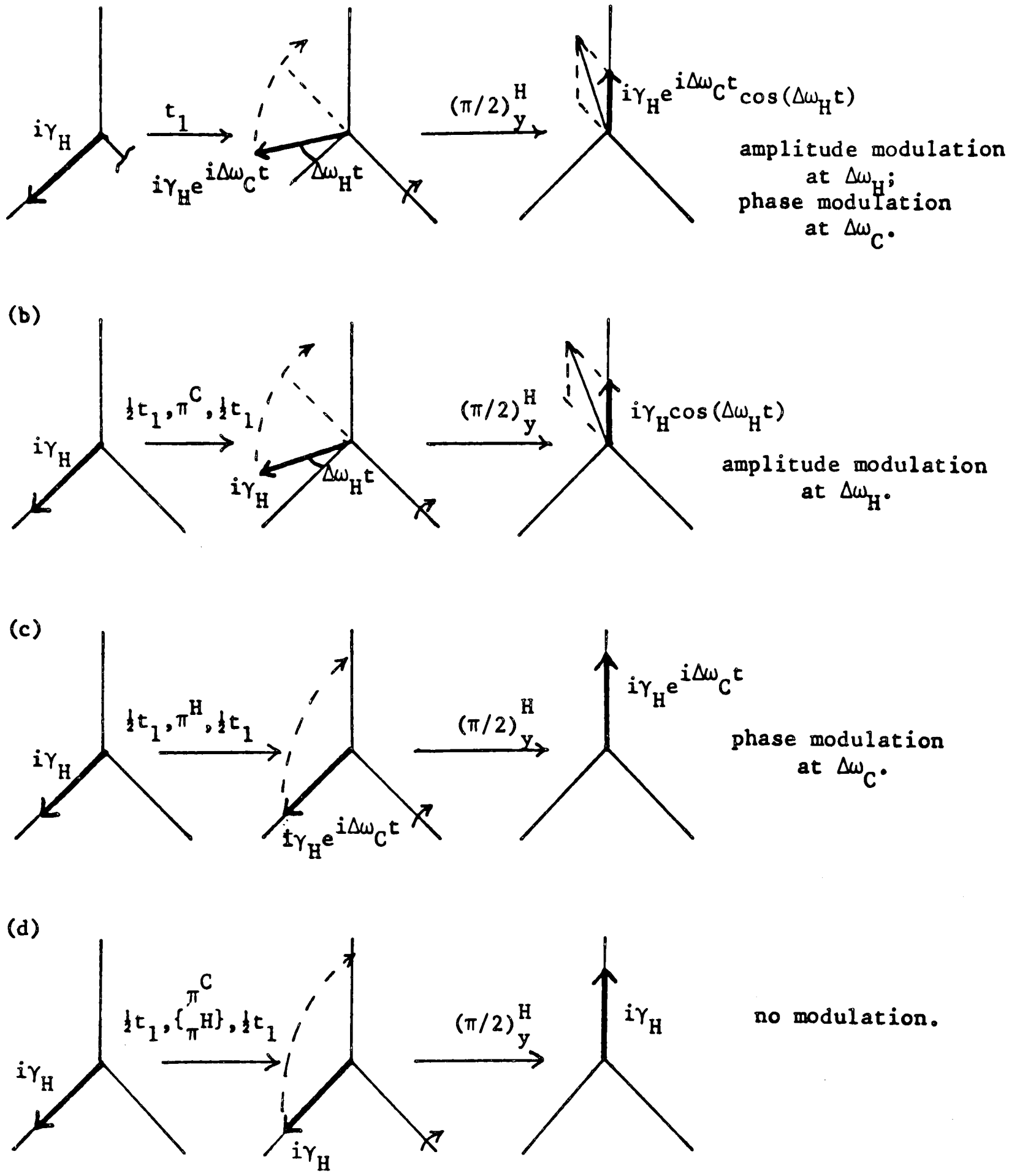

Fig.3.17 Interpretation of the results of Fig.3.16 in terms of ZDQ vectors.

In all cases the preparatory sequence

$$(\pi/2)_x^H - \tau - \pi_x^C\ \pi_y^C - \tau - (\pi/2)_x^C$$

results in an imaginary vector of magnitude $i\gamma_H$ along the x-axis of the ^{1}H-ZDQ frame. The vector precesses around the z-axis at a rate $\Delta\omega_H$ rad s^{-1}. Hence if it is wished to rotate the vector to the +z-axis by means of a $(\pi/2)_y^H$ pulse, the degree of conversion is proportional to cos $(\Delta\omega_H t)$, leading to an amplitude modulation of the transferred signals (a and b). This precession can be refocussed by introducing a π^H pulse (c and d). Similar evolution in the 'conjugate frame' leads to the multiplying factor $\exp(i\Delta\omega_C t)$, which determines the phase of the transferred signals, so that they are phase-modulated at angular frequency $\Delta\omega_C$ rad s^{-1} (a and c). This too can be refocussed, this time by using a π^C pulse (b and d).

The agreement of theory with experiment is a satisfying indication of the validity of the vector model.

An experimental verification has been made of this picture of ZDQ precession. The set of experiments described in Figure 3.15 was carried out on the heteronuclear AX ^{13}C-^{1}H system of formic acid. These are essentially INEPT pulse sequences in which the ZDQ coherence, created by a $\pi/2$ carbon-13 pulse acting on proton magnetization as described previously, is allowed to precess for an interval t_1 before transfer into carbon-13 transverse magnetization by the $\pi/2$ proton pulse. Experiments (b) to (d) differ in that the interval of free precession is bisected by π pulses applied to either or both of the carbon-13 or proton spin systems.

The behaviour of the carbon-13 signal as t_1 is varied is given in Figure 3.16. When no π pulses are present the carbon-13 signals undergo a simultaneous phase and amplitude modulation at two different frequencies. The application of π pulses to carbon-13 or proton spins at the centre of the t_1 period can remove either or both of these effects. This may be interpreted in terms of the ZDQ vector pictures as follows (Figure 3.17): When no π pulses are present the ZDQ vector precesses about the z-axis of the ^{1}H-ZDQ frame at angular frequency $\Delta\omega_H$, and also in the imaginary dimension at angular frequency $\Delta\omega_C$. To convert this vector into carbon-13 transverse magnetization requires the application of a $\pi/2$ proton pulse which can rotate the vector towards the z-axis of the ^{1}H-ZDQ frame. Thus the <u>magnitude</u> of the z-component produced is determined by the relative phase of the precessing vector and the proton pulse field. Because the vector is precessing in the transverse plane at angular frequency $\Delta\omega_H$, the carbon-13 magnetization produced is amplitude modulated at the same frequency. However the vector is also developing in the imaginary dimension, which determines the <u>phase</u>

of the transverse magnetization produced. Thus there is a simultaneous phase modulation of the carbon signals at the precession frequency in the 'conjugate frame' - this time $\Delta\omega_c$. But both amplitude modulation and phase modulation effects may be separated by refocussing the precessions in either or both of the two frames by using π pulses. This leads to pure amplitude modulation when a π carbon-13 pulse is used (case (b)), pure phase modulation with a π proton pulse (case (c)), and no modulation at all if both precessions are refocussed (case (d)). The experimental results are just as predicted, with the modulation frequencies also agreeing with the measured offsets from the two transmitter reference frequencies.

3.7 The homonuclear AX system

The homonuclear AX system is simply a special case of the heteronuclear AX system. The gyromagnetic ratios of the two nuclear species become identical and under normal circumstances the reference frequencies of the frames become the same, so that the interaction frame becomes equivalent to a simple rotating frame revolving at the one common transmitter frequency. Exceptions to this simple situation might occur however in some homonuclear double resonance experiments.

Now it must be remembered that the treatment given above is suitable only for pulses which selectively excite only one of the nuclear species in the AX system. For heteronuclear systems this is the normal state of affairs since the great difference in precession frequencies of the A and X spins ensures this condition.

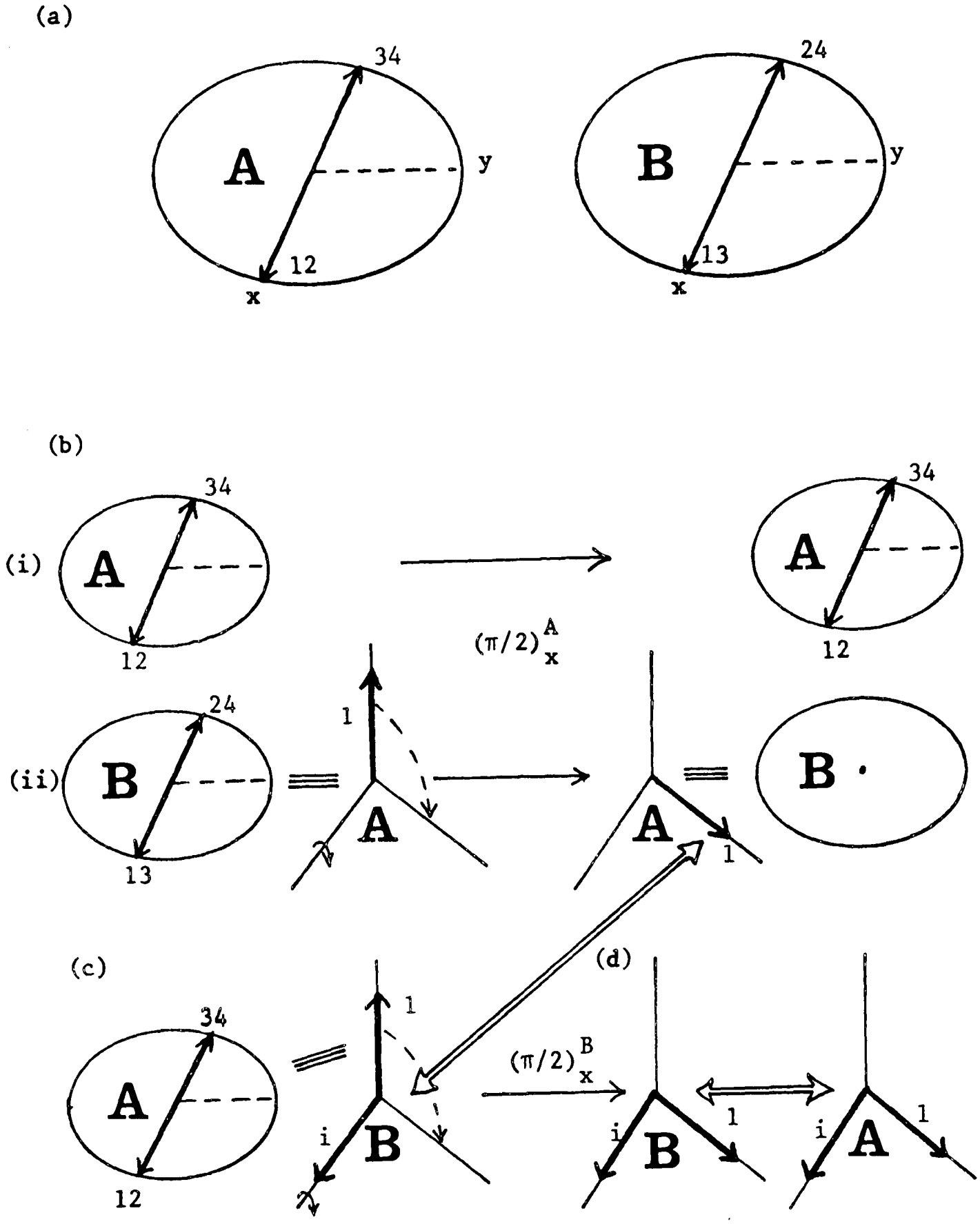

Fig.3.18 The creation of double-quantum coherence in the homonuclear AX system by the $(\pi/2)_x - \tau - \pi_x - \tau - (\pi/2)_x$ sequence.

(a) The state of the system immediately before the final $\pi/2$ pulse, which must be broken down into two elements, $(\pi/2)_x^A$ and $(\pi/2)_x^B$.

(b) The action of the $(\pi/2)_x^A$ element:-

(i) On A magnetization: It has no effect;

(ii) On B magnetization,expressed as the rotation of a vector in the AZDQ frame. All transverse magnetization is destroyed, having been converted into ZDQ coherence.

(c) The action of the $(\pi/2)_x^A$ element on A magnetization, expressed as the rotation of a vector in the BZDQ frame. Note that apart from the z-component in this frame, which is associated with A magnetization, there also exists a transverse component which was created by the previous pulse element.

(d) The final state, with the 'double vector' in the ZDQ frames, representing pure double-quantum coherence.

However in homonuclear systems strong pulses are routinely used which affect about equally all resonances in a spectrum, and it is essential that the vector model be able to handle such cases.

A strong non-selective pulse may be treated by decomposing it into a sequence of two hypothetical selective pulses, applied to the A and X spins in turn. Each of these selective pulses can then be treated in the usual way. This is a generalisation of the 'pulse cascade' analysis of G. Bodenhausen (122) which treats the influence of non-selective pulses on level populations by using the same hypothetical decomposition of a non-selective pulse into a 'cascade' of selective pulses. Here this idea has been extended to include transverse magnetizations and multiple-quantum coherences.

A simple example which illustrates the use of pulse cascades is a sequence which results in the conversion of longitudinal magnetization into double-quantum coherence. This is the three-pulse $(\pi/2)_x - \tau - \pi_x - \tau - (\pi/2)_x$ sequence in which each pulse is strong and non-selective, and the periods τ involve free precession such that $\tau = 1/(4J)$. The function of the first two pulses and precession periods is now familiar; it is a modulated spin echo designed to produce transverse magnetization components antiparallel along the x-axis at time 2τ, as illustrated in Figure 3.18(a). Note the similarity between this preparation sequence and that of the INEPT sequence, which also uses a modulated spin echo as preparation for the zero and double quantum coherence transfers. However there is a crucial difference in that in this example <u>both</u> species A and B possess transverse magnetization at time 2τ, so both of these transverse magnetizations contribute to the double- and zero-quantum coherence

created by the final non-selective $\pi/2$ pulse. In fact it will be seen that they interfere in such a way as to produce only double-quantum coherence and no zero-quantum.

The final $\pi/2$ pulse must be treated as a cascade of two selective pulses, $(\pi/2)_A$ and $(\pi/2)_B$. Remembering that each pulse affects both magnetizations and ZDQ vectors, the effect of the first cascade element $(\pi/2)_A$ is:

(i) it rotates the magnetization of the A spin transitions, and (ii) it also rotates B difference magnetization into ZDQ coherence. These two separate operations are indicated in Figure 3.18(b). In fact the first rotation leaves the A magnetizations unchanged provided the pulse is applied about the x-axis. On the other hand the initial state of B magnetization consists of anti-parallel components along the x-axis, which should as usual be represented as a real number along the z-axis of the AZDQ frame. This is then rotated by the $(\pi/2)_A$ cascade element into the transverse plane, signifying full conversion of B magnetization into ZDQ coherence. Accordingly the B magnetization vanishes at this point.

The second cascade component $(\pi/2)_B$ may now be applied and acts directly on B magnetization, and also on A magnetization via the B-ZDQ frame. As the B magnetization is now zero this former aspect may be ignored. In contrast the effect of the $(\pi/2)_B$ rotation in the B-ZDQ frame is interesting. The initial state of the vector in this frame comprises two contributions:

(i) a real vector along the z-axis, corresponding to the antiparallel components of A-magnetization, which, as may be recalled, escaped the first $(\pi/2)_A$ pulse, and

(ii) a vector in the transverse plane which represents the ZDQ coherence created by the first element. This transverse vector is related to the result of the first cascade rotation by a 'conjugate transformation', hence the double-headed arrow of Figure 3.18(b,c). It is a component of imaginary value i along the x-axis of the BZDQ frame.

The $(\pi/2)_B$ rotation can now be applied giving the result of Figure 3.18(d), all magnetization having been rotated into some combination of zero- and double-quantum coherence. In fact it can be easily shown that the state of Figure 3.18(d) represents pure double-quantum coherence, no zero-quantum coherence existing at this time. This can be verified by evaluating σ_{14} and σ_{23} from the Cartesian components in the ZDQ frames using equations such as 3.32.

Some comments are in order as to the nature and properties of the 'double vector' of Figure 3.18(d). Firstly it should be noted that decomposition into a single vector 'resultant' is not feasible because the two perpendicular components also have perpendicular phases in the 'imaginary' plane. This is yet another example of the hidden complexities of the ZDQ frames, with their concealed multi-dimensional character. Another property of the state of Figure 3.18(d) is that it has many degenerate representations in vector form, all of which are equivalent since they result in the same overall Cartesian components. This is illustrated in Figure 3.19.

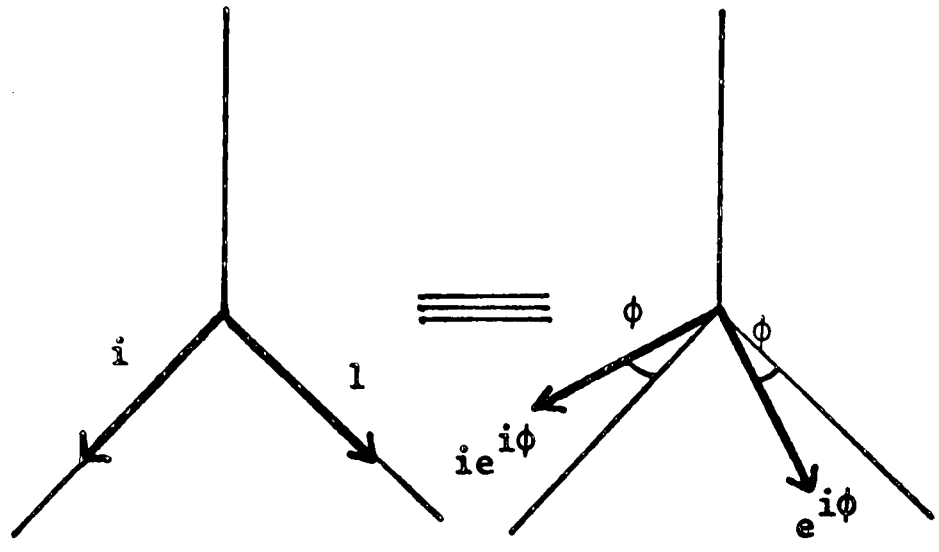

Fig.3.19. Equivalent representations of double-quantum coherence.

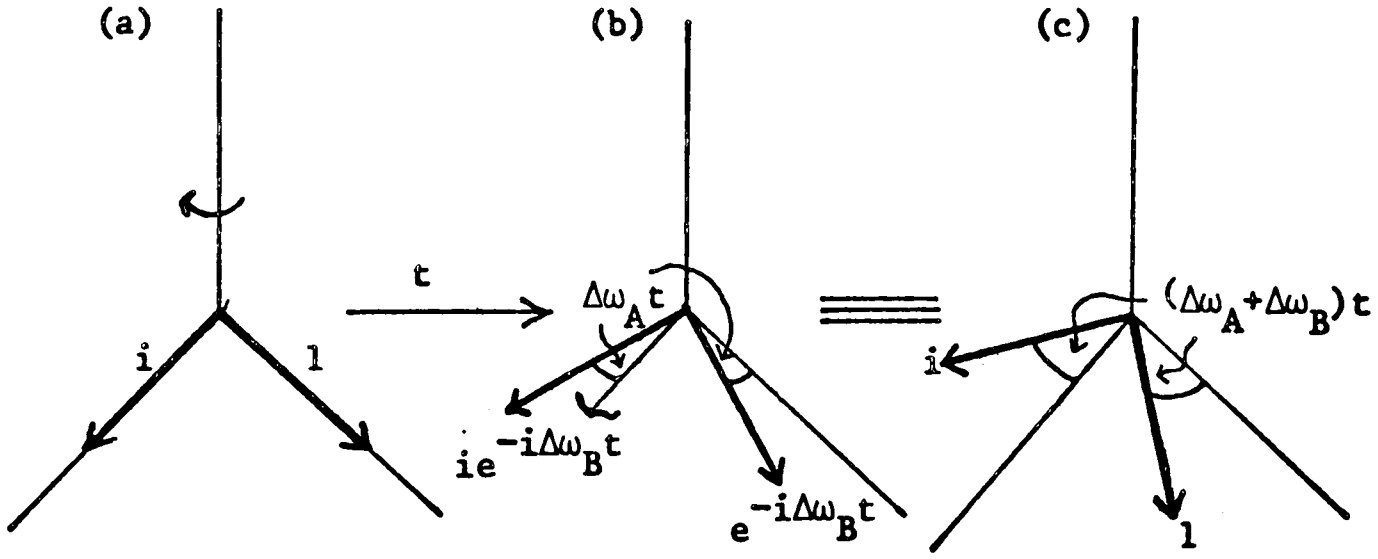

Fig.3.20. Double-quantum precession:
(a) Initial state.
(b) State after time t. Precession has occurred in the transverse plane at a rate $\Delta\omega_A$ rad s^{-1}, and in the 'conjugate frame' at a rate $\Delta\omega_B$ rad s^{-1}.
(c) Because of Fig.3.19, the two evolutions can be combined.

If the total x or y components of the double vectors are evaluated they are found to be independent of ϕ. Thus for the x-component,

$$ie^{i\phi}\cos\phi + e^{i\phi}\sin\phi = i \qquad 3.69$$

and for the y-component:

$$-ie^{i\phi}\sin\phi + e^{i\phi}\cos\phi = 1 \qquad 3.70$$

This has interesting consequences for the behaviour of the double vector under precession. As has been discussed, evolution in both the transverse and imaginary planes is involved in the precession of a ZDQ vector. For instance in the AZDQ frame, vectors rotate about the residual field $\gamma\Delta\omega_A$ along the z-axis, and also develop in the imaginary plane at angular frequency $\Delta\omega_B$, as represented by the inclusion of a complex multiplying factor $\exp(-i\Delta\omega_B t)$. A similar evolution is envisaged for the two parts of the double vector. The result is indicated in Figure 3.20(b), which expresses phase evolution in the transverse plane at angular frequency $\Delta\omega_A$ and also in the conjugate frame at angular frequency $\Delta\omega_B$. However because of the property illustrated in Figure 3.19, the two evolutions can be economically combined. The result is that of Figure 3.20(c) and expresses the well-known fact that double-quantum coherences evolve at the sum of the two transmitter offset frequencies.

This can be verified for a homonuclear AX system by using a double Fourier transform method to measure the rate of evolution of the double-quantum coherence, which is of course unobservable in a standard Fourier transform experiment. The double-quantum coherence

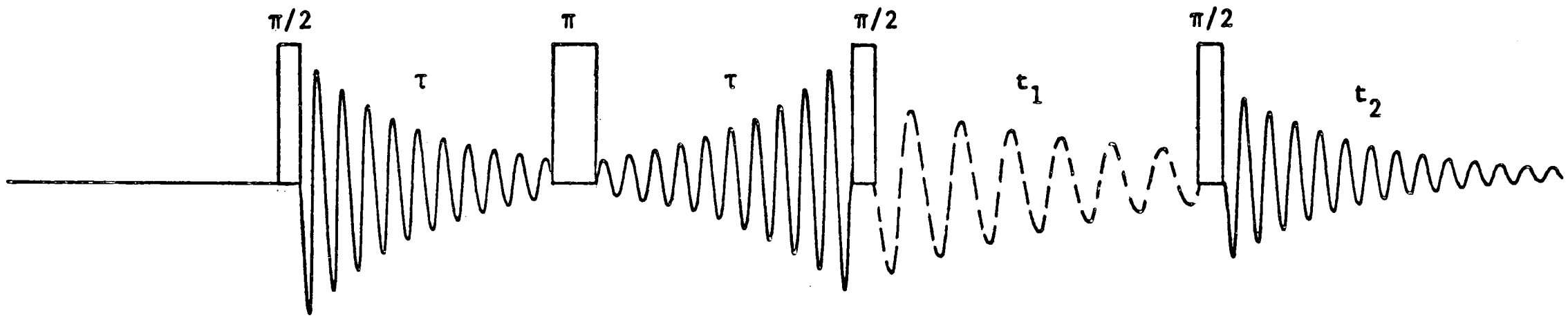

Fig.3.21. Pulse sequence for the study of double-quantum coherence.

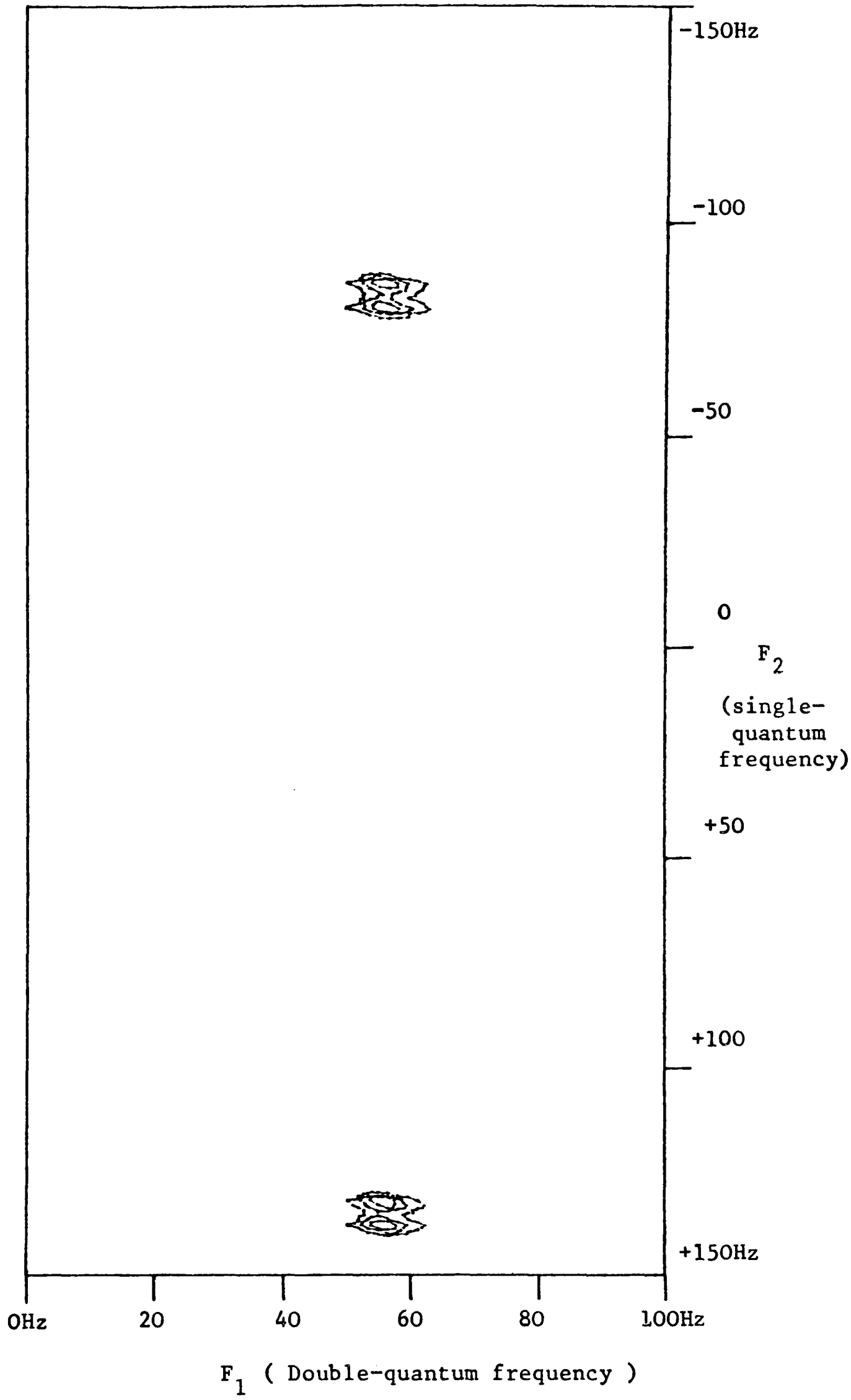

Fig.3.22. Experimental two-dimensional spectrum obtained with the pulse sequence of Fig.3.21, measured on the XL-200. The homonuclear AX system of 1,1-dichloro-2,2-diethoxyethane was used. (The ethyl resonances were placed outside the bandwidth of the analogue filters, so that after folding they appeared with too low an intensity to show on the contour plot).

The double-quantum frequency can be measured as 55 Hz, which is the sum of the two offset frequencies +135 and -80 Hz.

is created by the $(\pi/2)_x - \tau - \pi_x - \tau - (\pi/2)_x$ pulse sequence as discussed above. It is allowed to precess for a time t_1 and then transferred back into observable single-quantum coherences by a third pulse, producing in total the four-pulse sequence:

$$(\pi/2)_x - \tau - \pi_x - \tau - (\pi/2)_x - t_1 - (\pi/2)_x - \text{acquisition}(t_2) \quad 3.71$$

as illustrated in Figure 3.21.

The acquisition of a set of free induction decays during the t_2 period for different values of t_1 produces a two-dimensional data matrix $S(t_1,t_2)$ which may be subject to double Fourier transformation in the usual way. The resultant two-dimensional spectrum $S(F_1,F_2)$ is illustrated in Figure 3.22. Peaks which originate from precessing double-quantum coherence during the t_1 period are observed at the sum of the frequency offsets of the A and B spin resonances.

3.8 Selective detection of double-quantum coherence

In some experiments it is useful to suppress all signals from transverse magnetization which had not at some stage been transferred from double-quantum coherence. For instance such a facility could be used to selectively detect signals from a small number of coupled spin systems in the presence of a large excess of isolated spins, which cannot possess double-quantum coherence. This situation arises in natural abundance ^{13}C spectroscopy. Since the natural abundance of ^{13}C is only about 1%. most molecules in a sample of a given organic compound contain no ^{13}C at all, and only 1% contain a carbon-13 nucleus at a given molecular site. There also exist a small fraction,

about 0.01%, which contain ^{13}C nuclei at two specified molecular sites in the same molecule, and if these are reasonably close they have a scalar coupling, J_{CC}, and thus form an AB or an AX spin system. Signals from such molecules form weak satellite lines approximately symmetrically disposed about the main ^{13}C lines but typically 200 times weaker. It is of interest to study these satellite lines because the magnitudes and disposition of the couplings contain particularly direct information about the sequence and conformation of the carbon molecular 'backbone'. However this is often difficult or impossible in the presence of the large uncoupled centre line, particularly when the weak long-range ^{13}C-^{13}C couplings are the subject of interest. Then the small satellites lines are often swamped in the wings of the intense centre peak. One way to get round this problem is to enhance the satellites and deplete the centre line by chemical enrichment of specific ^{13}C sites, but this is an expensive and time-consuming process.

A more attractive alternative is to suppress the centre peak by some NMR method. If this can be done, time-averaging of the signals over long periods can be carried out to allow study of the very weak ^{13}C-^{13}C satellite signals in natural abundance materials.

Double-quantum coherence can be used in an experiment first suggested by A. Bax (123). The coupled ^{13}C-^{13}C spins are selectively detected in the following way. Firstly, homonuclear double-quantum coherence is generated by the three-pulse sequence

$$(\pi/2) - \tau - \pi_x - \tau - (\pi/2)_x \qquad 3.72$$

Step	Phase of ($\pi/2$) 'read pulse' ϕ	Reference phase for observation ψ
0	x	x
1	y	-y
2	-x	-x
3	-y	y

Table 3.1. Basic phase-cycling sequence for selective observation of double-quantum coherence.

Note that the reference phase ψ appears to cycle in the opposite sense to that of the 'read' pulse ϕ.

In practice, even better selectivity can be attained by incorporating a further phase cycling sequence in the double-quantum generation pulse sequence $(\pi/2)_x$-τ-$\pi_{\pm x}$-τ-$(\pi/2)_x$. Yet another phase cycling sequence can be added to remove the effects of any imbalance between the two channels of the quadrature detector. The complete sequences are detailed in references 123 and 145.

The operation of this has already been discussed. Now in contrast with the previous experiment, the double-quantum coherence is not allowed to evolve but immediately converted back into observable magnetization by a third $\pi/2$ 'read' pulse, which has a phase ϕ, and the signals generated measured against a reference signal which may have a different phase, ψ, thus:

$$(\pi/2)_x - \tau - \pi_x - \tau - (\pi/2)_x - (\pi/2)_\phi - \text{acquisition } (\psi) \qquad 3.73$$

Many such sequences are repeated (with adequate delays for relaxation) and the acquired free induction decays summed to enhance the signal-to-noise ratio.

Now it is possible to have the computer progressively change the phases ϕ and ψ in a cyclic manner as these sequences are repeated. If this is done correctly it is possible to suppress all signals generated from transverse magnetization which did not pass through double-quantum coherence, including the large uncoupled signal. This is because the conversion of double-quantum coherence into single-quantum magnetization has a rather peculiar dependence on the phase of the 'read' pulse. If the 'read' pulse is stepped in phase in a cyclic fashion, x, y, -x, -y, the transferred transverse magnetization is generated with phase -x, +y,+x,-y; it appears to cycle in phase in the opposite direction to the 'read' pulse. Hence if the 'read' pulse phase ϕ and the observed phase ψ are cycled in the fashion suggested in Table 3.1, all unwanted signals cancel out, and only the satellite signals remain, as required.

These phase properties may be interpreted using the vector

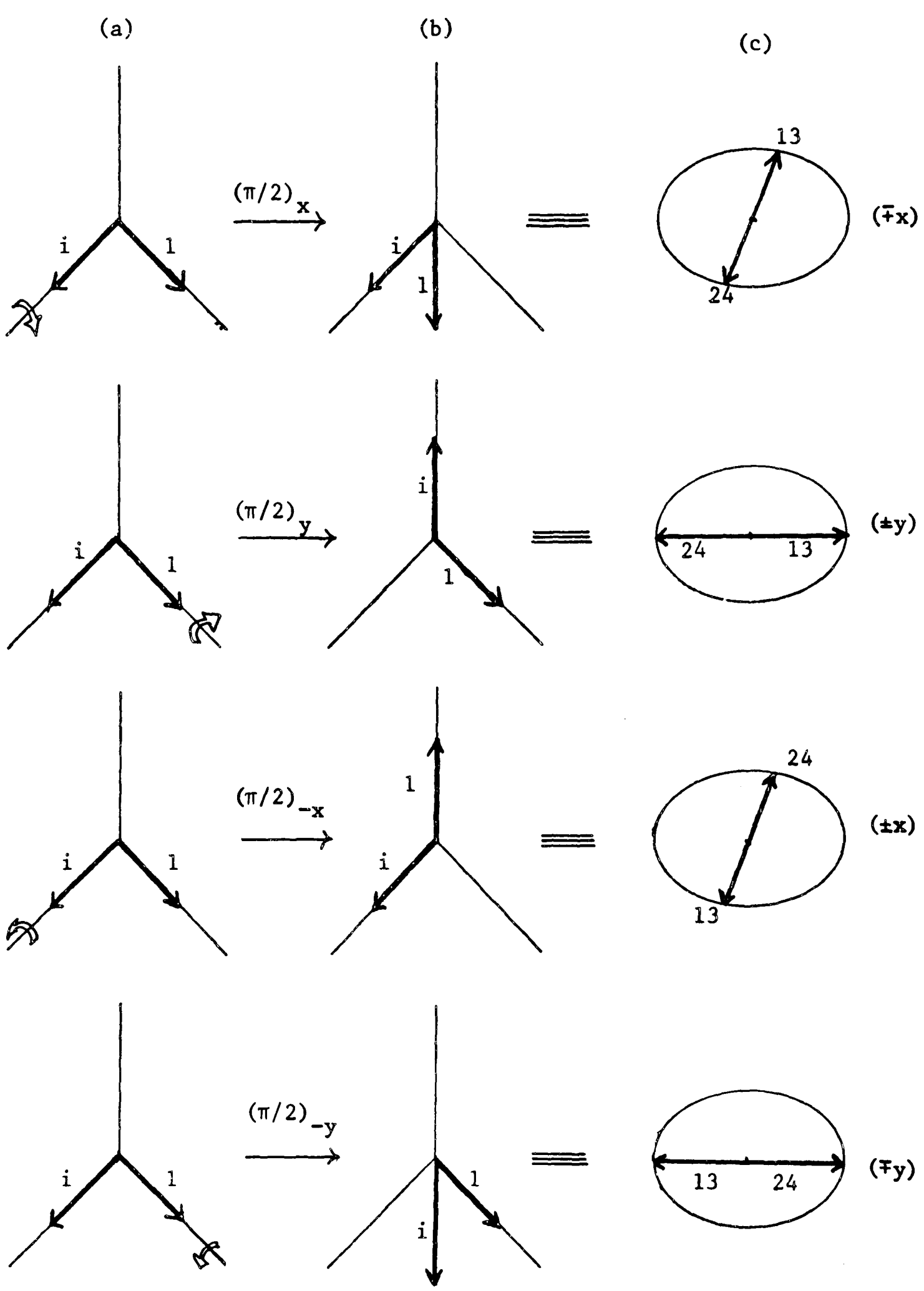

Fig.3.23. If single-quantum coherence is created from double-quantum coherence by the action of a $\pi/2$ pulse, the phase of the magnetization produced has an unusual form of dependence on the phase of the conversion pulse. This can be explained by performing rotations on the ZDQ vectors, as shown.

Fig.3.24. The natural-abundance ^{13}C - ^{13}C satellite spectrum of menthol, obtained on the XL-200.spectrometer by double-quantum transfer (see text). The resonances from molecules containing only one ^{13}C nucleus (which are normally about 200 times as intense) have been almost completely suppressed by a phase-cycling sequence (see Table 3.1).

model and this is done in Figure 3.23. On the left of these diagrams are representations of double-quantum coherence, as 'double vectors' in the transverse plane of the AZDQ frame. To each of these initial states a $\pi/2$ rotation is applied about the x, y, -x or -y axes of the reference frame. Each rotation generates a z-component in the AZDQ frame which must as usual be taken to represent antiparallel components of transverse B magnetization; the phase of the transverse magnetization produced is given by the value of the z-component generated in the AZDQ frame. A real number indicates antiparallel magnetization components along the x-axes of the rotating frame, whilst an imaginary number signifies components along the y axis. On inspection the results of these rotations will be seen to have the phase properties mentioned.

In practice the phase-cycling sequence is expanded to account for effects due to pulse imperfections and to relaxation which can otherwise result in imperfect suppression. When this is done suppression of the centre peak is essentially complete as shown in the example of Figure 3.24.

This experiment is probably the first really useful chemical application of multiple-quantum effects, but more are expected to follow.

CHAPTER FOUR

COMPOSITE PULSES

CHAPTER 4

COMPOSITE PULSES

4.1 Pulse Imperfections

Most techniques in nuclear magnetic resonance use strong short pulses of radio-frequency irradiation to manipulate the nuclear spin system. As was clear from the previous chapter, the desired rotations are usually by $\pi/2$ or π radians about an axis in the equatorial plane of the rotating frame, typically the x or y axis. In principle the rotation can be achieved by applying a pulse of duration determined by the condition:

$$\alpha = \gamma B_1 t_p \qquad 4.1$$

where t_p is the length of the pulse in seconds, α is the desired rotation angle, and B_1 the irradiation field strength. But in practice it is difficult to ensure such a rotation for all parts of the sample. In general, pulses are imperfect because:

(i) the radio-frequency field strength cannot be assumed to be uniform over the observable sample volume (radio-frequency field inhomogeneity);

(ii) the irradiation frequency may differ somewhat from the actual precession frequency. If the resonance offset is comparable to the radio-frequency field strength, rotation of the magnetization takes place about a tilted effective field which does not lie in the xy plane. The degree of tilt of the effective field depends

on the off-resonance parameter $\theta = \tan^{-1}(\Delta\omega/\gamma B_1)$ where $\Delta\omega$ is the frequency offset in rad s^{-1};

and (iii) there are practical difficulties in generating an oscillating B_1 field in the vicinity of the sample which rises instantaneously from zero to its full value at the start of the pulse and decays equally instantaneously at the end. Normally there are finite rise and fall times of a few microseconds which are related to the so-called 'Q-factor' of the coil, a parameter which quantifies the narrowness of the frequency response of the tuned circuitry. Normally it is desirable to increase the sensitivity of the coil by making it as frequency-selective as possible, but this can only be accomplished at the expense of problems associated with finite rise and fall times.

In addition there are a related set of problems known as 'phase glitch' or 'phase transients' which also occur at the start and end of a pulse but this time involve a momentary variation of the phase (rather than the amplitude) of the irradiating field. It has been shown that both of these types of imperfection are an intrinsic and unavoidable property of switched tuned circuits and hence cannot easily be removed without seeking alternative means of generating the signals such as digital waveform construction (124). Fortunately the effects seem to be quite small in practice and they will not be considered in detail. If phase glitch and rise and fall time effects are ignored, the radio-frequency pulses can be described by rotating frame fields which are constant in phase and which instantaneously rise from zero to their full value, and back again, at the beginning and end of the pulse.

In many of the sequences in this chapter, phase-shifted pulses are used which act along different axes in the transverse plane of the rotating frame, so that possible deviations in this phase-jump furnish another possible source of error. Throughout the reasonable assumption is made that the jump can be accomplished accurately enough for the effect of deviations to be ignored. The phase shifts in the two spectrometers used were certainly accurate to within 1^{o}.

The radio-frequency pulse is then subject mainly to imperfections due to radio-frequency field inhomogeneity and to resonance offset, both of which tend to obstruct the implementation of a desired rotation by the application of a single pulse. In this chapter the proposition is made that a desired rotation may be accomplished more effectively by using a sequence of a small number of pulses which combine in such a way as to give the required overall effect, but which collaborate so as to reduce the undesirable influences of pulse imperfections. Such a cluster of closely-spaced pulses will be known as a 'composite pulse' (89,125,126). The pulses are usually separated by intervals just sufficient to accomplish clean changes in the radio-frequency phase when this is required but not long enough to allow significant precession or relaxation. In some composite pulses longer intervals are left in which the free precession that occurs is then essential to the compensatory process.

It may be noted that if the spin ensemble were a linear system no compensation of errors would be possible in this way. If the response of the spin magnetization were simply proportional to the

perturbation, two pulses could do no better than one. Accordingly composite pulses always involve large rotations of the magnetization which take the response of the system well out of the linear region.

There is a problem in the nomenclature of pulses in the presence of imperfections. When there are B_1 inhomogeneity or off-resonance effects the usual terms '$\pi/2$ pulse' or 'π pulse' are somewhat misleading because the actual rotation experienced by the spins is not exactly $\pi/2$ or π radians and depends on the position in the sample and the resonance offset. Nonetheless these terms are retained for the sake of simplicity, but must be understood to refer to a hypothetical ideal situation in which off-resonance effects are negligible and which refers to a B_1 field of some nominal value B_1°. The nominal value usually represents the field intensity near the centre of the coil but its precise meaning depends on the method used to obtain the pulse lengths. A typical method is to adjust the pulse time until the signal excited passes through a null - this is taken to represent a flip of π radians so that the nominal value B_1° is given by

$$\gamma B_1^{\circ} t_{\pi} = \pi \text{ radians} \qquad 4.2$$

where t_{π} is the pulse duration at this condition.

It is not easy to derive a direct relationship between a nominal field defined in this way and the actual distribution of B_1 fields, but it is easy to show that B_1° is rather to the high side of the distribution curve. Analysing the problem in one spatial dimension only, denoted x, there is some variation of B_1 in space $B_1(x)$ and also in general some distribution of spin density $d(x)$. (In a

sample of restricted volume, d(x) falls off sharply beyond well-defined maximum or minimum boundaries of x). The magnetization per unit volume is proportional to d(x):

$$M_o(x) \propto d(x) \qquad 4.3$$

This magnetization may then be rotated by a local pulse field $B_1(x)$ for a time t_p to produce a transverse magnetization:

$$M_y(x) \propto d(x)\sin[\gamma t_p B_1(x)] \qquad 4.4$$

The signal contributed by a given volume element, S(x), is proportional to the transverse magnetization and also another factor which expresses the efficiency of coupling of the magnetization back to the receiver coil. In a single-coil instrument, the same coil is used for both excitation and detection of the precessing magnetization. Therefore the same coupling factor should be used both for the magnetic field experienced by a given volume element due to electrical currents in the coil, as for the signal induced in return in the coil by precessing magnetizations in that same volume element. Both are expressed by $B_1(x)$ so that:

$$S(x) \propto B_1(x)d(x)\sin[\gamma t_p B_1(x)] \qquad 4.5$$

The pulse duration t_p is now adjusted for a null in the integrated signal intensity which is the condition

$$\int_{-\infty}^{\infty} B_1(x)d(x)\sin[\gamma t_p B_1(x)]dx = 0 \qquad 4.6$$

$$\text{when } t_p = t_\pi \qquad 4.7$$

On change of variables, equation 4.6 becomes:

$$S(t_p) = \int_{-\infty}^{\infty} B_1 d(x).\sin(\gamma t_p B_1) \frac{\partial x}{\partial B_1} dB_1 = 0 \qquad 4.8$$

The function $\partial x/\partial B_1$ is an expression of the degree of homogeneity of a field of value B_1, since it denotes how far one must change x in order to experience a small change in field ∂B_1; the more homogenous is B_1, the greater is $\partial x/\partial B_1$. Thus equation 4.8 expresses the intuitive idea that the most homogenous parts of B_1 contribute most to the signal. However even in a hypothetical example in which B_1 has a uniform spatial gradient ($\partial x/\partial B_1$ is constant), the equation still suggests that regions with the strongest B_1 fields contribute most to the signal because of their strong coupling with the receiver coil. In real systems, both the strongest and the most uniform fields are designed to occur near the centre of the coil so that the nominal value B_1° tends to be much closer to the maximum B_1 value in a sample rather than some sort of 'average' value. This is sometimes of importance when inhomogeneity effects are being compensated. Local B_1 fields significantly smaller than nominal are encountered more often than those appreciably larger than nominal. It is possible to verify this conclusion by using a two-dimensional spectroscopic technique to measure the B_1 distribution throughout the sample space (127). This is done very simply by applying a strong pulse of length t_1 seconds to a sample which has a single resonance, such as that of protons in water. The pulse stimulates a free induction decay which is detected over a period t_2, and a data matrix $S(t_1,t_2)$ is built up as

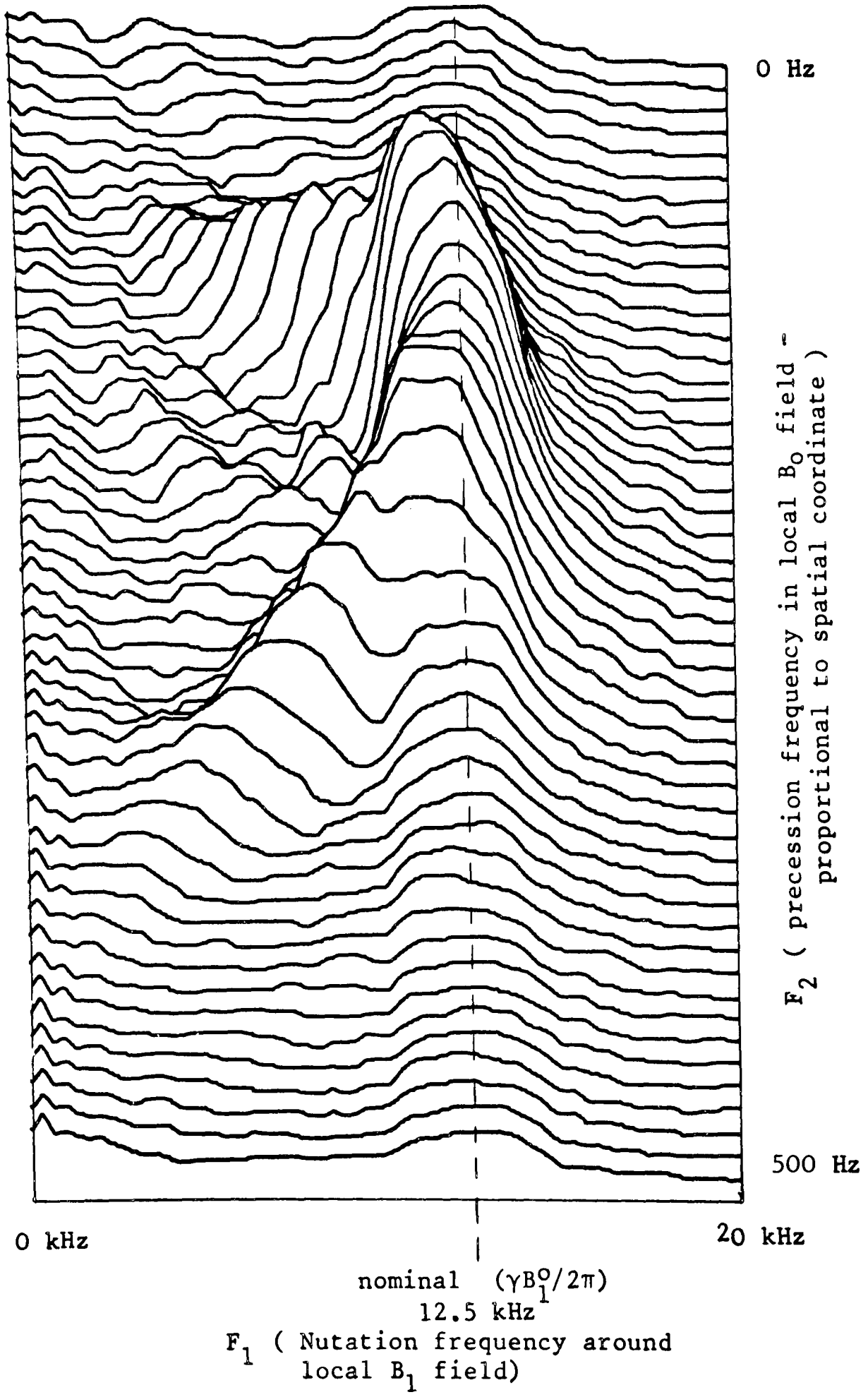

Fig.4.1. Experimental map of B_1 intensity with respect to spatial displacement along the spinning axis, for the CFT-20 spectrometer.

t_1 is incremented in a series of experiments. The signal components which comprise $S(t_1,t_2)$ originate from volume elements throughout the sample, and may be characterized by two frequencies, the nutation frequency $\gamma B_1(x)$ rad s^{-1} around the local effective pulse field $B_1(x)$ during the t_1 period, and the free precession frequency $\gamma B_o(x)$ rad s^{-1} during the t_2 period. Therefore this experiment can be adapted to measure the spatial distribution of B_1 fields by applying a large uniform static field gradient $\partial B_o/\partial x$, brought about by increasing the current through a suitable shim coil. If this static gradient dominates other contributions to magnetic fields, the precession frequency of a signal component during t_2 can be used as a direct indication of its position of origin in the sample volume. (Field gradients are used in a similar way in spin-density mapping experiments (127-131)). Double Fourier transformation of the data matrix correlates the precession frequencies of signal components during t_2 with their nutation frequencies during t_1, and gives a direct map of signal intensity against B_1 field strength in one dimension, and against spatial coordinate x in the other.

An experimental map for the CFT-20 spectrometer is shown in Figure 4.1. A single proton-decoupled carbon-13 resonance of methyl iodide was used as the test signal, with a static field gradient of about 20 mT m^{-1} applied along the long axis of the sample tube, perpendicular to the magnetic field in this case. This increased the linewidth of the carbon-13 signal to about 200 Hz, as can be seen from the projection of the two-dimensional spectrum onto the F_2 axis.

The crescent-shaped plot indicates an approximately quadratic variation of B_1 field strengths across the sample volume. The nominal value B_1^{o} derived from measurement of the condition for a rotation of π radians is also indicated on the diagram. It can be seen that the actual distribution of B_1 fields is skewed strongly to the low side of nominal.

4.2 Composite pulse analysis

There is a range of pictorial and mathematical tools which may be used to design a composite pulse which has a desired effect, and to analyse the degree of error compensation achieved. Firstly one can follow the physical trajectories of the magnetization vectors under the sequence of rotations, and allow each vector to be subject to the influence of inhomogeneity or of resonance offset. For simple sequences it may be possible to do this mentally or with the aid of a three-dimensional model. (Normally such a physical picture is a preliminary to the more sophisticated analyses). But for accurate results in complicated cases, such as when a sequence of many tilted rotations is applied, a computer simulation technique is advisable. To this end a range of FORTRAN computer programs were written and operated on the Oxford University ICL 1906A and 2980 computers. Some examples of their output are to be found on the following pages. The programs allow study of the individual trajectories of a range of magnetization vectors, to each of which may be assigned different pulse field strengths or resonance offset parameters, under an almost completely general sequence of pulses. Other programs allow a map to be made of a given characteristic of the pulse sequence (such as the degree of inversion of z-magnetization, or the phase of

transverse magnetization produced) against B_1 inhomogeneity or off-resonance parameters, or both. These programs were an invaluable aid in design and study of the composite pulses.

Another approach is to derive analytical expressions for the trajectories of the magnetization vectors during the sequence of pulses. This requires knowledge of the general rotation matrices $R(\alpha,\theta,\phi)$ which accomplish rotations by α radians about axes defined by elevations θ and azimuth ϕ. For a magnetization which experiences a local field of magnitude B_1, and is off-resonance by an amount $\Delta\omega$ in angular frequency units, the orf-resonance tilt angle θ is given by

$$\tan\theta = \frac{\Delta\omega}{\gamma B_1} \qquad 4.9$$

and the rotation angle of magnetization components about the tilted effective field is:

$$\alpha = [\Delta\omega^2 + (\gamma B_1)^2]^{\frac{1}{2}} t_p \qquad 4.10$$

The remaining argument ϕ of the rotation matrix $R(\alpha,\theta,\phi)$ represents the phase of the applied irradiation in the rotating frame, and usually takes values of multiples of $\pi/2$ radians, corresponding to fields applied along the x, y,-x and -y axes.

In general $R(\alpha,\theta,\phi)$ can be expressed:

$$\mathbf{R}(\alpha,\theta,\phi) = \begin{pmatrix} c\phi & s\phi & 0 \\ -s\phi & c\phi & 0 \\ 0 & 0 & 1 \end{pmatrix} \times$$

$$\begin{pmatrix} c^2\theta+s^2\theta c\alpha & +s\alpha s\theta & +s\theta c\theta(1-c\alpha) \\ -s\alpha s\theta & c\alpha & +s\alpha c\theta \\ -s\theta c\theta(1-c\alpha) & -s\alpha c\theta & s^2\theta+c^2\theta c\alpha \end{pmatrix} \begin{pmatrix} c\phi & -s\phi & 0 \\ s\phi & c\phi & 0 \\ 0 & 0 & 1 \end{pmatrix} \qquad 4.11$$

An abbreviated notation has been used:

$$s \equiv \sin; \quad c \equiv \cos \qquad 4.12$$

In the common case of pulses applied along the x or y axes of the rotating frame,

$$R_x(\alpha,\theta) = \begin{pmatrix} c^2\theta+s^2\theta c\alpha & s\alpha s\theta & s\theta c\theta(1-c\alpha) \\ -s\alpha s\theta & c\alpha & s\alpha c\theta \\ -s\theta c\theta(1-c\alpha) & -s\alpha c\theta & s^2\theta+c^2\theta c\alpha \end{pmatrix} \qquad 4.13$$

and

$$R_y(\alpha,\theta) = \begin{pmatrix} c\alpha & s\alpha s\theta & -s\alpha c\theta \\ -s\alpha s\theta & c^2\theta+s^2\theta c\alpha & s\theta c\theta(1-c\alpha) \\ s\alpha c\theta & s\theta c\theta(1-c\alpha) & s^2\theta+c^2\theta c\alpha \end{pmatrix} \qquad 4.14$$

Such matrices may then be used to generate new vectors (a', b', c') from old vectors (a,b,c) as follows:

$$\begin{pmatrix} a' \\ b' \\ c' \end{pmatrix} = R(\alpha,\theta,\phi) \begin{pmatrix} a \\ b \\ c \end{pmatrix} \qquad 4.15$$

Clearly the analytical expressions for the result of several such rotations will be very complicated unless simplifications can be made. These might take the form of ignoring the influence of off-resonance effects (when only compensation of inhomogeneity is being considered) or at least truncating these effects to first order.

A powerful alternative which can sometimes be applied renders unnecessary explicit matrix multiplication of this kind. It is possible instead to use the abstract mathematical properties of the rotation matrices to reveal the overall effect of some composite sequences, without the need to investigate the complicated motions which may take place during the sequence. This approach seems to be most useful in the field of composite π pulses and discussion is deferred until that section.

4.3 Composite $\pi/2$ Pulses

4.3.1 General considerations

$\pi/2$ pulses are of course most commonly used for the generation of transverse magnetization from longitudinal magnetization, as in the standard Fourier transform experiment. In this context the

intensity does not vary much with offset or inhomogeneity, and the phase errors tend to be approximately linear functions of offset and so are readily corrected.

However there are many cases in which imperfections in the $\pi/2$ pulses have a significant effect which may prevent proper operation of the experiment. These include techniques in which a preparatory $\pi/2$ pulse, applied to thermal equilibrium magnetization, is used to generate an initial transverse magnetization aligned along some specific axis (usually the y-axis of the rotating frame). Then some sequence of pulses or continuous fields is applied in which it may be essential for proper operation that the initial condition of the magnetization after the $\pi/2$ pulse is well-defined. Examples include spin-locking experiments, in which a continuous radio-frequency field is applied along the y-axis of the rotating frame. The transverse magnetization decays with a time constant $T_{1\rho}$, the relaxation time in the rotating frame. If however the magnetization is not prepared such that it lies exactly along this effective field, the relaxation is combined with a nutational motion which may complicate the analysis and also alter the effective relaxation time (132). Thus in this experiment imperfections in the initial $\pi/2$ pulse are critical in that they may prevent alignment of the magnetization along the proper axis before application of the phase-shifted spin-locking field.

Another example is the Carr-Purcell-Meiboom-Gill sequence for measuring spin-spin relaxation times (94,95). This experiment has already been discussed a little. It resembles the spin-locking experiment quite closely. Instead of a strong continuous radio-frequency field applied along the y-axis of the rotating frame,

a sequence of strong sharp π pulses is applied, also along the y-axis but separated by comparatively long intervals of free precession. The π pulses stimulate a sequence of echoes in which the effect of magnetic inhomogeneity is refocussed so that the echo train ideally decays with the spin-spin relaxation time T_2. The errors produced in this experiment by imperfections in the π pulses will be analysed in a later section. It will be found that under certain conditions, the decay of the echo train is insensitive to these errors. These are firstly that there should be no homonuclear coupling interactions, and secondly that the initial state of the magnetization should be along the y-axis of the rotating frame. So here too it is important that the initial $\pi/2$ pulse should prepare starting transverse magnetization exactly along the y-axis. Any deviation from this condition will cause cumulative errors in the echo train due to imperfections in the π pulses.

For both of these applications a composite sequence is required which will take magnetization from its equilibrium position along the z-axis to some specific orientation in the xy plane (such as the y-axis), independent of a given class of pulse imperfection. Although ways to do this have been found many experiments have a rather less stringent requirement which is easier to fulfil. For these experiments it is simply sufficient that the z-component of magnetization after the pulse is set as closely as possible to zero. The phase of transverse magnetization produced is not of great importance, but the z-component should be zero for <u>each volume element of the sample</u> - it is not a sufficient condition that the average z-magnetization be zero. Examples are the

'progressive saturation' (91) and 'saturation-recovery' (90) methods of measuring spin-lattice relaxation times mentioned in Chapter 1, section 4. Both of these experiments are very efficient methods of measuring spin-lattice relaxation times but are very susceptible to systematic errors caused by imperfect operation of the $\pi/2$ pulses. It is to be expected that these problems may be greatly alleviated by replacing the $\pi/2$ pulses with composite equivalents which produce much smaller residual z-components in the presence of imperfections.

4.3.2 Compensation of inhomogeneity (I):

The $(\pi/2)_x\,(\pi/2)_y$ sequence.

For most composite pulses a decision has to be made as to which class of imperfection is the dominant source of error. Some spectrometers possess transmitter coils which produce a very uniform B_1 field so that the errors produced are small and need not be compensated. In other applications off-resonance effects are more serious.

In this section off-resonance effects are neglected and only the influence of pulse field inhomogeneity is considered. In an inhomogenous radio-frequency field, a simple $\pi/2$ pulse can leave considerable residual z-components in regions of the sample in which the pulse field differs from the nominal. In these places the rotation angle of the magnetization may deviate by some small value Δ. If a rotation of $(\pi/2 + \Delta)$ radians is applied about the x-axis to an initial magnetization of unit magnitude along the +z axis, the residual z-component δz is of value

$$\delta z = - \sin \Delta \qquad 4.16$$

For small missets of the pulse length, or equivalently, small variations in the strength of B_1, this equation expresses a strong linear dependence of residual z-components on Δ. A more favourable sequence would generate a much weaker dependence, preferably only second-order or lower.

A simple solution is to add a second $\pi/2$ pulse, this time about the y-axis of the rotating frame. The result is a composite pulse $(\pi/2)_x(\pi/2)_y$, a rotation of $\pi/2$ radians about the x-axis followed almost immediately by a similar rotation about the y-axis, with the interval between the pulses being just long enough to allow a clean change in the radio-frequency phase but insufficient for significant free precession (125).

The rotation angles $\pi/2$ radians are here nominal values and any variation in flip angle must of course be taken to affect both pulses to the same extent. Thus the effect of pulse field inhomogeneity can be assessed by considering the result of a sequence $(\pi/2 + \Delta)_x(\pi/2 + \Delta)_y$. As has been seen the first rotation leaves a residual z-magnetization of magnitude $-\sin\Delta$. It also creates a much larger component of y-magnetization of magnitude $\cos\Delta$. The second, phase-shifted pulse leaves this desirable component unchanged but rotates the undesirable residual z-component away from the z-axis and toward the -x axis where it represents a small dispersion-mode signal. Were the second pulse exactly $\pi/2$ radians, all z-magnetization would be destroyed at this time, as required. Since the second pulse is also subject to errors

there is in fact a weak second-order dependence of z-magnetization on Δ, which is easily deduced as:

$$\delta z = \sin^2\Delta \qquad 4.17$$

For small imperfections the residual z-magnetization is negligible making the $(\pi/2)_x(\pi/2)_y$ sequence very suitable for applications to experiments such as progressive saturation.

An experimental test of the sequence can be made by measuring the residual z-magnetization produced by the composite pulse. This was done using a sequence:

$$P_1 - P_2 - \text{acquisition} \qquad 4.18$$

in which P_2 is a 'read' pulse of flip angle $\pi/2$ radians and P_1 is either the composite $\alpha_x\alpha_y$ sequence or a single conventional α_x pulse. Inhomogeneity effects were minimised by using a small, spherical bulb sample, the duration of the pulses comprising P_1 then being altered in order to cause a known variation in α around the $\pi/2$ condition. In this way the effect of inhomogeneity in B_1 could be simulated in a controlled way. The residual z-component of magnetization produced by the P_1 sequence was isolated and measured by repeating the experiment, but with inversion of the phase relationship between the P_1 and P_2 sequences. Then the transverse magnetization created by P_1 does not contribute to the average signal.

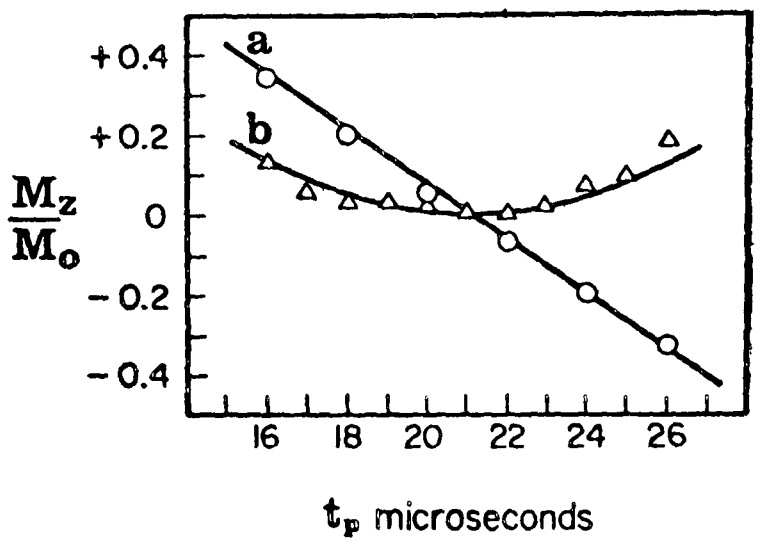

Fig.4.2. The residual z-magnetization remaining after (a) a conventional $(\pi/2)_x$ pulse, (b) a composite $(\pi/2)_x(\pi/2)_y$ sequence. The full lines represent calculations based on magnetization trajectories.

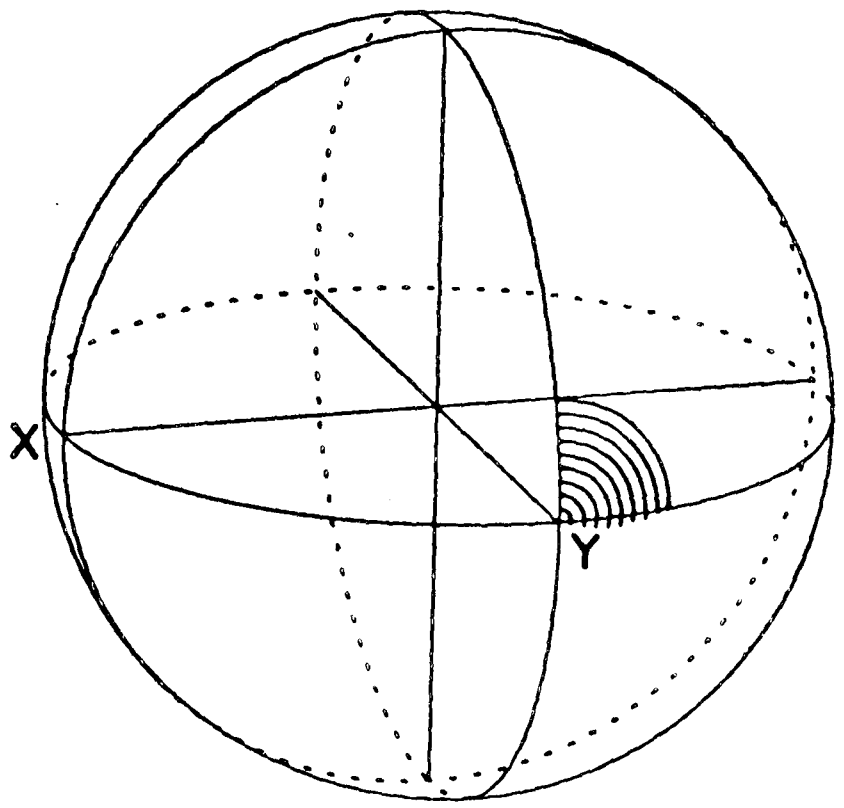

Fig.4.3. Trajectories of a family of magnetization vectors during a $(0.5\pi)_x(0.61\pi)_y$ sequence. The vectors have been assigned pulse length missets between 0.8 and 1.0 times the nominal value. Note the very small residual z-magnetization remaining at the end of the sequence.

The experimental results are summarised by Figure 4.2. When P_1 is a composite pulse, the residual z-components pass through a shallow minimum on variation of pulse times t_p. This corresponds to equation 4.17. In contrast, when P_1 is a single conventional pulse, the strong linear dependence of equation 4.16 is observed, the z-components only being close to zero at the exact condition $\gamma B_1{}^o t_p = \pi/2$ radians. The experimental points fit the theoretical curves quite well. The results suggest strongly that errors in relaxation time measurements caused by B_1 inhomogeneity should be less of a problem if a composite $(\pi/2)_x(\pi/2)_y$ sequence is used.

A further slight improvement to the sequence can be made by taking into account the fact that the distribution of B_1 fields is usually strongly skewed with far more volume elements experiencing B_1 fields significantly lower than nominal than higher than nominal. The pulse sequence can be biased such that it compensates negative deviations Δ particularly well. This can be done by increasing the length of the second pulse beyond the nominal value $\pi/2$ radians. An example chosen for computer simulation is the sequence $(0.5\pi)_x(0.61\pi)_y$ whose operation is illustrated in Figure 4.3. This diagram depicts the trajectories of a family of magnetization vectors which experience B_1 fields somewhat less than nominal, between 0.8 and 1.0 $B_1{}^o$. Note that their courses all terminate very close to the xy plane, and exactly so for the conditions

$$B_1 = B_1{}^o \text{ and } B_1 = \frac{0.5}{0.61} B_1{}^o \ (= 0.82\ B_1{}^o) \qquad 4.19$$

4.3.3 Compensation of inhomogeneity (II):

The $(\pi/2)_x\pi_y$, sequence.

The $(\pi/2)_x(\pi/2)_y$ sequence described above (and variations intended to compensate particularly well low B_1 fields), suffer the disadvantage that the residual error after the first pulse is simply converted into a residual error in the xy plane - that is, a phase error of the transverse magnetization produced. This may be problematic in some cases, for although the unwanted residual z-component has been set to zero, the precise orientation of magnetization components after the pulse is still to some extent indeterminate. This is a serious problem in those experiments which require exact alignment of the magnetization along the y axis for the best results, such as the spin-locking and Carr-Purcell-Meiboom-Gill sequences. The $(\pi/2)_x(\pi/2)_y$ sequence is no better than a single pulse in this context.

For these experiments a sequence has been found which has the very favourable property of 'focussing' magnetizations onto some pre-determined axis in the transverse plane, irrespective of small errors in the flip angles arising from pulse inhomogeneity. Unfortunately it is rather inconvenient to implement, since not only does it require an unusual phase shift of $\pi/6$ radians in the transmitter reference frequence, but also produces a magnetization oriented at the inconvenient angle of $\pi/3$ radians with respect to the y-axis. Thus its routine use would require the construction of computer-controlled circuitry capable of producing phase shifts in steps of $\pi/6$ radians, and this would probably only be worthwhile in extreme cases.

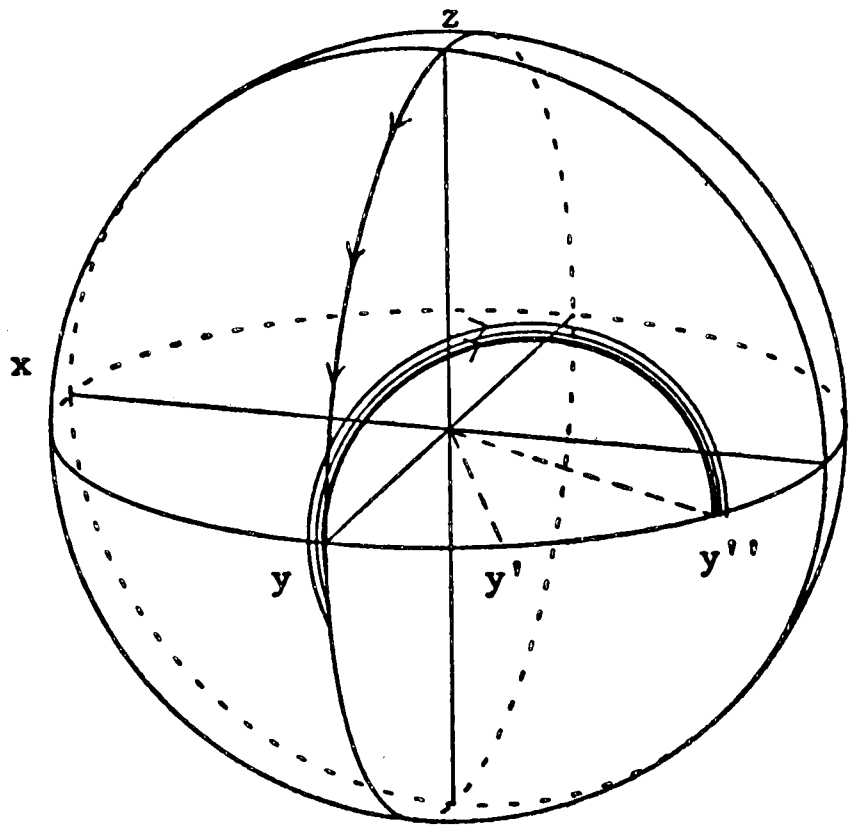

Fig.4.4. Trajectories of a family of magnetization vectors during the $(\pi/2)_x\ \pi_{y'}$ sequence, with pulse lengths misset between 0.85 and 1.15 times the nominal value. Note that all trajectories terminate very close to the axis y''.

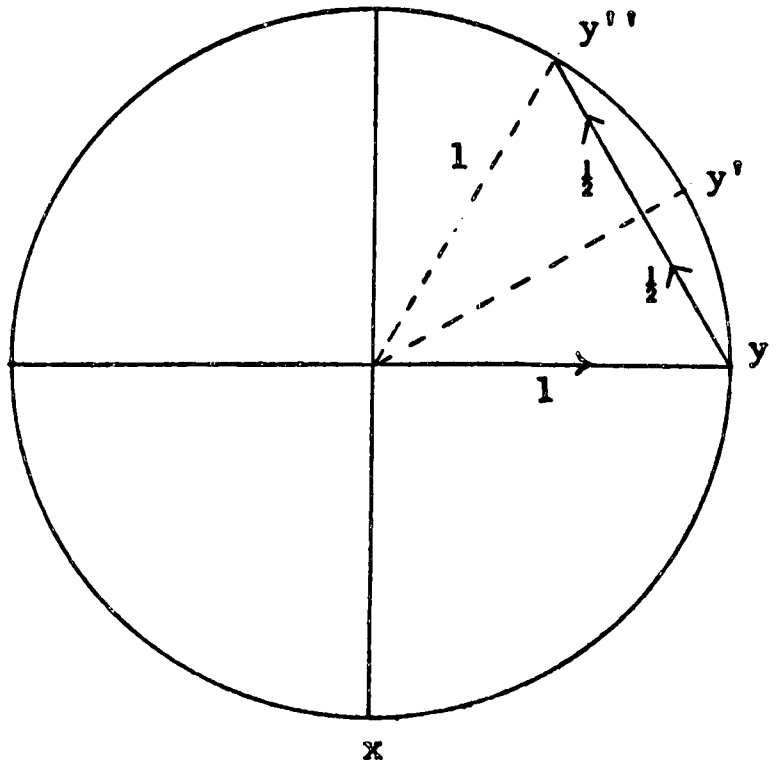

Fig.4.5. Geometry of the $(\pi/2)_x\ \pi_{y'}$ sequence. Since the rotation of π radians about axis y' has radius ½, the arc length during that excursion is the same as during the first pulse (which is by only $\pi/2$ radians but has radius 1). Hence the errors produced by the two rotations are of the same magnitude and may compensate each other.

Nevertheless this special sequence does have some interesting properties which merit its inclusion here. The sequence is as follows: Firstly a conventional $(\pi/2)_x$ pulse which brings magnetization from the z-axis to a position close to the y-axis of the rotating frame. This is followed by a rotation of π radians about an axis y', which lies in the xy plane between the y and -x directions, and at an angle of $\pi/6$ radians with the y-axis.

The operation of the proposed composite pulse is illustrated in Figure 4.4, which again concerns the trajectories of a group of magnetization components which experience a range of B_1 fields, and hence flip angles. After the first $(\pi/2)_x$ pulse, they lie in the yz plane, with residual z-components. As can be seen, the second π_y' pulse now takes them all on trajectories which terminate very close to the axis y", which is at an angle of $\pi/3$ radians from the y axis. Note that the errors in the two pulses seem to compensate each other almost completely. Although the first pulse may be rather short this is compensated by the short π pulse, so that all the isochromats appear to be 'refocussed' in some way onto the axis y".

The reason for this refocussing effect is that the trajectories during the first and second pulses are tangential, and in opposite directions. Hence small errors in the first rotation tend to 'unwind' during the second, even though this takes the magnetizations on a different path. There must be some point on the second trajectory at which the errors compensate each other, and at which all vectors refocus to a good approximation. It is simply necessary to define the condition that the refocussing point lie at some point in the

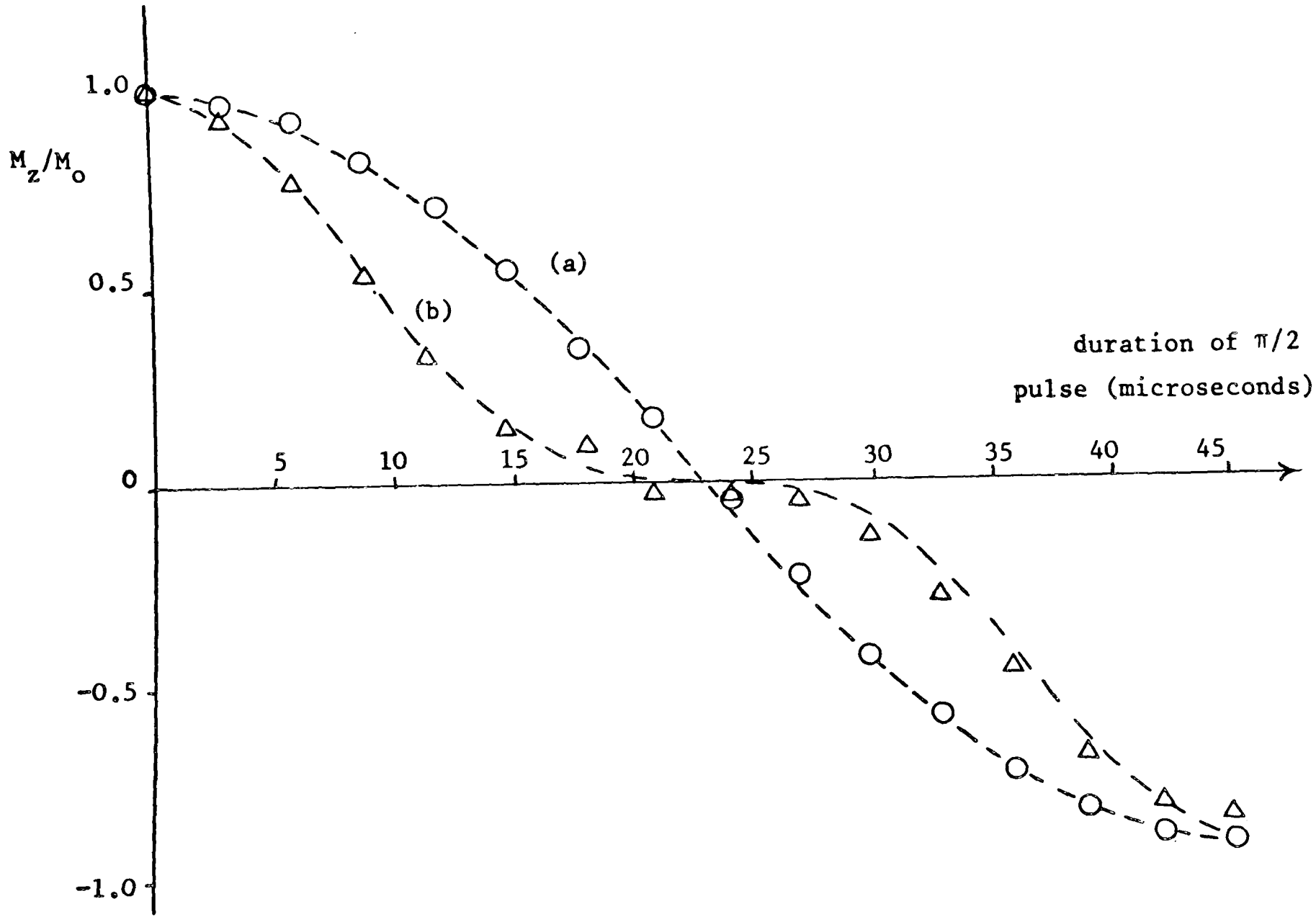

Fig.4.6. Residual z-components remaining after (a) a conventional single pulse of pulse length shown, and (b) after a composite $(\pi/2)_x\ \pi_{y'}$ sequence, with the duration of the second pulse always twice that of the first. The phase shift of $\pi/6$ radians was substituted by a period of free precession, calculated according the known frequency offset of the test resonance (carbon-13 signal of formic acid).

xy plane. This requires that the arcs traced out during the first and second pulses should be of equal length, which demands in turn that the second pulse be phase-shifted by $\pi/6$ radians from the y-axis. Only then is the arc during the first rotation, which subtends an angle of $\pi/2$ radians and is of radius 1, of the same length as the arc during the second rotation, which must subtend π radians and hence has to have a radius $\frac{1}{2}$. (see Figure 4.5). The result is a composite pulse which accurately locates magnetization components onto the axis y" of Figure 4.5.

The only errors produced by this sequence occur because the trajectories during the two pulses are no longer exactly tangential if large missets are considered. In fact the z-component is set to zero to third order in Δ, as can be verified by explicit calculation using rotation matrices giving

$$\delta z = \frac{1}{4}(\sin 3\Delta - 3\sin\Delta) \qquad 4.20$$

$$\simeq -\frac{1}{4}\Delta^3 \qquad 4.21$$

This can be verified experimentally in the same way as for the $(\pi/2)_x(\pi/2)_y$ sequence above. The results fit theoretical expectation very well. The residual z-components produced by the $(\pi/2)_x(\pi)_y$, sequence are small, having a cubic dependence and are represented in Figure 4.6. The curve for a single, conventional $\pi/2$ pulse is also shown and compares very unfavourably. In this test experiment, the difficult $\pi/6$ phase shift was accomplished for the chosen resonance by inserting between the two pulses an interval of free precession of duration τ where $\delta\tau = \frac{1}{6}\pi$ radians, and δ is the

offset of the resonance from the transmitter reference frequency. This is not a general method since it requires knowledge of the offset of the test resonance, and it is not possible to achieve compensation in this way for a full spectrum. Nevertheless the experiment served well to illustrate the feasibility of this pulse sequence.

4.3.4 Compensation for resonance offset (I):

The $(\pi/2)_x(3\pi/2)_y$-τ sequence

When a pulse is applied off-resonance, rotation of the magnetization takes place about an effective field tilted away from the xy plane. Thus a $\pi/2$ pulse no longer places an initial z-magnetization exactly along the y-axis. The vector finishes up close to the equatorial plane but with a large phase deviation from the y-axis and a smaller positive elevation above the xy plane. These imperfections produce effects similar to those due to inhomogeneity. In some experiments the residual z-components produced are the source of trouble, and composite sequences may be devised which leave vanishingly small residual z-components over a wide range of resonance offsets. But in a more demanding set of applications it is necessary to produce compensating pulse sequences which leave all magnetization vectors close to the y-axis, and not simply at some arbitrary orientation in the xy plane.

This is a complex problem. It is hard to visualise the overall effect of a set of rotations, each about a tilted field in the rotating frame: A set of pulses is required which has an overall effect, $z \rightarrow y$, independent of the tilt angle. Furthermore off-

resonance effects can be quite large and tilt angles of 10^{o} are not uncommon. Hence first-order approximations may not be sufficient in practical cases.

Nevertheless the first sequence which will be described does provide compensation only to first-order in the off-resonance parameter. However it does have a considerable practical advantage in being very easy to set up, and may also be thought of quite simply without resort to extensive computer simulation.

The proposed sequence in its simplest form is:

$$(\pi/2)_x(3\pi/2)_y - \tau \qquad 4.22$$

That is, a pulse of $\pi/2$ radians about the x-axis, followed by a pulse three times longer about the y-axis, and then a period of free precession τ, which will be shown to take the value

$$\tau = 1/(\gamma B_1{}^{o}) \text{ seconds.} \qquad 4.23$$

$B_1{}^{o}$ is as usual the nominal strength of the radio-frequency field, taken to be perfectly homogenous for the purposes of this section. (If the transmitter were turned on for a time τ, a pulse of nominal flip angle 1 radian would result.)

It will now be shown that this sequence rotates magnetizations from the z to the y axes of the rotating frame, independent of the off-resonance parameter θ, to first order.

To appreciate how this sequence operates it is necessary to become accustomed to the effect of tilted rotations. First consider the $(\pi/2)_x$ pulse, applied to thermal equilibrium z-magnetization of unit magnitude. Applying the rotation operator of equation 4.13 to initial z-magnetization according to equation 4.15 produces a vector:

$$R_x(\alpha,\theta)\begin{pmatrix}0\\0\\1\end{pmatrix} = \begin{pmatrix}\sin\theta\cos\theta(1-\cos\alpha)\\ \sin\alpha\cos\theta\\ \sin^2\theta + \cos^2\theta\cos\alpha\end{pmatrix} \qquad 4.24$$

θ is the off-resonance tilt angle and α the flip angle about the effective field, these being given by equations 4.9 and 4.10. Equation 4.10 shows that the tilted effective field is in fact stronger than the applied radio-frequency field by a factor $\sec\theta$, so that the flip angle α is also somewhat greater than the nominal flip angle of $\pi/2$ radians:

$$\alpha = \frac{\pi}{2}\sec\theta \qquad 4.25$$

This effect will be of considerable importance in some of the sequences to be described but it will be ignored here because it is a second-order effect. Retaining only first-order terms in θ, equation 4.24 becomes:

$$R_x(\tfrac{\pi}{2},\theta)\begin{pmatrix}0\\0\\1\end{pmatrix} \simeq \begin{pmatrix}\theta\\1\\0\end{pmatrix} \qquad 4.26$$

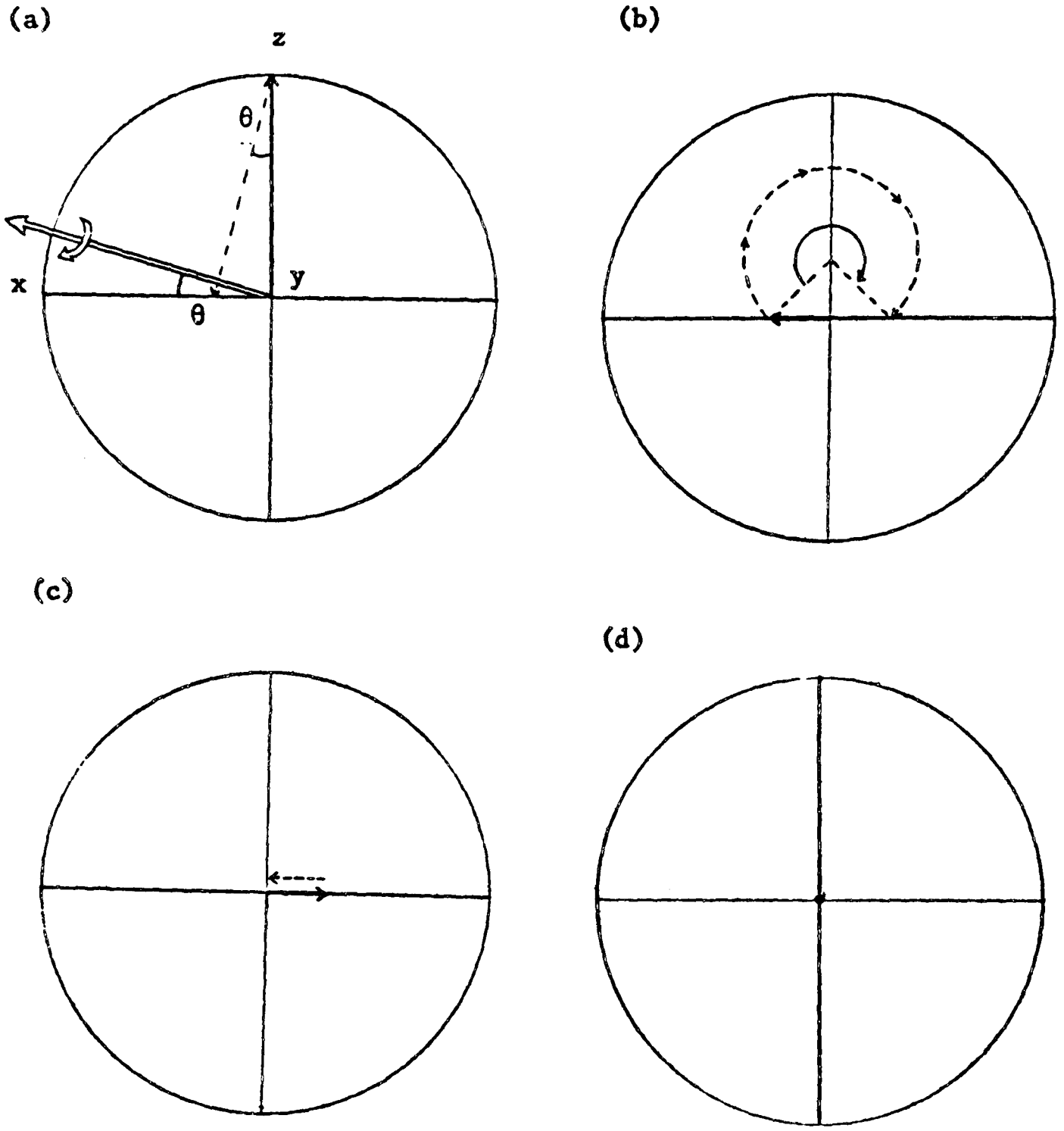

Fig.4.7. The trajectory of a vector during the $(\pi/2)_x(3\pi/2)_y$-τ sequence, as seen from along the y-axis of the rotating frame.

(a) Rotation by $\pi/2$ radians about a tilted field in the xz plane.

(b) Rotation by $3\pi/2$ radians about a tilted field in the yz plane then places the vector in a mirror-image position with respect to that plane.

(c) Precession for a time τ, where $\tau = 1/(\gamma B_1)$ seconds, brings the vector to the y-axis, independent of offset.

All of these operations are valid only to first order in θ.

This is a vector close to the y-axis but with a positive error in the x-component proportional to θ. This is shown in Figure 4.7(a).

The next step is to turn this vector into a mirror-image position with respect to the y-axis, Figure 4.7(c). Were the rotations not about tilted fields, a π pulse about the y-axis would be the obvious way to do this. However it is clear on examination that such a rotation about a tilted field would take the magnetization far above the xy plane. Another solution must be found. Simple geometry shows that the appropriate operation is a rotation by the much larger angle of $3\pi/2$ radians about the y-axis. This is because the initial position of the vector, the desired final position, and the rotation axis define a right-angled isosceles triangle as can be seen from Figure 4.7(b). Because only clockwise rotations are allowed a rotation of $3\pi/2$ radians is required. This can be verified by using the rotation operators. Applying the operator of equation 4.14 to the vector of equation 4.26, setting $\alpha = 3\pi/2$ and neglecting high-order terms in θ,

$$R_y(\frac{3\pi}{2},\theta)R_x(\frac{\pi}{2},\theta)\begin{pmatrix}0\\0\\1\end{pmatrix} \simeq \begin{pmatrix}0 & -\theta & 1\\ \theta & 1 & \theta\\ -1 & \theta & 0\end{pmatrix}\begin{pmatrix}\theta\\1\\0\end{pmatrix}$$

$$\simeq \begin{pmatrix}-\theta\\1\\0\end{pmatrix} \qquad 4.27$$

This is the mirror-image vector as anticipated. Now the signficance of the mirror-image position becomes clear if the vectors are

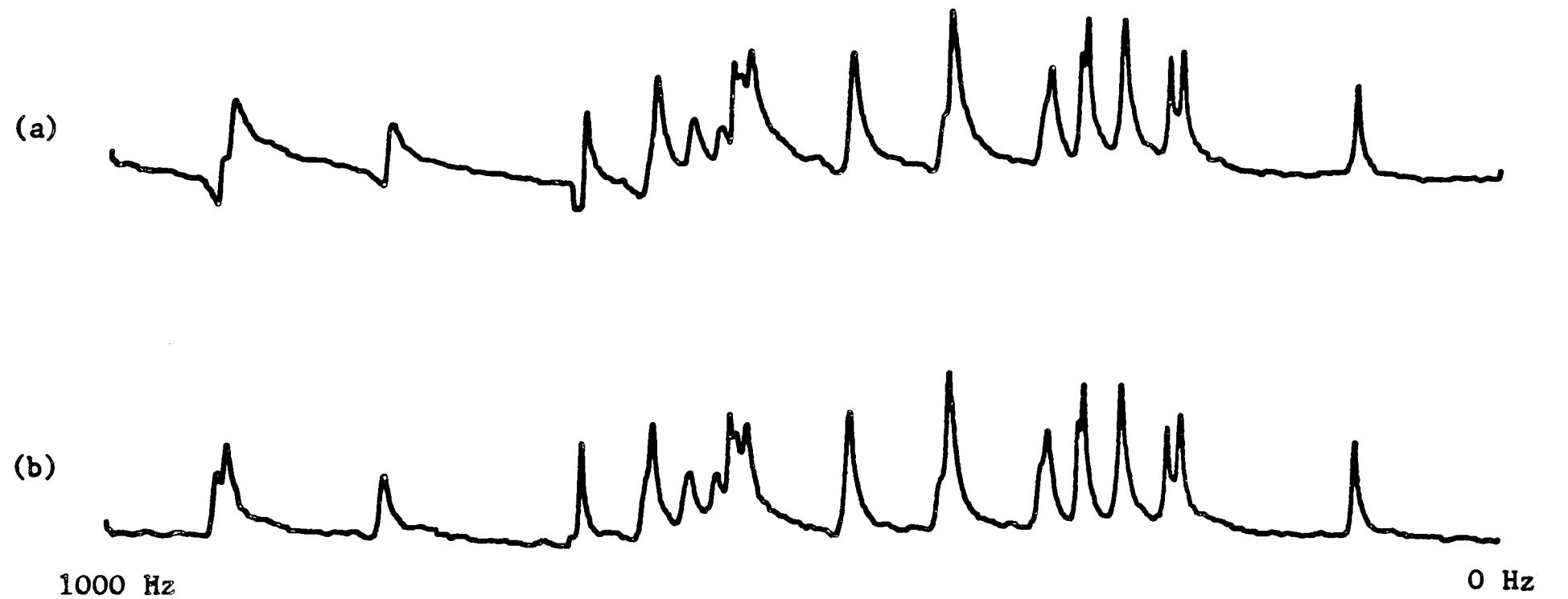

Fig.4.8. Experimental ^{13}C spectra of cholestryl acetate, obtained with a single $\pi/2$ pulse (a), or with a $(\pi/2)_x(3\pi/2)_y$-τ sequence (b). No phase correction has been applied to these spectra. The frequency-dependent phase error generated by the composite pulse is clearly much less than for the conventional pulse. (Spectra obtained on the CFT-20).

allowed to precess for some period according to their resonance offsets. The mirror-image vectors have the curious property that they then refocus onto the y-axis after a given interval, independent of their off-resonance frequencies. Vectors far off-resonance precess faster than vectors close to resonance, but they have been placed proportionately further from the y-axis by the preparatory $(\pi/2)_x(3\pi/2)_y$ sequence. The rate of precession in the rotating frame is $\Delta\omega$ rad s^{-1}, which is equal to $\gamma B_1\theta$ to first-order in θ. Hence for a given vector to cover the θ radians which lie between it and the y-axis an interval $1/(\gamma B_1)$ seconds should be left. This is independent of θ and so causes a refocussing at the y-axis as illustrated in Figure 4.7(d). The entire sequence becomes $(\pi/2)_x(3\pi/2)_y - \tau$, with $\tau = 1/(\gamma B_1)$ seconds.

For a typical B_1 field strength of $\frac{\gamma B_1}{2\pi}$ = 12.5 kHz, τ takes the value 13 μs. This is too short for relaxation to be a problem.

The refocussing property during the period τ may be thought of as a new sort of spin echo, taking place over a time period much shorter than the conventional echoes stimulated by π pulses. The analogy is quite complete, since any differences in precession frequencies, due to chemical shifts or magnet inhomogeneities, should be refocussed to form a small echo at the end of the τ period.

This sequence could be used for the straightforward excitation of transverse magnetization, whose phase should then be independent of offset, rendering unnecessary the usual application of a linear phase gradient to the Fourier transform spectrum. This capability is illustrated in Figure 4.8 which shows a wide spectrum excited by a composite pulse, or a conventional single pulse. The single

pulse generates a phase gradient which is clearly seen whilst the phase of magnetization excited by the composite pulse remains almost independent of offset. The phase errors generated by the conventional pulse are also augmented by the fact that a small period (~10 μs) must be left after the pulse in order to allow the recovery of the receiver electronics before data acquisition; this causes further precession and dephasing of off-resonance magnetization components. In the composite sequence there is no need to leave such an interval because it occurs quite naturally as part of the compensation process.

Note: In practice, a different problem is encountered in that a small interval must be left to allow change of phase between the $(\pi/2)_x$ and $(3\pi/2)_y$ pulses in the composite sequence. This can disrupt the compensation unless account is taken of it. Simple geometry leads to the conclusion that the appropriate action is as follows: If an interval ε must be left between the pulses, a similar period should be added to the τ period at the end of the sequence. In addition the length of the $(3\pi/2)_y$ pulse should be modified to the new value $2\pi - 2\tan^{-1}(1 + \gamma B_1 \varepsilon)$. These recommendations ensure that to first order the magnetization is still returned to a mirror-image position, and so still refocusses onto the y-axis. In practice, if $\frac{\gamma B_1}{2\pi}$ is 12.5 kHz and ε = 20 μs, the sequence should be modified to:

$$(\pi/2)_x - \varepsilon - (1.29\pi)_y - \tau \qquad 4.28$$

with τ = 33 μs.

These values were used for the experimental results of Figure 4.8.

4.3.5 Compensation for resonance offset (II):

The $(\alpha)_{-x} - \tau_1 - (\pi/2+\alpha)_x$ sequence

Just as for compensation for inhomogeneity, there are some applications of $\pi/2$ pulses in which it is most important that the residual z-component of magnetization after the pulse is always small. The phase of the transverse magnetization produced is not so important. The question arises whether this can be accomplished to any degree of accuracy for magnetizations experiencing homogenous, but far off-resonance, radio-frequency fields.

In fact it is well-known that a simple $\pi/2$ pulse is to some extent already internally compensated if only the residual z-component after the pulse is considered (91). The reason is that the tilt of the off-resonance effective field is counteracted by its increased magnitude. This can be verified algebraically. The result of applying a tilted $\pi/2$ pulse to z-magnetization has already been analysed and is given by equation 4.24, in which the effective flip angle α is somewhat greater than the nominal value of $\pi/2$ radians according to equation 4.25. Combining these two equations, the residual z-component of magnetization after the pulse is

$$\delta z = \sin^2\theta + \cos^2\theta\cos(\frac{\pi}{2}\sec\theta) \qquad 4.29$$

If terms higher than second-order in θ are ignored this can be reduced to:

$$\delta z \simeq (1 - \frac{1}{4}\pi)\theta^2 \qquad 4.30$$

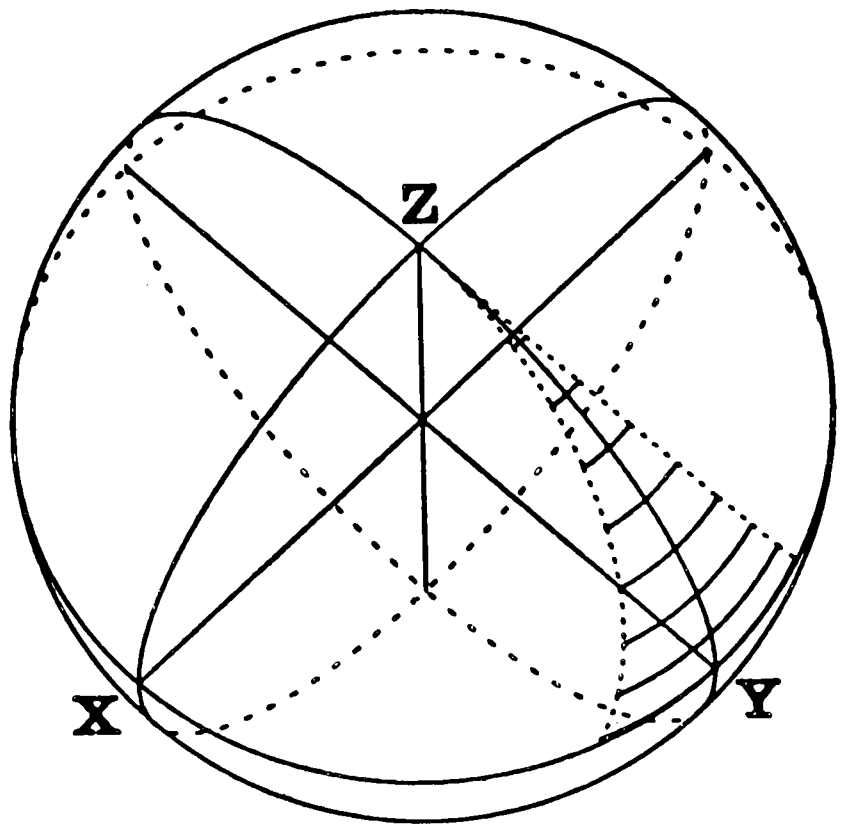

Fig.4.9. The self-compensating effect of a single $\pi/2$ pulse. A family of magnetization vectors representing offsets $\tan\theta$ between -0.33 to 0.33 has been considered, the locus of the tips of the vectors being drawn at regular intervals (full lines). Note that the final locus lies very close to the xy plane.

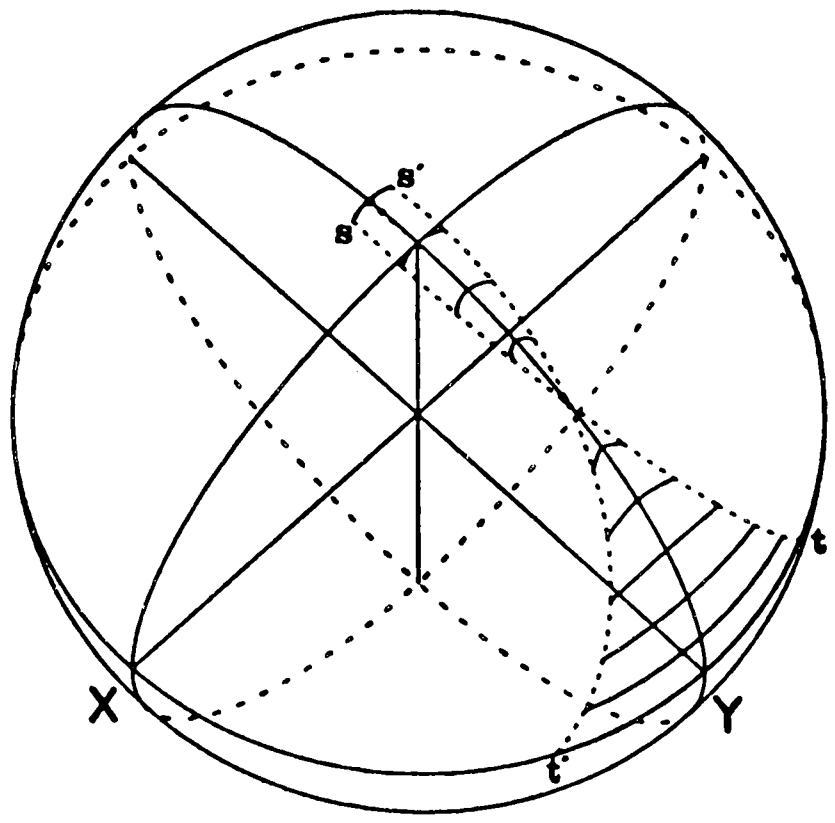

Fig.4.10. Compensation of resonance offset effects with a $(10^{o})_{-x}, \tau_1, (100^{o})_{x}$ sequence, with τ_1 chosen so as to minimise the residual z-magnetization after the pulse (with $\gamma B_1/2\pi$ = 10kHz, τ_1 = 9 μs).

Since $\frac{1}{4}\pi$ is not far from unity ($\frac{1}{4}\pi \simeq 0.79$), even this second-order term is small.

This point can also be illustrated by computer simulation. In Figure 4.9 a family of vectors representing a range of offsets is followed as they nutate around their respective effective fields. To illustrate their motion most clearly, the loci of the tips of the vectors are drawn at various stages of the trajectories; this gives an impression of the evolution in time. The curvature of the final locus is very small, so that it fits very close to the equator of the rotating reference frame. In contrast the phase errors are large, and essentially a linear function of offset.

If so desired a composite sequence can be used which reduces these small residual z-components even further. The sequence consists of two pulses, acting in opposite senses, and separated by a period τ of free precession which is adjusted so that it introduces a small curvature of the locus which exactly counteracts the curvature of Figure 4.9. This is illustrated in Figure 4.10. The sequence starts with a small pulse of 0.055π radians (10^{o}) about the -x axis, which takes the magnetization vectors from the z-axis to a position midway between points s and s' in Figure 4.10. Free precession for a period τ then causes the magnetization vectors to spread out and form the curved locus s-s'. Finally a pulse of 0.555π radians (100^{o}) carries the family of vectors towards the xy plane, the final locus lying very close to the equator. The computer simulation was carried out assuming a radio-frequency field strength of

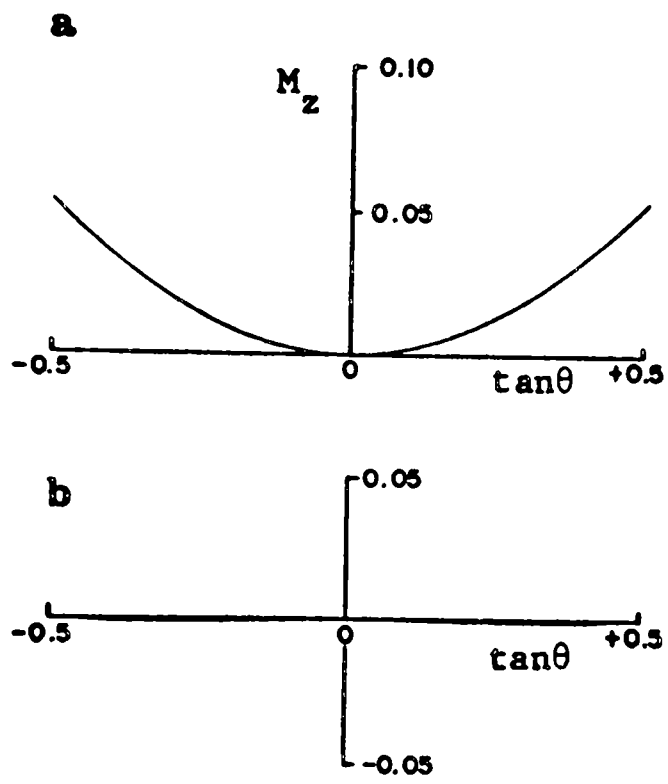

Fig.4.11. Compensation for resonance offset effects with a $(10^o)_{-x},\tau_1,(100^o)_x$ composite pulse. The residual z-magnetization after a conventional 90^o pulse (a) is compared with that after the composite two-pulse sequence (b).

$\gamma B_1/2\pi$ = 10 kHz, and the optimum value of τ found to be 9 μs. To apply this and following results to situations of different B_1 strengths, precession times should always be changed in inverse proportion. Thus if $\gamma B_1/2\pi$ were 20 kHz, the optimum sequence would be:

$$(0.055\pi)_{-x} - 4.5\mu s - (0.555\pi)_{x} \qquad 4.31$$

The improvement in residual component after the two-pulse sequence is clearly illustrated in Figure 4.11(a,b). These are graphs of z-component against offset parameter tanθ. For the conventional $\pi/2$ pulse (Figure 4.11a) there is an approximately parabolic dependence, whilst for the composite two-pulse sequence (Figure 4.11b), the curve is almost completely flat.

4.3.6 Compensation for resonance offset (III): 'Spin knotting'.

The two-pulse sequence of the previous section provides a clue for a composite sequence which compensates for both z-component and phase errors at the same time, over a wide range of resonance offsets. Although a scheme which does this has already been suggested in section 4.3.4, that pulse sequence provided compensation accurate only to first order and hence only applicable to small resonance offsets. The following scheme provides compensation over a wider range; for such a gain a sacrifice must usually be made, and in this case it is one of simplicity. The pulse sequence contains four independent variable parameters which must be optimised by computer simulation. The proposed sequence consists

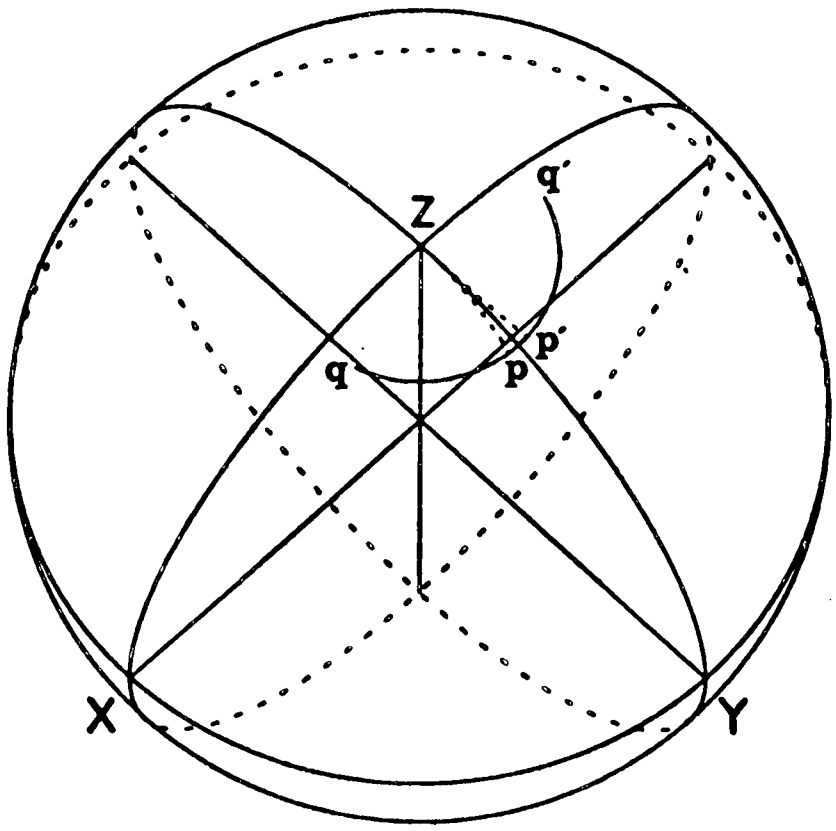

Fig.4.12. "Spin-knotting" pulse sequence. A 20° pulse along the x-axis places the family of magnetization vectors along the locus p-p'. A period of 30μs free precession then disperses the vectors along the line q-q'. A range of offsets tanθ = -0.5 to +0.5 has been treated. .

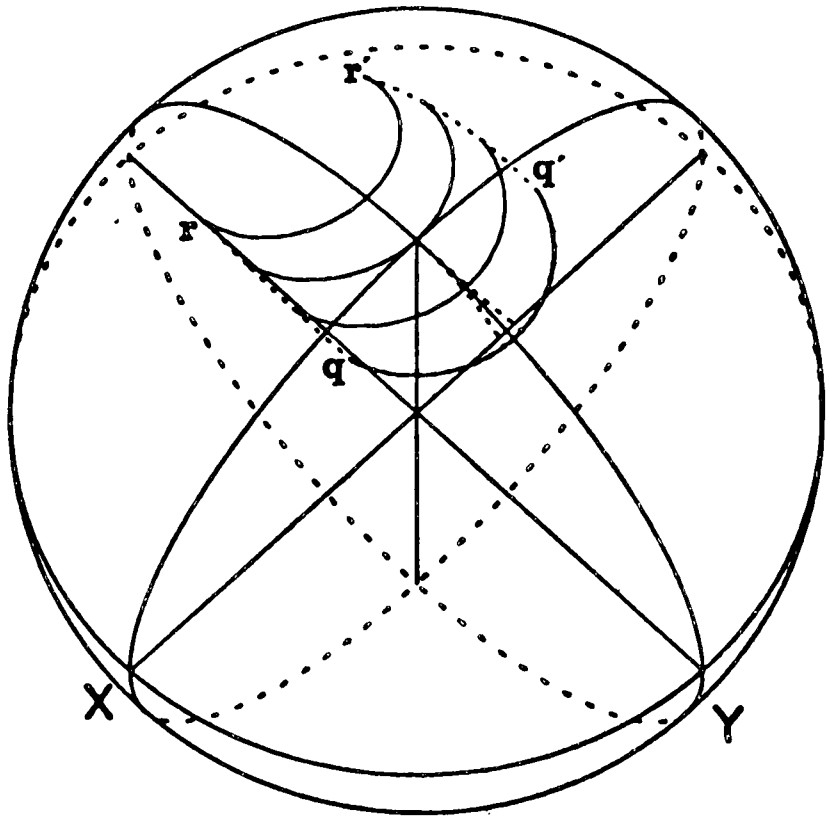

Fig.4.13. The second pulse, $(30^{o})_{-x}$ takes the locus from q-q' to r-r'.

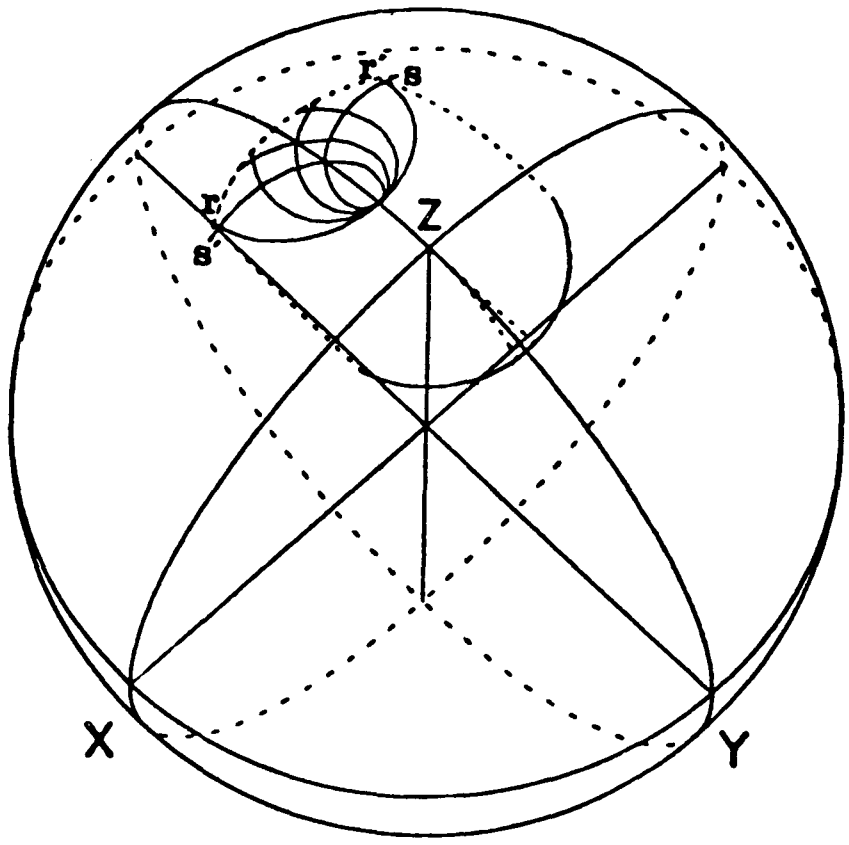

Fig.4.14. The second period of free precession, 30 μs long, causes the locus r-r' to fold in upon itself, to form the loop s-s'.

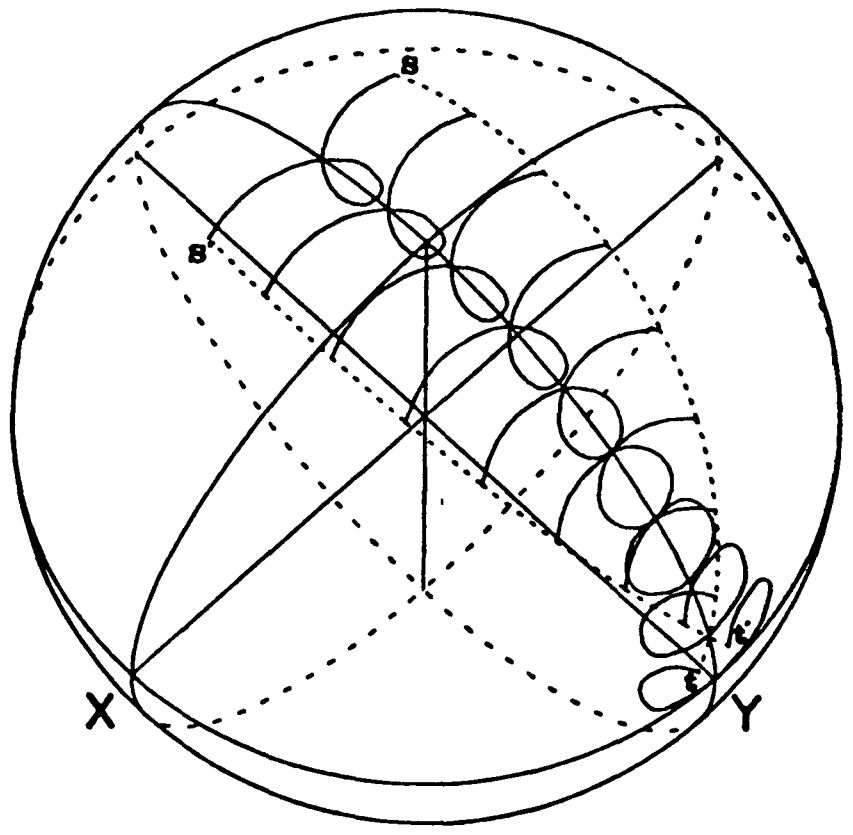

Fig.4.15. The final pulse, $(100^{o})_{x}$, takes the loop s-s' towards the y-axis, leaving it in the form of a a bow t-t'.

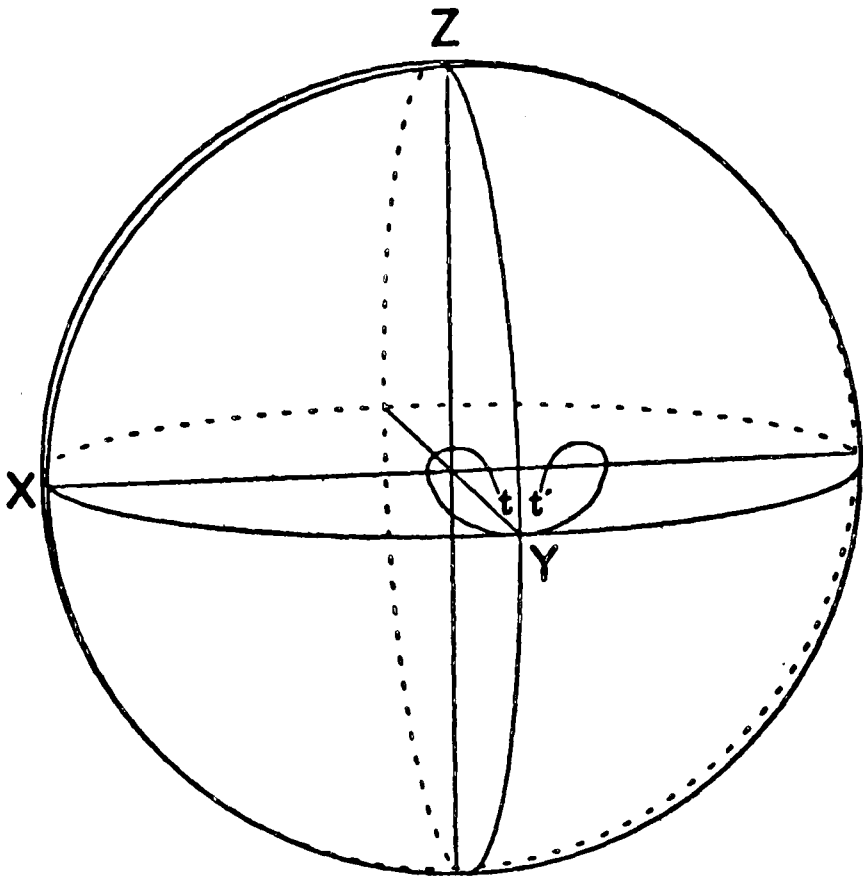

Fig.4.16. The final locus formed by the family of magnetization vectors, after a "spin-knotting" pulse sequence, as seen from approximately along the y-axis.

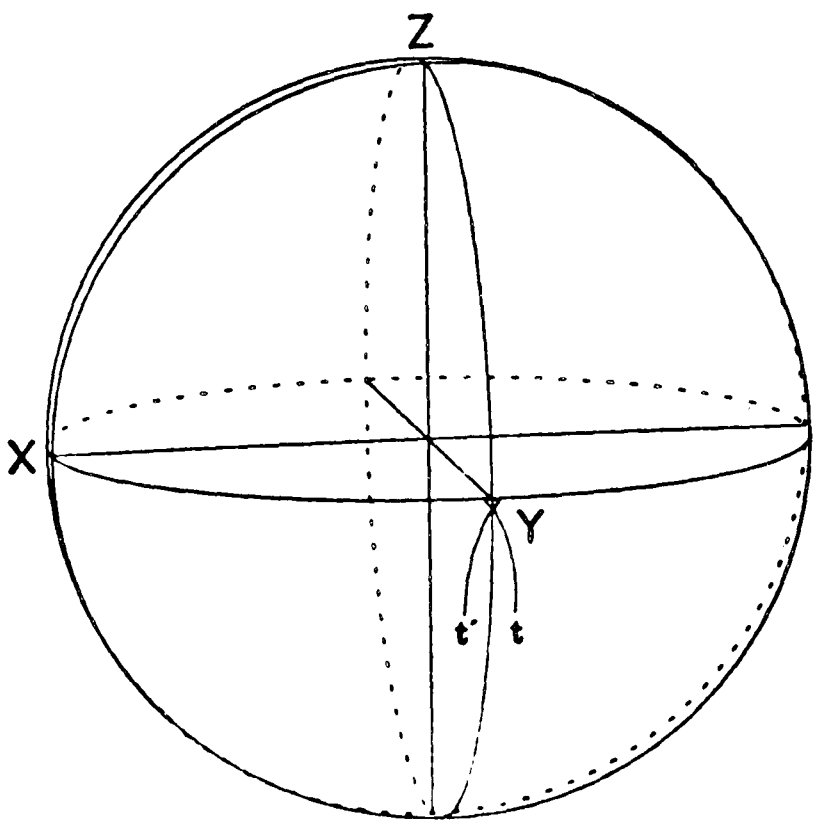

Fig.4.17. The bow can be tightened by optimisation of the variable parameters. This locus is the result of a $(10^{o})_{x}$,40μs,$(60^{o})_{-x}$, 11μs,$(140^{o})_{x}$ sequence.

of three pulses separated by two intervals of free precession. The algebraic sum of the three nominal flip angles is kept as $\pi/2$ radians, so that at exact resonance a vector is carried exactly from the +z axis to the +y axis. Thus there are four independent variables. The time evolution during the sequence is most clearly visualised if these do not at first take their optimum values.

The three pulses are applied about the +x, -x and +x axes respectively. The first pulse is given the nominal flip angle 0.111π radians (20^{o}), which is small enough that tilt effects are almost negligible. It is followed by free precession for a period of 30 μs. The loci of the tips of magnetization vectors with a spread in offset parameters of $\tan\theta$ between 0.5 and -0.5 are illustrated in Figure 4.12. At this time the vectors lie on a locus q-q'. The second pulse, of 0.167 radians (30^{o}) is now aplied about the -x axis, and takes the arc back over the pole (+z) to form a locus r-r' (Figure 4.13). A further 30 μs period of free precession follows. During this time the arc folds in upon itself reversing the relative positions of clockwise and counter-clockwise precessing vectors and producing the loop s-s' of Figure 4.14. The final pulse, of nominal flip angle 0.555π radians (100^{o}) takes this loop back over the pole where it forms a bow around the +y axis (Figure 4.15). The final bow-shaped locus t-t' is seen more clearly in the projection of Figure 4.16.

The 'knot' around the y-axis can be made tighter by optimising the variable parameters. Trial-and-error simulations indicate a sequence, which must be near-optimum, of

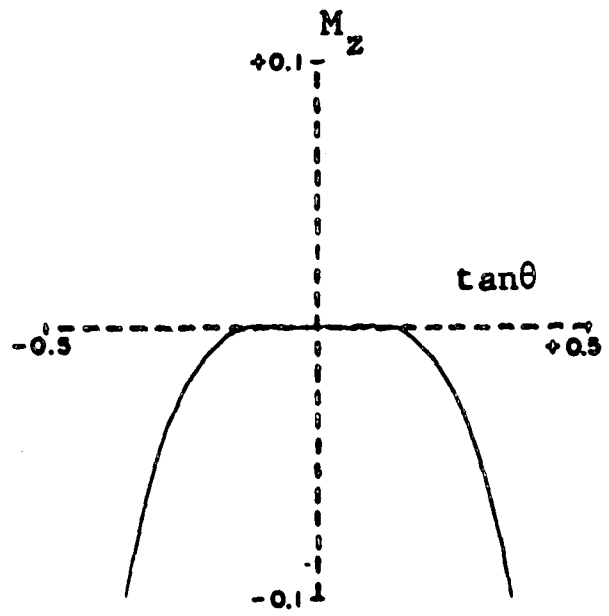

Fig.4.18. Residual z-components after an optimised "spin-knotting" sequence.

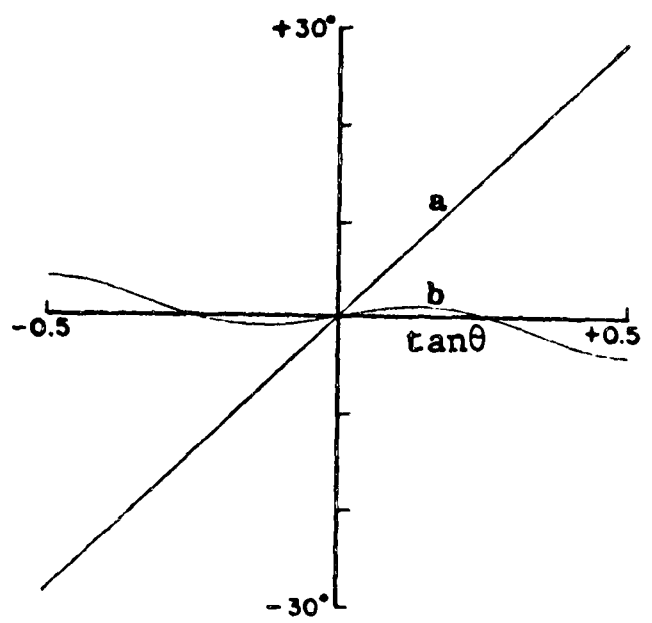

Fig.4.19. Compensation of resonance offset effects by the "spin-knotting" pulse sequence. The phase errors produced by a single pulse (a) are compared with those after a "spin-knotting" sequence (b).

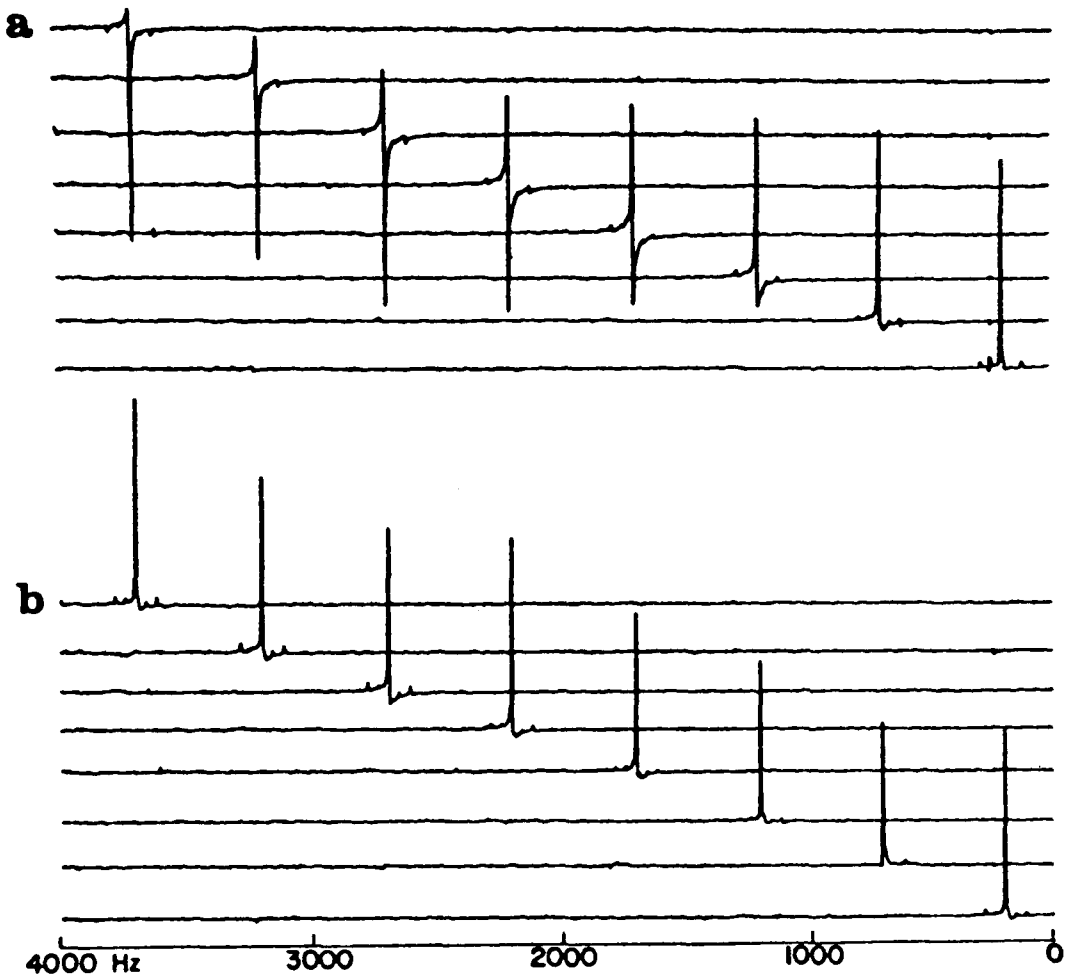

Fig.4.20. An experimental test of the compensation of phase errors by the "spin-knotting" sequence. (a) After a conventional single pulse, a signal which is correctly phased close to resonance rapidly acquires phase errors as it is moved away from resonance. (b) After the "spin-knotting" sequence, the errors are effectively compensated.

Table 4.1. A comparison of composite $\pi/2$ pulses.

Sequence	Compensation	Application	
		Saturation	Preparation for spin-locking or Carr-Purcell-Meiboom-Gill spin echo trains.
$(\pi/2)_x(\pi/2)_y$	B_1 inhomogeneity	✓	×
$(\pi/2)_x\ \pi_{y'}$	B_1 inhomogeneity	✓	✓
$(\pi/2)_x(3\pi/2)_y\text{-}\tau$	Resonance offset	×	✓
$\alpha_{-x}\ \text{-}\tau_1\text{-}(\pi/2+\alpha)_x$	Resonance offset	✓	×
"spin knotting"	Resonance offset	✓	✓

$$(0.555\pi)_{x} - 40\mu s - (0.333\pi)_{-x} - 11\mu s - (0.778\pi)_{x} \qquad 4.32$$

or in degrees:

$$(10^{o})_{-x} - 40\mu s - (60^{o})_{x} - 11\mu s - (140^{o})_{x} \qquad 4.33$$

Figure 4.17 shows that after this sequence the locus is a tight knot around the y-axis. The residual z-components after the sequence are vanishingly small for a range of offset parameters from -0.3 to 0.3, as can be seen from Figure 4.18. Phase errors are also reduced considerably (Figure 4.19).

The compensation of phase errors has been tested experimentally as shown in Figure 4.20. This illustrates the offset dependence of a single carbon-13 resonance after a conventional 90^{o} pulse as compared with an optimised 'spin-knotting' sequence. The signals vary in phase much less in the latter series.

A comparison of the various composite $\pi/2$ pulses is made in table 4.1.

4.4 Composite π pulses (I):

Population inversion.

Pulses of length π radians are used for two main purposes: Firstly to turn magnetization vectors which lie in the xy plane of the rotating frame into a mirror image position with respect to the pulse axis, and secondly, to take magnetization vectors from the +z to the -z pole, producing an inversion of level populations. In the first case the mirror image vectors refocus to form a spin echo, whose properties are familiar. Spin echoes are used in a variety of NMR techniques such as measurement of transverse relaxation times, and in two-dimensional spectroscopy. The second consequence of a π pulse, the inversion of spin state populations, is used in an equal variety of NMR experiments. A familiar example is the inversion-recovery method of measuring spin-lattice relaxation times in which an initial π pulse is used to invert the longitudinal magnetization. In less familiar experiments it is the populations of coupled spins which are inverted - in the formalism of the preceding chapter, this being an inversion of the z-component in the ZDQ frame, rather than in a magnetization frame. This 'interchange of spin labels' can be used in order to cause modulation of spin echoes by heteronuclear spin-spin coupling - the 'proton flip' technique in two-dimensional spectroscopy (47), and is also used in some heteronuclear spin-spin decoupling schemes (133). It is not the intention of this thesis to investigate these experiments too deeply. It is simply important to realise that their proper operation requires the

inversion of a z-component, of a magnetization vector, or possibly of a ZDQ vector, by a π pulse or an equivalent composite pulse.

Now in almost all of these experiments imperfections in the pulse have a significant effect. Spin echo experiments are impeded if the π pulse is unable to turn magnetization vectors into their proper mirror image positions, owing to pulse imperfections. It is possible to correct pulse imperfections by using composite π pulses but this requires a rather sophisticated analysis which is presented later. This is quite a complex problem because in a spin echo the starting position of the magnetization vectors is very general; they may be anywhere in the xy plane of the rotating frame. Ideally, each of these vectors should be rotated to a mirror-image position, irrespective of where it started. It is difficult to see how this can be fulfilled for all vectors, compensating for imperfections at the same time. This problem is clearly more challenging than the examples given so far, which assumed a fixed starting position for vectors along the z-axis, and a fixed ideal finishing point, along the y or some other axis. Discussion of the correction of imperfections in spin echo experiments will be deferred. Instead the easier subject of compensation for pulse imperfections in techniques involving population inversion will be addressed.

For these experiments the starting position of vectors is defined to be along the z-axis, and the composite pulse sequence should take these vectors to the -z axis, irrespective of a given class of pulse imperfection. A sequence which provides a particularly good inversion of z-magnetization in the presence of radio-frequency

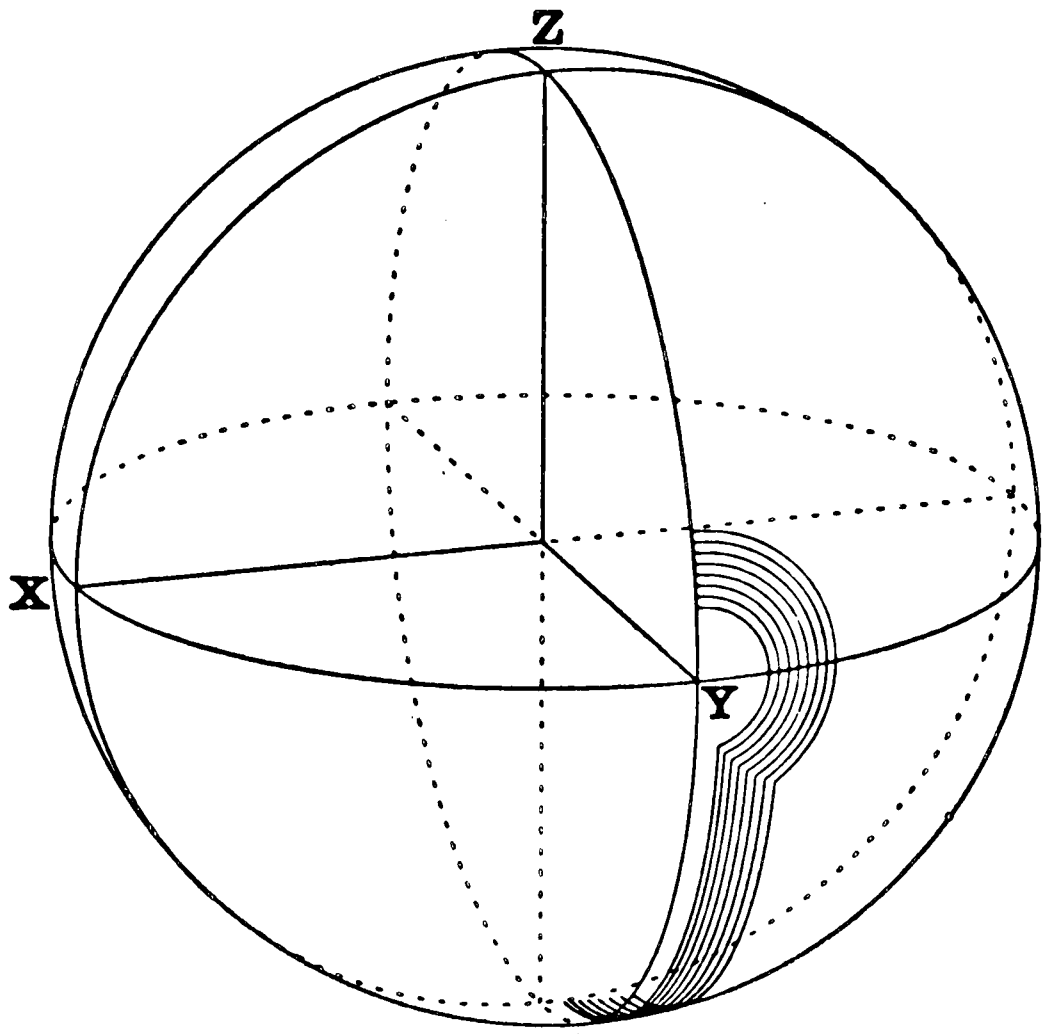

Fig.4.21. Population inversion by the $(\pi/2)_x\ \pi_y(\pi/2)_x$ composite pulse. A family of trajectories has been calculated with pulse lengths between 0.8 and 0.9 the nominal values. The ends of the trajectories are much closer to the -z axis than they would be after a conventional single π pulse.

field inhomogeneity is the $(\pi/2)_x(\pi)_y(\pi/2)_x$ sequence. This composite pulse was the first reported (89) and is probably the most generally useful of all. Its operation is illustrated in Figure 4.21. The first $(\pi/2)_x$ pulse rotates the magnetization vectors away from the +z pole and towards the +y axis. The trajectories of a family of vectors experiencing B_1 fields somewhat lower than nominal are illustrated. The first pulse leaves them in the yz plane but short of the y-axis. Now a π_y pulse is applied. If this operated perfectly it would place all vectors in mirror-image positions with respect to the xy plane; then the final $(\pi/2)_x$ pulse would bring them all to the -z axis, the imperfections in the first and last pulses having mutually cancelled. Of course the central π_y pulse is also subject to imperfections but these do not exert a great effect because the trajectory during the pulse is small. The inversion of z-magnetization proceeds almost independently of small deviations of the three rotations from their nominal angles. This can be verified both analytically and experimentally. A sequence of rotations $R_x(\pi/2+\Delta)R_y(\pi+2\Delta)R_x(\pi/2+\Delta)$ can be applied to a vector of unit magnitude initially at the +z pole, where Δ represents a misset parameter. The final z component (z^+) can be calculated and compared with that produced by a conventional single pulse $R_x(\pi+2\Delta)$.

For the single pulse,

$$z^+ = -\cos 2\Delta \simeq -1+2\Delta^2 \qquad 4.34$$

whilst for the composite sequence,

$$z^+ = -\cos 2\Delta + \frac{1}{4}(\cos 4\Delta - 1) \simeq -1 + 2\Delta^4 \qquad 4.35$$

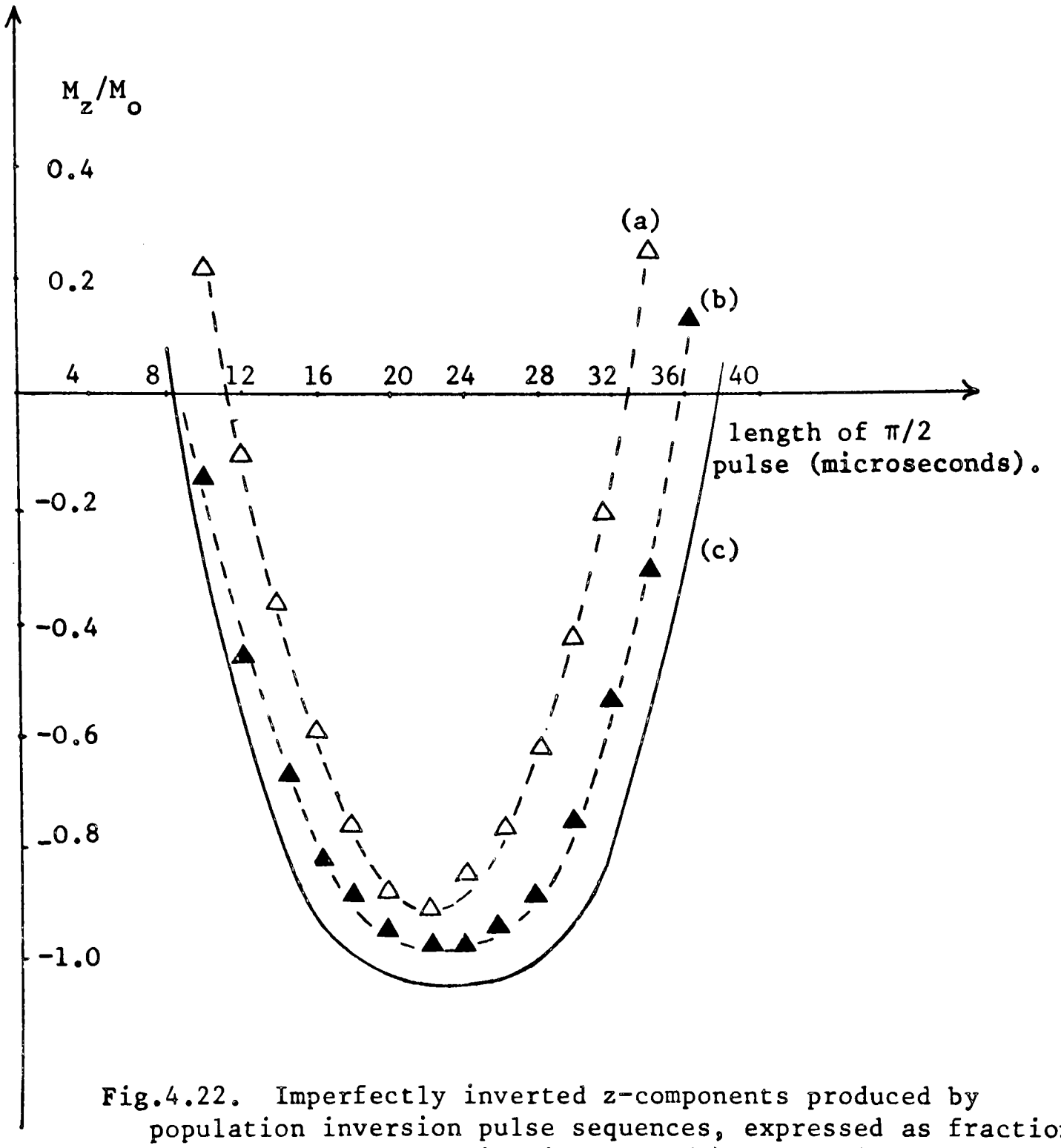

Fig.4.22. Imperfectly inverted z-components produced by population inversion pulse sequences, expressed as fractions of equilibrium magnetization M_o. (a) Conventional single π pulse (of duration twice the values shown). (b) Three-pulse sequence $(\pi/2)_x\ \pi_y(\pi/2)_x$. (c) Theoretical curve for the three-pulse sequence, assuming a perfectly homogenous B_1 field. The discrepancy between (b) and (c) may be attributed to the effects of B_1 inhomogeneity.

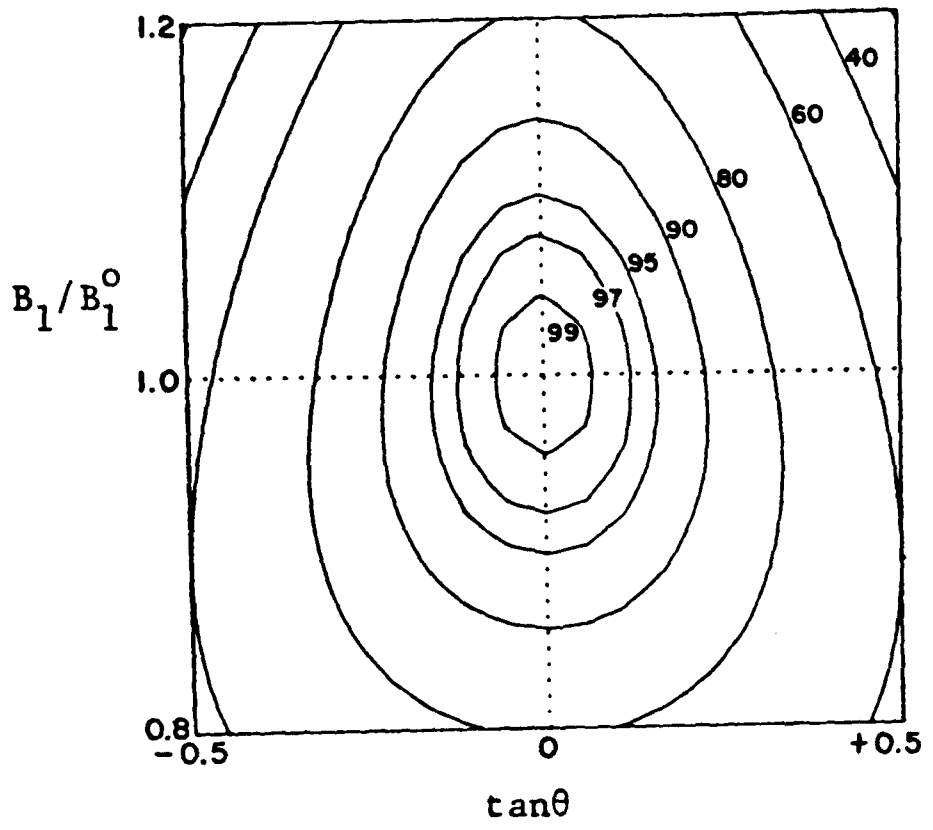

Fig.4.23. The contours of residual z-magnetization (expressed as a fraction of-M_o) after a conventional π_x pulse, as a function of pulse length misset B_1/B_1^o and resonance offset tan θ.

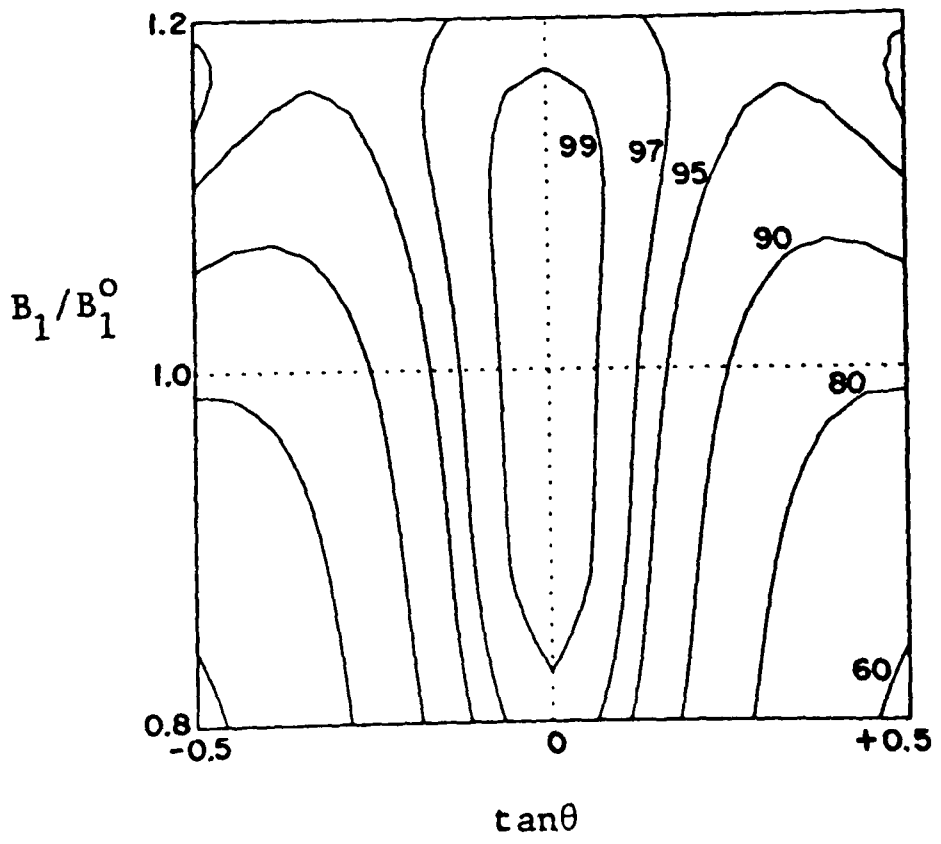

Fig.4.24. The equivalent contour diagram for the $(\pi/2)_x\pi_y(\pi/2)_x$ sequence, displaying the high tolerance to pulse length misset, and partial compensation for off-resonance effects.

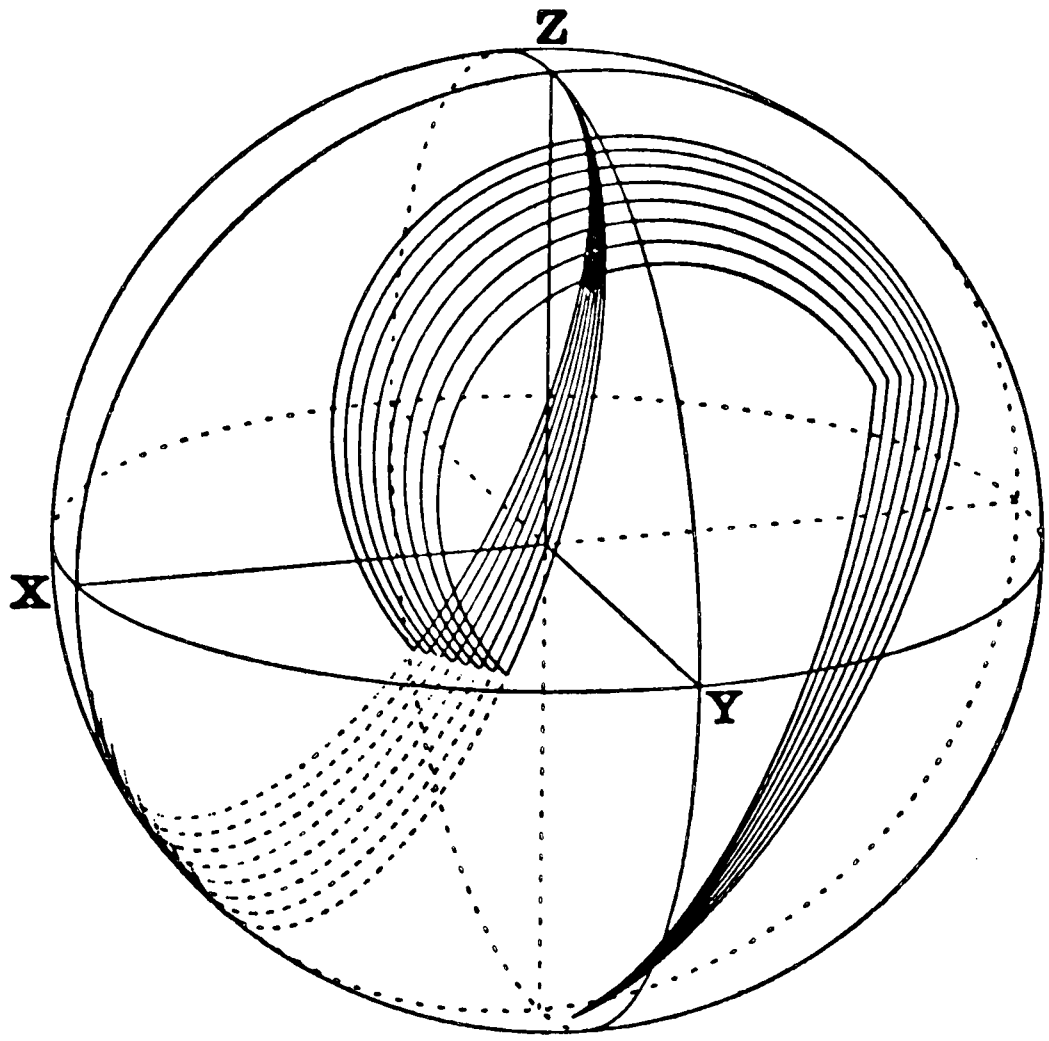

Fig.4.25. The effect of the $(\pi/2)_x\pi_y(\pi/2)_x$ sequence on a family of magnetization vectors, with offsets $\tan\theta$ between 0.4 and 0.6. Rotations occur about tilted fields in the xz, yz and xz planes. The overall effect is an imperfect refocussing of the family of vectors into a region not far from the south pole. Conventional single inversion pulses for the same offset range cause the vectors to continue along the dotted lines to end up far from the -z axis.

ignoring higher-order terms. Thus the composite sequence provides a good inversion which is much less sensitive to small missets Δ.

To verify these results the z-magnetization produced can be measured as a function of deliberate misset of the pulses in the same way as for the measurement of residual z-magnetization in sections 4.3.2 and 4.3.3. The experimental and theoretical results are compared in Figure 4.22.

Computer simulation can be used for a more detailed examination of the behaviour of the composite pulse. It is possible to plot contours of the z-magnetization produced as a function of pulse length error (α/α^{o}) and offset parameter $\tan\theta$. Figure 4.23 illustrates this for a conventional π pulse, showing that the single pulse has little tolerance of pulse length error or resonance offset. There is only a small area in which the z-magnetization after the pulse is within 99% of ($-M_o$). This should be compared with Figure 4.24 which represents the simulated behaviour of the composite $(\pi/2)_x(\pi)_y(\pi/2)_x$ sequence under the same conditions. The composite pulse is clearly much less sensitive to variations of the pulse lengths away from the nominal angles. It is possible to see from this diagram that off-resonance effects are also compensated to some extent, particularly for large offsets. This is also evident from computer simulation of the trajectories of a group of vectors under the three consecutive tilted rotations, Figure 4.25. The family of vectors responds to pulses applied off-resonance with correct nominal flip angles but with offset parameters in the range $\tan\theta$ = 0.4 to 0.6. The vectors end up much nearer

the South pole than they would have done after similarly tilted conventional π pulses (the dotted trajectories).

There is an interesting theoretical point in connection with these contour diagrams which also has some practical significance. It may be seen that both diagrams 4.23 and 4.24 are completely symmetrical with respect to sign of the offset parameter $\tan\theta$. In other words the degree of inversion, z to -z, under a three pulse sequence $\alpha_x\beta_y\alpha_x$ is independent of the sign of the offset from resonance. This has the practical consequence that with the aid of quadrature detection, the transmitter may be placed in the centre of the spectrum thus making best use of the available pulse power (4). The reasons for this symmetry are not obvious, but appear from the following argument which also serves as an example of rotation operator algebra.

The z-magnetization of a system described by a density matrix σ is given by:

$$\langle I_z \rangle = \mathrm{Tr}(\sigma I_z) \qquad 4.36$$

In this case the density matrix is initially at equilibrium proportional to I_z, but rotated by some operation R:

$$\langle I_z^+ \rangle \propto \mathrm{Tr}(RI_zR^{-1}I_z) \qquad 4.37$$

This equation may be manipulated as follows:

$$\begin{aligned} \langle I_z^+ \rangle \propto\ & \mathrm{Tr}(RI_zR^{-1}I_z) \\ =\ & \mathrm{Tr}[(I_zRI_z^{-1})I_z(I_zR^{-1}I_z^{-1})I_z] \qquad 4.38 \\ =\ & \mathrm{Tr}\,[(I_zR^{-1}I_z^{-1})I_z(I_zRI_z^{-1})I_z] \qquad 4.39 \end{aligned}$$

where in these lines the property Tr(AB) = Tr(BA) has been used.

Now the operation R is in some way dependent on the offset parameter θ - thus $R\{\theta\}$. Hence the three equations of 4.38 may be used to define the mathematical conditions under which $\langle I_z^+ \rangle$ is invariant on inversion of the offset parameter. $\langle I_z^+ \rangle$ is independent of the sign of θ if any one of the following conditions is satisfied:

$$R\{\theta\} = R\{-\theta\}, \qquad 4.39$$

or $$I_z R\{\theta\} I_z^{-1} = R\{-\theta\} \qquad 4.40$$

or $$I_z R^{-1}\{\theta\} I_z^{-1} = R\{-\theta\} \qquad 4.41$$

For any of these allows $R\{\theta\}$ to be replaced by $R\{-\theta\}$in equation 4.37 as shown by equation 4.38.

Of these three conditions the final one turns out to be the most frequently satisfied. The same equation can be expressed:

$$R_z(\pi) R^{-1}\{\theta\} R_{-z}(\pi) = R\{-\theta\} \qquad 4.42$$

since $R_z(\pi)$ is proportional to I_z.

As an example take a single rotation of α radians about a tilted axis in the xz plane. The rotation operator for this may be expressed:

$$R\{\theta\} = R_y(\theta) R_x(\alpha) R_{-y}(\theta) \qquad 4.43$$

giving

$$R^{-1}\{\theta\} = R_y(\theta)R_{-x}(\alpha)R_{-y}(\theta) \qquad 4.44$$

Hence

$$R_z(\pi)R^{-1}\{\theta\}R_{-z}(\pi) = [R_z(\pi)R_y(\theta)R_{-z}(\pi)].[R_z(\pi)R_{-x}(\alpha)R_{-z}(\pi)].$$
$$[R_z(\pi)R_{-y}(\theta)R_{-z}(\pi)]$$
$$= R_{-y}(\theta)R_x(\alpha)R_y(\theta) \qquad 4.45$$

which is just $R\{-\theta\}$. Hence condition 4.42 is satisfied and the z-magnetization produced by a single pulse is independent of the sign of θ, as verified in Figure 4.23

In contrast, for two tilted pulses it is easy to show that the condition is not satisfied if they act about non-parallel axes. For example, for two consecutive rotations, α_x followed by β_y,

$$R\{\theta\} = [R_{-x}(\theta)R_y(\beta)R_x(\theta)].[R_y(\theta)R_x(\alpha)R_{-y}(\theta)] \qquad 4.46$$

Hence

$$R^{-1}\{\theta\} = [R_y(\theta)R_{-x}(\alpha)R_{-y}(\theta)].[R_{-x}(\theta)R_{-y}(\beta)R_x(\theta)] \qquad 4.47$$

and

$$R_z(\pi)R^{-1}\{\theta\}R_{-z}(\pi) = [R_{-y}(\theta)R_x(\alpha)R_y(\theta)].[R_x(\theta)R_y(\beta)R_{-x}(\theta)] \qquad 4.48$$

But this is no longer equal to the desired operator

$$R\{-\theta\} = [R_x(\theta)R_y(\beta)R_{-x}(\theta)].[R_{-y}(\theta)R_x(\alpha)R_y(\theta)] \qquad 4.49$$

since the two terms in square brackets to not commute.

Thus for one pulse the contour plot is symmetrical, for two pulses about different axes it is not so. Of greater interest are the properties of three-pulse sequences of the form $\alpha_x\beta_y\alpha_x$. It can be shown that the symmetry in time of these sequences ensures that equation 4.43 is satisfied and hence the degree of inversion is also symmetric with respect to the off-resonance parameter. The operator for the three tilted pulses is:

$$R\{\theta\} = [R_y(\theta)R_x(\alpha)R_{-y}(\theta)].[R_{-x}(\theta)R_y(\beta)R_x(\theta)].[R_y(\theta)R_x(\alpha)R_{-y}(\theta)] \qquad 4.50$$

so that

$$R_z(\pi)R^{-1}\{\theta\}R_{-z}(\pi) = [R_{-y}(\theta)R_x(\alpha)R_y(\theta)].[R_x(\theta)R_y(\beta)R_{-x}(\theta)].[R_{-y}(\theta)R_x(\alpha)R_y(\theta)] \qquad 4.51$$

which this time is equal to $R\{-\theta\}$just as required.

Note that no such symmetry exists in the transverse components of magnetization produced by the three-pulse sequence, or in the intermediate trajectories of the vectors during the composite pulse.

Apart from these interesting symmetry properties Figure 4.24 demonstrates that the $(\pi/2)_x(\pi)_y(\pi/2)_x$ sequence provides partial compensation for off-resonance effects, as has already been observed. The compensation can be made better by lengthening the central pulse beyond the nominal value of π radians. The two outer pulses should be kept at $\pi/2$ radians to ensure that the sequence still behaves

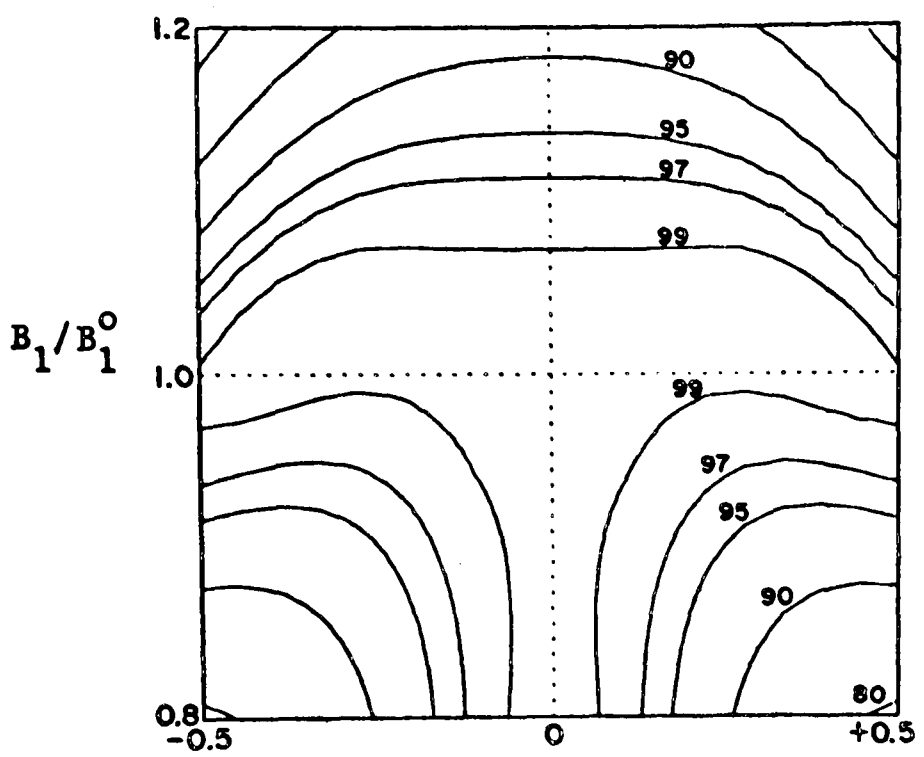

Fig.4.26. Contours of z-magnetization after the $(\pi/2)_x(4\pi/3)_y(\pi/2)_x$ sequence.

The tolerance to resonance offset has been much improved, without loss of compensation for pulse missets, to the low side of nominal. In a large T-shaped region M_z is held to within 1% of $-M_o$.

as a good π pulse when no imperfections are present. Computer simulation indicates that the optimum length of the central pulse is about $4\pi/3$ radians, producing a sequence:

$$(\pi/2)_x(4\pi/3)_y(\pi/2)_x \qquad 4.52$$

This composite pulse accurate inverts z magnetization for a wide range of offsets, approximately $0.5 > \tan\theta > -0.5$. The corresponding contour diagram is shown in Figure 4.26. Note the large T-shaped area in which the z-magnetization is held to within 1% of the ideal value. This assures that compensation for spatial homogeneity is also good providing the pulses are close to resonance, because the distribution of B_1 fields in the sample is skewed strongly to values lower than nominal, as has already been described. Thus this composite pulse sequence has the useful versatility of being able to compensate for either of the two major varieties of pulse imperfection, radio-frequency inhomogeneity or resonance offset, but not both at the same time.

A simple illustration of the advantage of being able to use a composite pulse to invert longitudinal magnetization is provided by the 'null-point' method of measuring longitudinal relaxation times. In this experiment equilibrium magnetization is inverted by an ordinary π pulse or a composite equivalent, allowed to relax, and then monitored by applying a $\pi/2$ pulse and measuring the transverse magnetization produced. If a relaxation interval t_N can be found for which the magnetization passes through a null the relaxation time constant T_1 is given by

$$T_1 = t_N/\ln 2 \qquad 4.53$$

Table 4.2. Apparent spin-lattice relaxation times by the null method: Effect of resonance offset.

Resonance offset $\Delta\omega/2\pi$ (kHz)	Offset parameter tan θ	Conventional pulse T_1	Composite pulse T_1
0	0.00	13.3 (-1)[a]	13.4(<1)
1	0.09	13.0 (-4)	13.4(<1)
2	0.18	12.0 (-11)	13.4(<1)
3	0.27	10.8 (-20)	13.4(<1)
4	0.36	9.7 (-28)	13.1 (-2)

[a] Systematic error (%) with respect to the value T_1 = 13.4 seconds measured by careful inversion-recovery experiments and least-squares fitting to an exponential.

Table 4.3 Apparent spin-lattice relaxation times by the null method: Effect of pulsewidth misset.

Ratio of pulse lengths to their nominal values t_p/t_p^o	Conventional pulse T_1 (seconds)	Composite pulse T_1 (seconds)
1.0	13.3 (-1)[a]	13.4(<1)
0.9	12.8 (-5)	13.4(<1)
0.8	12.1 (-10)	13.3(-1)
0.7	11.0 (-19)	13.3(-1)
0.6	6.2 (-54)	12.1(-10)
0.5	signal not inverted	10.2(-24)

assuming exponential relaxation, and an exact inversion of magnetization by the π pulse.

This is an excellent method of measuring T_1 since in principle only two measurements are needed which straddle the null point, but unfortunately T_1 will be underestimated if the inversion caused by the π pulse is poor. However the use of a composite pulse should allow the null-point method to be used even far from resonance or when the pulse field homogeneity is known to be imperfect.

This was tested by measuring the spin-lattice relaxation time of the proton-decoupled carbon-13 resonance of methyl iodide. As usual the real effects of inhomogeneity were minimised by using a small spherical sample, and then simulated in a controlled way by systematically missetting all pulses in the same proportion, so producing errors in the apparent T_1's derived from the null point. The relaxation times were compared with that estimated from a careful inversion-recovery experiment - a slow method but known to be very free from systematic errors.

Tables 4.2 and 4.3 summarise the results. Table 4.2 concerns the variation in the systematic errors with the off-resonance parameter $\tan\theta$. For a conventional inversion pulse the apparent T_1 values show large errors, increasing with the offset, whilst the use of the composite $(\pi/2)_x(4\pi/3)_y(\pi/2)_x$ sequence greatly reduces these errors, holding them below 1% for most of the offset range.

The effect of spatial homogeneity, as simulated by progressive misset of the pulse lengths, is shown in Table 4.3. Again large systematic errors in the apparent T_1 as determined from the null-point are produced if a single π pulse is used for population inversion. These errors are kept within acceptable limits when the composite π pulse is used instead.

4.5 Composite π pulses (II):

Spin echo experiments

4.5.1 Pictorial approach

Pulses of length π radians are used not only for population inversion but also for placing transverse magnetization vectors into mirror-image positions with respect to the pulse axis. A spin echo is formed and the refocussing can be repeated many times to generate a train of echoes whose decay rate is independent of the magnet homogeneity and provides access to the spin-spin relaxation time constant. This experiment (Carr-Purcell Method 'B') provides a considerable challenge to the philosophy of compensation of pulse imperfections by composite pulses. When long spin-spin relaxation times are involved, many hundreds of consecutive refocussing pulses may need to be applied, so that the experiment is very sensitive to any errors in the pulses which can have a cumulative effect.

This problem is sufficiently serious that it stimulated the first attempt at internal compensation of pulse errors - the Meiboom-Gill scheme which involves a phase shift of $\pi/2$ radians between the preparatory $\pi/2$ pulse and the train of π pulses (95).

The operation of this experiment is examined in a moment. It will be found that even with the Meiboom-Gill phase shift the multiple echo experiment tends to be very sensitive to pulse imperfections or misset, and in certain cases errors are not compensated at all. The use of composite π pulses will be shown to provide a powerful alternative (126). For example, in systems which involve homonuclear spin-spin coupling interactions, the Meiboom-Gill modification does not compensate pulse imperfections, whilst the composite pulse technique does provide effective compensation. Even when homonuclear coupling is absent and the Meiboom-Gill scheme is effective, the composite pulse method compensates imperfections to a significantly greater degree.

It has already been observed that the problem of error compensation in spin echo experiments is a particularly difficult one because the positions of the vectors at the time of the refocussing pulse are rather general. They are spread out in arbitrary positions in the xy plane and it is desired to rotate each of these vectors to the corresponding mirror-image position, independent of pulse field inhomogeneity or resonance offset. It will be shown that a composite π pulse can be used to do this, with the restriction that the precise <u>plane</u> in which the mirror images are formed is dependent on pulse imperfections. Thus for exact pulses a composite π_y pulse forms a mirror image with respect to the yz plane, just as would an exact conventional π_y pulse. It will be shown that even when the pulses are imperfect the composite pulse does place the vectors in mirror-image positions, but the <u>plane</u> of reflection may be slightly rotated about the z-axis according

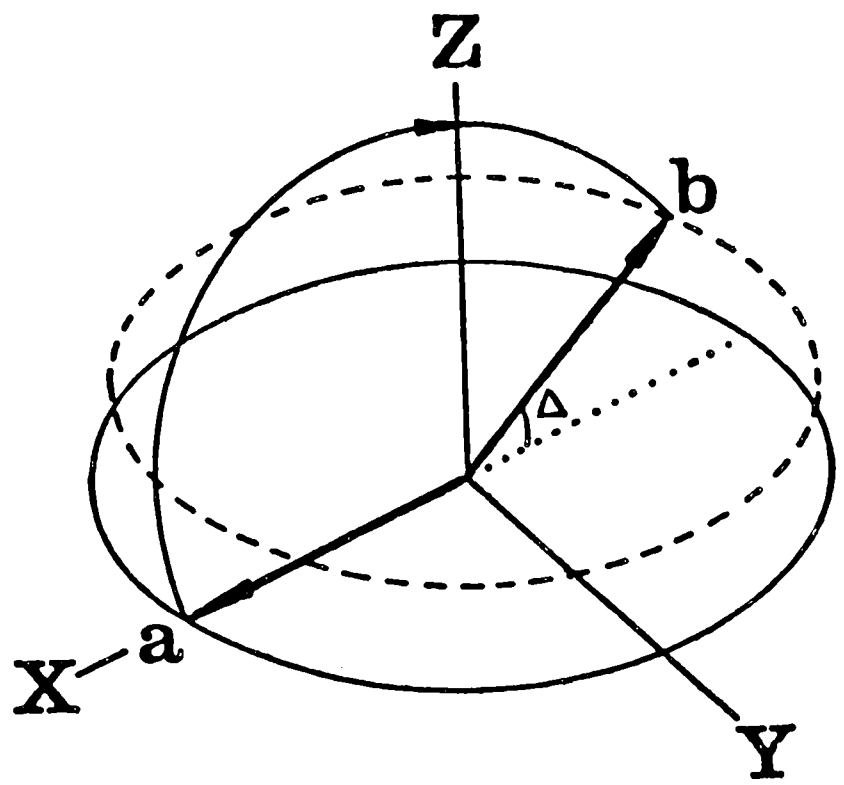

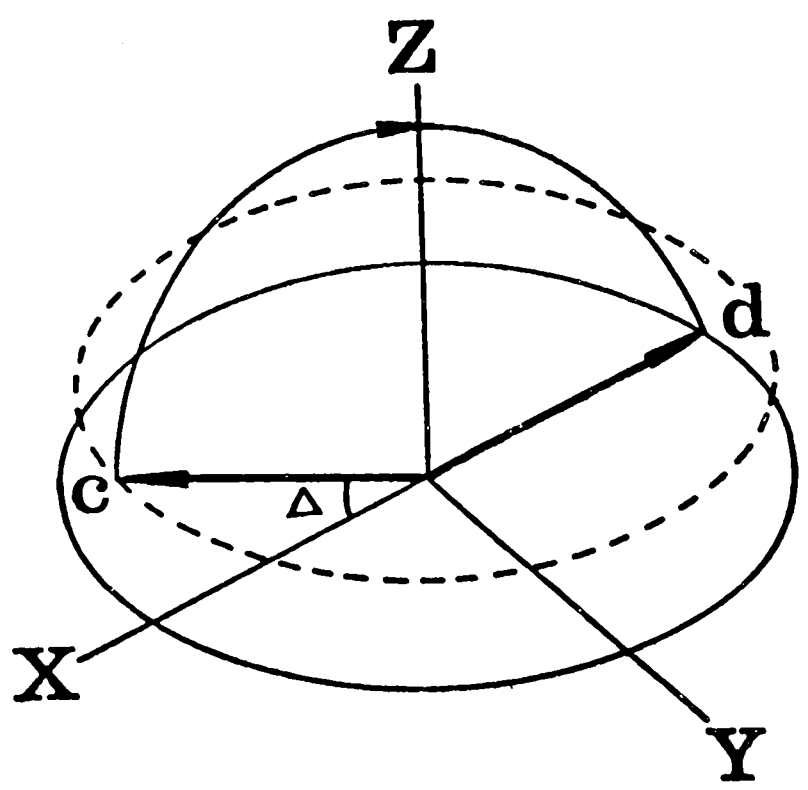

Fig.4.27. Compensation of pulse length errors by means of the Meiboom-Gill modification (see text).

to the degree of imperfection. This means that an echo does form properly but its phase depends somewhat on the local B_1 field strength, or the resonance offset. Thus in an inhomogenous radio-frequency field the echo will be somewhat reduced in intensity because it is composed of many component echoes each of slightly different phase. Fortunately this is not a problem because if the refocussing is repeated and a second echo formed, the phase shifts can be shown to cancel out exactly and the second echo will have the full intensity, independent of both B_0 and B_1 inhomogeneity to a first approximation. Thus in a full Carr-Purcell experiment involving a long sequence of composite refocussing pulses, every even echo is fully compensated for pulse imperfections.

Before the composite pulse method is explained more fully it is important to understand the classical method of compensation of pulse imperfections, the Meiboom-Gill modification. Here too the effects of pulse imperfections are made to compensate on the even-numbered echoes in the sequence. This can be illustrated by a simple pictorial argument (Figure 4.27). A magnetization vector is initially placed along the y-axis by a preparatory $(\pi/2)_x$ pulse. It now precesses in the xy plane for a time τ according to its offset from resonance. Consider a specific vector which happens to precess through $\pi/2$ radians, taking it to point a, at the x-axis. The π pulse is now applied and is subject to imperfections. Consider it to be rather shorter than its nominal value, so that it flips the vector through only $(\pi-\Delta)$ radians, taking it to point b in Figure 4.27, just above the -x axis. Free precession again takes place but with the vector in a plane

slightly above the equatorial plane, so that the echo at time 2τ is somewhat reduced in amplitude. However the next refocussing pulse takes the vector through another arc of $(\pi-\Delta)$ radians from c to d, back into the equatorial plane, so that the effect of imperfections in the two pulses is exactly cancelled. The second echo at time 4τ forms with the full intensity, and the sequence can be repeated, with every even-numbered echo in the train being formed independent of pulse imperfections.

The drawback to this scheme is that the chain of events which leads to compensation is easily disrupted. Firstly, in the general case where a is not along the x-axis, there are second-order errors to be considered, which although small can accumulate and cause difficulties in a long echo train. Secondly, the method requires exact symmetry in the motion of each magnetization vector and any factors which break the symmetry will bring about cumulative errors. Thus the magnetization must be prepared exactly along the y-axis - hence errors in the preparatory $(\pi/2)_x$ pulse can be important (though these can of course be overcome by using a composite $\pi/2$ pulse!). Also the precession frequency of the vector must remain the same throughout the 4τ period - but this is not so in the presence of homonuclear spin-spin coupling. Consider the simple AX case. Because the refocussing pulse interchanges the spin states of the coupled spin, each refocussing pulse causes a frequency jump of $\pm$ J Hz for a given precessing vector. A vector which has reached point b in Figure 4.27 no longer precesses exactly to point c in the next interval 2τ, so that the second refocussing pulse no longer brings it back to the equatorial plane. Pulse errors accumulate and the Meiboom-Gill compensation scheme

is not effective in systems with homonuclear spin-spin coupling.

Apart from this some quite different effects can be observed when using imperfect refocussing pulses on homonuclear coupled spin systems (85). If the π pulse does not produce a complete spin state inversion, some transverse magnetization is converted into zero- and double-quantum coherence. This is because the z-components in the ZDQ frames are not exactly inverted but are left short of the -z axis. The finite residual transverse components in the ZDQ frames represent zero- and double-quantum coherence. During a train of many imperfect refocussing pulses there is a continuous interconversion of precessing ZDQ coherence and transverse magnetization, producing very complicated modulation effects. Thus in homonuclear coupled systems spin echo experiments using single π pulses fail doubly: Firstly, they do not produce a refocussing effect compensated for pulse imperfections, and secondly, they introduce problems associated with poor spin state inversion.

If composite π pulses are used instead, it is immediately apparent that at least these latter difficulties should not arise because the composite pulse is known to give a good spin state inversion in the presence of small pulse imperfections (134). The effect of a composite π pulse on transverse magnetization is less clear. Suppose for the moment that the only pulse imperfection is spatial inhomogeneity of the transmitter field B_1, and that a composite pulse $(\pi/2)_x(\pi)_y(\pi/2)_x$ is used. The effect of B_1 inhomogeneity can be simulated by a proportionate increase in all three pulse lengths: $(\pi/2+\Delta)_x(\pi+2\Delta)_y(\pi/2+\Delta)_x$.

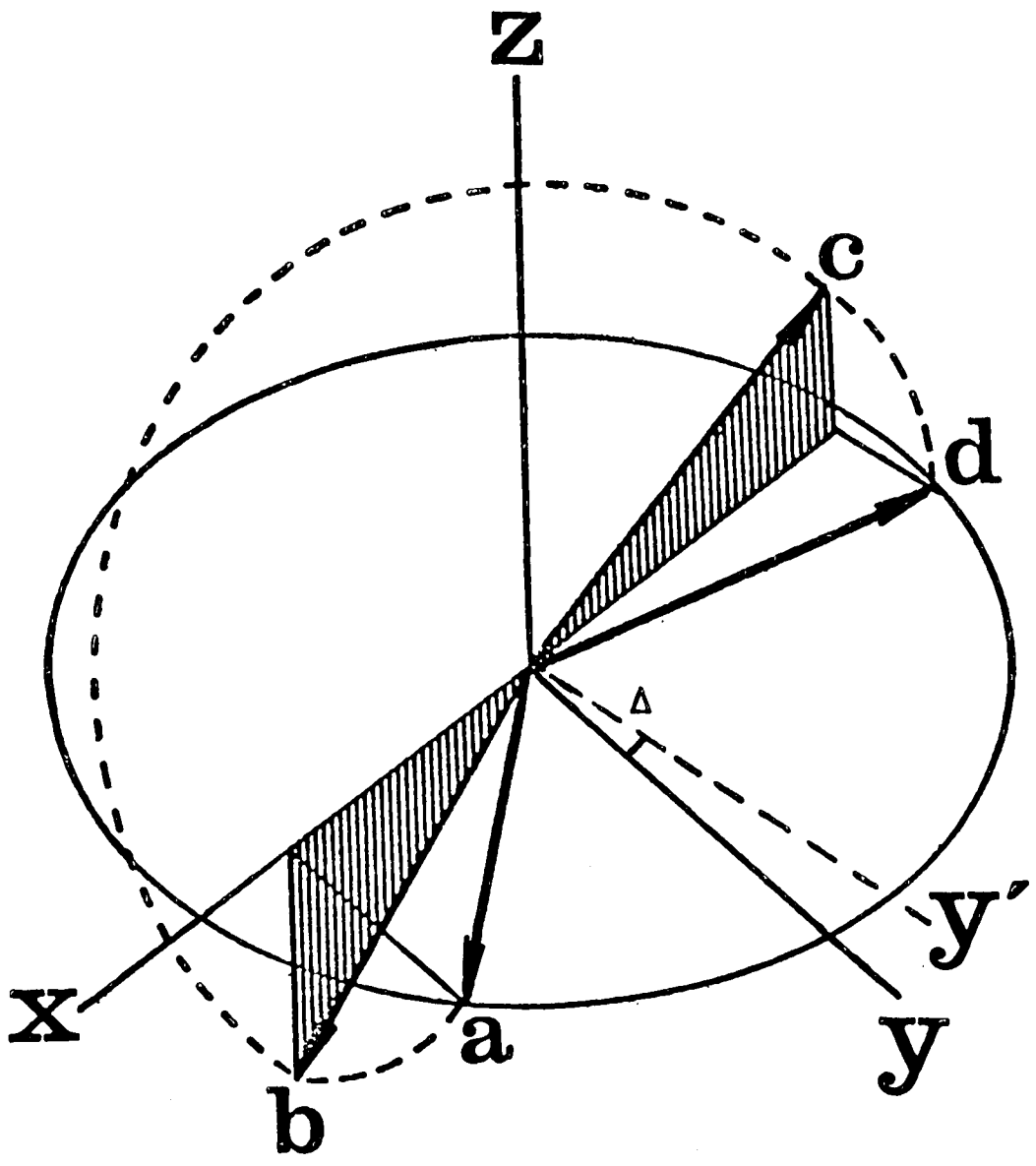

Fig.4.28. Compensation of pulse length errors by means of the $(\pi/2)_x\pi_y(\pi/2)_x$ sequence.

The effect on a typical component of transverse magnetization is demonstrated in Figure 4.28, in which the imperfections in the $(\pi/2)_x$ pulses are at first ignored. A typical vector starts at point a in the xy plane, subtending an angle ψ radians with the x-axis. The first $(\pi/2)_x$ pulse takes the vector out of the xy plane to point b, in the xz plane (shaded). The second rotation, of $(\pi+ 2\Delta)$ radians about the y-axis, takes it to point c, still in the xz plane, but subtending a reduced angle $\psi-2\Delta$ radians with the -x axis. Finally the last $(\pi/2)_x$ pulse places the typical vector back in the xy plane, where it still subtends the angle $\psi-2\Delta$ with the -x axis.

There are only minor changes to this picture if the imperfections in the first and last pulses are included. Point b then lies slightly behind the xz plane, but so does c, so that the imperfections in the first and last rotations compensate each other, to first order in Δ. With large missets Δ there will be second order effects and the vector is not taken exactly from a to d by the composite pulse.

Ignoring these second-order effects, the three-pulse sequence has an overall effect equivalent to a rotation by exactly π radians about an axis y', which lies in the xy plane but makes an angle Δ radians with the y-axis. In other words, the imperfections in the pulse lengths have been converted into a phase shift, which has considerable advantages. Firstly, because the overall effect is that of a rotation by π radians about an axis in the xy plane, the sequence accurately inverts longitudinal magnetization and

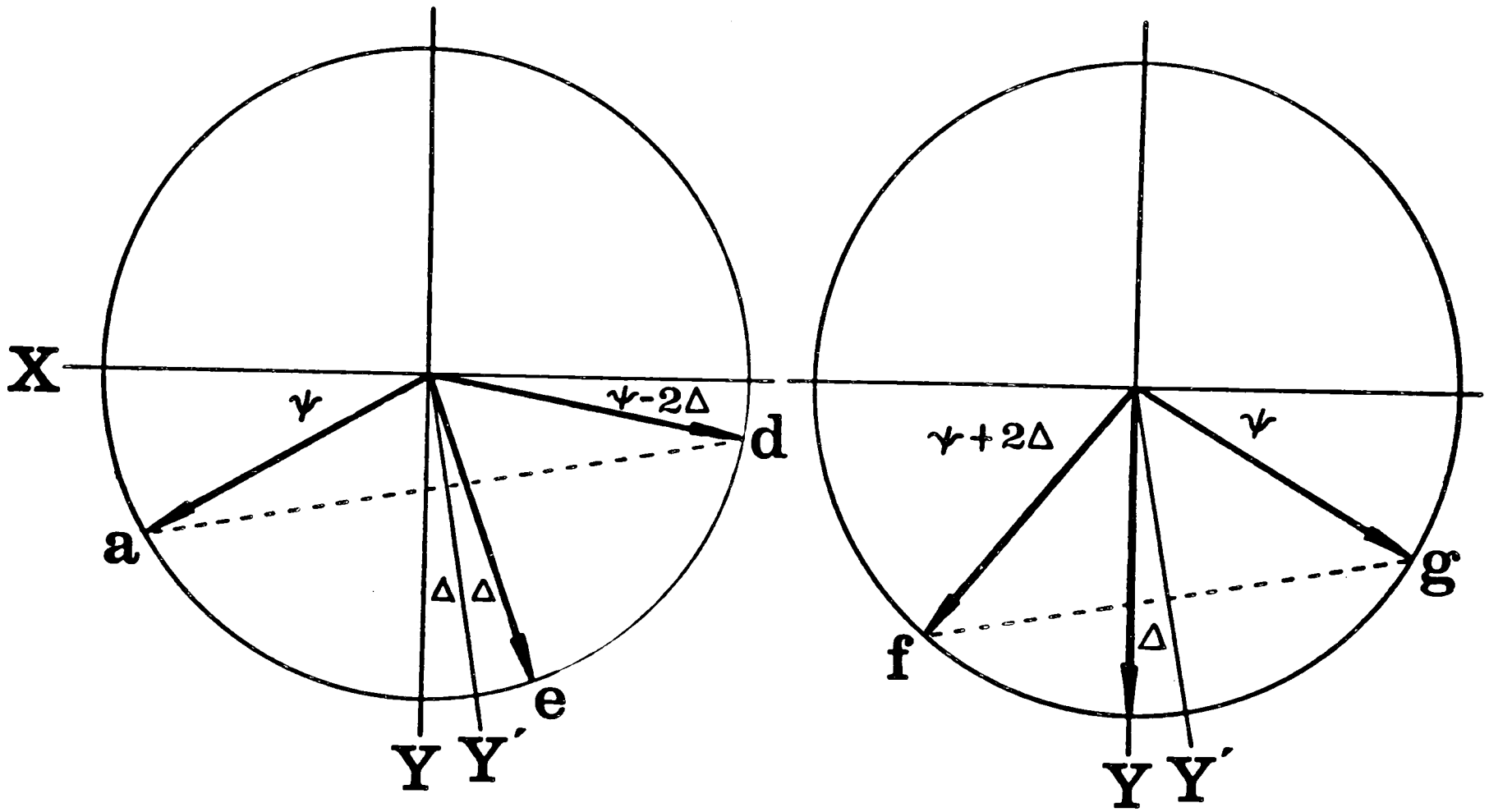

Fig.4.29. Compensation of spin-echo dephasing on the even-numbered echoes. The overall result of the composite pulse sequence $(\pi/2+\Delta)_x(\pi+2\Delta)_y(\pi/2+\Delta)_y$ has been represented as $\pi_{y'}$ so that all vectors precess in the xy plane.

and does not mix it with transverse magnetization. Secondly, the phase shift compensates itself on even numbers of echoes, as will now be shown.

Figure 4.29 concerns the evolution of transverse magnetization during two complete elements of a Carr-Purcell echo train (τ-R-2τ-R-τ) in which each refocusssing pulse R is a composite $(\pi/2)_x(\pi)_y(\pi/2)_x$ sequence. A typical vector starts along the y-axis and precesses to point a. The composite pulse carries it to a position d as described above, this being equivalent to a rotation about the phase-shifted axis y'. The next period τ of free precession carries it to e, independent of the precession frequency, providing this remains constant. Hence it forms an echo with a phase somewhat dependent on the B_1 field strength. Thus in a distribution of B_1 fields the echo amplitude is somewhat reduced because of the distribution of phases but this does not matter because the phase shifts cancel out after the next composite pulse. Further precession takes the vector to f, where the angle subtended with the x-axis is now $\psi+2\Delta$ radians. A flip about the effective axis y' places the vector at g, ψ radians from the -x axis, which is just where it would have been, had both the refocussing pulses been exact and operated about the y-axis. The final period of precession generates an echo along the y-axis in which pulse imperfections have no detectable effect to first order in Δ.

It is important to note the important differences between this method of compensation and the Meiboom-Gill method. Although Figure 4.29 assumed that the vector had a constant precession frequency throughout, this is not essential to the argument, which

still applies in cases such as when weak homonucldar coupling is involved, so that the vector jumps in frequency on each π pulse. Of course these frequency jumps generate a phase modulation of the echoes, but they do not impair the compensation process. This is in contrast to the Meiboom-Gill experiment, where jumps in frequency have a disastrous effect on the error compensation. Furthermore, the composite pulses do not mix longitudinal and transverse magnetization, whereas in the Meiboom-Gill method each imperfect pulse causes some interconversion of longitudinal and transverse components. Such mixing can be a further source of difficulties in the conventional technique because longitudinal magnetization is constantly being created by spin-lattice relaxation during the echo train.

4.5.2 Rotation operator analysis.

These conclusions can be given a theoretical justification by using rotation operators to clarify the overall effect of the three successive misset rotations:

$$R = R_x(\pi/2+\Delta)R_y(\pi+2\Delta)R_x(\pi/2+\Delta) \qquad 4.54$$

This approach renders unnecessary investigation of the motion of the magnetization vectors during the sequence.

As in the pictorial discussion, it is possible to ignore at first the imperfections in the first and last pulses, so that discussion is restricted to the operator:

$$r = R_x(\pi/2)R_y(\pi+2\Delta)R_x(\pi/2) \qquad 4.55$$

However it should be remembered that the full operator is given by

$$R = R_x(\Delta)rR_x(\Delta) \qquad 4.56$$

Now r can be reduced as follows: Firstly the rotation $R_y(\pi+2\Delta)$ is split into two equal parts, and then the unity operator $R_{-x}(\pi/2)R_x(\pi)R_{-x}(\pi/2)$ is inserted:

$$r = [R_x(\pi/2)R_y(\pi/2+\Delta)R_{-x}(\pi/2)].R_x(\pi).[R_{-x}(\pi/2)R_y(\pi/2+\Delta)R_x(\pi/2)] \qquad 4.57$$

using the associative property of the operators.

The bracketed terms can be simplified by using an identity

$$R_x(\pi/2)R_y(\alpha)R_{-x}(\pi/2) \equiv R_{-z}(\alpha) \qquad 4.58$$

which is a special case of equation 2.72 of Chapter 2, and is subject to cyclic permutation of the subscripts x, y and z. Such identities will be used extensively in the following pages. By such means equation 4.57 is expressed:

$$\begin{aligned} r &= R_{-z}(\pi/2+\Delta)R_x(\pi)R_z(\pi/2+\Delta) \\ &= R_{-z}(\Delta).[R_{-z}(\pi/2)R_x(\pi)R_z(\pi/2)].R_z(\Delta) \\ &= R_{-z}(\Delta)R_y(\pi)R_z(\Delta) \end{aligned} \qquad 4.59$$

This is just the operator which was expected, for it represents a rotation by π radians about the axis y', rotated away from the y-axis by an angle Δ radians. But before proceeding further it must be verified that the outer terms in equation 4.56 can legitimately be ignored. This is best done by expanding the operators $R_x(\Delta)$ as exponential series and ignoring high-order terms:

$$R = R_x(\Delta) r R_x(\Delta) \qquad 4.60$$

$$= \exp(i\Delta I_x) r \exp(i\Delta I_x)$$

$$\simeq r + i\Delta(I_x r + r I_x) \qquad 4.61$$

to first order in Δ.

Inside the brackets it is permissible to use the zeroth-order approximation for r:

$$r \simeq R_y(\pi) \qquad 4.62$$

which gives

$$R \simeq r + i\Delta(I_x R_y(\pi) + R_y(\pi) I_x) \qquad 4.63$$

The expression in brackets can be shown to be identically zero by judicious use of equation 2.75:

$$I_x R_y(\pi) = R_y(\pi)[R_{-y}(\pi) I_x R_y(\pi)] \qquad 4.64$$

$$= -R_y(\pi) I_x \qquad 4.65$$

Hence to first order in Δ, R = r.

This conclusion supports the pictorial arguments. To a first approximation the three-pulse sequence acts as a flip of Δ radians about the phase-shifted axis y'. Hence it provides the accurate inversion of z-magnetization described in section 4.5. Mathematically,

$$RI_zR^{-1} = [R_{-z}(\Delta)R_y(\pi)R_z(\Delta)].I_z.[R_{-z}(\Delta)R_{-y}(\pi)R_z(\Delta)]$$

$$= R_{-z}(\Delta).[R_y(\pi)I_zR_{-y}(\pi)].R_z(\Delta)$$

$$= -I_z. \qquad 4.66$$

4.5.3 Off-resonance effects

Correction for the effects of tilted effective fields requires a slightly different sequence than that used for spatial field inhomogeneity. In section 4.5 a sequence

$$(\pi/2)_x(4\pi/3)_y(\pi/2)_x \qquad 4.67$$

was used to provide accurate population inversion over a wide range of offsets, approximately $0.5 > \tan\theta > -0.5$. Can this sequence also be used in spin echo trains?

A rotation operator analysis can be done to show that it too is approximately equivalent to a rotation by π radians about an axis in the equatorial plane of the rotating frame. Hence it can indeed be used in the same way as the $(\pi/2)_x(\pi)_y(\pi/2)_x$ sequence, and

provides compensation of tilt effects on even echoes in the train.

Actually a detailed analysis is unnecessary. Because the set of rotations which leave a sphere unchanged form a group, any combination of two or more rotations is equivalent to some other rotation (the 'group property'). Now if a given set of rotations has been shown, by computer simulation or some other means, to give an inversion of z-magnetization, it is constrained to be one of the set of rotations by π radians about axes in the equatorial plane of the rotating frame. This can be verified easily by examination of a model . Because the z and -z axes lie at either end of a great circle, only this limited set of rotations connect the two points.

This is a useful result because it means that any sequence which can be devised which accurately inverts z-magnetization under some range of conditions necessarily works for spin echoes as well, providing error compensation on the even echoes. It is unnecessary to examine in detail the motion of vectors during the sequence, or even express the precise overall rotation by operator algebra.

This theorem can be proved formally as follows:
A rotation R inverts the z-component of magnetization:

$$RI_zR^{-1} = -I_z \qquad 4.68$$

Let R be a general rotation $R(\alpha,\theta,\phi)$ and then see what constraints equation 4.68 puts on the permissible values of α,θ and ϕ.

$$R(\alpha,\theta,\phi) = R_z(\phi)R_y(\theta)R_x(\alpha)R_{-y}(\theta)R_{-z}(\phi) \qquad 4.69$$

Hence

$$[R_z(\phi)R_y(\theta)R_x(\alpha)R_{-y}(\theta)R_{-z}(\phi)].I_z.[R_z(\phi)R_y(\theta)R_{-x}(\alpha)R_{-y}(\theta)R_{-z}(\phi)]$$

$$= -I_z \qquad 4.70$$

giving

$$[R_y(\theta)R_x(\alpha)R_{-y}(\theta)].\ I_z[R_y(\theta)R_{-x}(\alpha)R_{-y}(\theta)] \ = -I_z \qquad 4.71$$

Note that ϕ has disappeared from the equation so no constraints need be put upon its value. Equation 4.71 can be expressed:

$$R_x(\alpha).[R_{-y}(\theta)I_zR_y(\theta)].R_{-x}(\alpha) = -[R_{-y}(\theta)I_zR_y(\theta)] \qquad 4.72$$

The terms in brackets are:

$$R_{-y}(\theta)I_zR_y(\theta) = I_z\cos\theta + I_x\sin\theta \qquad 4.73$$

and comparing terms,

$$R_x(\alpha)I_zR_{-x}(\alpha)\cos\theta = -I_z\cos\theta \qquad 4.74$$

and

$$I_x\sin\theta \ = -I_x\sin\theta \qquad 4.75$$

which may be solved to give the constraints

$$\theta = 0 \quad \text{and} \quad \alpha = \pi \qquad 4.76$$

Thus equation 4.68 defines the operation:

$$R = R_z(\phi)R_x(\pi)R_{-z}(\phi) \qquad 4.77$$

which has the form of a rotation by π radians about some equatorial axis.

Thus since the composite pulse $(\pi/2)_x(4\pi/3)_y(\pi/2)_x$ is known to provide an accurate population inversion over a wide offset range, it has to be equivalent to a rotation such as given by equation 4.77, but in which ϕ is undefined, and may be a function of θ.

This is easily demonstrated for the simple on-resonance case:

$$R = (\pi/2)_x(4\pi/3)_y(\pi/2)_x \qquad 4.78$$

$$= [(\pi/2)_x(2\pi/3)_y(\pi/2)_{-x}].\pi_x.[(\pi/2)_{-x}(2\pi/3)_y(\pi/2)_x] \qquad 4.79$$

$$= (2\pi/3)_{-z}\pi_x(2\pi/3)_z . \qquad 4.80$$

On-resonance the composite pulse is equivalent to a rotation of π radians about the axis y' in Figure 4.4.

4.5.4 Composite pulses in a Carr-Purcell spin echo train

Rotation operators can now be used to analyse the properties of composite pulses in a Carr-Purcell spin echo train. Within the domain in which the composite pulse gives a good inversion of z-magnetization, it may be represented by an operator R such as

that of equation 4.77. Evolution of the density matrix during the echo train may then be treated by using the propagator ARA where A is the free precession operator over the period τ:

$$A = \exp[-iH_o\tau] \qquad 4.81$$

H_o is the free precession Hamiltonian in the rotating reference frame.

In a system of homonuclear spins, the Hamiltonian H_o consists of two parts:

$$H_o = H_o^a + H_o^s \qquad 4.82$$

$$\text{where} \quad H_o^a = -\sum_i \delta_i I_{zi} \quad \text{and} \quad H_o^s = -\sum_{j<k} J_{jk} \underline{I}_j . \underline{I}_k \qquad 4.83$$

For weakly coupled spins and low pulse repetition rates, the off-diagonal parts of H_o^s may be ignored (135) so that

$$H_o^s = \sum_{j<k} J_{jk} I_{zj} I_{zk} \qquad 4.84$$

which commutes with H_o^a.

This allowes the free precession operator A to be split up in a similar way:

$$A = \exp(-i\, H_o\tau) = A^a A^s \qquad 4.85$$

where

$$A^a = \exp(i\tau \sum_i \delta_i I_{zi}) \text{ and } A^s = \exp(i\tau \sum_{j<k} J_{jk} I_{zj} I_{zk}) \qquad 4.86$$

Hence the echo propagator ARA may be reformulated:

$$ARA = A^a A^s R A^s A^a$$

$$= A^a A^s (RA^s R^{-1})(RA^a R^{-1})R \qquad 4.87$$

Now consider the effect of R on the two parts of the free precession operator, A^s and A^a. A^a is inverted by the rotation:

$$RA^a R^{-1} = R\exp[i\tau \sum_i \delta_i I_{zi}]R^{-1} = \exp[i\tau \sum_i \delta_i R I_{zi} R^{-1}]$$

$$= \exp[-i\tau \sum_i \delta_i I_{zi}] = (A^a)^{-1} \qquad 4.88$$

In contrast R leaves A^s unchanged, because it acts on both sets of coupled spins j and k:

$$RA^s R^{-1} = R\exp[i\tau \sum_{j<k} J_{jk} I_{zj} I_{zk}]R^{-1}$$

$$= \exp[i\tau \sum_{j<k} J_{jk} (RI_{zj}R^{-1})(RI_{zk}R^{-1})]$$

$$= \exp[i\tau \sum_{j<k} J_{jk} (-I_{zj})(-I_{zk})]$$

$$= A^s \qquad 4.89$$

Hence the propagator ARA becomes

$$ARA = A^a A^s (A^a)^{-1} A^s R = (A^s)^2 R \qquad 4.90$$

For two echoes, the propagator may be simplified further:

$$(ARA)^2 = (A^s)^2 R (A^s)^2 R = (A^s)^4 R^2$$

$$= (A^s)^4 \qquad 4.91$$

Because R^2 is unity. (It is a rotation by 2π radians). Thus in general for even-numbered echoes n,

$$(ARA)^n = (A^s)^{2n} = \exp[-2ni\tau H_o{}^s] \qquad 4.92$$

Note that this expression no longer contains any reference to ϕ, the phase of the π rotations. Hence the propagator generates an echo train exactly the same as that produced by π pulses applied about the y-axis, providing only even-numbered echoes are examined. This is in agreement with the pictorial description given previously.

For example, if homonuclear spin-spin coupling is absent, $H_o{}^s$ is zero, so that $(ARA)^n$ is unity for even numbers n. The echo train is unmodulated. (Relaxation has been ignored). But if homonuclear coupling is present, the coupling part of the Hamiltonian $H_o{}^s$ generates a modulated echo train. For even values of n,

$$(ARA)^n = \exp[2ni\tau \sum_{j<k} I_{jk} I_{zj} I_{zk}] \qquad 4.93$$

The components of observable mgnetization can be calculated by applying 4.92 to an initial density matrix $\sigma(o)$:

$$\langle M_y \rangle_n \propto Tr\ [(ARA)^n \sigma(o) (ARA)^{-n} I_y] \qquad 4.94$$

$\sigma(o)$ is proportional to I_y if the system is prepared by a $(\pi/2)_x$ pulse applied to equilibrium magnetization. Then

$$\langle M_y \rangle_n \propto Tr[\exp(2ni\tau \sum_{j<k} I_{jk} I_{zj} I_{zk}) I_y \exp(-2ni\tau \sum_{j<k} I_{jk} I_{zj} I_{zk}) I_y] \qquad 4.95$$

which can easily be shown to give rise to the modulated echo

envelope:

$$\langle M_y \rangle_n \propto \sum_{j<k} \cos(4n\pi\tau J_{jk}) \text{ for n even.} \qquad 4.96$$

The argument above is dependent on R being of the form of equation 4.77 - a flip of π radians about an axis in the xy plane. Thus it is suitable for single π pulses of exact length, or for composite pulses in the domain in which they produce a good inversion of z-magnetization. Pulses which cannot be described by equation 4.77 do not have the simple effect of reversing the propagator A^a leaving A^s unchanged. A^a is modified in a relatively simple way which is capable of geometrical interpretation (see following sections), but A^s gives a very complicated result. The modified operator RA^sR^{-1} may be shown to inter-convert transverse magnetization and multiple-quantum coherences. The resulting dialogue between observable magnetization and invisible multiple-quantum coherence produces a very complicated modulation of the spin echo train.

4.5.5 Cumulative errors in a spin echo train

The interaction of pulse imperfections with the non-coupled part of the precession operator A^a will now be examined in more detail. This will give a greater insight into the limitations of the Meiboom-Gill compensation scheme, and the advantages to be accrued by using a composite pulse method.

There is a close formal similarity between the composite three-pulse sequence $(\pi/2)_x(\pi)_y(\pi/2)_x$ (by now familiar), and a single element of a Carr-Purcell sequence $R_zR_yR_z$, consisting of free precession for an interval $\tau(R_z)$, a refocussing pulse (R_y)

and a further precession period. For the composite pulse, operator algebra was used to clarify the overall effect in the presence of imperfections, and demonstrate an approximate equivalence with a rotation by exactly π radians about an axis in the equatorial plane of the rotating frame. Similar algebra can be used to treat a single element of the Carr-Purcell sequence $R_z R_y R_x$, or more specifically a pair of elements $(R_z R_y R_z)^2$, since it will be found that as usual error compensation tends to occur to the greatest degree on the even-numbered echoes in the train.

Treatment of the Carr-Purcell sequence does differ from that used for the composite pulse in that the angle of rotation R_z depends not on B_1 field strength but on the precession frequencies of the individual resonances, so that the overall result is dependent on the resonance chosen. This appears naturally in the algebra. An important assumption is made in the calculation that spin-lattice relaxation may be ignored. This allows the evolution during the free precession periods to be expressed as a simple rotation R_z. This is not strictly valid, but fortunately if spin-lattice relaxation is taken into account the conclusions of this section tend to be reinforced rather than invalidated.

Now it has already been shown that if the Hamiltonian contains a term H_o^S which represents homonuclear coupling, the corresponding propagator A^S interacts in a very complicated way with any refocussing pulse which is not a flip of exactly π radians. It has not been found possible to derive a closed expression for the modulation of the echo train in this case, which is expected to be a complicated combination of single and multiple-quantum precession

frequencies. Instead the easier problem of the interaction of an imperfect refocussing pulse with the non-coupled part of the Hamiltonian H_o^a will be addressed. This represents the common situation in which homonuclear coupling is unlikely, such as in natural-abundance ^{13}C spectroscopy.

Firstly consider a spin echo train in which imperfect conventional refocussing pulses are used, the main imperfection being spatial inhomogeneity of the radio-frequency field, represented as a misset in the flip angle, $R_y(\pi+2\Delta)$. (Tilting of the effective field caused by resonance offset could be handled in a similar way). The overall propagator for the element $R_zR_yR_z$ is then

$$A^aRA^a = \exp(-i\sum_i\theta_iI_{zi})R_y(\pi+2\Delta)\exp(-i\sum_i\theta_iI_{zi})$$

$$= \exp(-i\sum_i\theta_iI_{zi})R_y(2\Delta)\exp(+i\sum_i\theta_iI_{zi})R_y(\pi) \qquad 4.97$$

where $\theta_i = \delta_i\tau$ and indicates the angle through which a given resonance i precesses during the period τ.

The first three terms of this equation may be combined into a single rotation by using the identity 2.73. This gives

$$A^aRA^a = \exp\{2i\Delta\sum_i(I_{yi}\cos\theta_i - I_{xi}\sin\theta_i)\}R_y(\pi) \qquad 4.98$$

For two elements the overall propagator is

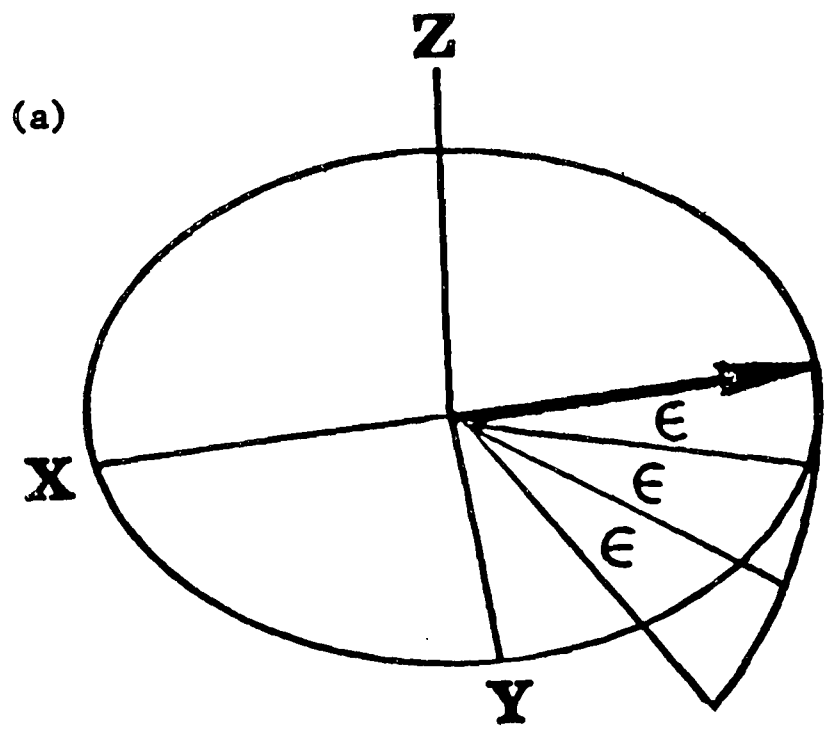

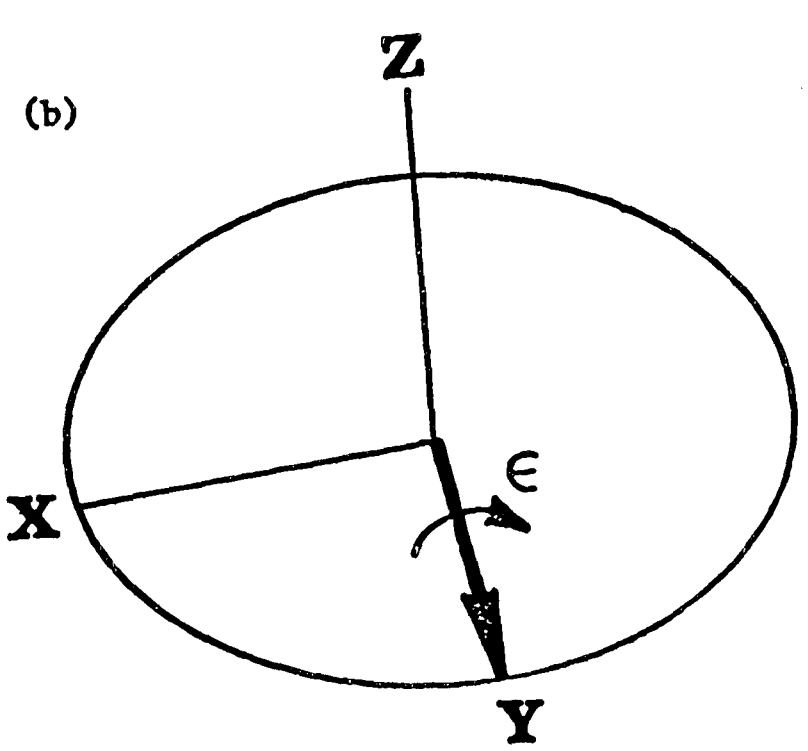

Fig.4.30. The overall effect of pulse length errors at the time of the even-numbered echoes if the refocussing pulses are $(\pi+\Delta)_y$. Each element $(\tau\text{-}R\text{-}2\tau\text{-}R\text{-}\tau)$ causes a small rotation $\epsilon = 2\Delta\cos\theta_i$ about the y-axis. Without the Meiboom-Gill modification (a), the magnetization starts out along the x-axis, so the small rotations have a strong cumulative effect. With the Meiboom-Gill phase shift, these small rotations have no significant effect (b).

$$(A^aRA^a)^2 =$$

$$\exp\{2i\Delta\sum_i(I_{yi}\cos\theta_i - I_{xi}\sin\theta_i)\}Ry(\pi)\exp\{2i\Delta\sum_i(I_{yi}\cos\theta_i - I_{xi}\sin\theta_i)\}Ry(\pi)$$

$$= \exp\{2i\Delta\sum_i(I_{yi}\cos\theta_i - I_{xi}\sin\theta_i)\}\exp\{2i\Delta\sum_i(I_{yi}\cos\theta_i + I_{xi}\sin\theta_i)\} \quad 4.99$$

Expansion of the exponentials to first order, and collection of terms gives

$$(A^aRA^a)^2 \simeq \exp\{2i\Delta\sum_i(I_{yi}\cos\theta_i)\} \quad 4.100$$

This operator represents the <u>overall</u> rotation brought about by two complete elements of the Carr-Purcell sequence $(R_zR_yR_z)^2$. Physically it turns a given vector i by a small angle $\varepsilon = 4\Delta\cos\theta_i$ about the y-axis. Thus the positions of a given magnetization vector at the centre of even echoes in the train can be predicted by repeated application of this small rotation to some initial condition. Firstly note that if the vector has a precession frequency such that $\theta_i = (m+\frac{1}{2})\pi$, where m is an integer, there are no cumulative errors to first order. But in general this is not so for all resonances in the spectrum, and some will experience the maximum effect of the imperfections, $\varepsilon = 4\Delta$.

Then the significance of the Meiboom-Gill modification can be understood. If the magnetization is initially prepared along the -x axis (by a preparatory $\pi/2$ pulse about the y-axis, the same phase as the refocussing pulses), the small rotations ε have a cumulative effect, and slowly rotate the vector in an arc away from the x-axis and towards the south pole (Figure 4.30(a)). The observed behaviour is a slow sinusoidal oscillation of the echo intensity at a low frequency proportional to the degree of

imperfection. In an inhomogenous B_1 field these oscillations destructively interfere to produce a premature decay of the echo amplitude. However these undesirable cumulative effects can be much reduced by preparing the initial magnetization along the y-axis, so that the small rotations have a minimal influence. This is the Meiboom-Gill modification and requires that the initial $\pi/2$ pulse be phase-shifted by $\pi/2$ radians with respect to the refocussing pulses. (Figure 4.30(b)). It is also clear under what conditions the Meiboom-Gill scheme breaks down. There are no first-order cumulative effects if, and only if, the magnetization is prepared exactly along the y-axis, and remains there at the times of the even-numbered echoes. This is not so in at least two important cases. Firstly, spin-lattice relaxation causes magnetization components to drift above the xy plane during the echo train, and so will cause a cumulative interaction with pulse imperfections. Secondly, magnetization components do not remain along the y-axis if there are homonuclear spin-spin coupling interactions. Then the echoes are phase modulated, so cumulative errors may build up here too. (There are also quite different effects in coupled spin systems associated with the poor spin state inversion caused by the imperfect π pulse (134)).

4.5.6 Second-order compensation with composite pulses

It was shown above that in the absence of homonuclear spin-spin coupling, and ignoring relaxation effects, pulse length errors are corrected to first order by the Meiboom-Gill modification. It will now be demonstrated that under the same conditions the composite pulse method achieves correction to second order, making

it superior to the Meiboom-Gill method even when the latter is operating as well as possible.

The rotation operator for a composite pulse subject to pulse length imperfections can be written:

$$R = R_x(\pi/2 + \Delta)R_y(\pi+2\Delta)R_x(\pi/2+\Delta) \qquad 4.101$$

As shown previously (equations 4.57 and 4.60), this is equivalent to:

$$R = R_x(\Delta)R_{-z}(\Delta)R_y(\pi)R_z(\Delta)R_x(\Delta) \qquad 4.102$$

Although the outermost terms can be dropped if an expression accurate only to first order in Δ is required, here the calculation will be carried through to second-order. The operator is expanded:

$$R = R_{-z}(\Delta).[R_z(\Delta)R_x(\Delta)R_{-z}(\Delta)].R_y(\pi).[R_z(\Delta)R_x(\Delta)R_{-z}(\Delta)].R_z(\Delta) \qquad 4.103$$

The expressions in square brackets can be approximated as follows:

$$R_z(\Delta)R_x(\Delta)R_{-z}(\Delta) = \exp[i\Delta(I_x\cos\Delta - I_y\sin\Delta)]$$

$$\simeq \exp(i\Delta I_x)\exp(-i\Delta^2 I_y)$$

$$\simeq R_x(\Delta)R_{-y}(\Delta^2) \text{ or } R_y(\Delta^2)R_x(\Delta) \qquad 4.104$$

since small rotations commute to a good approximation. Thus R

may be expressed:

$$R \simeq R_{-z}(\Delta)R_{-y}(\Delta^2).[R_x(\Delta)R_y(\pi)R_x(\Delta)].R_{-y}(\Delta^2)R_z(\Delta) \qquad 4.105$$

The central bracket can be simplified:

$$R_x(\Delta)R_y(\pi)R_x(\Delta) = R_y(\tfrac{\pi}{2}).[R_{-y}(\tfrac{\pi}{2})R_x(\Delta)R_y(\tfrac{\pi}{2})].[R_y(\tfrac{\pi}{2})R_x(\Delta)R_{-y}(\tfrac{\pi}{2})].R_y(\tfrac{\pi}{2})$$

$$= R_y(\tfrac{\pi}{2})R_{-z}(\Delta)R_z(\Delta)R_y(\tfrac{\pi}{2}) = R_y(\pi) \qquad 4.106$$

The final expression for the rotation operator is

$$R \simeq R_{-z}(\Delta)R_y(\pi-2\Delta^2)R_z(\Delta) \qquad 4.107$$

which is accurate to second order in Δ.

Whereas in first order the composite sequence behaves as an exact π pulse operating about a phase-shifted axis in the xy plane, the second order calculation reveals a small deficit $2\Delta^2$ in the length of the π pulse. Using this expression for the refocussing pulse R_y, the propagator for two echo periods can be recalculated and is:

$$(A^aRA^a)^2 \simeq R_{-z}(\Delta)\exp(-4i\Delta^2\textstyle\sum_i I_{yi}\cos\theta_i)R_z(\Delta) \qquad 4.108$$

where again approximations are carried to second order. This expression is unity to first order, so that a given magnetization vector is restored to its initial direction at the centre of the even-numbered echoes, whatever its initial position. However

Table 4.4. Compensation of pulse length errors in various spin echo experiments.

Experiment	No homonuclear coupling	Homonuclear coupling
Basic Carr-Purcell sequence $(\pi/2)_x - \{\tau - \pi_x - \tau\}^n$	cumulative errors	cumulative errors
Meiboom-Gill modification $(\pi/2)_x - \{\tau - \pi_y - \tau\}^n$	first-order compensation	cumulative errors
Composite pulses (x-axis) $(\pi/2)_x - \{\tau - (\pi/2)_y \pi_x (\pi/2)_y - \tau\}^n$	first-order compensation	first-order compensation
Composite pulses (y-axis) $(\pi/2)_x - \{\tau - (\pi/2)_x \pi_y (\pi/2)_x - \tau\}^n$	second-order compensation	first-order compensation

when second-order effects are taken into account, there is clearly a preferable initial phase of the magnetization analogous to that used in the Meiboom-Gill modification. If a train of composite $(\pi/2)_x(\pi)_y(\pi/2)_x$ pulses are used for refocussing, magnetization is best prepared with a $(\pi/2)_x$ pulse, placing it close to the y-axis where the small rotations of equation 4.108 have least effect. Under these conditions and in the absence of homonuclear spin-spin coupling and spin-lattice relaxation, pulse length errors are compensated to both first and second order. The comparative efficiency of the various schemes of error compensation are summarised in Table 4.4.

4.5.7 Experimental verification

These conclusions have been verified by performing spin echo trains on a sample of 1,1,2-trichloroethane in acetone-d_6. The relaxation properties of this molecule are well covered in the literature. The sample was degassed by bubbling helium through the solution, and the experiments performed on the XL-200 spectrometer in which the B_1 field is known to be very homogenous. This allowed a controlled simulation of the effects of inhomogeneity by a misset of all pulse lengths by -20%. To avoid spinner modulation effects a stationary sample was used.

The echo modulation induced by the homonuclear coupling was removed by calculating 'double-sided transforms' of the whole echo at the end of the sequence (Chapter 2). As described in that chapter, transformation of the whole echoes removes dispersion-mode contributions from the modulated signals, so that the absolute value can be used to remove the modulation and still avoid

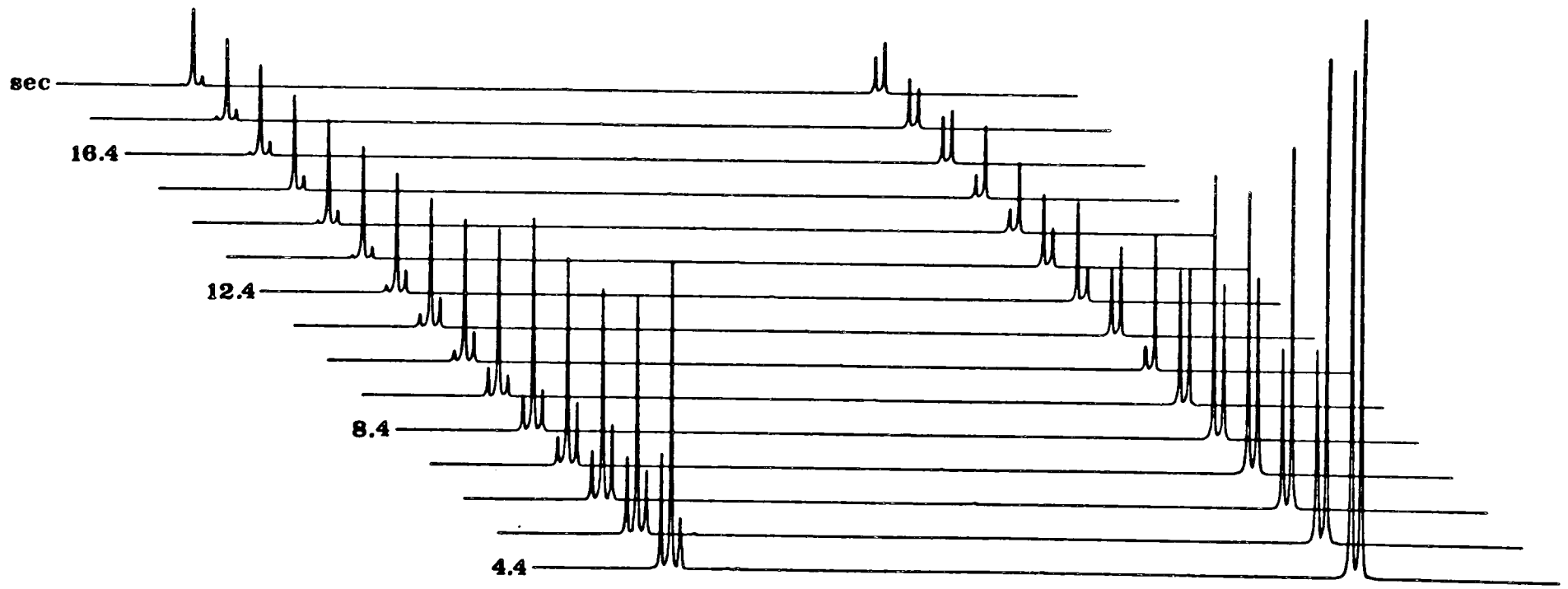

Fig.4.31. Spin-spin relaxation measurements on 1,1,2-trichloroethane, performed on the XL-200. The Meiboom-Gill modification was used with the refocussing pulses deliberately set 20% short. Echoes occurred at 0.5 second intervals, the final echo being preceded by a 3.4 second interval to allow acquisition of the whole echo. Since the Meiboom-Gill modification is ineffective in the presence of homonuclear spin-spin coupling, a gross fluctuation of the intensities is observed, partly obscuring the effects of spin-spin relaxation.

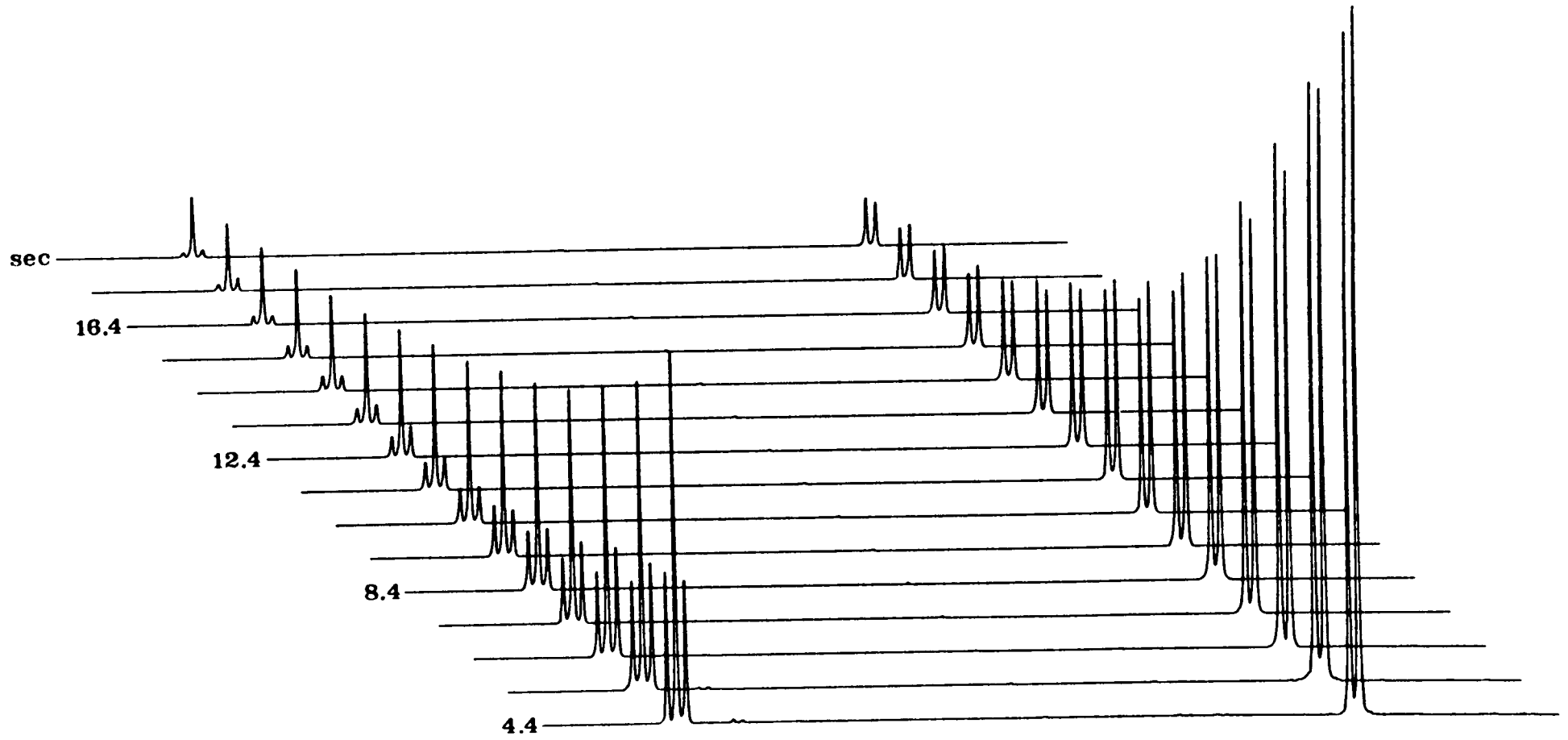

Fig.4.32. Spin-spin relaxation measurements on 1,1,2-trichloroethane, under the same conditions as for Fig.4.31, except that composite refocussing pulses were used, also misset by -20%. Note the monotonical decrease in intensities due to spin-spin relaxation.

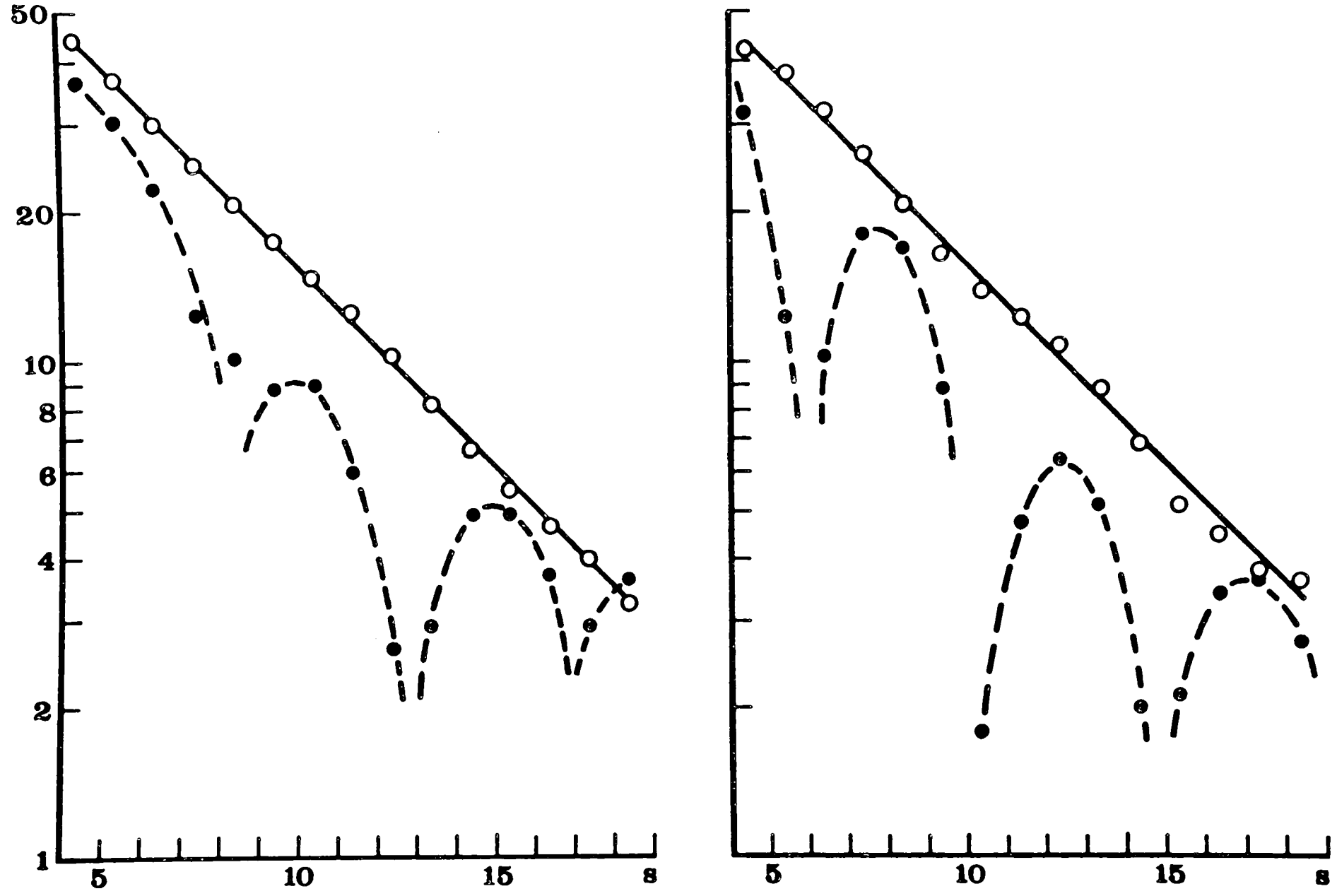

Fig.4.33. Comparison of the measurements of Figs.4.31 and 4.32. The intensities of the methylene doublet are shown, with the high-field line on the left, and low-field line on the right. Conventional refocussing pulses gave wild oscillations (black circles); the dashed lines have no theoretical significance. With composite refocussing pulses (open circles), the oscillations are much smaller and permit a good estimate to be made of the decay time constants (5.4±0.2 seconds).

interference effects between adjacent lines.

To allow an adequate acquisition time for the whole echo, the delay between the penultimate echo and the last refocussing pulse was extended to 1.7 seconds. This meant that the first spectrum in each series was taken after a delay of 4.4 seconds, so that the outer lines of the triplet have already decayed appreciably in comparison with the centre line. Figure 4.31 shows the results obtained with conventional pulses with the Meiboom-Gill modification. The pulse lengths had been deliberately misset by -20% in order to show a dramatic effect, but undesirable oscillations can still be observed with much smaller missets. Compare this with Figure 4.32 where the refocussing pulses were composite, again with the pulse lengths misset by -20%. An essentially smooth decay of the intensities of all five lines is observed. The comparison is most easily made from Figure 4.33 where the intensities of the two lines of the doublet are plotted on a logarithmic scale. The results for conventional single π pulses (black circles) show a strange bouncing pattern, which may be attributed to some sort of oscillation distorted by the absolute value presentation and the logarithmic scale. As mentioned previously it is very hard to derive an expression for this oscillation and the dotted lines have no theoretical significance. In contrast the results for composite pulses show only a small oscillatory component, which may be attributed to second-order effects.

4.6 Composite z-pulses

Although this chapter has so far concentrated on the use of composite sequences for the correction of pulse imperfections, some quite different applications are feasible. In fact what are essentially composite pulses have been used for many years in solid-state magnetic resonance to construct overall rotations about axes which are normally inaccessible, and a similar operator algebra has been used to treat them. An example is the 'WAHUHA' sequence (136) $\tau\text{-}(\pi/2)_{-x}\text{-}\tau\text{-}(\pi/2)_{y}\text{-}2\tau\text{-}(\pi/2)_{-y}\text{-}\tau\text{-}(\pi/2)_{x}\text{-}\tau$ which can be shown to resemble an overall rotation about the 'magic angle' axis (1,1,1). Thus repeated application of this sequence leads to decoupling of homonuclear dipolar interactions, with great increase in resolution in the solid-state. Much more sophisticated sequences have been constructed with a view to correction of pulse imperfections, in much the same way as the composite pulses described above (137). Thus the concept of composite pulses is not really new, but it is fair to say that the potential for high-resolution work in the liquid state has not been realised. However some sequences closely related to composite pulses have been used to achieve frequency selectivity, examples being the 'DANTE' sequence of Morris (138), the 'tailored excitation' technique of Tomlinson and Hill (139) and the '2-1-4' sequence of Redfield (140). The latter sequence bears some resemblance to the 'spin-knotting' pulse described above.

But in the liquid state the use of composite pulses is not restricted to the correction of imperfections, and here too they can be used to construct rotations about unusual axes. For

example it is not easy to rotate magnetization vectors by a given angle about the z-axis. A carefully chosen period of free precession could be left but this may introduce relaxation effects and the same rotation is not experienced by all resonances in the spectrum. Another means would be suddenly to increase the static magnetic field for a short interval, but this would require the introduction of extra coils in the neighbourhood of the probe, and construction of the appropriate driving circuitry. It would be hard to achieve a homogenous z-pulse over the sample volume, and the procedure might well be extremely dangerous in high-field superconducting magnets, where sudden field jumps could induce a 'quench', a disastrous transition to normal conductivity in parts of the superconducting wire. Much better is to use a composite pulse in which familiar rotations about the x and y axes are combined in such a way as to be equivalent to the desired z-rotation (141). For example a rotation of ϕ radians about the z-axis could be constructed by using a composite pulse

$$R_z(\phi) = R_{-x}(\pi/2)R_y(\phi)R_x(\pi/2) \qquad 4.109$$

ignoring the effects of pulse imperfections.

The use of such pulses should make unnecessary the complex phase-shifters which are starting to be used in liquid-state NMR (142). It <u>is</u> possible to build a digital delay line capable of providing shifts in the radio-frequency phase in as little as 1^{o} steps, but such lines are expensive and presumably make interfacing and programming complicated. It is presumably better to restrict the

available phase shifts to steps of $\pi/2$ radians and combine the orthogonal rotations in ways such as that of equation 4.109.

Small phase-shifts and z-rotations are most frequently of use in the field of multiple-quantum NMR (55,143). This is because coherences respond to a change in phase ϕ at a rate proportional to the difference in magnetic quantum number ΔM between the two connected levels (55). Double-quantum coherences respond twice as fast as the allowed single-quantum magnetizations, and triple-quantum coherences three times as fast. Zero-quantum coherences and energy level populations, both of which have $\Delta M = 0$, are unaffected by z-rotations.

This can be proved as follows: If an initial density matrix σ^- is perturbed by some rotation R the final density matrix σ^+ is given by

$$\sigma^+ = R\sigma^-R^{-1} \qquad 4.110$$

Expressed in terms of an individual coherence element σ_{mn}:

$$\sigma^+_{mn} = \sum_{ij} R_{mi}\sigma^-_{ij}R^{-1}_{jn} \qquad 4.111$$

Now let R be a rotation about the z-axis by ϕ radians:

$$R = \exp(i\phi I_z) \qquad 4.112$$

If the density matrix is expressed in the basis set of eigenfunctions of I_z (weak coupling), R is diagonal so that equation 4.111 can be much simplified:

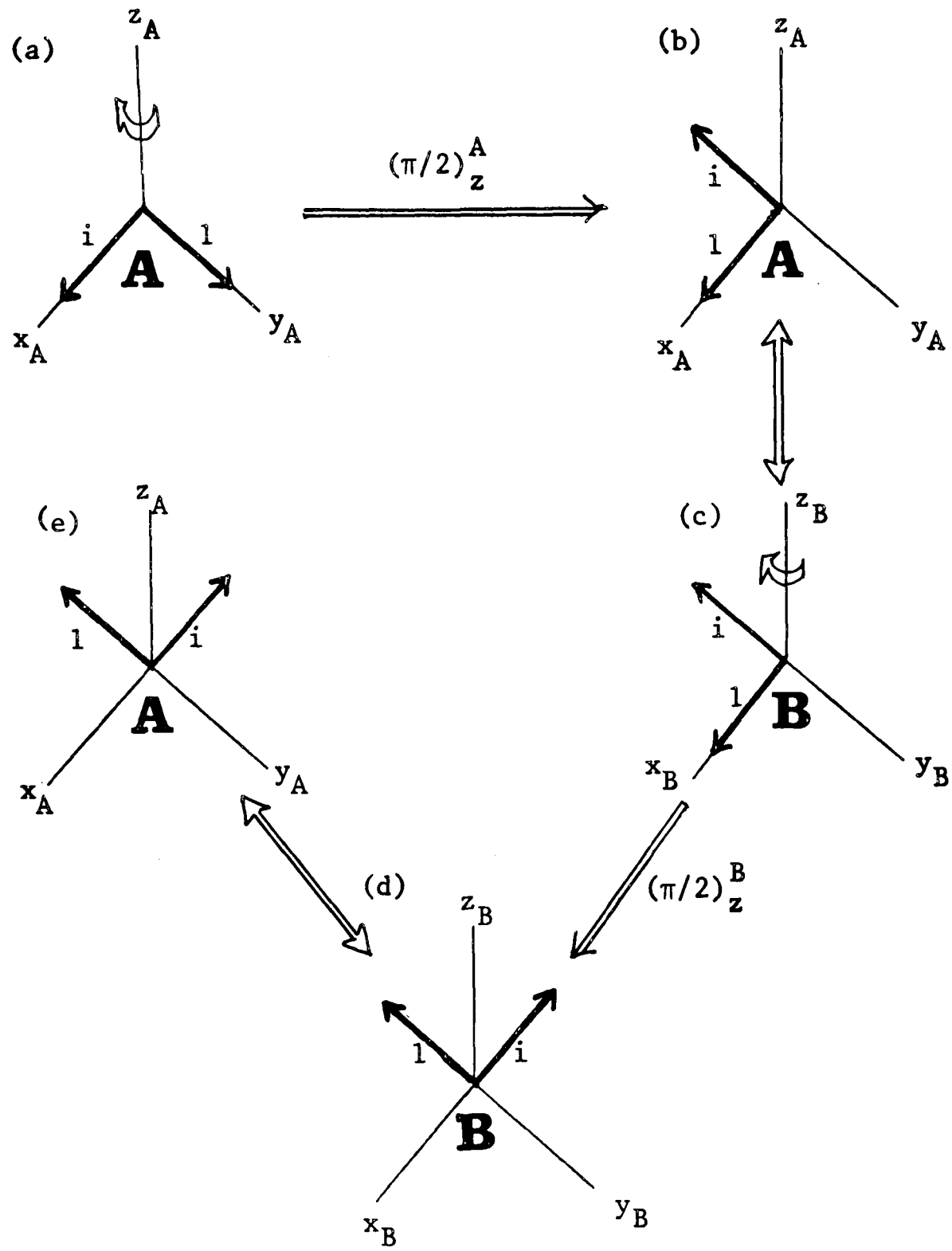

Fig.4.34. The effect on double-quantum coherence of a rotation about the z-axis of $\pi/2$ radians, expressed by manipulation of ZDQ vectors. As usual the non-selective $\pi/2$ rotation must be represented as a 'cascade' of two consecutive spin-selective rotations, $(\pi/2)_z{}^A$ and $(\pi/2)_z{}^B$.

(a)→(b): The vector (i,1) in the AZDQ frame is rotated to give (1,-i) by the first cascade element.

(b)→(c): (1,-i) transforms into the 'conjugate frame' without modification.

(c)→(d): The vector (1,-i) is rotated into (-i,-1) by the second cascade element $(\pi/2)_z{}^B$.

(d)→(e): The final vector transforms back into the AZDQ frame without modification.

The final state (e) is related to the initial state (a) by a rotation of π radians, twice the conventional value.

$$\sigma_{mn}^{+} = (R_{mm}R_{nn}^{-1})\sigma_{mn}^{-} \qquad 4.113$$

Thus σ_{mn} is multiplied by a factor $R_{mm}R_{nn}^{-1}$. Evaluating this factor,

$$R_{mm}R_{nn}^{-1} = \exp\{i\phi(I_z)_{mm}\}\exp\{-i\phi(I_z)_{nn}\} \qquad 4.114$$

$$= \exp(i\phi\Delta M) \qquad 4.115$$

since the magnetic quantum numbers M are defined as the eigenvalues of I_z.

The same conclusion can be reached by using the vector diagrams of Chapter 3. Figure 4.34 shows the effect of a rotation by $\pi/2$ radians on a vector representation of double-quantum coherence. In a homonuclear coupled system z-rotations must be applied to both the A and B spin systems, so that two 'conjugate transformations' are necessary to arrive at the result. Comparison of the initial state of Figure 4.34(a) and the final state of Figure 4.34(e) shows that in all the double-quantum vectors have moved through an angle of π radians - twice the applied rotation. The same conclusion can be reached if a more general rotation is chosen.

These properties of multiple-quantum coherence with respect to phase shifts or z-rotations lead to a multitude of interesting possibilities which cannot be discussed here. They include the selective detection of multiple-quantum coherence (55,143) and even the selective excitation of specified orders of multiple-quantum coherence in dipolar coupled systems (144). All of these experiments

involve small phase shifts which may have been accomplished more easily by using composite pulses. A paper is in preparation which uses a z-rotation by $\pi/4$ radians, produced by a composite pulse, to allow discrimination of positive and negative double-quantum precession frequencies (145). Such frequency discrimination would be difficult to achieve by other means.

CHAPTER FIVE

DISCUSSION

CHAPTER 5

DISCUSSION

Since the advent of pulse-Fourier transform nuclear magnetic resonance in 1966, the history of the subject has been one of steady replacement of continuous radio-frquency fields by short strong pulses as a means of manipulating the nuclear spin system. The advantages of pulse techniques are two-fold: Firstly, the non-selectivity of the strong pulses provides an important theoretical sensitivity advantage - as all resonances are manipulated simultaneously, examination of the complete spin system takes a shorter time in principle than the equivalent set of continuous-field experiments. This assumes firstly that an analysis technique exists for separating out the information, (usually a single or double Fourier transformation with respect to variable time parameters within the pulse sequence), and also that interest lies in more than just one or two resonances. The second major advantage of pulse techniques is that manipulation of the spins by this means tends to be a cleaner operation than the use of continuous fields at intermediate power levels. This is simply because the short durations of the pulses allows a very high power to be momentarily delivered to the probe. Ideally the B_1 field strengths can be made high enough that the interaction with the radio-frequency field dominates the rotating-frame Hamiltonian, so that the evolution of the system is accurately described by the simple pulse operators of section 2.3.3. In contrast, continuous

irradiation fields cannot be maintained at such high power levels without risking destruction of sample and probe, so that the simplified Hamiltonian cannot be used. Calculation of the evolution of the system then requires rediagonalization of the Hamiltonian, so that the positions and intensities of the existing resonances may be modified, and new ones may appear (34).

Thus apart from the replacement of continuous-wave detection by pulse-Fourier transformation, almost all double-resonance experiments can be replaced to advantage by an equivalent double Fourier transform method. Such pairs are INDOR (34-36) and Jeener spectroscopy (39-40), off-resonance heteronuclear decoupling (51,52) and heteronuclear shift correlation (60-65) or two-dimensional heteronuclear J-spectroscopy (42-48), and the detection of homonuclear multiple-quantum transitions by using strong continuous irradiation fields (53,54) as against two-dimensional multiple-quantum spectroscopy (55). However it should be pointed out that the sensitivity of the two-dimensional experiments can be markedly degraded by instrumental effects, which, together with the complexity of these methods, can make their practical advantages over the double-resonance techniques rather marginal in some cases (146).

Even when modification of the Hamiltonian is required, this is often more cleanly done by using repetitive pulse trains rather than continuous fields. A good example of this is in the solid state, where continuous rotation about an effective field tilted above the xy plane by the 'magic angle' $54^{o}44'$ is required, in order to produce a decoupling of homonuclear dipolar interactions. This was originally done by spin-locking about a continuous field applied off-resonance by an amount carefully designed to give the

desired tilt (147). More recently repetitive sequences of strong pulses are used which have an equivalent effect (136,137,150). The use of non-selective pulses ensures that the degree of decoupling is almost independent of resonance offset. In high-resolution liquid-state work, similarly tilted effective fields are sometimes applied in order to scale down heteronuclear J-coupling interactions (51-52). Once again, the modification of the Hamiltonian by the use of repetitive pulse trains may provide a favourable alternative, in which the dependence of average effective field tilt on resonance offset can be much reduced (151,152).

A further advantage of pulse techniques is that if desired, the effect of continuous fields can still be simulated. Thus a train of short non-selective pulses may have a strongly selective overall effect, as has been examined in detail by Morris (138). Pulse sequences can also be designed which produce a much more general dependence of excitation strength on frequency (139).

This extension of pulse methods to ever more sophisticated applications has made it particularly important that their effects are fully understood. In Chapter 3 it was demonstrated that these effects can be surprisingly complicated for even the simplest possible coupled spin system, the AX system. Nevertheless the geometry of interconversion of the various coherences is basically simple and is amenable to discussion using a vector model. The degree of utility of this particular model will probably only become apparent after a little time. It may be that it is too restricted in its applications, and that the explicit density matrix calculations, or the use of single-transition operators (114-116) (both of which

are more complicated) will see more light of day. The author is reasonably optimistic that the vector model is a helpful guide in the bewildering terrain of coupled spin systems, and it has already been a stimulus for the development of an experimental pulse sequence for the 'direct detection' of multiple-quantum coherence (153).

Composite pulses are of more certain utility. It is true that computer-aided design of transmitter coils in the most modern instruments has resulted in B_1 fields of very good homogeneity, so that this aspect of pulse imperfections may not be so much of a problem in the future, in high-resolution liquid-state machines. (But even then the use of composite pulses should reduce the need for very accurate pulse length calibration). However, nuclear magnetic resonance is now progressing into areas well removed from the small sample tube. There is an increasing amount of NMR being performed on large biological specimens, and magnets are now in production which are capable of accommodating an adult human torso. These experiments fall into two main classes:

(a) Mapping of the variation in density of proton spins throughout the sample volume, with a view to locating regions of high or abnormal proton densities, such as fluid-filled lesions (154), and

(b) *in vivo* studies of chemical changes within individual organs, by monitoring nuclei of large chemical shift range. (Phosphorus-31 seems to be of most promise for this purpose (155)). Both of these classes of experiment are likely to be of considerable medical, physiological or biochemical importance. But with such large, inhomogenous samples, it is likely that B_1 inhomogeneity will again

be a problem, and composite pulses may be of assistance in manipulation of the spins.

The second major class of pulse imperfection is resonance offset, which is likely to remain a problem for some time, for both large and small-sample NMR. Although technical developments in amplifier and probe design have resulted in the production of large B_1 fields at the sample, this has not significantly reduced effective field tilt because B_o fields have also been increasing due to equivalent developments in superconducting magnets. Once more composite pulses may allow the best to be made out of the available power input. For example, compare the computer simulations of Figures 4.23 and 4.26, which plot the degree of population inversion achieved by a conventional single pulse as against a composite three-pulse sequence. The improvement achieved with respect to resonance offset is approximately equivalent to a ten-fold increase in radio-frequency field strength. Very recently a self-compensating pulse sequence has been used to decouple proton spins from carbon-13 nuclei (156). The self-compensating action ensures essentially full decoupling over a very wide range of proton frequencies, the performance apparently being considerably better than any other scheme in current use, including noise irradiation (32), square-wave phase modulation (157) and phase-alternated chirp irradiation (158).

Finally, an examination of the way in which orthogonal rotations combine together has led to a proposal for entirely new manipulations of the spins, such as rotations about the z-axis (section 4.6). Such operations will almost certainly be of importance in the study of multiple-quantum coherence.

To summarise, it has been the intention of this thesis to make a detailed examination of the one operation of central importance in modern nuclear magnetic resonance - the radio-frequency pulse. The action of pulses on the observables of coupled and non-coupled spin systems has been examined, and a pictorial interpretation has been given for a simple coupled spin system. Then the possibility was discussed of combining two or more pulses so as to produce an advantageous overall effect. In some cases, the result is similar to that produced by a single pulse, but is often less sensitive to a given class of pulse imperfection, a result of practical importance. In other cases, the resultant operation on the spins would be almost impossible to achieve by other means. It is hoped that these results constitute a useful contribution to pulse-Fourier transform nuclear magnetic resonance.

APPENDICES

APPENDIX 1

INSTRUMENTATION

Two NMR spectrometers were available to the author, Varian CFT-20 and XL-200 machines. The XL-200 is far superior but restrictions of operator time meant that some of the experiments described were performed on the older instrument, the CFT-20. For each experiment, the spectrometer used is indicated in the figure caption.

Both machines consist of a spectrometer connected by a two-way interface to a central processing unit, which is also in communication with various peripheral devices: an oscilloscope or raster screen for spectral and parameter display, a printer, an incremental flat-bed plotter, and a magnetic disc unit for storage of data and programs. Both spectrometers had also been interfaced to fast drum plotters, for rapid output of two-dimensional spectra, although this is not a standard feature. To perform the experiments described, no modification of hardware was required for either instrument Computer control of the radio-frequency phases, (and improvement of the stability of the timer), had already been introduced on the CFT by previous workers (159). This facility is a standard feature in the XL-200.

The new pulse sequences were performed by modifications to the programming of the spectrometer. This presents no problem in the case of the XL-200, in which the implementation of very general pulse sequences is a standard feature, and simply involves

the creation of a few lines of PASCAL, followed by compilation into the 16-bit machine code used by the computer. At the time of the experiment the code is transferred into a free-running acquisition microprocessor which controls the spectrometer, leaving the main processor available for other operations. The CFT-20 possesses no such compiler so that the pulse programming must be made by machine code patches in the standard main program, 'BASIC-A'. These patches consist of a less than a hundred lines of 16-bit machine code for a simple pulse sequence, but can run into thousands of lines for ambitious programs such as that for display and phase-adjustment of two-dimensional spectra (see section 1.3). The programs for acquisition and double-Fourier transformation of two-dimensional data had already been created by Bodenhausen and Turner, and further developed by Niedermeyer and Morris.

The two spectrometers differ a great deal in instrumentation. The XL-200 possesses a 4T superconducting magnet of high inherent stability, whilst the CFT is content with a 1.9T electromagnet. Although the field intensities of both magnets are held constant by means of feedback from continuous monitoring of a deuterium resonance signal, the stability of the electromagnet is rather suspect. Fluctuations in field over the duration of a two-dimensional experiment may be responsible for the noisy ridges parallel to the F_1 axis in some two-dimensional spectra, see Figure 1.6. Accordingly the XL-200 is preferable for two-dimensional work. Also the XL appears to possess radio-frequency coils which produce B_1 fields of exceedingly good homogeneity. The homogeneity of B_1 fields in the CFT is very poor, as is evident from Figure 4.1.

APPENDIX 2

OPERATORS

Of central importance in the quantum-mechanical description of NMR are Hermitian and unitary operators, represented here by the symbols A and U. Hermitian operators are important because they are used to represent observable quantities. This is because their expectation values are real, as is easily proved from the definition of Hermicity (6):

$$A = \tilde{A}^{*} \qquad \text{A.2.1}$$

The density matrix σ is a Hermitian matrix, as are other important operators such as I_x, I_y, I_z and I^2. (I_+ and I_- are not).

Unitary operators are also important. Most evolutions of the density matrix may be represented as unitary transformations:

$$\sigma' = U\sigma U^{-1} \qquad \text{A.2.2}$$

This neglects relaxation.

The definition of a unitary operator is:

$$U^{-1} = \tilde{U}^{*} \qquad \text{A.2.3}$$

The expectation values of unitary operators are complex quantities so that unitary operators do not represent observables.

The algebra of unitary and Hermitian operators is conveniently expressed using exponential operators such as e^A defined as:

$$e^A = 1 + A + \frac{1}{2!}AA + \frac{1}{3!}AAA + \ldots \qquad A.2.4$$

Exponential operators are very powerful but care must be taken. For example, note that the expression

$$e^A e^B = e^{A+B} \qquad A.2.5$$

is only true if $[A,B] = 0$.

The unitary operators involved in the evolution of the density matrix are usually related to an Hermitian operator as follows:

$$U = e^{iAt} \qquad A.2.6$$

where A is time-independent.

The time-dependence of σ' as defined by equation A.2.2 above, can then be expressed:

$$\sigma' = U\sigma U^{-1} + i[A,\sigma] \qquad A.2.7$$

It is from such reasoning that come expressions such as equation 2.53.

Not all unitary operators are time-dependent. A particularly important class of time-independent unitary operators are those used for diagonalization of the Hamiltonian:

$$\Lambda = UHU^{-1} \qquad A.2.8$$

The transformations of the density matrix under strong pulses are usually expressed by unitary transformations with operators such as $R_x(\alpha)$:

$$R_x(\alpha) = \exp(i\alpha I_x)$$

$$= 1 + i\alpha I_x + \frac{1}{2!}(i\alpha I_x)^2 + \frac{1}{3!}(i\alpha I_x)^3 \qquad \text{A.2.9}$$

For a spin-$\frac{1}{2}$ system,

$$I_x^2 = \tfrac{1}{4}\mathbb{1} \qquad \text{A.2.10}$$

whence comes the expansion:

$$R_x(\alpha) = \mathbb{1}\cos\tfrac{1}{2}\alpha + 2iI_x\sin\tfrac{1}{2}\alpha \qquad \text{A.2.11}$$

Such expressions are used in the matrix representations of rotation operators, eqn. 2.71. A useful special case of this equation is when $\alpha = \pi$ radians:

$$R_x(\pi) = 2iI_x \qquad \text{A.2.12}$$

The important interactions of rotation operators with angular momentum operators, and of rotation operators with each other, have already been outlined in section 2.3.3.

REFERENCES

REFERENCES.

1) A.Abragam,'The Principles of Nuclear Magnetism', Clarendon Press, Oxford, 1971, Ch.8.
2) R.R.Ernst and W.A.Anderson, Rev.Sci.Instr., 37, 93 (1966).
3) F.Bloch, Phys.Rev., 70, 460 (1946).
4) A.G.Redfield and R.K.Gupta, J.Chem.Phys., 54, 1418 (1971).
5) B.C.Mayo, Chem.Soc.Revs., 2, 49 (1973).
6) P.W.Atkins, 'Molecular Quantum Mechanics', Clarendon Press, Oxford, 1970.
7) J.T.Arnold, S.S.Dharmatti and M.E.Packard, J.Chem.Phys., 19, 507,(1951).
8) N.F.Ramsey, Phys.Rev., 78, 699 (1950).
9) F.W.Wehrli and T.Wirthlin, 'Interpretation of Carbon-13 NMR Spectra', Heyden, New York, 1976, Ch.2.
10) N.Bloembergen, E.M.Purcell and R.V.Pound, Phys.Rev., 73, 679 (1948).
11) H.S.Gutowsky, D.W.McCall and C.P.Slichter, Phys.Rev., 84, 589 (1951).
12) E.L.Hahn and D.E.Maxwell, Phys.Rev., 84, 1246 (1951).
13) N.F.Ramsey, Phys.Rev., 91, 303 (1953).
14) J.A.Pople, W.G.Schneider and H.J.Bernstein, 'High Resolution Nuclear Magnetic Resonance', McGraw-Hill, New York (1959).
15) M.Karplus, J.Am.Chem.Soc., 85, 2870 (1963).
16) L.D.Hall and H.D.W.Hill, J.Am.Chem.Soc., 98, 1269 (1976).
17) D.E.Woessner, J.Chem.Phys., 37, 647 (1962).
18) H.Shimizu, J.Chem.Phys., 37, 765 (1962).
19) W.T.Huntress Jnr., Adv.Mag.Res., 41 (1970).
20) L.G.Werbelow and D.M.Grant, J.Chem.Phys., 63, 544 (1975).
21) R.L.Vold, R.R.Vold and D.Canet, J.Chem.Phys., 66, 1202 (1977).
22) T.E.Bull and J.Jonas, J.Chem.phys., 53, 3315 (1970).
23) J.Schaeffer, Topics in Carbon-13 NMR Spectroscopy, edited by G.C.Levy, (Wiley), Vol.1, Ch.4, 1974.
24) R.L.Vold and R.R.Vold, Prog.NMR.Spectroscopy, 12, 79 (1978).
25) I.Solomon, Phys.Rev., 99, 559 (1955).
26) P.S.Hubbard, J.Chem.Phys., 52, 563 (1970).
27) M.Inagaki, private communication.
28) H.S.Gutowsky, R.L.Vold and E.J.Wells, J.Chem.Phys., 43, 4107 (1965).
29) Ref.1, Ch.8.

30) G.C.Levy and W.Edmund, J.Am.Chem.Soc., 92, 5031 (1975).

31) P.S.Hubbard, Phys.Rev., 131, 1155 (1963).

32) R.R.Ernst, J.Chem.Phys., 45, 3845 (1966).

33) J.H.Noggle and R.E.Schirmer, 'The Nuclear Overhauser Effect', Academic Press, New York, 1971.

34) R.Freeman and W.A.Anderson, J.Chem.Phys., 37, 85 (1962).

35) E.B.Baker, J.Chem.Phys., 37, 911 (1962).

36) S.Sørensen, R.S.Hansen and H.J.Jakobsen, J.Mag.Res., 14, 243 (1974).

37) R.L.Vold, J.S.Waugh, M.P.Klein and D.E.Phelps, J.Chem.Phys., 48, 3831 (1968).

39) W.P.Aue, E.Bartholdi and R.R.Ernst, J.Chem.Phys., 64, 2229 (1976).

40) J.Jeener, Ampere International Summer School, Basko Polje, Yugoslavia, 1971.

41) K.Nagayama, P.Bachmann, K.Wüthrich and R.R.Ernst, J.Mag.Res., 31, 133 (1978).

42) G.Bodenhausen, R.Freeman and D.L.Turner, J.Chem.Phys., 65, 839 (1976).

43) G.Bodenhausen, R.Freeman, R.Niedermeyer and D.L.Turner, J.Mag.Res., 24, 291 (1976).

44) L.Müller, A.Kumar and R.R.Ernst, J.Mag.Res., 25, 383 (1977).

45) G.Bodenhausen, R.Freeman, R.Niedermeyer and D.L.Turner, J.Mag.Res., 26, 133 (1977).

46) R.Freeman, G.A.Morris and D.L.Turner, J.Mag.Res., 26, 373 (1977).

47) G.Bodenhausen, R.Freeman, G.A.Morris and D.L.Turner, J.Mag.Res., 28, 17 (1977).

48) D.L.Turner and R.Freeman, J.Mag.Res., 29, 587 (1978).

49) R.L.Vold and S.O.Chan, J.Chem.Phys., 53, 449 (1970).

50) R.Freeman and H.D.W.Hill, J.Chem.Phys., 54, 301 (1971).

51) H.J.Reich, M.Jautelat, M.T.Messe, F.J.Wiegert and J.D.Roberts, J.Am.Chem.Soc., 91, 7445 (1969).

52) B.Birdsall, N.J.M.Birdsall and J.Feeney, J.Chem.Soc.Chem.Comm., 316 (1972).

53) K.McLauchlan and D.H.Whiffen, Proc.Chem.Soc., 144 (1962).

54) W.A.Anderson, R.Freeman and C.A.Reilly, J.Chem.Phys., 39, 1518 (1963).

55) A.Wokaun and R.R.Ernst, Chem.Phys.Letts., 52, 407 (1977).

56) A.Bax, R.Freeman and T.Frenkiel, to be published.

57) A.Wokaun and R.R.Ernst, Mol.Phys., 36, 317 (1978).

58) G.Bodenhausen, N.M.Szeverenyi, R.L.Vold and R.R.Vold, J.Am.Chem.Soc., 100, 6265 (1978).

59) R.L.Vold, R.R.Vold, R.Poupko and G.Bodenhausen, J.Mag.Res., 38, 141 (1980).

60) A.A.Maudsley and R.R.Ernst, Chem.Phys.Letts., 50, 368 (1977).

61) A.A.Maudsley, L.Müller and R.R.Ernst, J.Mag.Res., 28, 463 (1977).

62) G.Bodenhausen and R.Freeman, J.Mag.Res., 28,471 (1977).

63) G.Bodenhausen and R.Freeman, J.Am.Chem.Soc., 100, 320 (1978).

64) R.Freeman and G.A.Morris, J.Chem.Soc.Chem.Comm., 684 (1978).

65) P.H.Bolton and G.Bodenhausen, J.Am.Chem.Soc., 101, 1080 (1979).

66) A.G.Avent and R.Freeman, J.Mag.Res., 39, 169 (1980).

67) G.A.Morris, to be published.

68) D.C.Finster, W.C.Hutton and R.N.Grimes, J.Am.Chem.Soc., 102, 400 (1980).

69) R.Freeman and G.A.Morris, Bull.Mag.Res., 1, 5 (1979).

70) R.K.Hester, J.L.Ackermann, V.R.Cross and J.S.Waugh, Phys.Rev.Letts., 34, 993 (1975).

71) M.Alla and E.Lipmaa, Chem.Phys.Letts., 37, 260 (1976).

72) R.K.Hester, J.L.Ackermann, B.L.Neff and J.S.Waugh, Phys.Rev.Letts., 36, 1081 (1976)

73) M.E.Stoll, A.J.Vega and R.W.Vaughan, J.Chem.Phys., 65, 4093 (1976).

74) S.J.Opella and J.S.Waugh, J.Chem.Phys., 65, 4919 (1977).

75) E.F.Rybaczweski, B.L.Neff and J.S.Waugh, J.Chem.Phys., 67, 1231 (1977).

76) G.Bodenhausen, R.E.Stark, D.J.Ruben and R.G.Griffin, Chem.Phys.Letts., 67, 424 (1979).

77) M.Polak, A.J.Highe and J.S.Waugh, J.Mag.Res., 37, 357 (1980).

78) M.H.Levitt and R.Freeman, J.Mag.Res., 34, 675 (1979).

79) R.Freeman, S.P.Kempsell and M.H.Levitt, J.Mag.Res., 34, 663 (1979); P.Bachmann, W.P.Aue, L.Müller and R.R.Ernst, J.Mag.Res., 28, 29 (1977).

80) A.Bax, A.F.Mehlkopf and J.Smidt, J.Mag.Res., 35, 373 (1979).

81) A.Bax, R.Freeman and G.A.Morris, to be published.

82) M.H.Levitt and R.Freeman, J.Mag.Res., 39, 533 (1980).

83) C.P.Slichter, 'The Principles of Nuclear Magnetic Resonance', Harper and Row, New York, 1963.

84) G.Bodenhausen, R.Freeman and D.L.Turner, J.Mag.Res., 27, 511 (1977).

85) G.Bodenhausen and D.L.Turner, J.Mag.Res., 41, 200 (1980).

86) G.Bodenhausen,D.Phil thesis, Oxford, 1977.

87) R.Freeman, H.D.W.Hill and R.Kaptein, J.Mag.Res., 7, 82 (1972).

88) E.L.Hahn, Phys.Rev., 76, 145 (1949).

89) M.H.Levitt and R.Freeman, J.Mag.Res., 33, 473 (1979).

90) J.L.Markley, W.J.Horsley and M.P.Klein, J.Chem.Phys., 55, 3604 (1971).

91) R.Freeman and H.D.W.Hill, J.Chem.Phys., 54, 3367 (1971).

92) D.Canet, G.C.Levy and I.R.Peat, J.Mag.Res., 18, 199 (1975).

93) H.Hanssum, W.Maurer and H.Rüterjans, J.Mag.Res., 31, 231 (1978).

94) H.Y.Carr and E.M.Purcell, Phys.Rev., 94, 630 (1954).

95) S.Meiboom and D.Gill, Rev.Sci.Instr., 29, 688 (1958).

96) R.Freeman and H.D.W.Hill, in 'Dynamic Nuclear Magnetic Resonance Spectroscopy', Ed. L.M.Jackman and F.A.Cotton, Academic Press, New York, 1975, Ch.5.

97) S.R.Hartmann and E.L.Hahn, Phys.Rev., 128, 2042 (1962).

98) A.Kumar and R.R.Ernst, J.Mag.Res., 24, 425 (1976).

99) A.G.Redfield, Phys.Rev., 98, 1787 (1955).

100) R.L.Vold, R.R.Vold and H.E.Simon, J.Mag.Res., 13, 226 (1974).

101) F.Bloch and A.Siegert, Phys.Rev., 57, 522 (1940).

102) E.L.Hahn, Phys.Rev., 80, 580 (1950).

103) D.L.Turner, J.Mag.Res., 39, 391 (1980).

104) W.P.Aue, J.Karhan and R.R.Ernst, J.Chem.Phys., 64, 4226 (1976).

105) K.Nagayama, K.Wüthrich, P.Bachmann and R.R.Ernst, Biochem.Biophys.Res.Comm., 78, 99 (1977).

106) L.D.Hall, G.A.Morris and S.Sukumar, Carbohydr.Res., 76, C7-C9 (1979).

107) L.D.Hall, G.A.Morris and S.Sukumar, J.Am.Chem.Soc., 102, 1745 (1980).

108) L.D.Hall, J.K.M.Saunders and S.Sukumar, J.Chem.Soc.Chem.Comm., 1980, 366.

109) G.Bodenhausen, R.Freeman, G.A.Morris and D.L.Turner, J.Mag.Res., 31, 75 (1980).

110) R.Feynmann, F.Vernon and R.Hellworth, J.Appl.Phys., 28, 49 (1957).

111) M.E.Stoll, A.J.Vega and R.W.Vaughan, J.Chem.Phys., 67, 2029 (1977).

112) R.Kaiser, J.Mag.Res., 40, 439 (1980).

113) P.M.Henrichs and L.J.Schwartz, J.Mag.Res., 28, 477 (1977).

114) S.Vega, J.Chem.Phys., 68, 5518 (1978).

115) A.Wokaun and R.R.Ernst, J.Chem.Phys., 67,1752 (1977).

116) M.Mehring, E.K.Wolff and M.E.Stoll, J.Mag.Res., 37, 475 (1980).

117) J.S.Waugh, Lecture notes, NATO Summer School, Villasimius, Sardinia, 1980.

118) G.A.Morris and R.Freeman, J.Am.Chem.Soc., 101, 760 (1979).

119) G.A.Morris, J.Am.Chem.Soc., 102, 428 (1980).

120) A.A.Maudsley, A.Wokaun and R.R.Ernst, Chem.Phys.Letts., 55, 9 (1978).

121) L.Müller, and R.R.Ernst, Mol.Phys., 38, 963 (1979).

122) G.Bodenhausen and R.Freeman, J.Mag.Res., 36, 221 (1979).

123) A.Bax, R.Freeman and S.P.Kempsell, J.Am.Chem.Soc., 102, 4849 (1980).

124) M.Mehring and J.S.Waugh, Rev.Sci.Instr., 43, 4 (1972).

125) R.Freeman, S.P.Kempsell and M.H.Levitt, J.Mag.Res., 38, 453 (1980).

126) M.H.Levitt and R.Freeman, J.Mag.Res., 42, 000 (1981).

127) D.Hoult, J.Mag.Res., 33, 183 (1979).

128) P.C.Lauterbur, Nature, 242, 190 (1973).

129) P.Mansfield and A.A.Maudsley, J.Mag.Res., 27, 101 (1977).

130) A.Kumar, I.Welti and R.R.Ernst, J.Mag.Res., 18, 69 (1975).

131) W.S.Hinshaw and P.A.Bottomley, Nature, 270, 722 (1977).

132) H.S.Torrey, Phys.Rev., 76, 1059 (1949).

133) R.Freeman, S.P.Kempsell and M.H.Levitt, J.Mag.Res., 35, 447 (1979).

134) R.Freeman and J.Keeler, to be published.

135) A.Allerhand, J.Chem.Phys., 44, 1 (1966).

136) J.S.Waugh, L.M.Huber and U.Haeberlen, Phys.Rev.Letts., 20, 180 (1968).

137) P.Mansfield, Phys.Letts., 32A, 485 (1970); P.Mansfield, J.Phys., C4, 1444 (1971); P.Mansfield, Prog.NMR.Spectroscopy, 8, 41 (1972); U.Haeberlen, 'High Resolution NMR in Solids', Academic Press, New York, 1976.

138) G.A.Morris and R.Freeman, J.Mag.Res., 29, 433 (1978).

139) B.L.Tomlinson and H.D.W.Hill, J.Chem.Phys., 59, 1775 (1973).

140) A.G.Redfield, 17th Experimental NMR Conference, Pittsburgh, Pennsylvania, April, 1976.

141) R.Freeman, T.Frenkiel and M.H.Levitt, to be published.

142) G.Bodenhausen, J.Mag.Res., 34, 357 (1979).

143) G.Bodenhausen, R.R.Vold and R.L.Vold, J.Mag.Res., 37, 93 (1980).

144) W.S.Warren, D.P.Wietekamp and A.Pines, Phys.Rev.Letts., 43, 1791 (1979)

145) A.Bax, R.Freeman, T.Frenkiel and M.H.Levitt, to be published.

146) G.A.Morris, D.Phil. thesis, Oxford, 1978.

147) M.Lee and W.I.Goldberg, Phys.Rev., 140, A1261 (1965).

150) U.Haeberlen and J.S.Waugh, Phys.Rev., 175, 453 (1968).

151) W.P.Aue and R.R.Ernst, J.Mag.Res., 31, 533 (1978).

152) W.P.Aue, D.P.Burum and R.R.Ernst, J.Mag.Res., 38, 375 (1980).

153) M.H.Levitt, J.Keeler and R.Freeman, to be published.

154) D.I.Hoult, in Annual Report, National Institute of Health, Biomedical Engineering Branch, Bethesda, Maryland, USA, 1979.

155) P.Bendel, C.M.Lai and P.C.Lauterbur, J.Mag.Res., 38, 343 (1980).

156) M.H.Levitt and R.Freeman, to be published.

157) V.J.Basus, P.D.Ellis, H.D.W.Hill and J.S.Waugh, J.Mag.Res., 35, 19 (1979).

158) J.B.Grutzner and A.E.Santini, J.Mag.Res., 19, 178 (1975).

159) G.Bodenhausen, R.Freeman, G.A.Morris, R.Niedermeyer and D.L.Turner, J.Mag.Res., 25, 559 (1977).

160) A.Bax, R.Freeman and G.A.Morris, J.Mag.Res., 42, 000 (1981).